DOCTOR OF PHILOSOPHY

Causes of light backscattering by particles in the open ocean and the coastal zone

Martinez-Vicente, Victor

Award date:
2010

Awarding institution:
Bangor University

Causes of light backscattering by particles in the open ocean and the coastal zone

by

Victor Martinez Vicente, B.Sc., M.Sc.

A thesis in partial fulfilment of the requirements of the University of Wales for the degree of Doctor of Philosophy

December 2009

University of Wales Bangor
School of Ocean Sciences
Menai Bridge
Anglesey
Wales
LL59 5AB

ABSTRACT

The aim of this study was to investigate the causes of optical particle backscattering (b_{bp}) in the ocean, with the central hypothesis being that the phytoplankton is a significant contributor to variations in b_{bp}. The question is important because of its implications on some algorithms that estimate primary productivity from space and the interpretation of ocean colour from remote sensing.

To test this hypothesis a separation into several components (i.e. the reductionist approach) was applied to two different scenarios, typical of the oceanographic studies: an open ocean cruise and a coastal time series.

In a case study at the open ocean (central North Atlantic, over the Mid-Atlantic Ridge), during summer 2007, the variation in b_{bp} was explained by Chl-a (R^2=63%, P<0.001) using a power law, which was consistent with previous studies.

The use of the "reductionist approach" on the open ocean dataset incorporated information on pico and nano plankton abundances using flow cytometry, pigments and particulate detritus absorption measurements. It was found that the concentration of phytoplankton cells between 2 and 20μm in size, explained 70% (P<0.001) of the variance in b_{bp}. Furthermore, using a budget analysis of the contributions from different phytoplankton types and bacteria abundances, it has been shown that the nanoplankton have a higher backscattering efficiency per cell than bacteria, but that the elevated bacteria abundances mean that, overall, bacteria dominate the b_{bp} signal in the oceanic case study presented here (52% of b_{bp} is due to bacteria).

A similar approach was used for analysis of a nine year time series of bio-optical and particle composition data (including phytoplankton diversity) at the L4 coastal site on the Western English Channel. Variability of b_{bp} was best explained (R^2=58%, P<0.001) by the inorganic fraction, with no clear seasonal variation.

The main conclusion is that the "reductionist approach" allows a better understanding of the causes for variability of optical properties and should be further use for the study of the causes of backscattering in other areas of the ocean.

LIST OF CONTENTS

LIST OF FIGURES

Chapter Six – Backscattering related to phytoplankton using flow cytometry in the open ocean

LIST OF TABLES

ACKNOWLEDGMENTS

I would like to thank Dr. Gavin H. Tilstone and Dr. Gay Mitchelson-Jacob for the friendly supervision and support of this Thesis.

Many thanks to Mr. Steve Groom at Plymouth Marine Laboratory not only for providing the funding for the registration fees over the duration of this PhD but also for his advice, interest in this work and encouragement throughout.

I would like to acknowledge the NERC Field Spectroscopy Facility (FSF) for providing the Wetlabs BB3 instrument for the ECOMAR cruise (Loan N: 519.1206).

My appreciation goes to Dr. Peter Miller for allowing the use of the ECOMAR data for this Thesis as well as his support for obtaining the instrument loan from the FSF. Thanks to NEODAAS for the provision of remote sensing images and data.

Thanks to the Captains and crews of the *R.V. James Cook* and *R.V. Plymouth Quest* for their help during the ECOMAR cruise and the sampling at L4.

In particular, I would like to thank Mr. Gerald Moore for organising the Hydroscat instrument comparison at PML presented in Chapter 4 and for maintaining the bio-optical sampling at L4 between 2003 and 2007.

Chapter 7, being a time series that spans beyond the duration of this PhD, has some data contributed from different researchers: Dr. Claire Widdicombe for data of phytoplankton counts; Dr. Peter Land for part of the data of suspended particulate matter (2007-2008); Dr. James Fishwick, Alex Menezes, Isobel Cook and Katie Chamberlain for the analysis of part (1999-2007) of the pigment samples using HPLC.

I would like to thank my colleagues at PML and in other institutions for valuable discussions and/or training in different analysis techniques, including: Dr. Peter Land, Dr. Glen Tarran, Dr. Jamie Shutler, Dr. Giorgio Dall'Olmo, Dr. Tim Smyth, Dr. James Fishwick, Dr. Ruth Airs, Dr. Kadija Oubelkehir, Dr. Shubha Sathyendranath and Dr. Trevor Platt.

Finally, I would like to thank to my family. It would not have been possible to complete this work without their support. Thanks for the delicious meals to my mother in law, Nina. Thanks for the help in finishing doing up my house (at the same time as I was finishing this thesis) to my father in law, Mastro Carlo. Thanks to Victoria and Lorenzo for their laughter. Thanks to my parents.

Especially, I would like to dedicate this work to my wife, Rossana, for her unconditional support and patience over these years.

Chapter One

Motivation, introduction, rationale and objectives

CHAPTER ONE: MOTIVATION, INTRODUCTION, RATIONALE AND OBJECTIVES

1.1 Motivation

The research in this thesis is a contribution to the field of marine optics, the branch of the oceanography concerned with light propagation in the ocean. It focuses on marine bio-optics and the relationship between biological and biogeochemical variables and optical properties, specifically the backscattering coefficient (b_b), which quantifies the fraction of light scattered in the backward direction. Documenting the natural variability of b_b and investigating the causes of this variability in the marine environment should provide new optical information associated with different biological and biogeochemical properties of marine waters.

1.2 Aims and objectives

The **'reductionist approach' will be used throughout the thesis and applied to in-situ scenarios** (in an oceanic and a coastal location) **to address the question** of **whether the phytoplankton is a significant contributor to backscattering**. In this thesis, the results are presented both considering the suspended matter as a bulk component as well as splitting the suspended matter into compartments using the 'reductionist approach'.

Therefore, the specific objectives of this thesis are:

- To document the natural variability (spatial, temporal and spectral) of b_b in oceanic and coastal regions.
- To interpret the spectral variations of b_b supported by biogeochemical and other optical properties.
- To compare and complement the results from using the reductionist approach to the more classic approach of using bulk biogeochemical properties of the suspended matter.

1.3 Introduction and rationale

The light illuminating a particle can be absorbed and dispersed (scattered) in different directions. Intuitively, the spectral backscattering coefficient ($b_b(\lambda)$) is a measure of the proportion of incident light that travels in the backward direction after interacting with the particle.

Backscattering is, to a first order (Gordon and Morel, 1983), directly proportional to the remote sensing of ocean colour from the space. From ocean colour, standing stocks of phytoplankton biomass (through the quantification of its ubiquitous pigment, the chlorophyll-a) as well as the photosynthetic capacity of phytoplankton (primary production) can be estimated (Eppley *et al.*, 1985). Improvements in the understanding of b_b have contributed to the progress of remote sensing products to help the understanding of the Global Carbon Cycle in the ocean in the context of Climate Change (Behrenfeld *et al.*, 2006; IPCC, 2007). Estimations of chlorophyll concentration from satellites provide data for the synoptic validation of Global Circulation Models (GCM), improving predictions of the response of the ocean to Climate Change, and are at the heart of most algorithms used to derive both primary production from remote sensing (Behrenfeld and Falkowski, 1997) and to produce budgets of carbon at the global scale (Dunne *et al.*, 2007). New remote sensing algorithms use phytoplankton carbon derived from b_b, instead of chlorophyll-a, as the basis for estimating primary production in the open ocean (Behrenfeld *et al.*, 2005). At regional scales, there is an increased need for water quality monitoring indicators from satellites, such as SPM which can be derived from b_b, due to the implementation of directives for environmental protection (EU Water Framework Directive, 2000/60/EC).

The interest in the study of the sources of b_b in the ocean originated from the importance of b_b in interpreting remotely sensed images. The approaches to retrieve information about substances in the sea from ocean colour (IOCCG, 2000) can be split into three types of algorithm: empirical, semi-analytical and analytical. Empirical algorithms retrieve one biogeochemical component (e.g. chlorophyll in phytoplankton) from the ratio of two or more wavelengths (O'Reilly *et al.*, 1998). Semi-analytical algorithms use the relationships between inherent optical properties (like backscattering) and seawater components (like chlorophyll-a content) to interpret ocean

colour by making assumptions about the bio-optical relationships (Gordon *et al.*, 1988; Morel, 1988). Analytical algorithms interpret the ocean colour in terms of the inherent optical properties (with no need to make assumptions about the bio-optical relationships) (Lee *et al.*, 2002; Smyth *et al.*, 2006). Initial attempts to describe b_b variability as a function of in-water components (i.e. algal chlorophyll content) were done as part of the development of semi-analytical algorithms (Gordon *et al.*, 1988; Morel, 1988). However, there were large differences between the bio-optical relationships used for b_b and chlorophyll content (Morel and Maritorena, 2001). Part of these uncertainties both in magnitude and in spectral variation of backscattering was due to the **lack of fundamental knowledge about the sources of b_b** (and the inability to measure b_b in situ).

Not only semi-analytical algorithms require the improvement of bio-optical relationships for b_b. Analytical algorithms produce inherent optical properties (including b_b) as outputs from the inversion of satellite ocean colour signal. It is necessary to transform the b_b (as well as the other inherent optical properties) into biogeochemical and biological parameters. There is already a good knowledge of the relationships between the other inherent optical properties (IOPs). For instance, absorption is highly correlated with phytoplankton pigments (Bricaud *et al.*, 2004), and attenuation is commonly used as a descriptor of particulate organic carbon concentration (Gardner *et al.*, 2006). Theoretically (Morel, 1973), b_b is a proxy for particle abundance but it also depends on distribution of particle size (i.e. relative proportions of larger and smaller particles) and on particle composition (e.g. whether particles are organic or inorganic) (Jonasz and Fournier, 2007). Thus, satellite algorithms, producing backscattering from ocean colour, can be related to suspended matter via the mass-specific coefficients (Dall'Olmo and Gitelson, 2006). However, before b_b can be used in an inverse way (i.e. a measurement of b_b used to provide information about the suspended particles), there are some **questions about the causes of variability of b_b** (i.e. the forward problem) **that need addressing**.

The work presented in this thesis, is a **bio-optical study of backscattering which aims to improve the understanding of the relationships between b_b and other components in marine waters. In particular, research is needed on whether the**

phytoplankton is a significant contributor to particle backscattering or not as it will be argued here after.

The question on the importance of phytoplankton on backscattering arises from the observation that although a significant relation between Chl-a and backscattering has been documented (Huot *et al.*, 2008), phytoplankton is not the only contributor to backscatter (Stramski *et al.*, 2004). There are currently two tendencies in the scientific literature that provide conflicting evidence. One, supported by modelling studies and some laboratory experiments, which state that b_b from particles (b_{bp}) in the ocean is dominated by minerals (Stramski *et al.*, 2001), and in their absence, the most important living contributor is bacteria (Stramski and Kiefer, 1991). This could be a plausible explanation as bacterial abundance co-vary with Chl-a. Evidence for the relationship between bacteria and backscattering was supported by experiments on cultures carried out in the early 1990s (Ahn *et al.*, 1992; Morel and Ahn, 1990, 1991; Morel *et al.*, 1993) which complemented the, then state of the art, modelling tool proposed by Bricaud and Morel (1986). This model (based on Mie theory), which can be used to predict backscattering, makes two important assumptions: first, particles are spherical and second, they are homogeneous (Bohren and Huffman, 1983; van de Hulst, 1957). In contrast to this line of research, some experiments and in-situ observations, suggest that the phytoplankton may have a larger role than predicted by models (Dall'Olmo *et al.*, 2009; Vaillancourt *et al.*, 2004). This trend has emerged more recently thanks to the development of instrumentation that directly measures the b_b in the water (Maffione and Dana, 1997; Moore *et al.*, 2000). The supporters of this line of thought argue that the assumptions of earlier modelling work considering the phytoplankton homogeneous spheres are underestimating the role of phytoplankton in producing backscattering, hence giving rise to what has been coined as the 'missing backscattering' (Stramski *et al.*, 2004). Evidence on the enhancement of backscattering from inhomogeneities in the phytoplankton cells come from detailed measurements of the scattering intensity at several angles around particles (Volten *et al.*, 1998) and from advanced formulations of the scattering models using two layered geometries (Aden and Kerker, 1951; Bernard *et al.*, 2009; Meyer, 1979) and three layered models (Kitchen and Zaneveld, 1992). This dichotomy has not yet been resolved and the main objective of this thesis is to try to move the subject forward **by providing evidence on whether the phytoplankton is a significant source of backscattering or not**.

Globally, the results of the work from Stramski *et al.* (2001) confirmed those of ten years before: the phytoplankton contribution to b_b is very small and that bacteria may be greatest living contributors to b_b (Morel and Ahn, 1991; Stramski and Kiefer, 1991). However, these studies make an important assumption which may be a cause of uncertainty: that modelled cells are homogeneous spheres. The real plankton cells have an external cellular wall and a cytoplasm where the organelles reside. Modelling studies with coated spheres that simulate real cells show enhanced backscattering compared with homogeneous spheres by as much as one order of magnitude (Kitchen and Zaneveld, 1992; Zaneveld and Kitchen, 1995). Differences for backscattering have been shown between centred and off centred nucleus in a coated spheroid (Quirantes and Bernard, 2004). Preliminary results (Bernard, 2005) have shown that heterogeneous geometry can produce an increase on phytoplankton b_b from 5 to 25 times compared to the homogeneous case.

To do so, an **in-situ approach has been chosen** (as opposed to a laboratory experiment). In-situ sampling has the advantage of characterising the natural variation in optical properties, especially since new instruments have become available as profiling tools which can be relatively easily deployed in the field. Previous in-situ studies relating backscattering to suspended matter composition refer mainly to bulk properties of the suspended matter: chlorophyll-a concentration (Chl-a), particulate organic carbon (POC) and suspended particulate matter (SPM), including the inorganic and organic particulate matter fractions (PIM and POM, respectively). Oceanic studies have mainly focused on obtaining relationships between backscattering and Chl-a (Huot *et al.*, 2008; Reynolds *et al.*, 2001; Stramska *et al.*, 2003) and with POC (Stramski *et al.*, 2008; Stramski *et al.*, 1999), while coastal studies have referenced the backscattering coefficient to SPM and its various components (Snyder *et al.*, 2008).
The relationship between POC and IOP has been studied for twenty years. Morel (Morel, 1988) showed a relationship between b at 550 nm ($b(550)$) and Chl-a, and a relationship between Chl-a and POC. However, the relationship between POC and Chl-a is very variable and difficult to predict as it is dependent on several factors, such as the physiological status of cells (photoacclimation), types (and sizes) of phytoplankton cells and relative amounts of detritus (Geider *et al.*, 1997; MacIntyre *et al.*, 2002; Sathyendranath *et al.*, 2009). Therefore, the best way to correlate IOP with POC is to

compare directly POC with optical measurements, instead of relating the IOP to Chl-a and then to transform the Chl-a to POC.

Studies in the laboratory have provided an insight into the relationship between POC and scattering. The mass-specific scattering relative to POC is relatively constant in a variety of growth conditions (Stramski and Morel, 1990), and the cause of this relatively robust relationship is the link between cell size and carbon content (Montagnes *et al.*, 1994) and the connection between carbon content and refractive index (Stramski, 1999). The largest amount of field data relating an optical property and POC is between the particulate attenuation coefficient at 660 nm ($c_p(660)$) and POC. The most recent database used nearly 4500 data pairs from different parts of the ocean (Gardner *et al.*, 2006), and catalogued a significant linear regression, but with large regional variability in the slope of the regression (~2 fold) and in the correlation coefficient (varying between 0.5 and 0.9). A limited number of studies have used in-situ measurements of POC and backscattering to produce empirical relationships of use for remote sensing algorithms (Stramska and Stramski, 2005; Stramski *et al.*, 2004; Stramski *et al.*, 2008; Stramski *et al.*, 1999).

However, it has been recognised that bulk matter properties are not sufficient to resolve the question of whether the phytoplankton is a significant source of backscattering (Huot *et al.*, 2008; Stramski *et al.*, 2001). Therefore, Stramski *et al.* (2004) proposed a **'reductionist approach'**. In practice this approach consists of separating the contributions to the backscattering into different components:

$$
\begin{aligned}
b_b &= b_{bw} + b_{bp} \\
b_{bp} &= b_{bpSPM} = b_{bpPOM} + b_{bpPIM} = b_{bpliving} + b_{bpnonliving} + b_{bpPIM} = \\
&= \sum_{i=1}^{n} b_{bppla,i} + b_{bpnonliving} + b_{bpPIM} = \\
&= \sum_{i=1}^{n} C_{ppla,i}\sigma_{bbp,pla,i} + C_{nonliving}\sigma_{bbp,nonliving} + C_{PIM}\sigma_{bbp,PIM}
\end{aligned}
\qquad \textbf{Eq.1}
$$

where the total backscattering coefficient (b_b) is equal to the sum of pure seawater contribution to backscatter (b_{bw}) and particle backscattering (b_{bp}). Backscattering by bubbles could be important in high wind conditions, but in this thesis the focus is on

particles so bubbles and their effect are not considered. In turn, particle backscattering is due to suspended particulate matter (b_{bpSPM}) which can be split into its organic and inorganic fractions (b_{bpPOM} and b_{bpPIM}). The organic contributions to backscatter come from the living pool, through a number (*n)* of different sources (including viruses, bacteria and several phytoplankton types), ($b_{bpliving}$). The other organic component is from non-living organic matter ($b_{bpnonliving}$), which includes phytodetritus locally produced and organic detritus from other sources (riverine or re-suspended, in coastal waters).

If the contributions to particulate components in Equation 1 are expressed in terms of mass concentration, C (mg C m^{-3} for the phytoplanktonic components, g m^{-3} for SPM) then, the backscattering cross-section is a mass-specific coefficient for each particle type per unit of mass, σ_{bbp} (m^2 (mg C)$^{-1}$ for phytoplanktonic, m^2 g^{-1} for SPM).

If C is the number concentration of each particle type (i), N_i (in m^{-3}), then, the backscattering cross-section, σ_{bb} has units of m^2 for a single particle of the ith component. The backscattering cross-section is the product of the geometric cross-section of the particle and the efficiency factor (dimensionless) for backscattering of the particle:

$$\sigma_{bbp,pla,i} = S_i \times Q_{bbpi} \qquad \textbf{Eq.1b}$$

The efficiency factor, Q_{bbpi}, is the ratio of radiant power backscattered by the particle to radiant power intercepted by the geometric cross-section of the particle, S_i (Bricaud and Morel, 1986). Although the 'reductionist approach' has been used successfully in modelling, it has not been investigated or applied to natural waters.

To address the questions posed above, the thesis is structured as follows: a revision of the fundamental theory behind the backscattering process and the current knowledge about the contribution of each particulate component is carried out in ***Chapter 2.*** ***Chapter 3*** *outlines the methods used in collecting the data set to address the objectives.*

Chapter 4 *is a methodological study on the precision and accuracy of instrumentation to measure backscattering of particles in water. It compares two different instruments that measure backscattering and provides a study on the possible causes of error between them and in the measured* b_b.

The causes of backscattering in an open ocean environment are investigated in ***Chapters 5 and 6****. During summer 2007, a cruise took place (hereafter the ECOMAR cruise) at the Mid-Atlantic Ridge - MAR (between 48 and 54°N), providing the opportunity to sample in a region away from continental influences (with no external sources of minerals or organic detritus). This specific oceanic region has not been previously sampled for biological or bio-optical parameters, hence, the added importance of these measurements. Two chapters are dedicated to this area:* ***Chapter 5*** *is a study of the bulk matter components in relation to the optical backscattering and its spectral variations. It is necessary to verify that the measurements presented in this thesis agree with the current state of knowledge, therefore the bulk properties of the matter are studied as a preliminary (and necessary) step previous to further analysis. It is concluded that bulk components can provide only limited information about the causes of backscattering, therefore, introducing* ***Chapter 6,*** *which is a study considering the phytoplankton components separately.*

In order to extend the study into more optically complex waters, in ***Chapter*** *7 results from a coastal site are presented. The L4 coastal station (part of the Western Channel Observatory) is ideally suited as a case study to test the "reductionist approach" on a seasonal scale, not only because it is a regular sampling site for a variety of variables from nutrients to zooplankton, including bio-optics, but of its optical complexity through the influence of different types of phytoplankton, SPM and coloured dissolved organic matter (CDOM).*

Finally, the results presented in ***Chapters 4 to*** *7 are discussed in* ***Chapter 8*** *and a summary of conclusions and recommendations for future work is presented.*

Chapter Two

Background on the relationships between backscattering and the biogeochemical properties of marine particles

CHAPTER 2 : BACKGROUND ON THE RELATIONSHIPS BETWEEN BACKSCATTERING AND THE BIOGEOCHEMICAL PROPERTIES OF MARINE PARTICLES

Synopsis

This chapter is dedicated firstly to defining backscattering (b_b) and to providing the fundamental physical basis of the light interaction with particles. Secondly, to describe what is known, on a per particle type basis, about the contribution of each type to b_b. Thirdly, to summarise the relationships obtained from in-situ studies and finally to give an overview on the applications to derive the nature of the particles either from satellite or from direct bio-optical observations.

The definitions of b_b are made both in the context of the bulk Inherent Optical Properties (IOP) (Kirk, 1994; Mobley, 1994) and by the theory of scattering by small particles (Bohren and Huffman, 1983; Jonasz and Fournier, 2007; van de Hulst, 1957). The elements of the Mie theory presented here are intended for interpreting the in-situ measurements collected during this thesis, hence the non exhaustive nature of the review, which can be found in the books above.

2.1 Bulk inherent optical properties

The propagation of light in natural waters is affected by the nature of the substances present in it. Their optical influence is quantified by a set of coefficients, grouped by Preisendorfer (1961) into inherent optical properties (IOPs) and apparent optical properties (AOPs). The IOPs quantify the influence of these substances on the light field, while the AOPs characterize the way the geometry of the radiative field is modified by their presence. Therefore the AOPs depend on the IOPs and on the directional structure of the ambient light field. Radiative transfer theory provides the connection between the IOPs and the AOPs (Mobley, 1994).

This double attribute of the IOPs, being exclusively linked to the substances in the marine environment but at the same time influencing its light field, make the IOPs the object of this study. The two fundamental IOPs are the absorption coefficient and the volume scattering function. Other IOPs include the scattering and backscattering coefficients, index of refraction, the beam attenuation coefficient and the single-scattering albedo.

An intuitive way of defining the IOPs is by assuming a light balance on a small volume (ΔV), of thickness Δr (Figure 2.1). This volume is illuminated by a narrow collimated beam of monochromatic light of spectral radiant power, $\Phi_i(\lambda)$, measured in Wm^{-1}. Part of the incident power is absorbed within the volume of water, $\Phi_a(\lambda)$; part is scattered $[\Phi_s(\theta,\lambda)]$ out of the beam at an angle θ; and the remaining power $[\Phi_t(\lambda)]$ is transmitted through the volume with no change in direction. Let $\Phi_s(\lambda)$ be the total power that is scattered in all directions, and assume that no inelastic scattering[1] occurs. By conservation of energy,

$$\Phi_i(\lambda) = \Phi_a(\lambda) + \Phi_s(\lambda) + \Phi_t(\lambda) \qquad \textbf{Eq. 1}$$

[1] Inelastic scattering implies that there is a change in wavelength of the scattered light (i.e. Raman scattering or fluorescence)

The spectral absorbance, A(λ), is a fraction of the incident power that is absorbed within the volume (dimensionless):

$$A(\lambda) \equiv \frac{\Phi_a(\lambda)}{\Phi_i(\lambda)} \qquad \textbf{Eq. 2}$$

Likewise, the spectral scatterance B(λ) is the fraction of the incident power that is scattered out of the beam and T(λ) is the spectral transmittance. The sum of these three IOPs equals 1.

The inherent optical properties usually employed in marine optics are the spectral absorption and scattering coefficients, which are respectively the spectral absorbance and scatterance per unit distance in the water. Using the nomenclature of Figure 2.1.a, the spectral **absorption coefficient,** $a(\lambda)$, is defined as

$$a(\lambda) \equiv \lim_{\Delta r \to 0} \frac{A(\lambda)}{\Delta r} \qquad \textbf{Eq. 3}$$

and the spectral **scattering coefficient,** $b(\lambda)$, is

$$b(\lambda) \equiv \lim_{\Delta r \to 0} \frac{B(\lambda)}{\Delta r} \ (\mathrm{m}^{-1}) \qquad \textbf{Eq. 4}$$

The spectral beam **attenuation coefficient,** $c(\lambda)$, is defined as

$$c(\lambda) \equiv a(\lambda) + b(\lambda) \ (\mathrm{m}^{-1}) \qquad \textbf{Eq. 5}$$

with B(θ,λ) being the fraction of incident power scattered out of the beam through an angle θ into a solid angle ΔΩ centered on θ (Figure 2.1.b). This angle is called the scattering angle; its values lie in the interval 0 to π. If the medium is axially symmetrical about the direction of propagation of the incident light beam, then the angular scatterance per unit of distance and unit of solid angle, β(θ,λ), is

$$\beta(\theta,\lambda) = \lim_{\Delta r \to 0} \lim_{\Delta\Omega \to 0} \frac{B(\theta,\lambda)}{\Delta r \Delta\Omega} = \lim_{\Delta V \to 0} \frac{I_s(\theta,\lambda)}{E_i(\lambda)\Delta V} \qquad \textbf{Eq. 6}$$

where $I_s(\theta,\lambda)$ is the spectral radiant intensity scattered into direction θ, $E_i(\lambda)$ the corresponding incident irradiance and ΔV the volume of water illuminated by the incident beam. This form of the β(θ,λ) suggests the name of spectral **volume scattering function** (**VSF**) and the physical interpretation as the scattered intensity per unit incident irradiance per unit volume of water ($\mathrm{m}^{-1}\mathrm{sr}^{-1}$).

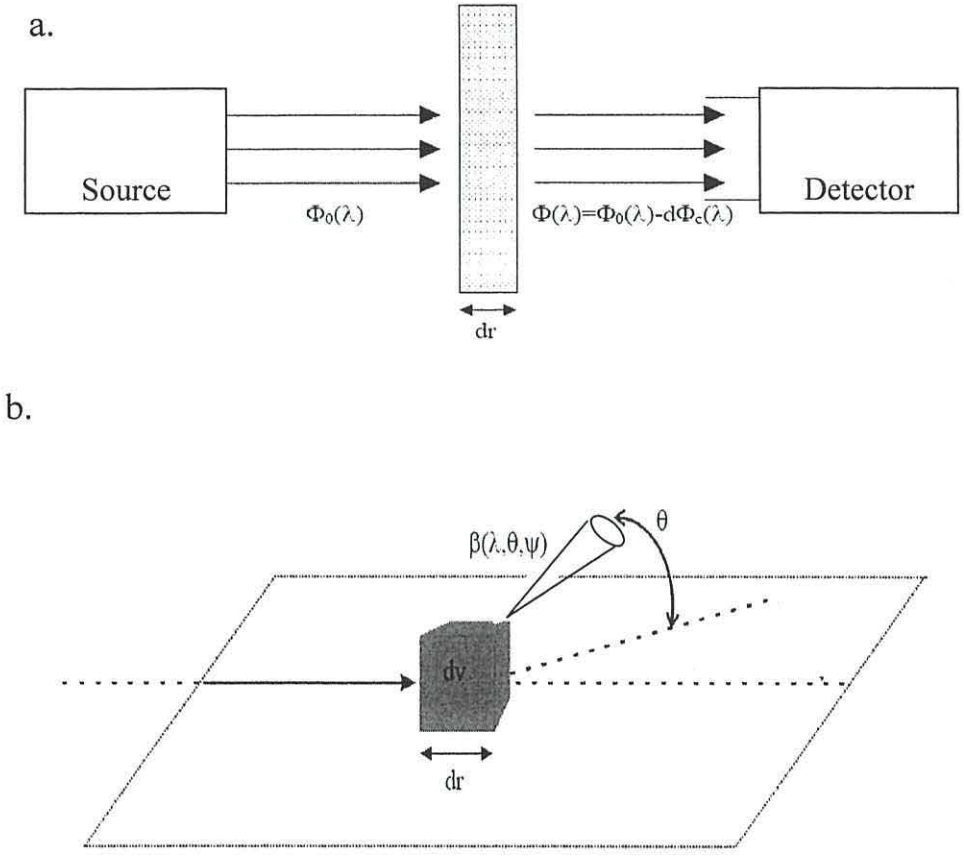

Figure 2.1 Schematic representation used for the definition of the bulk optical properties (Adapted from A. Morel Lecture). a) Absorption b)Scattering and volume scattering function (β). The cone around β highlights the fact that it is a magnitude per solid angle.

Integrating $\beta(\theta,\lambda)$ over all directions gives another way of defining the spectral scattering coefficient:

$$b(\lambda) = 2\pi \int_0^{\pi} \beta(\theta,\lambda)\sin\theta d\theta \qquad \text{Eq. 7}$$

This integral is possible due to the azimuthal symmetry with respect to the incident direction (for unpolarized sources and for randomly oriented scatterers). The integration is often divided into **forward** and **backward scattering (backscattering)**, with the corresponding coefficients being respectively,

$$b_f(\lambda) \equiv 2\pi \int_0^{\pi/2} \beta(\theta,\lambda)\sin\theta d\theta \text{ and}$$

$$b_b(\lambda) \equiv 2\pi \int_{\pi/2}^{\pi} \beta(\theta,\lambda)\sin\theta d\theta \qquad \textbf{Eq. 8}$$

Based on the above IOPs, there are some useful ratios: the **backscattering ratio** and the **volume scattering phase function (or normalized VSF)**, $\tilde{\beta}(\theta,\lambda)$, defined respectively by:

$$\tilde{b}_b(\lambda) = \frac{b_b(\lambda)}{b(\lambda)} \qquad \textbf{Eq. 9}$$

$$\tilde{\beta} \equiv \frac{\beta(\theta,\lambda)}{b(\lambda)} (\text{sr}^{-1}). \qquad \textbf{Eq. 10}$$

Another IOP of use in marine optics is the spectral **single scattering albedo** $\omega_0(\lambda)$, defined by

$$\omega_0 \equiv \frac{b(\lambda)}{c(\lambda)}. \qquad \textbf{Eq. 11}$$

Single scattering albedo is near to one in waters where the beam attenuation is due primarily to scattering and near zero where the beam attenuation is due primarily to absorption.

The preceding description has assumed that no inelastic (trans-spectral) scattering processes are present. However, trans-spectral scattering occur in natural waters, due to fluorescence by dissolved matter or chlorophyll, and to Raman or Brillouin scattering by the water molecules themselves. The detailed study of the inelastic scattering is outside the aims of the present work.

2.2 A model of scattering by small particles applicable to marine optics

A definition of scattering is "the redirection of energy of an 'infinite' 'plane-parallel' electromagnetic wave due to interaction with matter". Interaction means that the wave travels at different speeds at different locations within the medium due to inhomogeneities within the medium. These can be caused by particles of different optical properties to the medium or 'fluctuations', that is regions within the medium with slightly different concentrations of molecules. The 'relative' index of refraction (m) of a particle relative to the medium in which it is embedded, is the ratio of the speeds of lights propagating through the medium and the particle (not to confuse with refractive index, n, see below). For a given size and shape of particle, the more different the index of refraction is from 1 the more pronounced is the scattering.

Scattering is the sum of (Figure 2.2):

1. Reflection: at a boundary of a particle with different *m* than the medium in which it is embedded, a certain amount of radiation is reflected back.

2. Refraction: at a boundary of a particle with different *m* than the medium in which it is embedded, a certain amount of radiation penetrates into the particle, usually at a different angle than the angle of incidence (Snell Law).

3. Diffraction: the light propagating along the boundary of the particle responds to the boundary causing a change in direction.

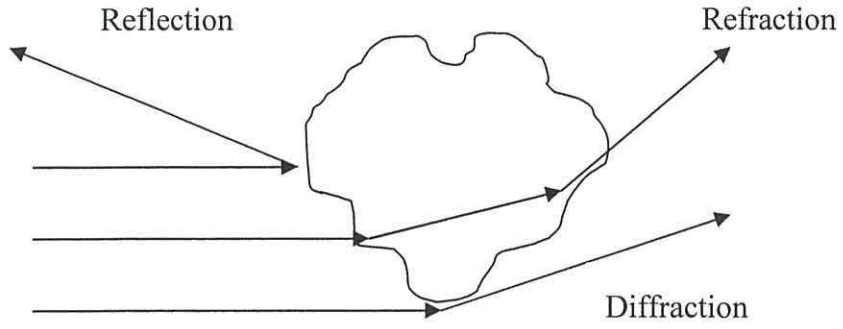

Figure 2.2 Interactions of the light with a particle constituting the total scattering.

van de Hulst (1957) derives what is called the optical theorem using as a point of departure for its reasoning that the incident wave is a plane scalar wave and that the scattered wave is a spherical wave with amplitude inversely proportional to the distance:

$$C_{attn} = \frac{4\pi}{k^2}\mathrm{Re}\{S(0)\} \qquad \textbf{Eq. 12}$$

where C_{attn} is the total attenuation cross-section. C_{attn} is equal to C_{scat} when the imaginary part is 0. k is the wavenumber of the incoming wave ($k = 2\pi/\lambda$) and $\mathrm{Re}\{S(0)\}$ is the real part of the amplitude function of the scattering by the particle in the forward direction ($\theta=0$), which is just the integral over the spherical coordinates of the two dimensional angular scattering cross-section.

According to the above optical theorem, it is possible to define the geometrical cross section, S_g, of any particle as being the projected ("shadow") area of this particle on

the plane wave (Morel, 1991). The processes of absorption and scattering are described at a single particle level by two dimensionless "efficiency factors", Q_a and Q_b, which are respectively the ratios of the radiative energy absorbed and scattered by the particle, to the energy incident on its geometrical cross section.

The sum, $Q_a+Q_b= Q_c$, defines the efficiency factor for attenuation, which expresses the global removal of energy. Therefore $S_g\ Q_i = C_i$ (dimensions of L^2) is the cross section of the particle for absorption, scattering and attenuation if i=a,b,c respectively.

The Mie theory is the analytical way to compute efficiency factors (Q_i) and the intensity of the scattered light, including its polarization state, for any scattering angle. This theory is a rigorous solution of Maxwell's equations and is able to account for scattering by spherical, variously sized and absorbing particles. For very small (compared to wavelengths) spheres it reduces to the Rayleigh theory of the radiating dipole, where scattering is dominated by refraction and reflection, and the response is proportional to the particle's volume. For large spheres, it provides a rigorous sum of the geometrical optics pattern where the scattering is dominated by diffraction, as the light going through the particles is likely to be absorbed, and the response is proportional to the particle's cross sectional area, which is sensitive to the shape of the particle. The Mie theory initially developed for homogeneous spheres has been extended to different shapes and/or non-homogeneous particles.

What follows is an overview of the modifications to the Mie theory, that will be relevant for the rest of this work, including: simplifications (like the anomalous diffraction approximation, ADA), effects of considering absorption (the anomalous dispersion, AD) and effects of considering multiple particles (mono and polydispersed) for the simple case of homogeneous spherical particles, which may be of use to interpret the measurements of b_b presented later.

The parameters intervening in the Mie theory (Morel, 1991) are: the relative size (α), the relative index of refraction (m), the phase lag (ρ) and the optical thickness due to absorption (ρ') that are defined by the following relationships:

$$\rho = 2\alpha(n-1)$$

$\rho' = 4\alpha n'$

where

$\alpha = \pi d / \lambda_w = \pi d n_w / \lambda_0$

$$m = \frac{n_s - in'_s}{n_w} = n - in'$$

λ_0 is the wavelength in vacuo and n_w is the index of refraction of the water. The index of refraction of a homogeneous substance (index *s*) is relative to the real refractive index of the water (n_w) in the visible domain. The complex refractive index is composed by a real (n) and imaginary parts (n'), related respectively to the scattering and absorption by

$n = v_0 / v_s \, n_w$

$n' = a_s \lambda / 4\pi \, n_w = a_s \lambda_w / 4\pi$

where v_0 and v_s are the speed of light in vacuo and in the substance, and a_s is the absorption coefficient of the substance.

If the index of refraction of the particle differs only slightly from that of the surrounding medium (i.e. near to 1 in the marine environment), the "anomalous diffraction approximation (ADA)" (van de Hulst, 1957), can be applied to obtain estimates of Q_a, Q_b and Q_c. Under this assumption, the general formulation of the attenuation and absorption efficiency factors (Q_c and Q_a) as a function of the parameters above is simplified into:

$$Q_c = 4\,\mathrm{Re}\left\{\frac{1}{2} + \frac{\exp(-i\rho)}{i\rho} + \frac{\exp(-i\rho)-1}{(i\rho)^2}\right\} \qquad \textbf{Eq. 13}$$

$$Q_a(\rho) = 1 + 2\frac{\exp(-\rho')}{\rho'} + 2\frac{\exp(-\rho')-1}{\rho'^2} \qquad \textbf{Eq. 14}$$

The efficiency factor of scattering (Q_b) is calculated as the difference between Q_c and Q_a. The efficiency factors are shown in Figure 2.3 as a function of ρ with increasing absorption (n'). For n'=0 (non absorbing particles) Q_b and Q_c present regularly decreasing oscillations around their limiting values, which are met for large values of ρ. These oscillations originate from favourable (constructive) or unfavourable (destructive) interferences between the rays having passed through the particle, and those diffracted around the particle. When absorption intervenes, Q_a departs from zero

and increases with ρ, tending to a limiting value of 1, the same as Q_b. The effect of the absorption on Q_c in general is to reduce the amplitudes of its oscillations.

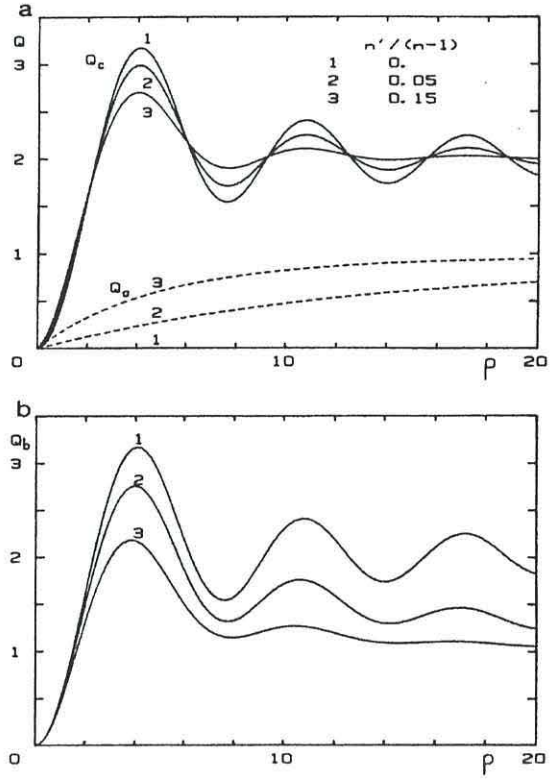

Figure 2.3 Variation of the optical efficiency factors: a) attenuation (Q_c) and absorption (Q_a). b) scattering (Q_b) (taken from Morel and Bricaud, 1986).

This theory can be expanded from a single particle to a group of particles of variable size (polydispersed). The size structure of a population of particles is characterized by a size distribution function:

$$F(d) = \frac{1}{V}\frac{d(N)}{d(d)} \qquad \textbf{Eq. 15}$$

F(d)d(d) is the number of cells per unit volume in the size range $d \pm 1/2 d(d)$, where *d* is the diameter of the particles. The integral of this function provides N/V, the total number of particles N in the volume V of suspension (Bricaud and Morel, 1986). With λ and *n* fixed, *d* can be transformed into ρ, and the distribution function can be written as $F(\rho)$. Mean efficiency factors can be defined and computed for a "mean" particle, which represents the actual polydispersed population according to:

$$Q_i(\rho_M) = \frac{\int_0^\infty F(\rho) Q_i(\rho) \rho^2 d\rho}{\int_0^\infty F(\rho) \rho^2} \qquad \textbf{Eq. 16}$$

with $i=a,b,c$; where ρ_M is the ρ value which corresponds to the maximum of the size distribution function. In this equation, the numerator represents the cumulated cross section for absorption, scattering and attenuation and the denominator represents the geometrical cross section of the entire population ($Q_i = \sigma_i / S_g$).

Figure 2.4 shows the Q_c plotted as a function of ρ_M for a non absorbing population. The size distribution functions are log-normal with increasing dispersion (wider peak). As it is observed, the polydispersion results in a smoothing effect, which is greater as the distribution becomes wider. The Q_c reaches a maximum at ρ=4.09 for monodispersions, slightly shifted for polydispersions, and beyond this point, Q_c tends asymptotically to 2. The interpretation of this behaviour is that size is an important factor for the attenuation due to smaller particles (2 to 5 μm), while for particles greater than 10 μm or 20 μm, Q_c is practically independent of size. Q_b is also weakly size dependent and the scattering (the product S_g x Q_b) by larger particles appears to be only proportional to their geometrical cross-sections.

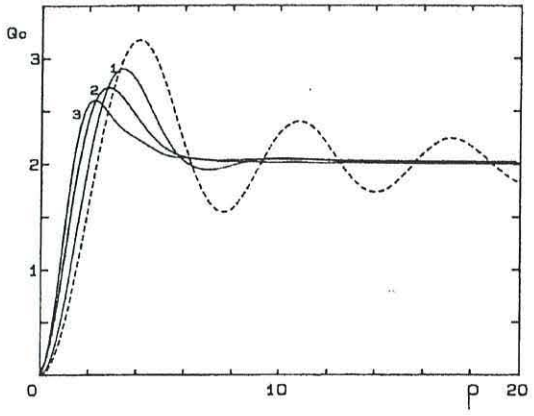

Figure 2.4 Mean efficiency factor for attenuation (Q_c) of a mean particle representative of a polydispersed population as a function of ρ (taken from Morel and Bricaud, 1986).

However, rigorous Mie theory has to be applied to determine the angular distribution of the scattered energy. Q_{bb} (efficiency factor of backscattering) and the angular distribution of the scattered light ($\beta(\theta,\lambda)$, see Section 2.1) have to be described. The full solution of Mie theory involves the computation of the (dimensionless) angular scattered intensities $i_1(\theta,\alpha,m)$ and $i_2(\theta,\alpha,m)$. These intensities are the squares of the moduli of the complex amplitude functions relative to the electric fields perpendicular

to and parallel with the plane of scattering and are functions of Mie coefficients (polarisation components). Q_{bb} is obtained from the integral of $i_1(\theta,\alpha,m)$ and $i_2(\theta,\alpha,m)$ values according to:

$$Q_{bb}(\alpha,m)=\alpha^{-2}\int_{\frac{\pi}{2}}^{\pi}\frac{i_1(\theta,\alpha,m)+i_2(\theta,\alpha,m)}{2}\sin\theta d\theta \qquad \textbf{Eq. 17}$$

where the intensity parameter is $i(\theta,\alpha,m)=[i_1(\theta,\alpha,m)+i_2(\theta,\alpha,m)]/2$, that can be related to the dimensionless volume scattering phase function, $\tilde{\beta}(\theta)$, for a particle becomes:

$$\tilde{\beta}(\theta)=i(\theta,\alpha,m)/\pi Q_b\alpha^2 \qquad \textbf{Eq. 18}$$

For a polydispersion, similar equations to the Q_a, Q_b and Q_c can be written as long as the size distribution function of the geometrical size d is expressed as a function of α. Then the previous equations become

$$Q_{bb}(\alpha_M)=\frac{\int F(\alpha)Q_{bb}(\alpha)\alpha^2 d\alpha}{\int F(\alpha)\alpha^2 d\alpha} \qquad \textbf{Eq. 19}$$

$$\tilde{\beta}(\theta,\alpha_M,m)=\frac{\int i(\theta,\alpha,m)d\alpha}{\pi\int Q_b(\alpha,m)\alpha^2 d\alpha} \qquad \textbf{Eq. 20}$$

where α_M is a modal value corresponding to the maximum frequency in the distribution and the limits for the integrals must encompass the entire population.

The variation of the angular distribution predicted from the Mie theory for the marine particles is now presented as a function of size, absorption properties and refractive index. It is well known that for a given size (i.e. the corresponding α value), the scattering pattern shows a succession of maxima and minima due to interferences (Figure 2.5). The number of oscillations increases with increasing α. As the particles in the ocean exhibit a continuous size spectrum over a given interval, the oscillations are annihilated (Figure 2.6) and they cannot be used as a "fingerprint" for identification.

The marine particles, "large" from an optical point of view (i.e. the phytoplanktonic cells), produce a scattering pattern where the forward scattering predominates over the backscattering. This dissymmetry in the $\beta(\theta,\lambda)$ is, in general, enhanced with increased size. For very large particles, the forward peak (central spot of diffraction) continues to be increased and simultaneously becomes narrower (Figure 2.6).

The absorption inside the particle reduces slightly the intensity of the light crossing the particle, which then interferes with the diffracted radiation (unchanged). The resulting scattered radiation is reduced accordingly, mainly in the backward directions but the position of the oscillations remains unmodified (Figure 2.5). For instance, in the case of phytoplankton, the low values of the imaginary part of the refractive index produce significant effects only for large particles and for backscattering. As a rule, the smaller the index is, the more pronounced is the general dissymmetry of the $\beta(\theta,\lambda)$. This rule progressively vanishes when the size becomes very small (Figure 2.5.b). In the Rayleigh domain ($\alpha \sim 0.2$), the $\beta(\theta,\lambda)$ is completely independent from the index, and in the extended Rayleigh domain (or Rayleigh-Gans domain), a progressive dependence on n appears. For instance, for picoplankton, with possible α values less than about 10, it can be conjectured that the $\beta(\theta,\lambda)$ will almost be insensitive to the index and solely determined by the size.

a. b.

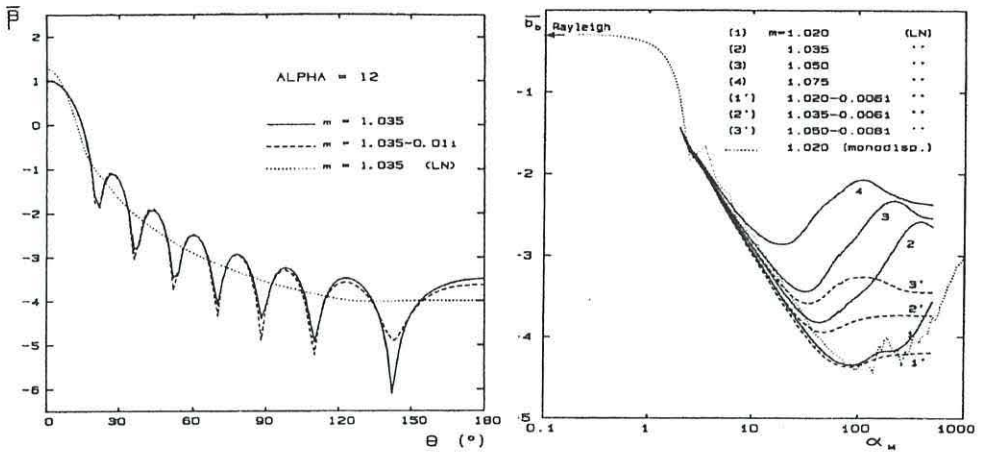

Figure 2.5 a) Normalized VSF, for a particle of relative size α=12, when the refractive index is 1.035 and 1.035-0.01*i*. The dotted curve represents the same normalized VSF for a polydispersed population of particles with n=1.035. b) Variations of the backscattering ratio as a function of the modal relative size parameter (taken from Morel and Bricaud, 1986).

a. b.

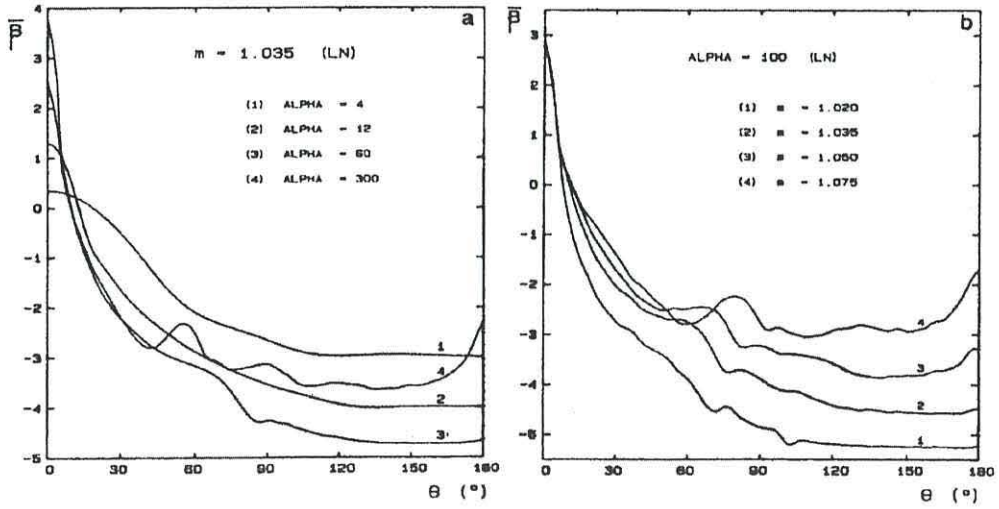

Figure 2.6 Normalized VSF a) for increasing α_M values and for m=1.035; b) for increasing real index of refraction and for α_M=100 (taken from Morel and Bricaud, 1986).

The "anomalous dispersion" (AD) is the case in which the absorption is taken into account and the imaginary part of the refractive index (n') influences the scattering (real part, n). The inclusion of this phenomenon is important to allow for the spectral

theory considers the effect of the absorption on scattering via the refractive index. An absorption band corresponds to an oscillator which absorbs energy at its frequency, and also in its vicinity but with a lesser efficiency. If ν_0 is the wave number of the resonance peak (maximum absorption) and ν that of the incident radiation, the absorption in this spectral region is governed by the number $\upsilon=2(\nu-\nu_0)/\gamma$. The band is symmetrical to ν_0 and its width is depicted by the damping γ. If n is equal to $1+\varepsilon$ (with ε small) far from the absorption region, in the neighbourhood of the absorption band it becomes

$$n = 1 + \varepsilon - \varepsilon K \frac{\upsilon}{(1+\upsilon^2)} \qquad \textbf{Eq. 21}$$

In response to the variations in n', is expressed as

$$n' = \varepsilon K \frac{\upsilon}{(1+\upsilon^2)} \qquad \textbf{Eq. 22}$$

The oscillator strength or the absorption intensity are described by K. The effect of considering the anomalous dispersion of *m* on the Q_{bb}, shows an increase of Q_{bb} with increasing *n* and a decrease of Q_{bb} with increasing *n'*, with this influence being more important for sufficiently high values of the modal relative size (Figure 2.7).

a. **b.**

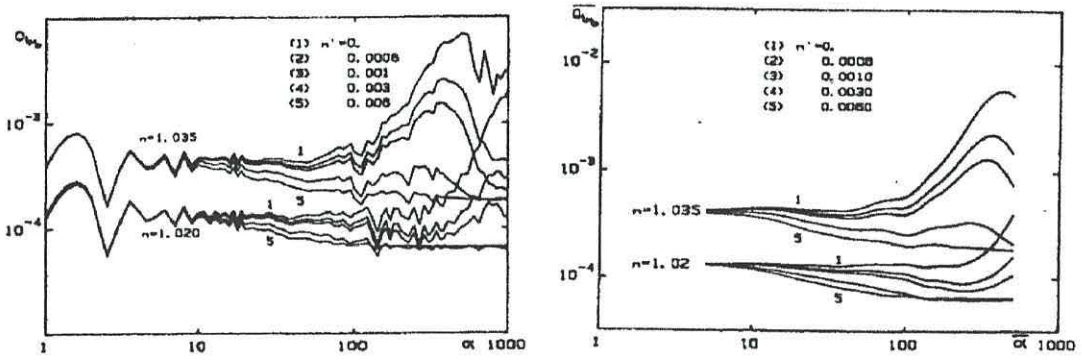

Figure 2.7 Variations of the efficiency factor for backscattering Q_{bb}: a) for a particle, as a function of the relative size for two values of the real part of the refractive index and increasing values of the imaginary part; b) for a population of particles, as a function of different modal relative size for two values of the real part of the refractive index and increasing values of the imaginary part (taken from Bricaud and Morel, 1986).

In this section the Mie theory has been presented including the ADA, the AD and the effects of considering a population of particles. However, this theory extends further, due to the possibility of considering different shapes such as cylinders, disks and spheroids (Aas, 1984). In the case of arbitrary shapes other theories have been used such as the T-Matrix, the finite difference time domain and the discrete dipole approximation (DDA). These methods are very expensive computationally when applied to ensembles of particles (Bohren and Huffman, 1983) and hence have not been applied to the study of b_b by marine particles as much as the Mie theory. Another potential complication is the consideration of internal structures (Aden and Kerker, 1951), which in the marine environment is difficult to apply because the parameters of the model (for instance, thickness of the layers) are not well known. A more complete analysis of these effects can be found in Jonasz and Fournier (2007) and the references therein.

2.3 Contributions to the backscattering coefficient

The bulk IOP is a sum of contributions by the various constituents of a water body (reductionist approach proposed by Stramski *et al.* (2004)). The backscattering coefficient contributions can be decomposed as:

$$b_b(\lambda) = b_{bw} + \sum_{i=1}^{N} b_{bi}(\lambda) \qquad \textbf{Eq. 23}$$

being b_{bw} the backscattering by pure sea water and b_{bi} the backscattering due to the ith-component considered up to N, total number of types of particles.

A review of the current knowledge on the subject has been done by Stramski *et al.* (2004). The following section will present a summary of their results, concerning laboratory experiments and modelling, complemented with other sources where appropriate.

2.3.1 Pure water and pure sea water

Morel (1974) reviewed the theory and observations, and his findings on the features of molecular scattering by water can be summarized as:

1. Scattering of pure water is small compared to other liquids because its packed molecular structure produces low isothermal compressibility and refractive index.
2. Scattering of pure seawater is better explained by fluctuation theory than by Rayleigh scattering.
3. The angular distribution of scattering has maxima in the forward ($\theta=0$) and backward ($\theta=\pi$) directions and minima in the side directions ($\theta= \pi/2$),
4. Due to this particular angular distribution of the scattering, the molecular backscattering coefficient $b_{bw}(\lambda)$, is half of the total molecular scattering coefficient, $b_w(\lambda)$, and the backscattering ratio $\tilde{b}_{bw}=0.5$,
5. The wavelength dependency of the $b_{bw}(\lambda)$ is proportional to $\lambda^{-4.32}$

The molecular scattering of water is considered to be known and constant. There are accepted values in oceanography (Buiteveld *et al.*, 1994; Morel, 1974; Shifrin, 1988; Smith and Baker, 1981). In a recent review by Twardowski *et al.* (2007), according to their Figure 2, the best description for the variation of the b_{bw} is a combination of Buiteveld's (Buiteveld *et al.*, 1994) values and the salinity dependency based on Morel's study (Morel, 1974) of the form [1+ 0.3S/37], where S is salinity.

Changes in salinity affect those values, but variations in temperature or pressure have non-significant effects. The range of values for pure sea water (for a typical S=35) using the latest model (Twardowski *et al.*, 2007), decreases from about 0.00451 m^{-1} at 442 nm to 0.000799 m^{-1} at 671 nm; compared to the non saline pure water 0.00351 m^{-1} and 0.000622 m^{-1} (Figure 2.8). On average pure sea water backscatters 30 % more than de-ionised pure water at all wavelengths. This effect can be important in coastal areas where there are large inputs of fresh water, although compared to the contribution of other substances suspended, to the total b_b the effects of salinity on the change of the water backscatter will not be critical.

The contribution of pure seawater backscattering to the total backscattering of seawater is important in very clear oceanic waters. In those areas with low concentrations of particles and bubbles, $b_{bw}(\lambda)$ is on the order of tens of percent of the $b_b(\lambda)$. In the clearest natural waters, this contribution can exceed 50 % and reach even 80 % in the blue spectral region (Morel and Gentili, 1991).

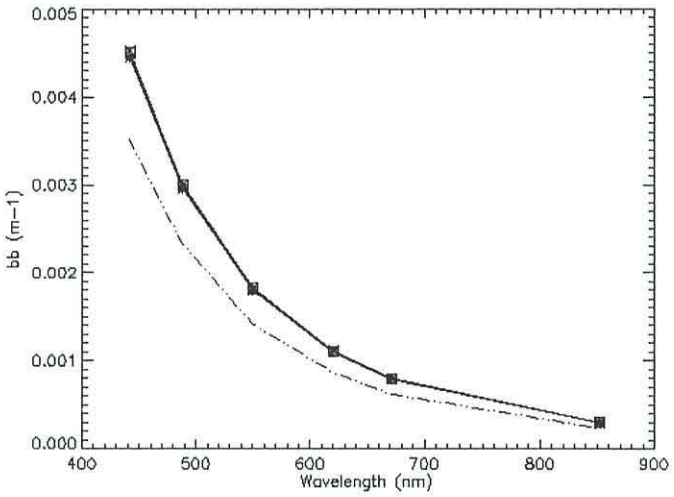

Figure 2.8 Spectral backscattering coefficient of pure seawater (Twardowski *et al.*, 2007) for a temperature of 13.0 °C. Dotted line is backscattering by pure water (S=0.0). Symbols are super-imposed backscattering for S from 33 to 35.5 in 0.5 increments and at selected wavelengths corresponding to the instrument for measuring in-situ backscattering at PML (Hobilabs Hydroscat-6).

2.3.2 Turbulence

The variations caused by turbulent mixing of temperature and salinity cause fluctuations in the density of the fluid, which in turn affects the refractive index of the fluid. The ocean is dominated by turbulent flows at different scales of size and duration. The inhomogeneities of the refractive index of the water produced by this motions influence the forward scattering of the light (Bogucki *et al.*, 1998), but this behaviour has not been observed in natural waters. The physical explanation for the increase of scattering in the forward direction is that the interaction of eddies of different sizes with photons produce slight but continuous changes in the direction of the photons as these cross the mixing mass of water. Therefore, the observed forward peak would come from an integrated effect of the turbulence induced deviations.

The effect of turbulence on light backscatter is orders of magnitude weaker compared to the effects on small angle scattering. Using a relationship based on effects of turbulent variations of temperature on the volume scattering functions, the magnitude of backscattering due to turbulence ($b_{bt}(\lambda)$) can be estimated to a first order (Stramski *et al.*, 2004). According to their calculations, $b_{bt}(640)$ can vary within a broad range, between 10^{-9} and 10^{-2} m^{-1}, being typical values in oceanic turbulent flows values the between 10^{-7} to 10^{-6} m^{-1}. This estimate is small compared to the typical values of b_{bw} between 10^{-4} to 10^{-3} m^{-1}.

Given the magnitude of b_{bt} it is unlikely that the turbulence may be an important contributor to the backscattering in the ocean. However, part of the large variation estimated comes from the uncertainties and assumptions underlying the relationships used between turbulence and light scattering, which need to be further investigated.

2.3.3 Bubbles

The generation of air bubbles in the ocean is mainly due to the injection of air by breaking waves, but other causes include rainfall, biochemical processes such as oxygen release by phytoplankton or decomposition of organic matter and release from the ocean floor. The influence of bubbles on b_b has been studied using a modelling approach (Zhang *et al.*, 1998). This contribution has been estimated to be 1-10% in calm sea conditions or even higher, due to coating of bubbles (Zhang *et al.*, 1998).

In nature, bubbles acquire organic films quickly after their formation. These organic films are composed mainly of protein or lipids, whose mean relative refractive indices are approximately 50 % higher than that of the air inside the bubble. Zhang *et al.* (1998) suggested that the role of bubbles as backscatterers could be increased up to 40 % (λ=550nm) by this coating. In situ observations of high values of bubble backscattering, exceeding $10^{-2}m^{-1}$ (Zhang *et al.*, 2002), tend to verify the theoretical studies. The importance of bubble coatings in backscattering may be limited by the fact that little is known about the composition and therefore, the optical properties (particularly imaginary part of the relative refractive index) of these coatings. Another constraint to the study of the role of bubbles in backscatter is that very little is known about the smaller size range (1-20 μm), which, if detected in persistent and sufficient

numbers, could indicate an important source of optical backscattering. Although the spectral variations of b_b have not been so far studied in detail, their effects in remote sensing of ocean colour could be very important. Through enhanced backscatter over the whole visible domain: (1) bubbles can produce a non negligible reflectance in the near infrared, thus invalidating the atmospheric correction in waters optically dominated by phytoplankton and its related compounds; and (2) bubbles can produce and increase in the green reflectance bands, thus producing overestimation of the chlorophyll concentration.

2.3.4 Living particles

Characterisation of the living particles, from an optical point of view, is done using their size (in terms of the radius or diameter of a sphere of equivalent volume), the abundance (in numbers per unit of volume) and their refractive index.

Figure 2.9 shows the size range of living particles in the marine environment compared to other substances that contribute to b_b. The particle abundance or concentration typically shows a decrease with increasing size. This implies that concentrations of viruses, with typical diameters (D) less than 0.2 μm, can be between 10^{12} and 10^{14} cells m^{-3}; while heterotrophic bacteria ($0.2<D<1$ μm) concentrations can range between 10^{11} and 10^{12} cells m^{-3}; and picoplankton ($0.5<D<2$ μm) concentrations as high as 10^{10} and 10^{11} cells m^{-3} (Li, 1995). The concentration of non-living submicrometre particles can be a few orders of magnitude higher than that of the viruses (Koike *et al.*, 1990). The relation between particles' size and concentration is described by the particle size distribution (PSD), which together with the optical properties of a single particle determine the bulk inherent optical properties (Section 2.2).

These optical properties of a single particle are in turn determined mainly by their refractive index and their diameter relative to the wavelength of the incident light. Other influencing factors are the shape, external and internal structures. The refractive index (relative to water) of the living plankton cells is very low, less than 1.1, typically around 1.04-1.05. This low value is related to the high water content in the

protoplasm, while cells with a hard inorganic skeletal or shells may have an increased refractive index of about 1.15 (Aas, 1996).

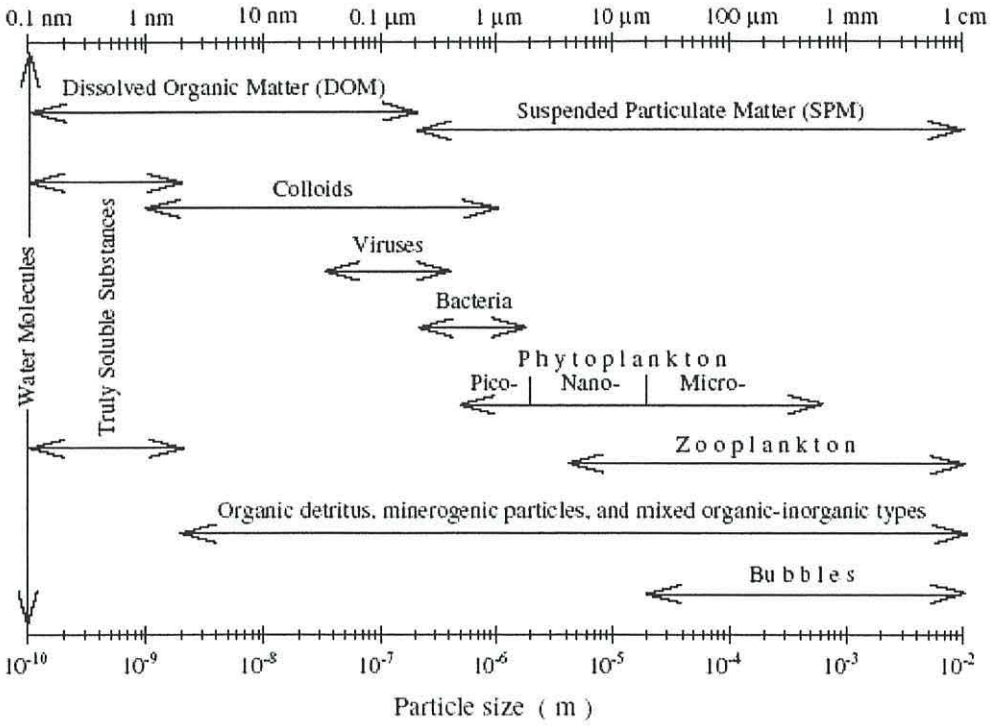

Figure 2.9 Particle size range that characterises the different compartments that contribute to the backscatter coefficient and are considered in the text (taken from Stramski *et al.* (2004)).

A summary of the contribution of marine micro-organisms to the total b_b was performed using a modelling approach (Stramski *et al.*, 2001). By means of a compilation of optical properties from 18 planktonic components of previous works (Ahn *et al.*, 1992; Bricaud *et al.*, 1988; Morel *et al.*, 1993), an oligotrophic case was simulated (total chlorophyll concentration ~0.18 mg m^{-3}). This study considered a mixed population of particles, whose size distribution obeyed a power law with an exponent of -4, which is normal in the aquatic ecosystem (Mobley, 1994). In addition to living viruses, bacteria and phytoplankton, biogenic detritus, minerals and bubbles were considered. With these constraints, the small nanoplankton species (those with sizes between 4 to 8 µm, while nanoplankton sizes go from 2 to 20 µm) represent a high proportion of the total chlorophyll concentration (45.8 %), while picoplankton contributes with 24.9 % and big flagellates and dinoflagellates contribute with 29.3 % to total chlorophyll. Under these hypothetical conditions of size distribution and chlorophyll concentrations for each of the components considered, Stramski *et al.*

(2001) found that the contribution of all the planktonic microorganisms to the b_b was only between the 1.8 and 3.6 %. This small contribution is dominated by the bacteria and by the combined picoplankton components (up to 80 % of the plankton contribution). The contribution of viruses to planktonic backscattering is only appreciable at short wavelengths (i.e. nearly 12 % at 400nm). Experimental work verified this result concerning the viruses, whose small backscattering is due to their low refractive index (Balch *et al.*, 2000). However they may have a role in rapidly changing the IOPs when they infect cells in a bloom (Balch *et al.*, 2002).

Globally, the results of the work from Stramski *et al.* (2001) confirmed those of ten years before: the phytoplankton contribution to b_b is very small and that bacteria may be greatest living contributors to b_b (Morel and Ahn, 1991; Stramski and Kiefer, 1991). However, these studies make an important assumption which may be a cause of uncertainty: that modelled cells are homogeneous spheres. The real plankton cells have an external cellular wall and a cytoplasm where the organelles reside. Modelling studies with coated spheres that simulate real cells show enhanced backscattering compared with homogeneous spheres by as much as one order of magnitude (Kitchen and Zaneveld, 1992; Zaneveld and Kitchen, 1995). Differences for backscattering have been shown between centred and off centred nucleus in a coated spheroid (Quirantes and Bernard, 2004). Preliminary results (Bernard, 2005) have shown that heterogeneous geometry can produce an increase on phytoplankton b_b from 5 to 25 times compared to the homogeneous case.

Measurements of the volume scattering function (Volten *et al.*, 1998) and b_b (Vaillancourt *et al.*, 2004) of phytoplankton cultures have provided evidence that the modelling using homogeneous spheres produce less backscatter than what is measured. Including the description of the phytoplankton external shape can be done using modelling based on Mie theory (Section 2.2). Non spherical particles have been modelled (Aas, 1984) concluding that the shape may be a second order factor compared to size distribution and refractive index.

2.3.5 Non living particles

The amount of information available on the contribution of "soft" detritus (i.e. decaying organic matter) and minerals to ocean backscattering is even smaller than the information on the phytoplankton contribution. Modelling (Stramski *et al.*, 2001) indicates that inorganic mineral particles, with high refractive index, are the most important contributors to total backscatter (between 80 and 85 %), while organic detritus, with a high water content, contributes ~9 %. As for the phytoplankton, the validity of these results is limited by the assumption of homogeneous and spherical particles that follow a very precise size distribution slope (in this case -4). Using a similar approach, Wozniak and Stramski (2004) modelled the optical properties of some mineral particles to highlight their effects on backscattering and on the marine remote sensing applications, highlighting that the presence of small amounts of minerals in water, can produce significant errors in retrievals of chlorophyll-a, Chl-a, using standard algorithms. However theirs was a purely modelling approach based on assumptions on size distribution and refractive index. Recent work (Bowers and Binding, 2006; Twardowski *et al.*, 2007) have added more data concerning the scattering by minerals, however, specific papers on backscattering by mineral particles do not exist so far.

Special attention has been given to the backscattering from coccoliths, the calcium carbonate shells detached from phytoplankton species such as *Emiliana Huxleyi*. They produce a very characteristic signature in the satellite imagery (Holligan *et al.*, 1983) by modification of the light field (Smyth *et al.*, 2002). The b_b from the coccoliths can produce up to 30 % of the backscattering even outside of the bloom (Balch *et al.*, 1996). A detailed study of the backscattering of light affected by the shape of liths detached from *Emiliania Huxleyi* (Gordon and Du, 2001) evaluated different models for accounting on the light backscattering: discrete dipole approximation and the T-matrix theory (Mishchenko *et al.*, 2000). When these models were applied to the specific shape of the coccoliths, the results showed that the backscatter was underestimated by a factor of two when the shape of the liths (disks) where approximated by a spherical shape.

2.3.6 Colloids

Colloids are particles in the size range between 1 nm and 1 μm, which are small enough not to suffer sedimentation by gravity, but large enough to have an interface and interior, chemically distinct from the surrounding water (Vold and Vold, 1983). The interior of a colloidal particle has a great variety of compounds: organic polymers such as polaysaccharides, proteins, peptides, humic and fulvic acids, cellular debris; as well as inorganic particles such as oxides and hydroxides of metals, carbonates and clay minerals; organic-inorganic complexes; living microbes and viruses (Wells and Goldberg, 1991, 1992). Colloids can be grouped by their size into two fractions with different abundances: small colloids, with size ranges between 5 and 200 nm have abundances greater than 10^9 cm^{-3}; large colloids, with size ranging from 0.4 to 1μm and abundances that can reach 10^7 cm^{-3}. Colloids are more abundant than the organisms present in their size ranges. Smaller colloids abundance is typically one order of magnitude greater than viruses and larger colloids are one to two orders of magnitude greater than bacteria (Koike *et al.*, 1990; Stramski *et al.*, 2004b). The investigation of the role of the colloids in marine bio-optics has been limited by their arbitrary inclusion in the "dissolved matter" compartment. The operational definition in bio-optical oceanography is that all the substances that pass through a 0.2 μm pore-size filter is dissolved and is treated as an absorbing only component (the coloured dissolved organic matter, CDOM). However, also as an operational definition, the suspended particulate matter (SPM) encompasses all the substances retained on a GF/F filter (0.45 μm nominal pore size). The SPM has often been related to the scattering and backscattering, when in fact, according to the above abundances, one could be ignoring the smaller colloidal particles. A modelling study using 21 measured colloidal size distributions and abundances from the North Atlantic, Sargasso Sea, Southern Ocean and Pacific Ocean (Stramski and Wozniak, 2005), attempted to quantify the role of colloids on backscatter of light. They estimated that adding the averaged backscattering from small and large colloids would result in a b_b twice b_{bw} over most of the visible region. Small colloids contributed 44 % at 350 nm and 19 % at 750 nm to the average total colloidal backscattering. Spectrally, the total colloidal backscatter was more important at longer wavelengths; for instance, it was more than five times the b_{bw} at 700 nm.

2.4 In-situ observations of the natural spectral variability of b_b

The studies on the specific effects of a particular type of particle on the backscattering coefficient are an attempt to find out the causes of the observations of backscatter in the marine environment. These observations have produced a rapidly growing literature to the commercial availability of instruments that measure in-situ the spectral backscatter (Maffione and Dana, 1997; McManus *et al.*, 2003). Although there are differences among the design of these instruments, they agree to less than 10 % (Boss *et al.*, 2004; Boss *et al.*, 2007). In order to place the results of this thesis in context, the range of available studies (from clear oceanic waters to coastal areas) and their findings concerning to b_b will be summarized in this section.

Twardowski *et al.* (2007) measured b_b in the South East Pacific Ocean, considered as the optically "clearest" waters of the world (Chl-a down to 0.001 mgm^{-3}). They used a ECO-BB3 (WET Labs) to measure $\beta(117°)$ at 462, 532 and 650 nm, and then to derive b_{bp}. They found that the aggregate values of b_{bp} were less than 20 % higher of the b_b of pure seawater (Section 2.3).The spectral variability of b_{bp}, indicated by the exponent of $1/\lambda$ fitted to the data, varies between 1.22 in the surface to ~4 below the deep chlorophyll maximum, DCM (~300m). The surface spectral variation of b_{bp} is predicted by Mie theory for particles with little absorption and a Junge-type distribution with a slope of 4. The spectral slope at the below the DCM is similar to the Rayleigh scattering, indicating that the particle population is dominated by particles much smaller than the wavelength of the light scattered.

Sub-polar regions of the ocean, with higher Chl-a, have been also been object of bio-optical sampling. Stramska *et al.* (2003) surveyed the north polar Atlantic (~75°N) during three summer cruises between 1998 and 2000, measuring b_b with a HOBI Labs Hydroscat-6 (Maffione and Dana, 1997). The range of Chl-a encountered during this study was 0.2-1.1 mg m^{-3} and the spectral slope of b_b varied between 1 and 3. In a later visit to the same area, (Stramska *et al.*, 2006) higher values of the b_b spectral slope were found, indicating a low concentration of particles (minimum Chl-a was ~0.1mg m^{-3}). In the Southern Ocean (Reynolds *et al.*, 2001), using a HOBILabs Hydroscat-6 the measured spectral slope of the particle backscatter ranged from 3 to 0.8 with a general tendency to decrease with increasing Chl-a.

There are fewer studies of spectral variation of b_{bp} in more productive oceanic waters. For instance, a recent survey of an upwelling area, at the shelf edge off the coast of Calfornia (Kudela *et al.*, 2006) does not give information about the spectral variability of b_{bp} but points to its relation with the fluorescence as an indicator of the upwelling/relaxation of upwelling. During the active phase of the upwelling (pumping of deep water to the surface) there is low fluorescence and high b_{bp}; while during the relaxation (bloom), b_{bp} increases with increasing fluorescence. Combining this information with concurrent attenuation measurements, the authors interpret this to be the succession of detrital and biogenic material respectively to upwelling/relaxation events.

Bio-optical studies at the coastal zone have been more common in the recent literature, generally as a part of a global scientific effort to validate remote sensing algorithms (Kostadinov *et al.*, 2007; Tzortziou *et al.*, 2007). However, few studies have focused on the spectral variability of b_{bp} (Berthon *et al.*, 2007; Chami *et al.*, 2005). Using a multispectral volume scattering meter (MVSM) (Lee and Lewis, 2003), the b_{bp} was derived from measurements of the spectral volume scattering function in coastal waters of the Black Sea (Chami *et al.*, 2005) and in the coastal northern Adriatic Sea (Berthon *et al.*, 2007). Chami *et al.* (2005) detected a spectral variation of expressed as the ratio $b_{bp}(443)/b_{bp}(555)$ varying from 0.82 to 1.17 in waters with a Chl-a varying from 0.2 to 2 mgm^{-3}. The range of variation of b_{bp} in the blue band was attributed to the anomalous dispersion (see Section 2.2) caused by the high absorption due to the non algal fraction, which composed at 443 nm between 66 and 88 % of the total particulate absorption. Using a newer version of the same instrument, Berthon *et al.* (2007) did not find this effect, as the average contribution of non algal particles in their samples had an average value 47±7 % (their average Chl-a ranging between 1 and 1.62 mg m^{-3}). In terms of backscattering spectral slope (or in their paper $\beta(140°)$), they find a variation from 0.28 to 1.24 at three different times of the year (October 2004, July 2005 and April 2006). They also validate the measurement of b_{bp} using a HOBILabs Hydroscat-6, for which they find a mean absolute percentage difference of ~15 % with an underestimation by the HOBILabs Hydroscat-6, which they attribute to the low extrapolation factor used (χ_p), in agreement with other studies (Boss and Pegau, 2001; Chami *et al.*, 2006).

So far, only the visible domain was considered in these studies. However there may be an interest in extending the study of the spectral properties of b_{bp} into the near infra red, as it has been done for the b_p (Doxaran *et al.*, 2009).

2.5 Forward and inverse models that use b_b

The advance of satellite ocean colour algorithms for retrieval of the biogeochemical components requires an improvement on the bio-optical models underlying. According to Gordon and Morel (1983), the satellite algorithms can be classified by the way they relate the reflectance to the components in seawater. This classification divides the algorithms in: empirical, semi-analytical and analytical.

The first satellite algorithms developed for ocean colour retrieved with the CZCS were empirical and related reflectance ratios to the Chl-a (Gordon and Morel, 1983). The semi-analytical approach represents an evolution from the empirical, as they relate the reflectance signal to the absorption and the backscattering, and those IOP to the Chl-a (Gordon *et al.*, 1988; Morel, 1988). The analytical algorithms use bio-optical relationships between all the components (like Chl-a, SPM and CDOM) and their optical signatures, to decompose the signal detected by the satellite. This approach is theoretical and not in use in operational remote sensing, as it is impossible to do a full characterisation of the optical properties of all the components in the seawater. Other techniques, with more complex mathematical approaches exist, such as non-linear optimisation, principal components or neural networks (IOCCG, 2000).

The semi-analytical algorithms rely on bio-optical models for the description of the relationship between the biogeochemical components and their IOPs. There is a substantial body of knowledge on the absorption and its relation to the biogeochemical components is relatively well known. However, there are a number of empirical relationships between the biogeochemical components and the backscattering that need to be validated. This is mainly due to the uncertainties about the sources of backscattering (see Section 2.3). This section will concentrate firstly on reviewing the direct relationships between backscattering and its causes, from the perspective of their use in remote sensing algorithms.

2.5.1 Models based on Chlorophyll-a (Chl-a)

The semi-analytical parameterizations of the backscattering coefficient take the general form:

$$b_b = b_{bw} + F_{bb} Chl - a \qquad \textbf{Eq. 24}$$

where algal and detritus contributions are merged into a certain function (F_{bb}) of Chl-a. Therefore, all terms are related to chlorophyll and the reflectance from the satellite can be directly related to the Chl-a. In the late 80s there were two key publications of semi-empirical algorithms: Gordon *et al.*(1988)- hereafter G88 and Morel (1988)- hereafter M88. These models have shaped the way subsequent models have developed, and for this reason it is worth considering the assumptions behind their formulation.

Both models depart from the empirical relationship between scattering and Chl-a (Gordon and Morel, 1983):

$$b_{p550}(Chl - a) = b^0 (Chl - a)^{0.62} \qquad \textbf{Eq. 25}$$

They differ in the way the wavelength and Chl-a dependency is modelled. G88 describes the spectral variation of b_{bp} using coefficients as follows:

$$b_{bp}(\lambda) = \alpha(\lambda) \cdot 0.3(Chl - a)^{\beta(\lambda)}, \qquad \textbf{Eq. 26}$$

where α and β are tabulated constants, that produce the dependency of b_{bp} with Chl-a and with wavelength, and are derived from the following observations and assumptions:

- Concerning the dependency of b_{bp} with Chl-a, G88 base their modelling of b_{bp} upon the fact that even though the backscattering ratio $\tilde{b}_b$ of the phytoplankton is low (0.5 % according to Morel and Bricaud (1981)), its role on the optical properties of the medium increases non linearly relatively to the role of other components, as the proportion of phytoplankton carbon to detrital carbon increases in the higher chlorophyll environment. Accordingly, G88 assumed that the particulate $\tilde{b}_b$ decreases with increasing chlorophyll concentration: Chl-a=0.1 mg m^{-3} has a $\tilde{b}_b$ of 2 % while 20 mg m-3 have a $\tilde{b}_b$ equal to 0.5 %.
- Concerning the dependency of the backscattering coefficient on the wavelength, G88's model is based on two observations: first, at low pigment concentration (Chl-a less than 0.1 mg m^{-3}) the scattering coefficient for ocean

water exhibits a λ^{-1} wavelength dependence; second, at wavelengths where particles are strong absorbers, the scattering is reduced, such that the total attenuation is not spectrally dependent. Therefore, G88 assumes that for Chl-a less than 0.1 mg m^{-3}, the $\tilde{b}_{bp}$ =(560/λ) x 2 %, and for 20mg m^{-3} $\tilde{b}_{bp}$ takes the value of 0.3 % within the pigment absorption bands and the default 0.5 % for the rest of the wavelengths.

Independently, M88 uses a similar equation to Eq. 26, giving to b^0 a value of 0.30 and leaving the exponent the same. This power law with an exponent less than one indicates that, in oligotrophic waters, the scattering by particulates is relatively higher than in eutrophic waters. According to M88, the chlorophyll specific scattering coefficient, that is b_p/Chl-a, decreases from 1.15 to 0.10 $m^2(mgChl)^{-1}$, when Chl-a increases from 0.03 to 20 mg m^{-3}. This trend supports the hypothesis of an increment of the relative role of detritus when the algal mass diminishes (Morel, 1987).

The choice of the spectral dependence of $\tilde{b}_{bp}$ results from the following observations and hypothesis:

- The particle scattering had been shown to vary approximately with a λ^{-1} (Morel, 1973), at least for a size distribution of the particles following a Junge law with an exponent -4.
- The $\tilde{b}_{bp}$ of about 2 % is representative of the detritic particles (Morel, 1973).
- The $\tilde{b}_{bp}$ of algal cells is very low from experimental (Bricaud *et al.*, 1983) and theoretical (Bricaud and Morel, 1986) studies.

Hence the $\tilde{b}_{bp}$ could be modelled and combined with Eq. 26 into:

$$b_{bp}(\lambda) = b_{p550}(Chl-a)\cdot\left\{0.002+0.02\left(0.5-0.25\log Chl-a\right)\left(\frac{550}{\lambda}\right)\right\} \qquad \textbf{Eq. 27}$$

The rationale of this modelling is similar to the one in G88, in that the $\tilde{b}_{bp}$ changes from an oligotrophic situation where detritus are relatively more abundant (detrital particles with a $\tilde{b}_{bp}$ of 2 % and λ^{-1} scattering dependency) to an eutrophic situation where algal cells are the predominant particles, with low $\tilde{b}_{bp}$ (0.2 %) and practically no spectral dependency. In the case of M88, there is not a dependency on the absorption peaks of the chlorophyll.

The model in M88 was revised by Morel and Maritorena (2001), from now on MM2001. The Eq.25 was modified to take into account the scattering of water in the original relation:

$$b_{p550}(Chl-a) = 0.30 \cdot (Chl-a)^{0.62} - b_{w550} \qquad \textbf{Eq. 28}$$

MM01 used a recent and much larger dataset (Loisel and Morel, 1998), then the Eq. 28 was transformed into

$$b_{p550}(Chl-a) = 0.416 \cdot (Chl-a)^{0.766} \qquad \textbf{Eq. 29}$$

Additionally, other changes were done to Eq. 27:

-The $\tilde{b}_{bp}$ maximum value due to biogenic particles is too high (2%) for case 1 waters, incorporating the discussion by Ulloa *et al.* (1994), so this value is reset to 1 %.

-Taking into account that the $\tilde{b}_{bp}$ of the algal cells is very low (Ahn *et al.*, 1992), it is very difficult to accept that they are very important contributors to the spectral variability of backscatter. Therefore, the modification to the original M88 model is to diminish progressively the spectral dependency of the $\tilde{b}_{bp}$ with increasing Chl-a.

With both these modifications, Eq. 27 is transformed into

$$b_{bp}(\lambda) = \{b_{p550}(Chl-a)\} \cdot \left\{0.002 + 0.01(0.5 - 0.25\log(Chl-a))\left(\frac{550}{\lambda}\right)^{\upsilon}\right\} \qquad \textbf{Eq. 30}$$

where the varying exponent υ is expressed as:

$$\upsilon = 0.5(\log_{10}(Chl-a) - 0.3), 0.02 < Chl-a < 2 mgm^{-3}$$
$$\upsilon = 0, Chl-a > 2 mgm^{-3} \qquad \textbf{Eq. 31}$$

The following models, used in remote sensing, are relationships based on the three models presented above.

The relation of Loisel and Morel (1998) linking scattering to Chl-a was used by Ciotti *et al.* (1999) to develop a semi-empirical algorithm looking at the phytoplankton community structure. The $\tilde{b}_{bp}$ and wavelength variability are inversely related to the Chl-a using a re-formulation of the G88 model

$$b_{bp}(\lambda) = \tilde{b}_{bph+\det} b_{ph+\det}(660)\left(\frac{660}{\lambda}\right)^{\gamma} \qquad \textbf{Eq. 32}$$

It is worth noting that the range of γ in this model is from 2 (Sathyendranath *et al.*, 1989) to 0 following a logarithmic shape

$$\gamma = 1 - 0.768 \log_{10}[Chl - a] \quad \textbf{Eq. 33}$$

Ciotti *et al.* (1999), in their sensitivity analysis, find that the effect of the inclusion of a non phytoplankton wavelength dependent component in the backscatter model would affect the retrieval of $K_d(490)$ significantly (their figures 10a and b). A wavelength independent detrital backscatter with a $\tilde{b}_{bp}$ of 1 % would not have a noticeable effect on the retrieval of $K_d(490)$.

Reynolds *et al.* (2001) derived a semi-empirical algorithm for inversion of spectral remote sensing reflectance into chlorophyll using bio-optical models constructed from observations in the Southern Ocean. Two regions within the Southern Ocean were studied: the Ross Sea and the Antarctic Polar Zone Front (APFZ). In the Ross Sea high Chl-a were measured (up to 14 mg m^{-3}) and predominance of larger particles in the size spectrum, while more oceanic conditions were found in the APFZ, where the chlorophyll was lower (less than 2.5 mg m^{-3}) and smaller particles dominated the size spectrum. These characteristics influence the particle backscattering coefficient measured with a Hydroscat-6 (Maffione and Dana, 1997). The relationships between the Chl-a and the b_{bp} are different:

Ross Sea

$$b_{bp}(555) = 0.001[Chl - a]^{0.667}, \quad r^2=0.85, \text{ n=67} \quad \textbf{Eq. 34}$$

APFZ

$$b_{bp}(555) = 0.004[Chl - a]^{0.822}, \quad r^2=0.86, \text{ n=27} \quad \textbf{Eq. 35}$$

showing that at a given Chl-a, the magnitude of the particle backscattering is significantly higher in the APFZ than in the Ross Sea. There are two possible explanations for this. First, that the Chl-a in the Ross Sea is contained in larger particles, therefore the efficiency of backscatter (Chl-specific particle backscattering) in the Ross Sea is low. This explanation is supported by the measurements of the particle size distributions, as mentioned above. The second possible explanation is that small nonchlorophyllous particles such as detritus are less abundant in the Ross Sea than in the APFZ.

These models (Reynolds *et al.*, 2001) do not agree with the one proposed by M88 (see their figure 6a), but would be consistent at moderate Chl-a in the APFZ. The measured spectral slope of the particle backscatter ranges from 3 to 0.8 with a general tendency to decrease with increasing Chl-a. The greatest spectral variability of particle backscattering occurs in waters with low Chl-a, where the magnitude of b_{bp} is low and hence its contribution to total backscatter. The empirical relationship constructed using the combined data of the two regions, relates the total backscatter coefficient (including particles and pure water) to the spectral slope of the total backscatter as:

$$\gamma = -3.616 \log_{10}[b_b(555)] - 6.866 \text{ , } r^2=0.93, \text{ n=88} \qquad \textbf{Eq. 36}$$

Finally, Loisel *et al.* (2006) attempted the indirect retrieval of the spectral dependency of γ on Chl-a from remote sensing. Using his algorithm for the inversion of the remote sensing reflectance (Loisel and Stramski, 2000) at three wavelengths, to retrieve b_{bp} (i.e. 490, 510 and 550), he found that the value of γ ranges between 0 and 3.5 with a mean value of 1.37 (standard deviation ±0.42). The relationship of γ to $\log_{10}$Chl-a showed a high regional variability and a global slope of -1.45.

The models summarised in this section describe the dependency of backscatter on the Chl-a. These models share common parts: first is the description of the scattering at a reference wavelength related to the Chl-a and second, a value for the scattering efficiency, $\tilde{b}_b$. The empirical relationship constructed on data (Gordon and Morel, 1983) presents a great dispersion, that is not reduced by the use of a larger and more accurate data set (Loisel and Morel, 1998). Some authors attribute this dispersion to the size of the pores in the filters used in the determinations of the Chl-a or SPM (Babin *et al.*, 2003). This may point to the important role of smaller particles in the light scattering processes that are not retained by the filters currently used for sampling for Chl-a or SPM (i.e. colloids, see Section 2.3).

The second step, expressing the $\tilde{b}_{bp}$, implies three assumptions, about its magnitude, about its variation with Chl-a and about its wavelength dependence. It is worth noting that the scattering and backscattering coefficients do not necessarily have the same spectral behaviour. The depressive effect of absorption is generally more marked on

b_b than on b by algal cells (Ahn *et al.*, 1992) and by detrital material (Chami *et al.*, 2005).

2.5.2 Models based on Particulate Organic Carbon (POC)

Light scattering may be related to particulate organic carbon (POC), and measurements in the Southern Ocean and Arabian Sea verify this (Balch *et al.*, 2001; Stramski *et al.*, 1999). Some algorithms have made use of this relationship to produce maps at the Mediterranean (Loisel *et al.*, 2001) and others have used it for deriving primary production maps (Behrenfeld *et al.*, 2005).

Stramski *et al.* (1999), established a relation between POC concentration and in-situ $b_{bp}(510)$ for two regions in the Southern Ocean. Similarly to Reynolds *et al.* (2001) they obtained:

Ross Sea

$$[POC] = 476935.8(\pm 1.5) b_{bp}(510)^{1.277(\pm 0.061)}, \quad r^2=0.953, n=24 \qquad \textbf{Eq. 37}$$

APFZ

$$[POC] = 17069.0(\pm 1.3) b_{bp}(510)^{0.859(\pm 0.046)}, \quad r^2=0.918, n=33 \qquad \textbf{Eq. 38}$$

with the standard errors of the estimates of the regression coefficients in parenthesis, and the r^2 for the log-transformed variables. These relationships show that the particulate assemblages in the Ross Sea tend to backscatter less than the APFZ, especially at moderate to high POC concentrations. This difference was attributed to the dominance by phytoplankton cells, whose contribution to b_{bp} is generally small, have a comparatively higher contribution to POC concentration in the Ross Sea. In the latest validation of his model, Stramski *et al.* (2008) use samples from the South Pacific Subtropical Gyre and Eastern Atlantic, ranging in POC concentrations between 10 to 270 mg m^{-3}, to show that the normalized root mean square error of the retrieval of POC concentration is about 20 %.

In the case of the Mediterranean (Loisel *et al.*, 2001), the b_{bp} are outputs from an algorithm for inverting the remote sensing reflectance (Loisel and Stramski, 2000) to produce maps of POC in the Mediterranean, based in the relation:

$$[POC] = 37750 b_{bp}(555) + 1.3 \qquad \textbf{Eq. 39}$$

This formulation was derived from two sources: in situ measurements and the SeaBASS database. The former provided a relation between POC concentration and $b_p(555)$ and the latter, a relation between $b_{bp}(555)$ and $b_p(555)$. The relation between POC and $b_p(555)$ was:

$$[POC] = 453 b_p(555) + 1.3 \text{ , } r^2=0.85 \qquad \textbf{Eq. 40}$$

was retrieved during a cruise conducted within the Mediterranean in late summer 1999 (Oubelkheir, 2001). This relation is similar to one previously established in the north Western Mediterranean in December 1998-January 1999 (Claustre *et al.*, 2000).

From the SeaBASS database, the $\tilde{b}_{bp}$ was fixed at 0.012, selecting concurrent data of b_{bp} and b_b in open ocean. The criterion to select data from SeaBASS was that the ranges of Chl-a and b_p had to be similar to those observed in the Mediterranean. Using this approach (Loisel *et al.*, 2002), the seasonal variability of POC (or b_{bp}) in the global ocean has been found to be out of phase with the Chl-a, supporting further the idea of the small non-living detritus as an important source of backscattering.

Finally, Behrenfield *et al.* (2005) developed a model of primary production using b_{bp} to calculate the phytoplanktonic carbon biomass (C). Satellite-based Chl-a and $b_{bp}(440)$ produced by a statistical inversion algorithm (Garver and Siegel, 1997) from 28 regional bins for the September 1997 to January 2002 period revealed two distinct regimes: one where bbp is constant and one where b_{bp} covaries with Chl-a. In oligotrophic waters Chl-a ranges from 0.03 to 0.14 mg m^{-3}, while the b_{bp} varies very little (from 0.0010 to 0.0016m^{-1}). In more productive regions where Chl-a ~0.14mg m^{-3}, there is a good correlation (r^2=0.74). The interpretation for this pattern is that Chl-a variability is due to intracellular changes in pigmentation in impoverished ocean regions, while in more enriched regions, changes in b_{bp} are due to changes in phytoplankton biomass. To estimate phytoplankton carbon biomass from b_{bp}, the following equation is proposed:

$$C = 13000\left(b_{bp}(440) - 0.00035\right) \qquad \textbf{Eq. 41}$$

The fixed value represents a global estimate of b_{bp} by the stable heterotrophic and detrital components. The value 13000 was chosen to give satellite Chl:C consistent with laboratory results and an average phytoplankton to POC of ~30 % consistent

with estimates from satellite data using the two previously introduced relationships between [POC] and b_{bp} (Loisel *et al.*, 2001; Stramski *et al.*, 1999).

The current division of the causes of backscattering is moving away from the traditional relations with bulk biogeochemical properties (i.e. Chl-a or POC), towards the separation into a number of biogeochemical compartments. This is referred to as the "reductionist approach" (Stramski *et al.*, 2004), and has been adopted throughout this thesis (Section 2.3).

2.5.3 Inverse models in bio-optical field measurements

The bio-optical models introduced in Section 2.5.1 and 2.5.2 are used to simulate a backscattering signal from a known concentration of substances for use in remote sensing algorithms. The inverse process (i.e. retrieve the concentration from a given signal) is much more complex. The properties of marine substances that could be obtained from inversion of bio-optical measurements in the ocean are (Boss, 2006a):

1. Concentration of biogeochemical variables such as Chlorophyll a, particle volume, SPM, POC, DOC (dissolved organic carbon).
2. Size distribution, from c_p or the forward part of VSF.
3. Composition information, or the refractive index.
4. Rate of processes, as primary production parameters.

Inversion of attenuation spectra to retrieve particle size distribution has been investigated since the 70's (Boss and Pegau, 2001; Boss *et al.*, 2001a; Boss *et al.*, 2004; Boss *et al.*, 2001b; Sullivan *et al.*, 2005; Twardowski *et al.*, 2001; Zaneveld and Pak, 1973). Other attempts tried to invert a scattering signal from flow cytometry for single particles (Ackleson *et al.*, 1988; Green and Sosik, 2004; Green *et al.*, 2003a; Green *et al.*, 2003b). Some of them are based on the backscattering ratio (Twardowski *et al.*, 2001), but need further independent validation.

2.6 Summary and conclusions from this chapter

After a critical review of the basic knowledge and the current literature on backscattering, a major lack of knowledge has been identified in the area of the **relationships between particle backscattering and living particles**. Although a number of studies have addressed the relationship with Chl-a, simultaneous measurements of abundance of different types of particles with b_{bp} are rarely found in the literature, as highlighted by Stramski *et al.* (2001). In Section 2.2, the current theory used to explain backscattering from marine particles has been presented. A simplified version of this theory will be used throughout the thesis. The counts of the abundance of different types of particles (methods described in Chapter 3) make the implicit assumption that the particles of a given type have the same geometrical cross section.

In order to progress the knowledge on this field, the **'reductionist approach' will be used throughout the thesis and applied to in-situ scenarios** (in an oceanic and a coastal location) **to address the question** of **whether the phytoplankton is a significant contributor to backscattering**. In this thesis, the results are presented both considering the suspended matter as a bulk component as well as splitting the suspended matter into compartments using the 'reductionist approach'.

Therefore, the **specific objectives** of this thesis are:

- To document the natural variability (spatial, temporal and spectral) of b_b in oceanic and coastal regions.
- To interpret the spectral variations of b_b supported by biogeochemical and other optical properties.
- To compare and complement the results from using the reductionist approach to the more classic approach of using bulk biogeochemical properties of the suspended matter.

Chapter Three

Study areas and methods

CHAPTER THREE: STUDY AREAS AND METHODS

Synopsis

In-situ sampling approach in open ocean and coastal waters has been used throughout this thesis to address the main hypothesis: the phytoplankton is a significant contributor to backscattering (b_b). This chapter is devoted to the description of the sampling, instruments used, deployment techniques, sample collection, and details of the storage, analysis, processing and quality control of the data.

The backscattering measurement, b_b, is the principal focus here; however, the other inherent optical properties (IOPs) have to be quantified simultaneously. Therefore, methods that measure total spectral absorption and scattering are described in this section, together with techniques used to separate their components (i.e. pigmented from non pigmented).

In order to relate b_b to the biogeochemical components, the following have to be measured simultaneously as discrete samples: total suspended matter, pigments abundance, phytoplankton counts and particle size distributions. These components have been measured following the methods detailed in this section.

3.1 Regions sampled

3.1.1 The Mid-Atlantic Ridge ecosystem – ECOMAR Cruise

Between 13 July and 18 August 2007, the area of the Mid-Atlantic Ridge (MAR) around the Charlie Gibbs Fracture Zone-CGFZ (Figure 3.1) was sampled. Biological and bio-optical sampling took place around three main stations: the South, the TOPEX transect and the North.

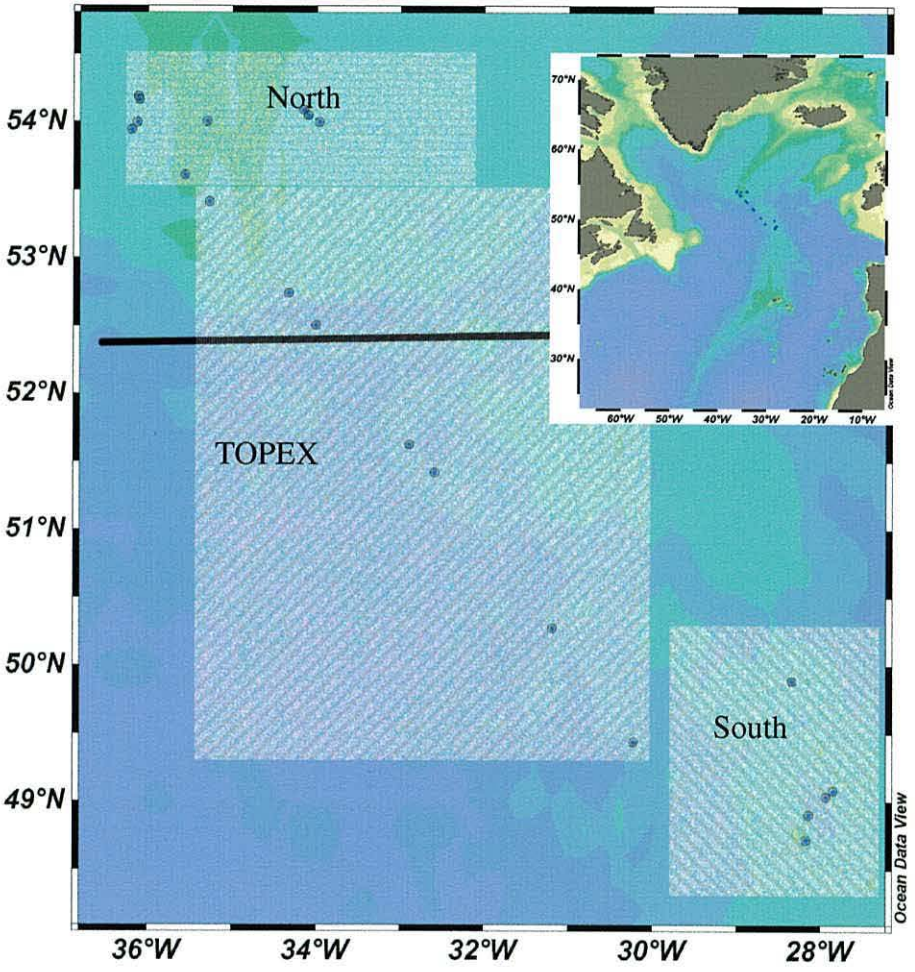

Figure 3.1 Map of cast positions. Shaded areas indicate the three areas in which stations were grouped. Some casts occurred in the same positions. Thick line highlights the position of the Charlie Gibbs fracture zone.

A total of 24 optical casts were measured coincident with discrete water samples taken from a CTD rosette were collected for the analysis of biogeochemical properties. In the South area, located to the South of the CGFZ in the subpolar gyre (Figure 3.1), six casts were measured, at the TOPEX transect, across the front, seven casts and in the North area, ten casts. Casts in the North and South were located also east and west of the Mid

Atlantic Ridge, and in this study they have been pooled together. The data from this cruise will be used in Chapters 5 and 6 of this thesis.

Table 3.1: ECOMAR sampling stations and measurements. (from the JC011 cruise report).

Area	Stn. No.	Date	Time GMT (start - end station)	Latitude N	Longitude W	Discrete sample depths (m)	Measurement taken*
Test station (out of the domain)	5	17 Jul	1610 2015	50° 07.8'	20° 03.9'	10 40 70 90	HPLC, Pabs, POC,FCM, optics rig.
South	9	19 Jul	1536 1620	49°04.84'	27°50.78'	5 20 40 70 100 130	HPLC, Pabs, POC, FCM, optics rig
South	15	20 Jul	1425 1458	49°04.54'	27°50.80'	5 20 50 80 100	HPLC, Pabs, POC,FCM, optics rig
South	25	23 Jul	1445 1637	49°02.20'	27°55.62'	5 20 40 70	HPLC, Pabs, POC,FCM, optics rig
South	30	24 Jul	1058 1423	48°54.09'	28°08.37'	5 30 50 80	HPLC, Pabs, POC,FCM, optics rig
South	34	26 Jul	1126 1327	49°53.26'	28°20.21'	5 25 50 80	HPLC, Pabs, POC,FCM, optics rig
South	40	27 Jul	0720 0833	48°43.21'	28°10.21'	5 30 50 70	HPLC, Pabs, POC,FCM, optics rig
TOPEX	44	28 Jul	1013 1303	49°26.29'	30°13.65'	5 20 40 60	HPLC, Pabs, POC, FCM, optics rig
TOPEX	48	29 Jul	0647 0927	50°16.45'	31°11.29'	5 30 50 70	HPLC, Pabs, POC,FCM, optics rig

Area	Stn. No.	Date	Time GMT (start - end station)	Latitude N	Longitude W	Discrete sample depths (m)	Measurement taken*
TOPEX	54	30 Jul	0814 1047	51°25.21'	32°35.02'	5 30 60	HPLC, Pabs, POC,FCM, optics rig
TOPEX	55	30 Jul	1318 1627	51°39.77'	32°53.54'	5 30 60	HPLC, Pabs, POC,FCM, optics rig
TOPEX	59	31 Jul	0919 1145	52°30.29'	34°00.12'	5 25 50	HPLC, Pabs, POC,FCM, optics rig
TOPEX	60	31 Jul	1419	52°44.59'	34°19.64'	5 25 60	HPLC, Pabs, POC,FCM, optics rig
TOPEX	64	1 Aug	0802 1020	53°24.74'	35°16.13'	5 30 40 55	HPLC, Pabs, POC,FCM, optics rig
North	65	1 Aug	1238 1430	53°36.46'	35°33.20'	5 15 40	HPLC, Pabs, POC,FCM, optics rig
North	70	4 Aug	0730 0953	53°59.74'	36°07.67'	5 35 55	HPLC, Pabs, POC, FCM, optics rig
North	76	5 Aug	0925 1018	54°11.14'	36°05.66'	5 30 60	HPLC, Pabs, POC,FCM, optics rig
North	82	6 Aug	1708 1755	54°09.85'	36°05.96'	5 35 60	HPLC, Pabs, POC,FCM, optics rig
North	85	7 Aug	1252 1320	53°56.49'	36°11.41'	5 30 50 65	HPLC, Pabs, POC,FCM, optics rig
North	89	8 Aug	0823 1056	54°00.10'	35°17.60'	5 30 50 60	HPLC, Pabs, POC,FCM, optics rig
North	99	9 Aug	1426 1633	54°00.00'	33°57.97'	5 25 50 70	HPLC, Pabs, POC,FCM, optics rig
North	108	11 Aug	1310 1342	54°05.40'	34°09.2'	5 30 45 60	HPLC, Pabs, POC,FCM optics rig
North	113	12 Aug	1338 1432	54°03.01'	34°05.98'	5 20 40 60	HPLC, Pabs, POC,FCM, optics rig

Area	Stn. No.	Date	Time GMT (start - end station)	Latitude N	Longitude W	Discrete sample depths (m)	Measurement taken*
North	118	13 Aug	1505 1533	54°02.30'	34°09.78'	5 25 55	HPLC, Pabs, POC,FCM, optics rig

* HPLC – phytoplankton pigments by High Performance Liquid Chromatography, Pabs – particulate, phytoplankton & detrital absorption coefficients, POC – particulate organic carbon, FCM – flow cytometry, Optics rig including : Wetlabs ac-9, ac-s, bb3 and HOBIlabs Hydroscat-6

3.1.2 Western English Channel coastal station - L4 station

Station L4, at 50° 15' N, 4° 13' W (~55m depth) is located ~10 km south of Plymouth (Figure 3.2) though ~6.5 km away from the nearest land on Rame peninsula. It is part of a sampling network maintained by the Marine Biological Association and Plymouth Marine Laboratory. In-situ sampling is undertaken on-board *RV Plymouth Quest* weekly at station L4 and comprises vertical profiles of hydrographic and optical parameters. Several publications have used these data sets as the object of their study in this area (See a review on this by Southward *et al.* (2005)). The data from L4 will be used in Chapters 4 and 7 of this thesis.

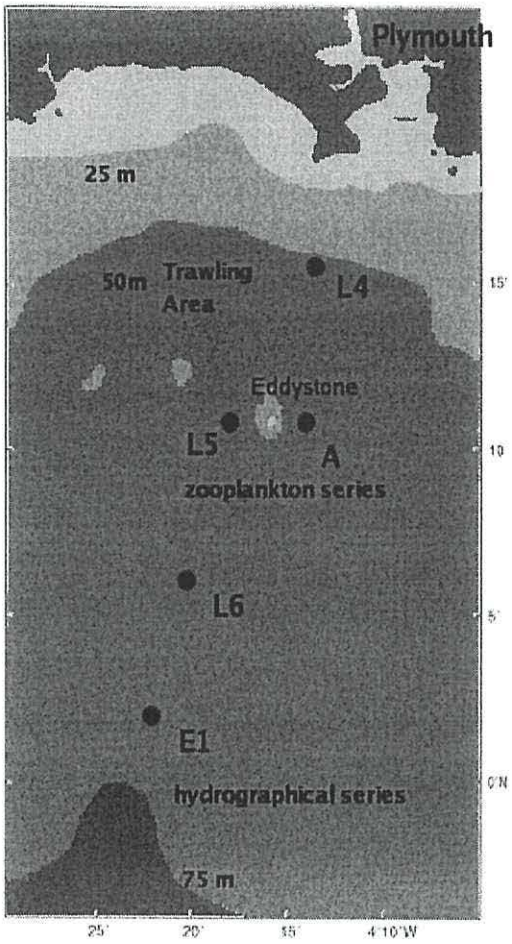

Figure 3.2 Location of L4 with respect to other near-shore sampling sites south of Plymouth (taken from Groom *et al.*, 2009).

3.1.3 Additional sampling at the North Sea –REVAMP cruises

One of the aims of the EU funded project REVAMP (REgional VAlidation of MERIS chlorophyll Products in the North Sea), was to test algorithms for interpretation of ocean colour satellite images. In this context, the cruises BE02/14 and BE03/12 aimed to:

- collect the maximum amount of in-situ observations in coincidence with the overpasses of the ESA MERIS sensor in optically complex waters;
- collect the in-situ observations to improve parameterisation of regional algorithms.

Both cruises took place on board the RV Belgica. BE02/14 sampled the North Sea between the 17th June and the 21th June 2002 , while BE03/16 sampled same region between the 16th June and the 20th June 2003 (Figure 3.3). Absorption data from these cruises are given in Tilstone *et al.*(in revision, JGR-Oceans). In Chapter 4 of this thesis, both the absorption and backscattering data from the North Sea are used in a sensitivity analysis of a backscattering instrument.

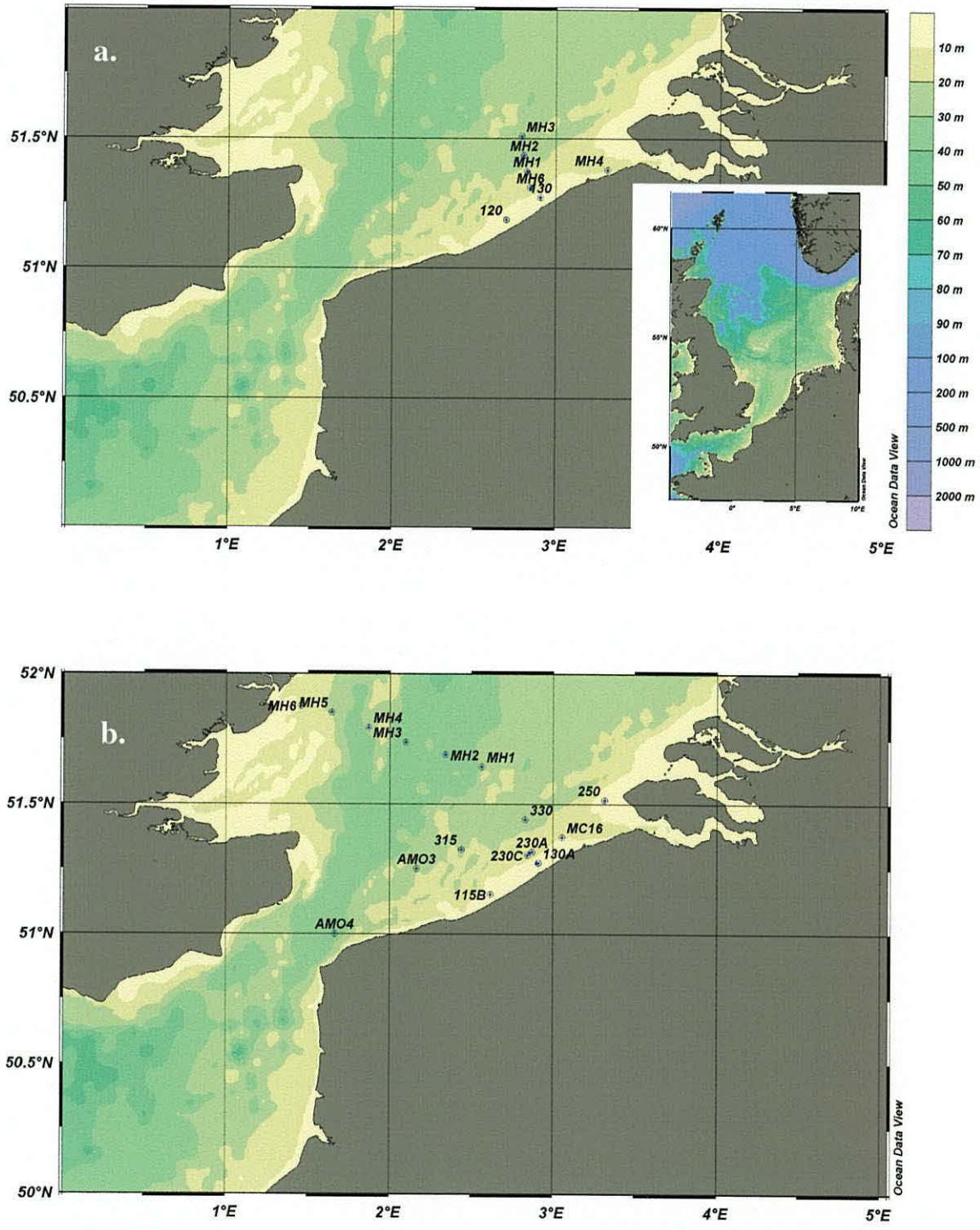

Figure 3.3 a) BE02/14 cruise stations, with insert of the North Sea area, and b) BE02/16 cruise stations. The label indicates actual station names.

In summary, data from four cruises have been used in this thesis which is summarised in Table 3.2. It is important to note that different instruments were used in each cruise to

measure backscattering. In Chapter 4 a comparison of backscatter using different instruments is performed on ECOMAR, L4 and North Sea data. In Chapters 5, 6 and 7, the relationship between biogeochemical properties and backscattering is studied with data from ECOMAR and L4 only.

Table 3.2: Summary of the combination of instruments used at each location and the chapter of this thesis in which they are used.

Cruise	Cruise dates	ac9	CTD	Backscattering instruments deployed	Responsible	Data presented in Chapter (data used)
BELGICA 2002/14	17-21 June 2002	n/a	SBE911+ (rosette)	HS-6, sn: 020332	Deployment, cleaning, calibration and processing V. Martinez Vicente (PML)	Chapter 4 (HS-6)
BELGICA 2003/16	16-20 June 2003	n/a	SBE911+ (rosette)	HS-6, sn: 020332 VSF-046G	Deployment, cleaning, calibration and processing V. Martinez Vicente (PML)	Chapter 4 (HS-6)
ECOMAR JC011	13 July – 18 August 2007	acs sn:023	SBE911+ sn: 4307	ECO-BB3 sn:366	Deployment, cleaning, calibration and processing V. Martinez Vicente (PML)	Chapter 5 and 6 (ECO-BB3)
L4	2003-2009	Ac9+ sn:265 and 277	SeaBird 19+ sn:4307 sn: 4180	HS6, sn:020332 VSF3-076	Deployment and cleaning: J.Fishwick/G.F. Moore (PML) Calibration and processing: V. Martinez Vicente (PML)	Chapter 7 (VSF3)

3.2 In-situ continuous optical measurements

3.2.1 In-situ spectral backscatter coefficient - b_b [m-1] - using HOBILabs HydroScat-6: instrument principle, calibration and data quality control

The HydroScat-6 is a self-contained instrument for measuring optical backscattering [b_b] at six different wavelengths in natural waters. Its unique optical geometry also permits auxiliary measurements of fluorescence. It was developed by HOBILabs Inc. based on the optical design proposed by Maffione and Dana (1997).

The PML HydroScat-6 (HS-6) is a metal cylinder (length 34.5 cm and diameter 20.3 cm) that includes the emitter and detector optics and electronics, a depth transducer, rechargeable batteries, a data logger with real-time clock, and an external switch for the control of logging (Figure 3.4). The rear end cap has only one connector in the case of the PML – HS-6.

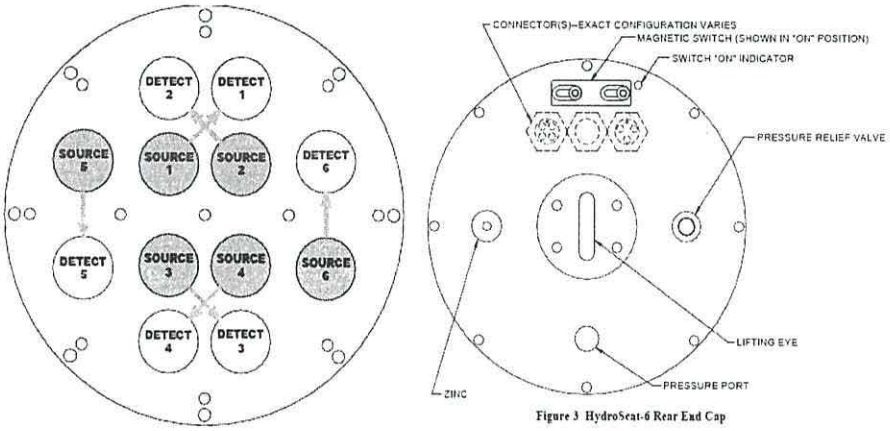

Figure 3 HydroScat-6 Rear End Cap

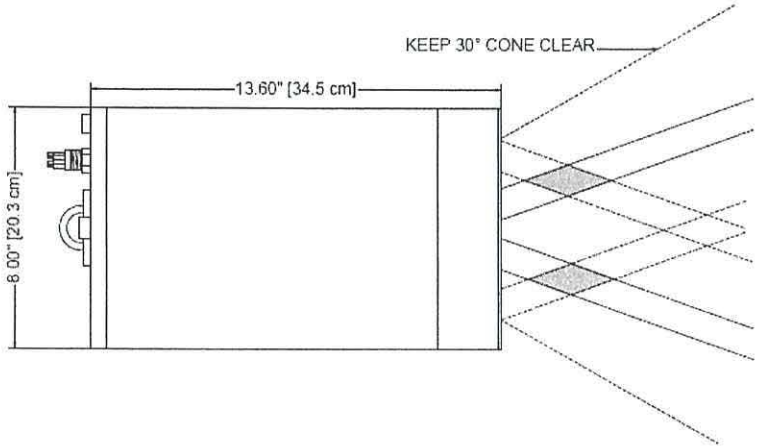

Figure 3.4 HOBILabs HS-6 of PML (taken from HOBILabs manual (2007)).

The optical sensors are located at the front end cap, where the HS-6 has six independent channels, each sensitive to a different wavelength (10 nm band widths). Each channel consists of separate source and receiver optics. Each source beam originates from a light-emitting diode (LED) selected to match the desired measurement wavelength. The beam from the LED goes through a lens to adjust its divergence, then through a prism that bends the beam before it enters the water. The receiver consists of an identical prism that bends the field of view toward the source beam, a bandpass interference filter that determines the exact wavelength range of the measurement, and lens that focuses the received rays onto a silicon detector.

The divergences of the source beam and receiver field of view, the angles of the prisms, and the distance between the source and receiver windows, determine the range of scattering angles over which the measurement is made. The HS-6 geometry results in a measurement centred on a scattering angle of 140°, so that the value actually measured by the instrument is the volume scattering function at 140° at each of the six wavelengths [$\beta(140°; \lambda)$]. The in-situ b_b is then derived as an extrapolation over the backward direction of this single direction measurement grace to an empirical relationship that uses a particular coefficient (χ_{bb}). The spectral variability of this coefficient is a subject of discussion (Chami *et al.*, 2006). The fraction of the transmitted light scattered in the desired range of angles is extremely small, and one of the prime considerations in the optical design is maximising this inherently low throughput. Thus at least a 2 cm opening throughout the optical path is maintained. Due to this aperture, the signal detected can be significantly modified (reduced) because of the attenuation of the light on its way back to the sensor. This produces the need to correct the quantities by a factor ("sigma correction", explained below).

Data can be stored internally in different formats, or broadcasted real-time into a PC.

Calibration of the HS6 is performed following the calibration procedures given by the manufacturer (HOBILabs (2006)). It consists of retrieving the coefficients needed for the transformation and correction of the measured signal into b_b. These coefficients are: Mu, dark offsets and gain ratios. Mu (μ) is the overall coefficient of sensitivity for a channel, which allows converting its normalized electronic response to absolute backscattering. This is measured by continuously moving a target with known

reflectivity (cross calibrated PTFE plate with a Spectralon NIST certified plate) through a range of distances in front of the sensor using a specific fixture (Figure 3.5). The resulting curve is integrated and weighted by known geometric factors in order to calculate μ. Because of electronic factors, the instrument may produce a non-zero signal even when no scattering signal is present. These offsets (which vary from channel to channel and with gain settings) are measured by blocking the face of the instrument to prevent any light from the LEDs from entering the receivers. The dark offsets are measured out of water. The HydroScat uses the dark offset measurements internally, subtracting them in real time from the "raw" data it produces. Finally, the HS6 has five different gain settings. These are different levels of signal amplification, which allow automatic operation in a wide variety of conditions. The lower gain settings also make possible the method of using a highly reflective target for the μ calibration. The ratios between adjacent gain settings are measured by recording the signal value while a channel is set to a certain gain, changing the gain by one step, and recording the new signal value.

For a complete calibration the sequence is to measure the dark offsets first, since this is done outside the calibration fixture, then perform the μ calibration, then the gains. From these parameters, the k_{exp} and k_0 are derived using the formulas in the calibration manual.

During this study, the calibration of the PML HS6 was performed by HOBILabs and at PML, using an in-house built calibration fixture (Figure 3.5).

Figure 3.5 Calibration setup for the HS6 at PML.

3.2.2 In-situ spectral backscatter coefficient - b_b [m-1] - WetLabs ECO VSF1, VSF 3 and BB3.

The ECO VSF measures the optical scattering at 100, 125, and 150 degrees, thus providing the shape of the Volume Scattering Function (VSF) throughout its angular domain. It can provide the total backscattering coefficient by integration and extrapolation from 90 to 180 degrees (Wetlabs, 2007c).

Figure 3.6 shows the optical configuration for the VSF for 1 wavelength configuration. The ECO VSF is a cylinder housing that contains the signal processing and controller circuitry. The optics include three LED-based transmitters that couple to a single receiver. The transmitters and receiver are located to establish centroid light scattering angles of approximately 100, 125, and 150 degrees respectively. For each angle the region of intersection encompasses width of about 18 degrees.

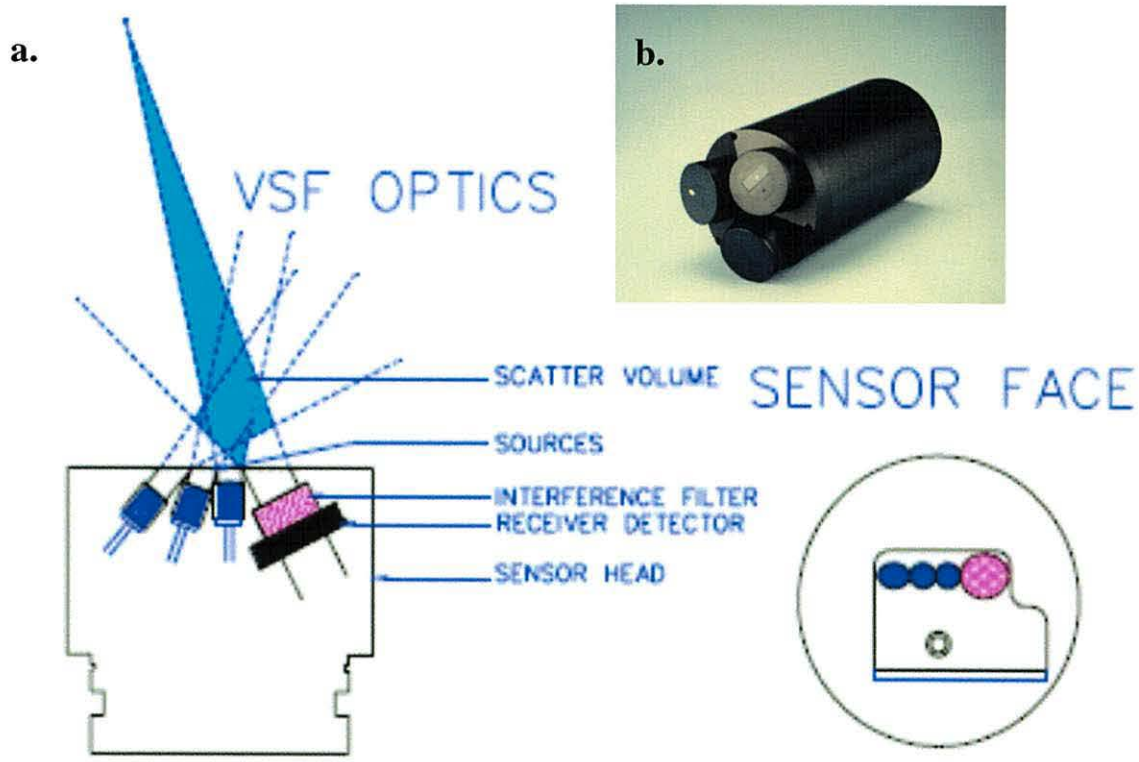

Figure 3.6 a) Optical configuration of ECO-VSF b) ECO VSF-3. (Taken from Wetlabs manual (2007))

The controller electronics do a sequence through the individual transmitters at approximately 1 Hz per sample cycle. The individual transmitters operate

synchronously with the receiver to reject ambient light. A directly coupled reference detector indicates relative LED intensity during operation. Signals from the receiver and reference detector are digitized and subsequently stored or telemetered from the instrument. Two VSF meters are available at PML, VSF-1 and VSF-3, measuring one and three wavelengths, namely 530 nm and 470 nm, 530 nm, and 660 nm respectively (Wetlabs, 2007b). Because the ECO VSF incorporates very short pathlengths and scattering volumes in its measurements, it is relatively immune to the pathlength attenuation. For attenuation coefficients up to approximately 5 m^{-1} no data correction is required. The ECO-BB3 uses the same optical principle that the VSF but it measures 117° scattering (β_t). It therefore applies a similar transformation to the Hydroscat: it requires an extrapolation factor (χ_{bb}) specific to 117°. However, because the angle is smaller, it does not get attenuation effects (i.e. no "sigma correction" needs to be applied), similarly to the ECO VSF

3.2.3 In situ spectral beam attenuation coefficient - c [m^{-1}] and absorption coefficient - a [m^{-1}] - Wetlabs ac9+

The ac9+ - Dual Path Absorption and Attenuation Meter (WET Labs Inc., USA) is the first spectrophotometer that measures in-situ the spectral absorption, *a*, and attenuation, *c*, of the natural waters at nine wavelengths (Wetlabs, 2006, 2007a).

It consists of two cylinders joined by two tubes of 25 cm length (Figure 3.8). The seawater circulates through the tubes. *a* and *c* are measured simultaneously on the same water body. In the larger cylinder there are separate detectors and a system for electronic acquisition and control of the unit. The smaller cylinder hosts the two independent light sources and separate filters for the light emitted to the wavelengths used (width of 10 nm per band).

The functioning of this instrument is based on the different structure of the two tubes in which the measurements take place (tube A and tube C). Tube C has black walls, so that all the diffused photons in the tube are absorbed by the walls. The light that is propagated through the tubes is subject to a loss of radiant energy due to absorption and scattering (Figure 3.7). The wall of the A-tube is covered by reflective material, so that all the photons hitting it are sent back to the tube, and the light that exits the end of it is

recovered by a diffuser and a big surface detector. The reflective material is in fact transparent quartz surrounded by a thin layer of air. Knowing the refractive indices of quartz and air and the thickness of the materials, using Fresnel's equations it is possible to calculate that total reflection of a beam takes place at an angle lower than 41.7° (with respect to the optic axis). A fraction of the light (i.e. the fraction scattered at angles greater than 41.7°) is not measured by the detector (Zaneveld *et al.*, 1994). This loss of light produces a 19% overestimation on average of the absorption (Wetlabs, 2007a). There are several methods that take into consideration this effect and correct it (see below). Also there is a difference in the C-tube between the true c and the measured value (underestimation of the true value), which is due to the acceptance angle of the instrument (0.7°). Correcting attenuation measurements for the errors caused by collection of scattered light is not recommended in the manufacturer's manual as it is "extremely difficult and of questionable benefit" (Pegau and Zaneveld, 1993). However, they note that transmissometers with different acceptance angles will provide slightly different measurements because they measure different portions of the scattering function.

Data containing the a and c at each measured wavelength are stored in binary format in the data storage unit of the ac9s available at PML (ac9+).

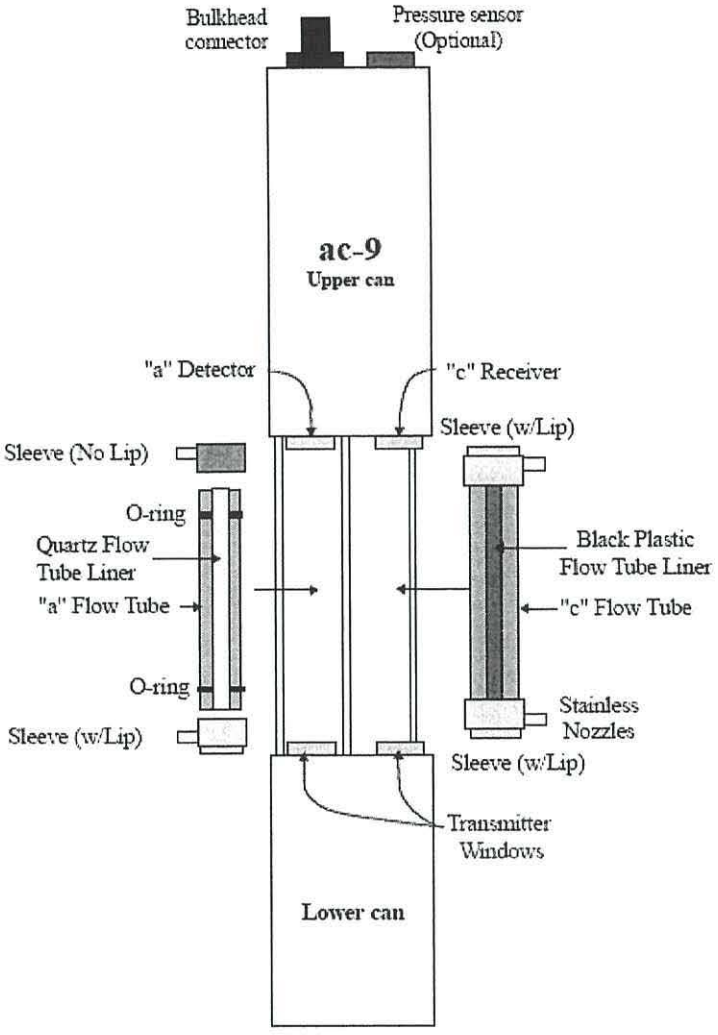

Figure 3.7 AC-9 unit (taken from WETlabs manual (2007))

For calibration of the instrument, the protocol proposed by Wetlabs is followed (Wetlabs, 2007a), however, the salient points regarding calibration and the deviations from the standard protocol are highlighted below. According to these protocols, there are two types of calibrations: air and water calibrations. Air calibrations are used to check for the cleanliness of the tube and windows of the instrument prior to deployment and to check for potential misalignments that occurred as a result of transport or mounting in a deployment frame.

Water calibrations are used to take into account the contribution of pure water in the attenuation and absorption and to follow the drift of the sensor. Because of the way the instruments are factory referenced to the pure water values to measure c and a above and beyond what is considered to be pure water values, they need to be offset back to

produce zero as a reading when they are measuring pure water outside the factory, after a period of functioning. The drift of the sensor be can due to degradation of the colour filters, a change in transmission of the windows or a deterioration of the walls of the flow tube. Given its greater importance, only field pure water calibrations have been documented.

The instruments were regularly calibrated in the field with pure water (milli-Q water), in its deployment configuration, in order to remove the effects of small misalignments of the optical system and/or to track possible long-term drift. The calibration is performed by making milli-Q water pass through the flow tubes (by pressurising a water deposit) and measuring the resulting offsets.

During cruises the milli-Q water comes from a de-ionising system on board. At PML, a reverse osmose membrane is coupled with a UV lamp, a Carbon cylinder, a de-ioniser cylinder and a 0.2 μm filter to produce pure water (i.e. particle and dissolved organics free water).

Milli-Q water is placed in to a clean tank (80 l polycarbonate carboy) at least 12h before the measurement to allow for degassing. Water is checked for particles or air bubbles before use. All tubing used was black and the set up is as described in Figure 3.8.

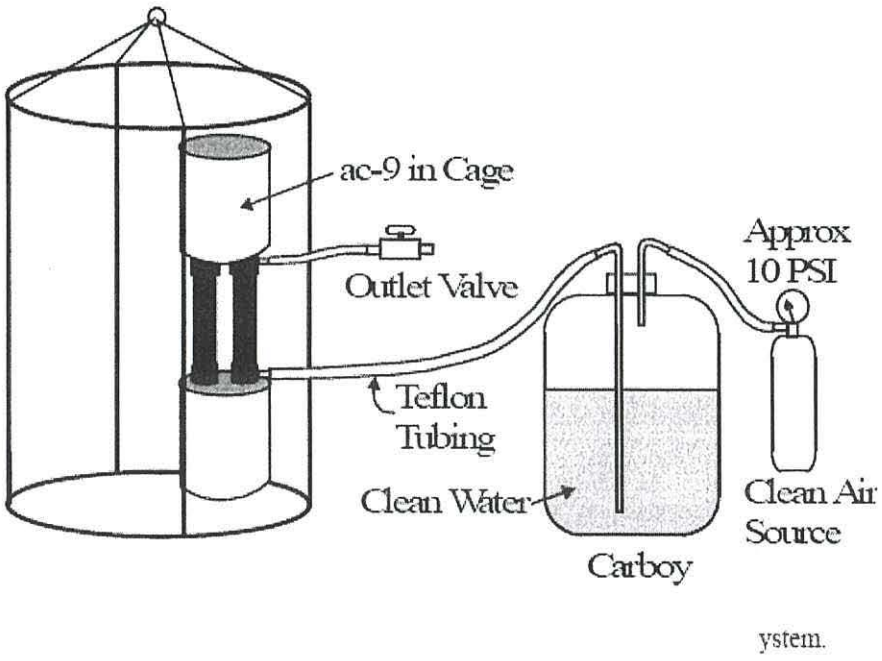

Figure 3.8 Schematic of a field water-calibration delivery system (taken from Wetlabs manual, 2007).

The instrument (flow tubes and optical windows) is cleaned using wetted Whatman Lens cleaning tissue firstly with milli-Q and then with methanol. This preparation is done at least 12 h previous to the calibration. Water temperature is recorded, several times during the calibration if necessary, for post-correction, using a hand held digital thermometer.

The instrument is left in operation mode for at least 30 minutes before starting to collect data, in order to warm up the electronic components of the instrument. Measurements are taken for about 60 seconds for each flow tube with the WETVIEW software: the measured offset must be stable (within 0.005) for each wavelength. Then, a portion of (stable) data is averaged. Such a sequence is repeated 3 times for each flow tube and the measured offsets must not differ by more than 0.005. In particular, during the calibration one has to check for bubbles that can cause large spikes in the data recorded. The resulting mean offsets are averaged and subtracted from the measurements before they are corrected for temperature, salinity and scattering. During this study, the calibration of the PML ac9s was performed at PML and during cruises. Figure 3.9 shows the temporal evolution of the calibrations in terms of the values of the mean offsets.

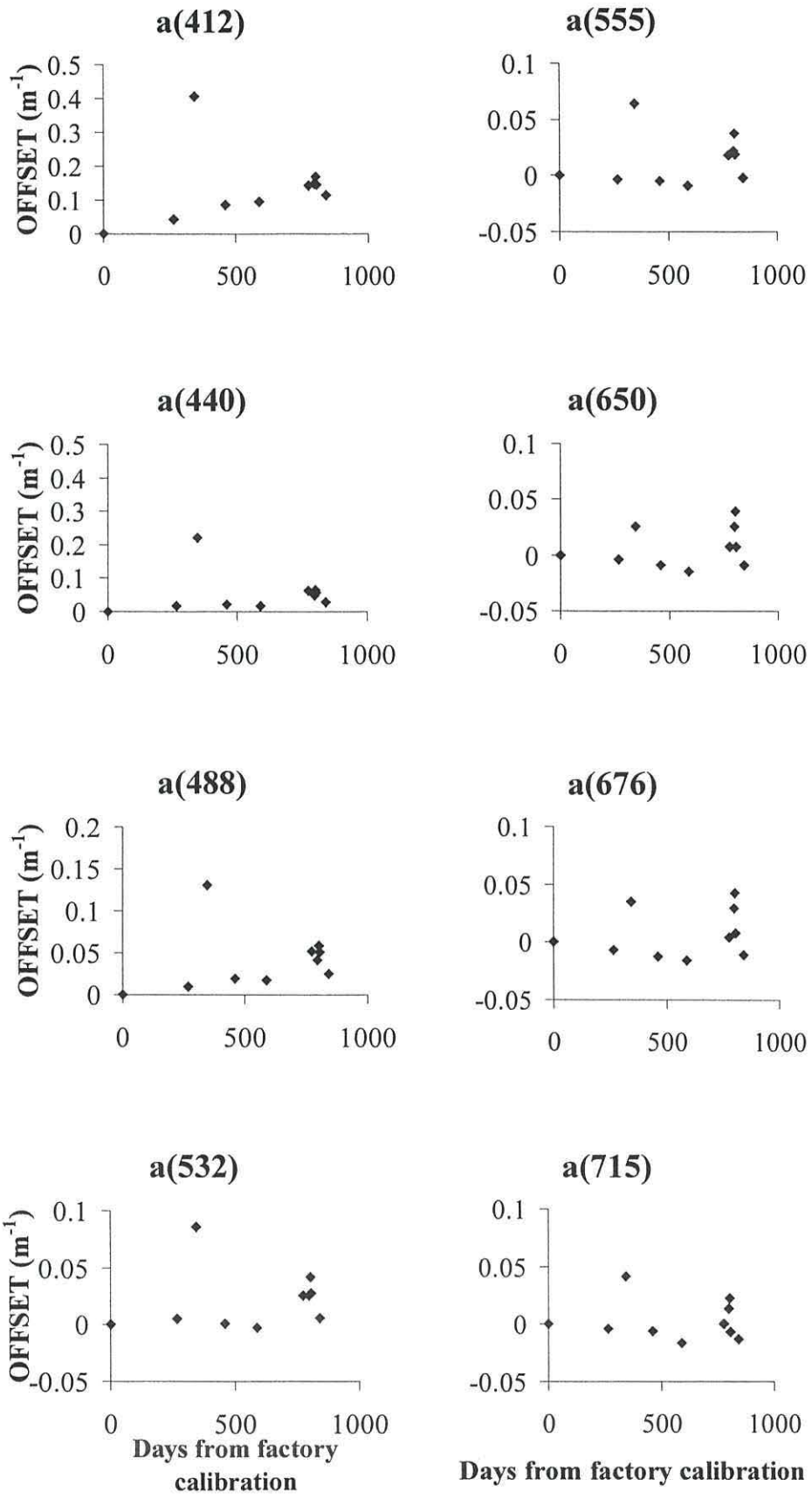

Figure 3.9 Temporal evolution of the absorption offsets of the PML ac9 (sn: 265) calibrations

3.2.4 Mounting and deployment of the instruments in-situ

During the ECOMAR cruise, the Wetlabs BB3 was deployed together with an acs (a hyperspectral ac9) in the PML optics rig (Figure 3.10.a). The temperature and salinity used for correction came from the CTD in the rig (Table 3.2). At L4, the Wetlabs VSF3 was deployed in the PML optics rig (Figure 3.10.a), with other instrumentation, including ac9+ and Seabird Electronics Inc. CTD. During REVAMP cruises, the Hydroscat-6 was deployed on its own, in a purpose made rig (Figure 3.10.b).

In every instance, care was taken to follow the recommendations of the manufacturers as to put the backscattering instruments facing down and give a clearance of 30° to the detector windows of the backscatter meters for a minimum of one metre. The frequency of acquisition was 4 samples/second, which allows the quasi-simultaneous measurement of fluorescence at two channels for the Hydroscat-6 and the lowering speed was between 0.1-0.2 m s^{-1}.

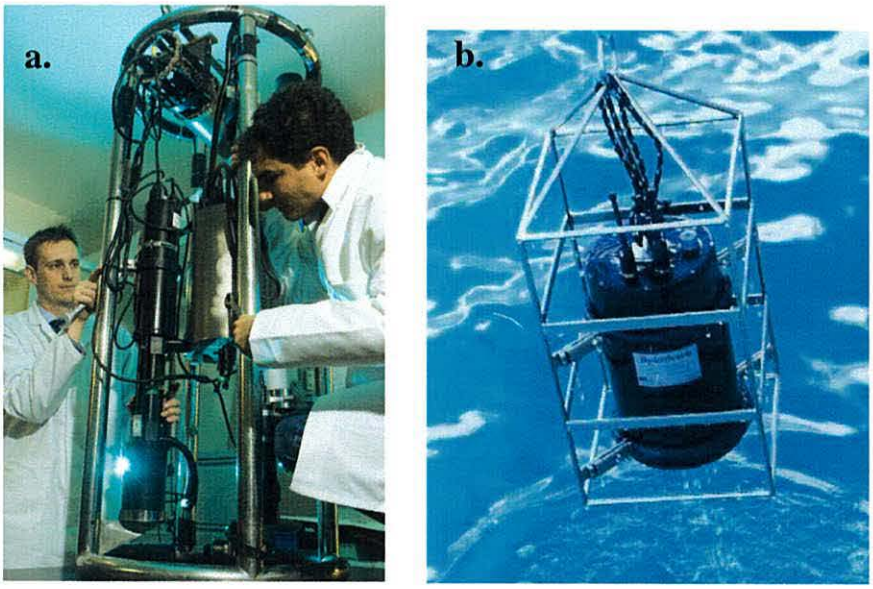

Figure 3.10 a)The PML optics rig, including an ac9+, a SeaBird CTD and a VSF meter; b) The HS-6 deployed in its own rig.

The ac9+ was deployed upright, on a frame lowered into the sea by means of a winch. A small pump (Type Seabird 3K, with a nominal flow rate of 3 litres/min) brings the water through the ac9+ flow tubes. All tubing is of Viton type (inert) to avoid contamination by coloured substances and covered with black tape to avoid direct light into the tubes. The lowering speed, for a frequency of acquisition of 6Hz, was about 0.1-0.2 m s^{-1}.

Air bubbles passing through or even remaining trapped into the flow tubes when the instrument is at surface and/or in the first meters (according to sea state), can affect measurements and induce differences between down- and up-cast values profiles according to REVAMP protocols (Tilstone *et al.*, 2004). During the deployments in-situ, the instruments were left at depth (at least 10 metres) for 10 minutes to help purging the system for bubbles and only the up-cast profiles are considered here, as the instrument optics is supposed to be warmed up during the downcast. Data were recorded in the internal memory and downloaded daily to a PC using the Wetlabs Inc. software for Archiving and Processing (WAP). A summary of the coincident wavelengths of the in-situ instrumentation used in this work is presented in Table 3.3.

Table 3.3: Summary of spectral matching among the instruments used in this work. The (±) indicates the width of the spectral band in nm. These are not available for the VSF.

Instruments	Wavelengths (nm)								
ac9+, sn:265 (±5)	412	440	488	510	555	630	650	676	715
ac9+, sn:277(±5)	412	440	488	510	555	630	650	676	715
VSF1, sn:46G				530					
VSF3, sn:076			470	530			660		
BB3, sn:366			470	532			660		
HS-6, sn:020332		442 (±5)	488 (±5)		550 (±5)	620 (±5)		671 (±10)	852 (±20)

3.2.5 Data processing

3.2.5.1 HOBILabs HS-6

The most recent Hydroscat processing scheme (HOBILabs, 2007a, 2007b) has three processing stages: firstly, the transformation of the scattered intensity received by the sensor into the physical value of the volume scattering function or VSF at approximately 140° [$\beta_u(140°)$]; secondly, the σ correction processing is done to account for the spectral modification of the signal measured due to the attenuation of the light beam in its way back to the sensor; finally, the extrapolation of $\beta_u(140°)$ to obtain corrected backscattering [b_b].

In the first stage of the pre-processing, the signal (S_{norm}) is converted to calibrated units to obtain b_{bu}, by dividing by a temperature dependent term and a gain matrix, to produce $\beta_u(140°)$:

$$\beta_u(140°) = \frac{S_{norm} \cdot \mu}{(1 + k_T(T - T_{cal})) \cdot G_g \cdot R_{norm}} \quad \textbf{Eq. 1}$$

The set of parameters in Equation 1 were obtained from water calibrations carried out by HOBILabs and at PML (see Section 3.2.1). The temperature term (k_T) was set to zero.

The sigma correction formula is an approximation to a complicated function of the geometry of the sensor and the sampling volume, and can be written as:

$$\beta(140°) = \sigma(K_{bb}) \cdot \beta_u(140°) \quad \textbf{Eq. 2a}$$

where σ is an exponential function of K_{bb} in the form of:

$$\sigma(K_{bb}) = k_1 \exp(k_{exp} K_{bb}) \quad \textbf{Eq. 2b}$$

where k_{exp} is instrument specific and is saved in the calibration file, k_1 is set so that the value of σ is 1 during the calibration process (assuming that the water used for calibration is optically pure). K_{bb} is the coefficient of attenuation for light travelling from the sensor to the sensing volume and back. It is described by:

$$K_{bb} = a + 0.4 \cdot b \quad \textbf{Eq. 2}$$

If measurements of a and b are available, they can be used to calculate sigma corrections with the best possible accuracy. However within HydroSoft, a is estimated from a priori data, and b is estimated from the measured b_b.

In the final stage of the processing, $\beta(140°)$ is subtracted by $\beta_w(140°)$ (Morel, 1974) to obtain the particle fraction, $\beta_p(140°)$ which is then extrapolated and integrated in the backward direction ($90°<\theta<180°$), to obtain b_{bp} (Maffione and Dana, 1997) and added to b_{bw} (Morel, 1974) to obtain total b_b:

$$b_b = 2\pi\chi_{bb}[\beta(140°) - \beta_w(140°)] + b_{bw} \quad \textbf{Eq. 3}$$

It is assumed that the factor χ_{bb}=1.08, although this factor is known to vary with θ, and, for instance χ_{bb}=1.18 has been proposed from $\beta_p(\theta)$ measurements (Boss and Pegau, 2001), but there is still some discussion on the variability of this parameter (Chami *et al.*, 2006). Comparisons of measurements with Hydroscat-6 and a volume scattering measuring instrument (Berthon *et al.*, 2007) produce differences in the determination of b_b ~15%.

Backscattering data were processed using the following protocol:

1. Conversion of raw data to ASCII, with Hydrosoft v2.72
2. Selection of the upcast part of the profile
3. Binning of the data to 0.5 m and application of a median filter
4. Correction for attenuation of the signal, "sigma correction"
5. Transformation of $\beta(140°,\lambda)$ into $b_b(\lambda)$
6. Addition of pure water values

Steps 2-6 were performed using IDL routines. The program used in step 2 was provided by G. Moore (PML), while the code for steps 3-6 was done by V. Martinez Vicente.

3.2.5.2 Wetlabs VSF and BB3 meters

The processing of the data from the VSF and BB3 meter was done in three steps: firstly, conversion of digital counts into $\beta(\theta)$ done using the calibration parameters supplied by the manufacturer. Secondly, a pathlength correction in turbid or very absorbing water (i.e. $c>5m^{-1}$). Given the geometry of the sensor and the characteristics of the water sampled, the pathlength correction was neglected, which implies a maximum error not greater than 5% of the measurement. Finally, calculation of b_{bp} from $\beta(\theta)$ at three angles. This was done by fitting a third order polynomial through all the measurements

points of $[2\pi\beta(\theta)\sin(\theta)]$ including $\theta = \pi$, where $\beta(\theta)\sin\pi = 0$. Then, the area under the polynomial was integrated using Newton method from the IDL library.

For the Wetlabs BB3, after subtraction of the pure seawater scattering, $\beta(117)$ becomes β_p, which needs to be transformed into particle backscattering (b_{bp}) using a factor $\chi_p(117°)$ following Twardowski *et al.* (2007):

$$b_{bp} = 2\pi\chi_p(117°)\beta_p(117°)$$

A value of 0.90 was adopted for $\chi_p(117°)$, assuming that $\chi_p(117°)$ is not significantly different to $\chi_p(125°)$ measured by Sullivan *et al.* (2005). Because of the small effective pathlength of the instrument, the correction with absorption and attenuation was considered negligible and therefore not applied to the data. Calibration of the instrument was performed by the manufacturer previous to the cruise. No dark offset measurements were performed during the cruise and it was assumed that there was no significant instrumental drift, as in the literature (Twardowski *et al.*, 2007).

In summary, the VSF and BB3 data were processed using the following protocol:

1. Conversion of data from binary to ASCII, using WAP v4.17
2. Merging of data from different sources connected to the instrument, using WAP 428a
3. Selection of the upcast part of the profile
4. Binning of the data to 0.5 m and application of a median filter
5. Integration of the VSF values to obtain b_b

Steps 2-5 were performed using IDL routines. The program used in step 2 was provided by G. Moore (PML), while the code for steps 3-5 was done by V. Martinez Vicente.

3.2.5.3 Calculation of the scattering and backscattering spectral slope

The spectral slope of the scattering and backscattering coefficients was calculated by fitting (Markwardt, 2008) a power law function of the wavelength, with 532 nm as the reference wavelength and the exponent being the spectral slope (γ_S):

$$b_p = b_p(532) \times \left(\frac{\lambda}{532}\right)^{\gamma_S} \qquad \textbf{Eq.5}$$

The R^2 associated with this fit was typically lower than 0.5, indicating the inadequacy of the model to our dataset. This may be due to effects of absorption as discussed by Snyder *et al.* (2008). However, this model has been chosen to be representative of the spectral variations in order to have results comparable to previously published works.

The spectral slope of b_p was calculated using all the available wavelengths of the ac9 (γ_S), except for 2007 and 2008, when the 676nm channel was malfunctioning and therefore those data were not used in the calculation of the slope. The spectral slope has also been computed using only three wavelengths: 555, 650 and 715 nm, with 715nm used as the reference wavelength, referred to as γ_{S3}. This differentiation was made according to recent findings (Doxaran *et al.*, 2009), that related particulate absorption (a_p) to the changes in the increase of b_p with respect to a b_p calculated using γ_{S3} (b_{pmod}). The spectral backscattering slope (γ_{BS}) was computed using an equation of the same form as Equation 5.

The backscattering ratio slope γ_{BSR} was computed as :

$$\gamma_{BSR} = \gamma_{BS} - \gamma_S$$

3.2.5.4 Wetlabs ac9+

Offset correction

Wetlabs ac9+ data were inspected visually to check for abnormal tendencies. Absorption and attenuation at three depths (surface, thermocline and bottom) were plotted and these quicklooks were saved as .png files. If no "suspicious spectral shapes" were detected, data were transferred to the next processing step. By "suspicious spectral shapes" one relies very much on experience with this kind of data: artefacts such as bumps, peaks in attenuation spectra between 488 and 600 nm. Data were corrected using values from field water calibrations in the case of presence of "suspicious spectral shapes". If, even when using different water calibrations corrections, the quality of the spectra did not improve, then the data were discarded.

Temperature and salinity corrections

After offset correction, data must be corrected for the in-situ temperature and salinity effects. This is done to correct for differences between the absorption coefficient of the optically pure water used as a reference when calibrating the instrument and the absorption coefficient of the water in which the measurements are performed. These effects are removed by applying following algorithms to the measured c_m and a_m:

$$c_{mts}(\lambda)=c_m(\lambda) - [\psi_t(\lambda)*(T-T_{cal}) + \psi_{sc}(\lambda)*(S-S_{cal})] \quad \textbf{Eq. 6}$$

$$a_{mts}(\lambda)=a_m(\lambda) - [\psi_t(\lambda)*(T-T_{cal}) + \psi_{sa}(\lambda)*(S-S_{cal})] \quad \textbf{Eq. 7}$$

where T and S are the temperature and salinity of the water during measurement, respectively, and T_{cal} and S_{cal} are the temperature and salinity (S = 0) of the water during field pure water calibration, respectively. The values used for ψ_t, ψ_{sc} and ψ_{sa} are the ones in Wetlabs Protocol L Tables 2 and 3. c_{mts} and a_{mts} are the attenuation and absorption corrected for the T and S effects.

Scattering correction

The portion of the scattered light not reaching the detector of absorption, causes an overestimation of a_{mts}. Presently, three methods are available to perform this correction, and methods 2 and 3 imply that c is measured simultaneously with a:

1. $a_{mtsb}(\lambda)= a_{mts}(\lambda)-a_{mts}(715)$,

by assuming no absorption at 715 nm and no spectral dependence of scattering.

2. $a_{mtsb}(\lambda)= a_{mts}(\lambda)-\varepsilon*[c_{mts}(\lambda)-a_{mts}(\lambda)]$,

by assuming the error is a constant proportion of scattering. Typically, ε=0.14 but can vary between 0.08 (phytoplankton dominated) and 0.3 (sediment dominated).

3. $a_{mtsb}(\lambda)=a_{mts}(\lambda) - ([a_{mts}(715)]/[c_{mts}(715)-a_{mts}(715)]) *[c_{mts}(\lambda)-a_{mts}(\lambda)]$

by using a reference wavelength (715 nm) to determine the proportion of scattering variable with the types of materials present at each cast.

Although method 3 is reputedly the most accurate, the Wetlabs protocol suggests the use of the most appropriate method for the specific site being studied. In the data presented here, using methods 2 or 3 sometimes produced overcorrection of the data, which made some of the values in the spectra become negative. Finally, to obtain total a and b, the addition of pure seawater values is required, taken from Table 2 of Wetlabs manual L.

In summary, the ac9 data were processed using the following protocol:

1. Conversion of data from binary to ASCII, using WAP v4.17
2. Merging of data from different sources connected to the instrument, using WAP 428a
3. Selection of the upcast part of the profile
4. Binning of the data to 0.5 m and application of a median filter
5. Correction of offsets, using the field pure water calibration values where appropriate
6. Correction for temperature and salinity
7. Correction for scattering
8. Addition of pure water values

Steps 3-8 were performed using IDL routines. The program used in step 3 was provided by G. Moore (PML), while the code for steps 4-8 was done by V. Martinez Vicente.

3.3 Instruments comparison: experimental set-up

The first step to understand the contribution of different particles to b_{bp} and its spectral slope (γ_{BS}), is to separate the variations caused by the methodology from those due to marine particles. To test the instrumental effects a comparison between a Wetlabs BB3 and HOBILabs Hydroscat backscatter meters is presented in Chapter 4. Because some differences are found among the instruments, the causes of those differences are investigated by a detailed analysis of the Hydroscat instrument and signal corrections. This included an inter-comparison of four Hydroscats, and a sensitivity analysis, to assess the uncertainty caused by the σ correction on γ_{BS}. Finally, the uncertainties on γ_{BS}, deduced from the inter-comparison and the sensitivity analysis, were compared to the natural variability of γ_{BS} in coastal waters. Details about the methodology of these tests are presented hereafter. The results and discussions concerning these tests are presented in Chapter 4.

The comparison between the Wetlabs BB3 and the HOBILabs Hydroscat-6 was done during the ECOMAR cruise, where both instruments were deployed simultaneously and coincident data from 14 casts are presented. BB3 data were processed according to Section 3.2.5.2 and Hydroscat-6 was processed according to Section 3.2.5.1. Because of failiures in the simultaneous ac-s data, the default parameters of sigma correction were used to process Hydroscat-6. Therefore the comparison presented tested the

backscattering coming from BB3 and that coming from a default processing of Hydroscat-6 (see default parameters in the sensitivity analysis hereafter).

Four Hydroscats (Table 3.4) were deployed in: a) an experimental tank with two concentrations of suspended matter; b) in-situ at two coastal stations typically exhibiting Low Sediment and High Sediment waters off Plymouth Sound.

Table 3.4: Characteristics of the instrument used in the inter-comparison

Instrument	Wavelengths e
HS4-1997	415, 440, 510, 676
HS2-1999	488, 676
HS6-2001	442, 488, 510, 555, 620, 676
HS6-2002	442, 488, 550, 620, 671, 852

During the tank experiments, the instruments were deployed sequentially from a winch to approximately 25 cm from the bottom (Vaillancourt *et al.*, 2004) in a black coated tank filled with $1m^3$ of de-ionised water, maintained at room temperature by re-circulating refrigerated water. The tanks were seeded with 1.0 gm^{-3} (tank 1) and 5.0 gm^{-3} (tank 2) total suspended matter (SPM) samples from the Tamar estuary (Figure 3.12). The sediments in this area have a typical composition of 30% fine silt and clay (<15 μm diameter) (Bale, 2005), however, no particle size distribution measurements were available simultaneously to the optical measurements in the tank experiments. A pump was used to circulate the water and to keep the material in homogeneous suspension and was turned off just before starting the measurements so that all bubbles disappeared.

For the in-situ comparison two stations were sampled: a Low Sediment station (SPM=0.80 gm-3), approximately 15 km outside Plymouth Sound, (50° 15.013' N; 4° 12.507'W), and a High Sediment station (SPM=2.43 gm-3), only a few km from the Sound (50° 20.026'N; 4° 10.021'W) (Figure 3.11). The four instruments were deployed at each station with three of them mounted vertically on the same horizontal crossbar about 30 cm apart, while the HS4-1997 was deployed on a separate frame, 1-2 metres

away from the other instruments. The Hydroscats were suspended below the surface to avoid bubble contamination. At the Low Sediment station, data were recorded at 3-4 m depth for 22 minutes, while at the High Sediment station they were recorded at 1-2 m depth for 7 minutes. $b_b(\lambda)$ data were binned in a similar way for the tank and in-situ comparisons. The tank data were reduced by using a median filter and binned to one second intervals. The in-situ data were also median filtered and binned to one metre intervals. The signal from bubbles was present down to 1.5 m depth in the raw data. This effect was completely removed by considering only data of depths greater than 1.5 m.

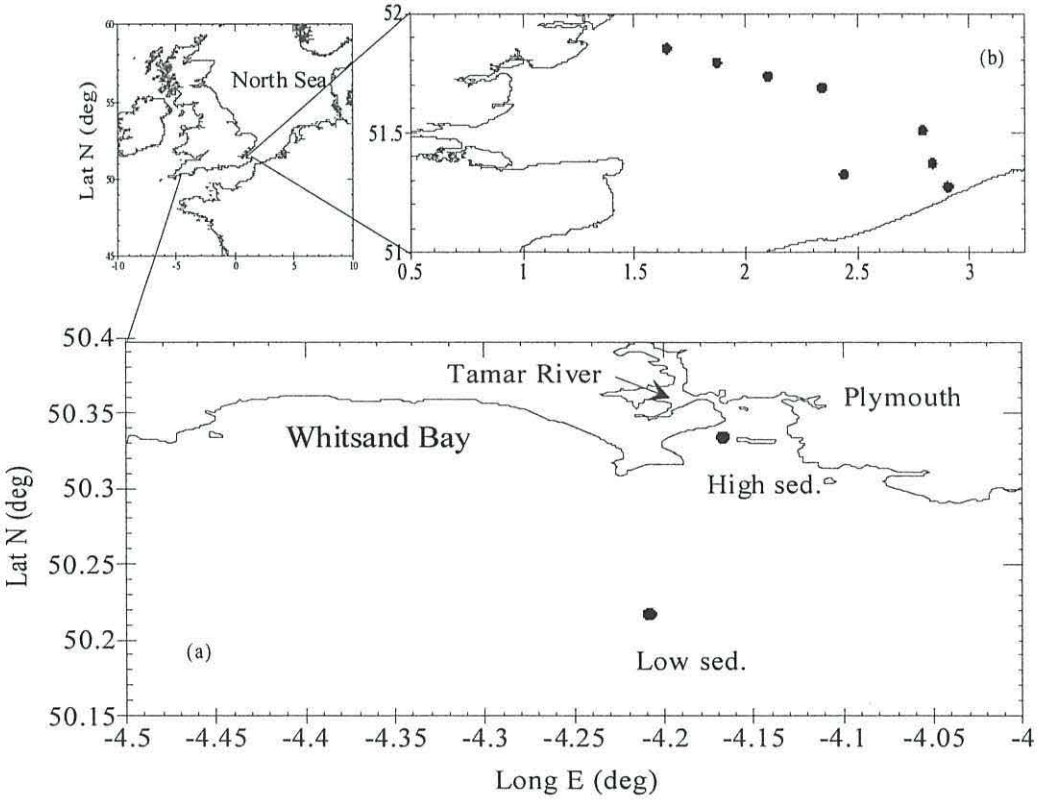

Figure 3.11 Positions of the stations used for: (a) the instrument inter-comparison in the Plymouth Sound, Low Sediment station and High Sediment station, and (b) the parameters range in the sensitivity analysis (North Sea).

The processing scheme used for this experiment was derived from Hydrosoft v2.71 which is slightly different to the processing in v2.73 (presented above). The difference lies in the order of application of the sigma correction. It has been verified that the change in order causes no significant difference to the final results. There are three processing stages: firstly, the transformation of the scattered intensity received by the sensor into the physical value of the volume scattering function or VSF at

approximately 140° [$\beta^u(140°)$]; secondly, the extrapolation of $\beta^u(140°)$ to obtain $b_b{}^u(\lambda)$; thirdly, the σ correction processing to obtain the final product, $b_b(\lambda)$. The comparison between the instruments was done using the values of $b_{bpu}(\lambda)$, and the details of these are given below. The σ correction procedure is described in Section 3.

In the first stage of processing, the signal (S_{norm}) is converted to calibrated units to obtain $b_{bpu}(\lambda)$, by dividing by a temperature dependent term and a gain matrix, to produce $\beta^u(140°)$, using Equation 1. Each instrument used a different set of parameters for this equation. These were obtained from absolute calibrations on each instrument carried out in the same way by HOBILabs (Dana and Maffione, 2002). The temperature term (k_T) was set to zero for all of the instruments. The gain (G_g) and the other calibration constants (R_{nom},α) had different values for each instrument. The effects of the differences in these parameters on $\beta^u(140°)$ are shown in Figure 3.12. For an arbitrary value of S_{norm} and the calibration constants of each instrument at different wavelengths, $\beta^u(140°)$ was calculated using Equation 1. For the three matching wavelengths among instruments, 488, 510 and 620 nm, the coefficients of variation (V) were 41.2, 41.8 and 25.5 % respectively.

In the second stage of processing, $\beta^u(140°)$ was subtracted by $\beta_w(140°)$ (Morel, 1974) to obtain the particle fraction, $\beta_p{}^u(140°)$ (Boss et al., 2004) which was then extrapolated and integrated in the backward direction ($90°<\theta<180°$), to obtain $b_{bpu}(\lambda)$, by using Equation 4 (Boss and Pegau, 2001; Maffione and Dana, 1997)

A factor $\chi_p(140°)=1.08$ was used for all the instruments (Maffione and Dana, 1997; Oishi, 1990). This factor is known to vary with θ, and $\chi_p(140°)=1.18$ has been proposed from $\beta_p(\theta)$ measurements (Boss and Pegau, 2001). Hydroscat is thought to be accurate to 10% (Boss and Pegau, 2001) in the retrieval of $\beta_p{}^u(140°)$ due to the variation in the molecular contribution of water in $110°<\theta<150°$. However, as the focus of this work is on the spectral changes in $b_{bp}(\lambda)$ and the spectral changes of $\chi_p(\theta)$ are unknown, the manufacturer's fixed value for both the instrument inter-comparison and the sensitivity analysis has been used.

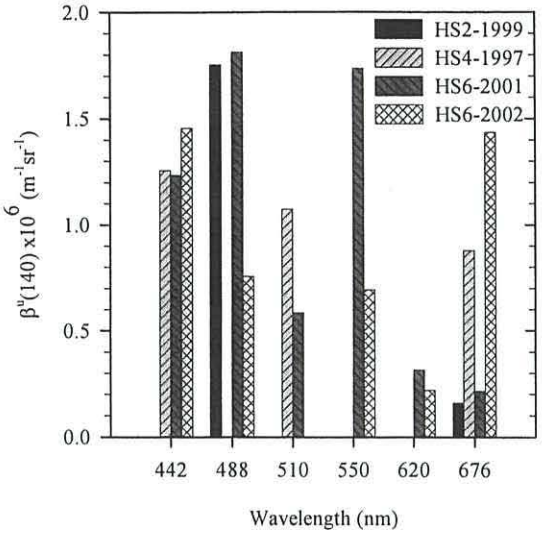

Figure 3.12 Sensitivity of βu(140°) due to differences in the absolute calibration parameters for each instrument (see text).

Once the signal has been transformed into a physical value (i.e. $\beta_u(140°)$), it needs to be adjusted for the attenuation on the way to and back from the sampling volume (Equations 2a and 2b). If a(λ) and b(λ) sampling takes place concurrently to the measurements of $b_b(\lambda)$, their values can be directly substituted into Equation 3 Otherwise, a(λ) has to be modeled according to:

$$a(\lambda) = \{0.06a^*(\lambda)[Chl]^{0.65}\} \cdot \{1 + 0.2\exp[-\gamma_y(\lambda - 440)]\} + \{a_{det}(400)\exp[-\gamma_d(\lambda - 400)]\} \quad \textbf{Eq.8}$$

This formulation for absorption takes into account Chl-a and CDOM using a well established model (Morel, 1991), with an additional term for detrital material [$a_{det}(\lambda)$]: The default values for the parameters are assigned as follows: the specific spectral absorption of phytoplankton ($a^*(\lambda)$) is derived from the literature (Figure 3.14)(Prieur and Sathyendranath, 1981) the Chl-a values, $a_{det}(400)$, spectral slopes of CDOM (γ_y) and detrital absorption (γ_d), are shown in Table 3.5. The scattering term in Equation 3 is modeled by:

$$b_p(\lambda) = [b_b^u(\lambda) - b_{bw}(\lambda)] / \tilde{b}_b \quad , \quad \textbf{Eq.9}$$

which comes from the definition of the backscattering ratio, $\tilde{b}_b = b_b(\lambda)/b(\lambda)$, subtracting the backscattering due to water from the uncorrected values of $b_b(\lambda)$. The default values of $\tilde{b}_b$ are also given in Table 3.5.

Table 3.5: Range of parameters: default from Hydrosoft v2.7, maximum and minimum from in-situ sampling.

Parameter	Minimum	Default	Maximum
$k_{exp}(442)$ ‡	0.137	0.143	0.143
Chl-a	0.42	0.1	9.4
a*(442) ‡	0.05	1.0	0.108
a_{det} (400)	0.06	0.01	0.227
γ_{det}	0.010	0.011	0.014
γ_y	0.010	0.014	0.018
a(442) ‡	0.26		0.671
$\tilde{b}_b$†	0.005	0.015	0.05

‡ Values shown as an example from $k_{exp}(\lambda)$, $a(\lambda)$ and $a^*(\lambda)$ in Fig. 3.

† Literature values (Prieur and Sathyendranath, 1981)

Quality control checks on the inter-comparison data led to the exclusion of some data when the instruments saturated: HS6-2001 saturated at 555 and 676 nm in both tank experiments. For HS4-1997 in the tank experiment with SPM 5.0 gm-3 no data were recorded. Some points were eliminated from the analysis due to calibration problems: 676 nm of HS2-1999 and 620 nm of HS6-2001. The band at 852 nm of HS6-2002 was not considered since none of the other Hydroscats measured at this wavelength. For the tank experiments only the HS6-2002 data were useful, as three of the six wavelengths of HS6-2001 were discarded. Once these data were removed, a Dixon's test was performed to detect outliers in the remaining data and none were detected. To assess the precision of the measurement at each wavelength, the effect of the spectral variation was removed by calculating the residuals of the linear fit between λ and $b_{bp}(\lambda)$. The residuals have an

average V of 3.15 % for the Low Sediment station, 1.63 % for the High Sediment station, 1.21 % for tank 1 and 2.85% for tank 2 comparisons. One way analysis of variance (ANOVA) was used to assess significant differences between instruments.

3.4 Discrete samples

3.4.1 Sample collection and storage

During the cruises, seawater from a CTD rosette was collected in an 8L carboy which was then measured into plastic bottles using a 2000 mL measuring cylinder. This water was used for the SPM, a_p and pigment analyses. Between 250-2000 ml of seawater was filtered under low vacuum pressure onto 47-mm Whatman GF/F filters for SPM, and onto 25-mm Whatman GF/F filters for a_p and pigments analysis. SPM samples were stored in -60°C freezer while a_p and pigments samples were kept in liquid N. In addition to the 8L collected, a further 0.5L was collected in dark, boro-silicate glass bottles for the determination of a_y (see below). During REVAMP cruises only, a_y filtrate was transferred to dark Winchester bottles pre-spiked with 1% NaN_3 and was then kept in fridge until analysis in the laboratory.

Data is presented in Chapter 4 and 7 from weekly sampling at L4 station (50°15'N, 4°13.02'E, bottom depth 55 m) between January 1999 and December 2008. Discrete water samples were collected at a nominal depth of 3 m using the non-toxic supply from the vessel as detailed in Groom *et al.* (2009) followed by the deployment of optical profiling instruments mounted on a stainless steel frame and lowered to a depth of 50 m. The optical data from the profiling instruments were selected at a 5 m depth to minimise bubble effects. For the enumeration of phytoplankton and microzooplankton species abundance and biomass, paired samples were collected from a depth of 10 m. It is worth highlighting the mismatch of sampling depths as a potential source of error in this study: discrete samples (collected at 3 m using the non-toxic supply), profiling instruments data (selected at 5 m) and phytoplankton samples (collected at 10 m using an oceanographic sampling bottle).

The protocols for the analysis of the SPM, pigments and particle absorption given below are based on the REVAMP Protocols (Tilstone *et al.*, 2004) and Groom *et al.*(2009), which contain further details not included here.

3.4.2 Inherent optical properties

3.4.2.1 Particle Absorption coefficients – $a_p[m^{-1}]$

The absorption coefficient of particulate matter (a_p), including that of phytoplankton (a_{phy}) and non phytoplankton (a_{nap}) was determined on a Perkin-Elmer Lambda 800 spectrophotometer retrofitted with a 60 mm spectralon coated integrating sphere (Tilstone *et al.*, 2004). The spectral stability of the instrument was checked at least once a year using absolute standards provided by the manufacturer.

The instrument was auto zeroed with free entrance ports, using high-grade spectralon plates at the exit ports. Baseline flatness was at least ±0.004 A units. Then, 8 spectrophotometric measurements on every sample were made: four before bleaching (to obtain a_p) and four after bleaching (to obtain a_p). The bleaching agent was 3.33% NaClO, (1 % active chlorine). A small volume (~5 ml) of MilliQ was re-filtered through the bleached GFF filter to remove any residual NaClO (Tassan and Ferrari, 1995). Blank filters were also bleached and re-filtered using the same procedure. The disappearance of the peak at 675 nm in the bleached sample and the concave shape of the absorbance spectrum near to 440 nm were used as evidence of complete filter bleaching. Care was taken to ensure that both sample and blank filters did not dry out since this adversely affects the optical density of the sample.

For processing the data there are several path length correction factors that can be used , but the original method by Tassan and Ferrari (1995) was applied in this study and implemented in an IDL routine by G. Moore.

3.4.2.2 Coloured dissolved organic matter absorption coefficient or yellow substance absorption – $a_y[m^{-1}]$

The a_y sample was obtained by filtration through pre-rinsed 0.2µm Whatman Anopore 47mm filters. Glassware was acid cleaned and rinsed with milli-Q water. The filtrate of the MilliQ water was collected in dark boro-silicate glass bottles and used as blank. The samples were prepared and stored as per milli-Q and were allowed to warm to the same temperature as the blank

Samples were run in 10cm cuvettes in dual beam mode Perkin-Elmer Lambda 800 spectrophotometer, same instrument as for a_p measurement but with no integrating sphere. The measurement order was as follows: first, a baseline was done after Autozero the instrument with no sample in the measurement slot. The data collected were monitored to a variance <0.0005 A units and no spectral tendency. A milli-Q scan was then run and between every three samples to check the stability of the instrument. The milli-Q water was discarded and the cuvette was rinsed three times with 5 to 10 ml of the next sample before the scan was performed. Triplicates of the same sample were performed when duplicates were not coincident.

The data processing was automated using an IDL routine that implemented Babin *et al.* method (Babin *et al.*, 2003).The milli-Q water spectrum was subtracted from the sample spectra. A scattering offset correction was performed subtracting to the spectra the average absorbance between 680 and 690 nm. The spectral absorption coefficient of the coloured dissolved organic matter was then calculated from the measured absorbance as:

$$a_y(\lambda) = \frac{2.303A}{l} \qquad \textbf{Eq. 10}$$

where A is the measured absorbance (relative units) and l is the cuvette path length (m).

3.4.3 Biogeochemical measurements

3.4.3.1 Suspended particulate matter and inorganic – organic proportions

Suspended particulate matter concentration is defined operationally as the matter retained by 0.47μm pore filters (Eisma, 1993). Filters were pre-treated and pre-weighed following EU-JRC protocols, with an improvement in the rinsing of the filters following REVAMP protocols (Tilstone *et al.*, 2004), which are based on a precedent study (Van der Linde, 1998). Suspended Particulate Matter concentration (SPM) was calculated for each replicate as the difference between the weight before and after filtration of the sample divided by the volume in litres of sample filtered. A blank filter was weighed for each sample to monitor the drift of the balance (Sartorius R200D).

Mean and standard deviation were calculated from the three replicates. As a quality control criterion for the SPM data, the replicates that produced a coefficient of variation [V=100x(std.dev./mean)] greater than 15% for the same sample were discarded.

Similarly to SPM, other the proportions of Inorganic and Organic Suspended Matter (PIM and POM respectively) were measured. After the SPM was weighed, the filters were burnt at 550°C for four hours in order to remove the organic fraction. Once the filters cooled down, they were weighed. Subtracting that weight from the weight of the filter prior to baking divided by the volume of sample filtered gives the POM. The SPM minus the POM gives the PIM. The PIM and POM have greater associated errors than the SPM determination, given the small amounts present in the filter in relation to the sensitivity of the scale used.

3.4.3.2 Particulate organic carbon concentration – POC

ECOMAR cruise samples were analysed in the laboratory to obtain the particulate organic carbon concentration (POC), by removing inorganic carbonates from the filters by acidification with Sulphurous Acid under vacuum for 24 - 48 hours (Hilton *et al.*, 1986). The filters were dried at 60°C for 48h, packaged in pre-combusted aluminium foil (Verardo *et al.*, 1990) and analysed on a Thermo Finnegan flash EA1112 elemental analyser using Acetanilide as the calibration standard.

3.4.3.3 Chlorophyll-a and phytoplankton pigment determination

Phytoplankton pigment contents used in this PhD were determined using high-performance liquid chromatography (HPLC) by the pigment analytical group at PML. The PML method, based on the method presented by Barlow *et al.* (1997) and adapted for the Agilent 110 series HPLC. The PML method successfully resolves and quantifies over 20 chlorophyll and carotenoids from a variety of water types, ranging from estuaries to oligotrophic oceans. A C_8 column is used in combination with a methanol based binary solvent system following a linear gradient. The method provides good resolution with a run time of 32 minutes excluding a post run time of 7 minutes prior to the next injection. Diode array detection is used with a primary monitoring wavelength at 440 nm to determine chlorophylls and carotenoids and at 660 or 667 nm for the

determination of chlorophyllide and phaeo-pigments. Using this method it is possible to correct the chlorophyll c_1c_2 concentration for any chl-ide contribution. The internal standard, apo-8-carotenal, is used in the extraction solvent to help improve the accuracy of the analysis by taking into account any losses due to evaporation in extraction solvent any inadvertent losses, or incorrect injection volumes. The separation of monovinyl and divinyl chlorophylls a + b plus the carotenoids zeaxanthin and lutein, is achieved over a run time of 32 minutes α- + β-carotene and chlorophylls c_1 and c_2 are not separated by this method.

3.4.3.4 Particle size distribution using a Multisizer

The principle of operation of this instrument is of a resistive particle counting, which relies on sizing and counting pulses of electrical resistance (Jonasz and Fournier, 2007). These pulses are caused by the passage of a particle and the fluid in which it is contained, through a small aperture connecting two chambers containing an electrolyte solution. The resistance is measured by the difference in voltage, at a constant current, between two platinum electrodes submerged in each of the chambers. The intensity of the resistance pulse is approximately proportional to the particle volume. Hence this method defines the particle size as the diameter of a sphere with volume equal to that of the particle (i.e. the equivalent spherical diameter, ESD). The relationship between the intensity of the resistance pulse and the ESD is regularly calibrated using spheres of a known diameter with near monodispersed distributions (generally latex microspheres). The particle size range is defined by the diameter of the aperture between the electrolytes, its diameter ranging from 12 to 1000 μm. The nominal particle size range is 2 to 60 % of the aperture diameter. Potential errors may be associated with the following effects: coincidence, particle shape and breakage. Coincidence of particles produces a reduction of the measured concentration of particles and an increase of concentration of large particles. When this is observed, the sample must be diluted with a particle free electrolyte. The divergence from the spherical shape (i.e. elongated, disk like particles) can produce 20-30 % differences in the response of the Coulter counter. Finally, the breakage of particles passing through the aperture is more likely to happen to detrital (non living organogenic) particles, which are more fragile than living cells. This points out that the use of resistive methods may be more suitable for open ocean

waters than for coastal waters, due to higher amounts of detritus in the coastal environment.

For L4 analysis, particle size distribution was measured using a Coulter Multisizer II, fitted with a tube with an orifice of 100 μm. The setup was fixed to take a measurement on 500μl of sample, which usually took ~12 s. The sampling routine was to use 0.2 μm filtered seawater as the blank and electrolyte. Samples were measured three times and the output was saved on a PC. The data were processed to obtain the particle size distribution slope between 2 and 200 μm by fitting a power law (Bader, 1970) to the data (Markwardt, 2008):

$$N(D) = KD^{-j}$$

where N is the number of particles of diameter D per cubic meter and per micrometer, K is the concentration of particles and j (the Junge exponent) is the slope of the distribution. The R^2 associated with this fit was typically greater than 0.9.

3.4.3.5 Phytoplankton counting using flow cytometry -FCM

This instrument is a laser scanner particle counting (Jonasz and Fournier, 2007). The operation of a flow cytometer relies on two principles: (1) hydrodynamic focusing of a thin filament of sample fluid (including the particles to be measured) at the centre of a particle free fluid (sheath fluid) in order to maintain the optimal position of the filament to obtain the best signal to noise ratio, (2) the rapid measurement of the optical properties of the sample on a single particle basis (i.e. light scattering, fluorescence).

Analytical flow cytometry (AFC) samples for the ECOMAR cruise were fixed with pre-filtered (0.2 micron) gluteraldehide to a final concentration of 1%. Samples with gluteraldehide were left during at least 1h at 4°C in the dark and then flash frozen in liquid N and stored at -80 °C until analysis in the laboratory. Analysis was carried out using Becton Dickinson FACSort and Coulter FACScan flow cytometers. Following standard procedures (Tarran *et al.*, 2006; Tarran *et al.*, 2001) the following planktonic groups were quantified in the samples: heterotrophic bacteria, *Prochlorococcus* spp., *Synechococcus* spp., picoeucaryotic phytoplankton, nanophytoplankton, cryptophytes and coccolithophores. Heterotrophic bacteria were separated into high nucleic acid

content and low nucleic acid content. Coccolithophorid abundances were non significant throughout the cruise, and are not reported here. It is worth stressing that the organisms counts were triggered by fluorescence rather than by side scattering, which means that only fluorescent particles (photosynthetic or stained bacteria) were counted, and not the whole particle population.

3.4.3.6 Phytoplankton counting using microscopy identification - Microscopy

Additional to the phytoplankton counts using FCM, in this thesis phytoplankton counts from microscopy are used in Chapter 7, as detailed by Widdicombe *et al.* (JPR, accepted). Briefly, samples are preserved with 2% Lugol's iodine solution and 4% buffered formaldehyde. Between 10 and 100 ml of sample, depending on cell density, are settled for >48 hours and cells are identified where possible to species level and enumerated. Cell sizes between 2 and 200 μm were converted to volume and then to carbon using the equations of Menden-Deuer *et al.* (2000). The use of this updated method to calculate carbon from cells counts reduced carbon estimates by less than 10% globally compared with previous estimates (Llewellyn *et al.*, 2005). From the species carbon, phytoplankton was grouped into: diatoms, dinoflagellates, phyto-flagellates (between 2 and 10μm), *Phaeocystis* spp., coccolithophorids and heterotrophic Dinophyceae. Phytoplankton carbon (phytoplankton-C), is hereafter referred to the sum of the carbon contributions from each of the phytoplankton groups above (i.e. diatoms, dinoflagellates, phyto-flagellates, *Phaeocystis* spp. and coccolithophorids) plus the heterotrophic Dinophyceae, because of the presence of photosynthetic pigments (Roger Harris pers. comm.). Percentages of each phytoplankton component are referred to the total phytoplankton-C as defined here. It is worth stressing that no picoplankton nor bacteria counts were included in this phytoplankton-C estimate.

3.5 Summary of measurements

In Table 3.6 a summary of the parameters available at each sampling region with number of data for each parameter, is presented. Chapter 4 will make use of the data from the North Sea cruises (BE 02/14 and BE 03/16). Chapter 5 and 6 will make use of the information derived from the data collected during ECOMAR cruise, while Chapter 7 will make use of the data from L4.

Table 3.6: Summary of the parameters available (√) or not (X) at each in-situ study site and number of stations visited (or sampling dates for the time series at L4).

	In situ			
Parameters Available	North Sea BE 02/14	North Sea BE 03/16	ECOMAR JC011	L4
N of stations	19	19	22	175
HS6	√	√	√	X
VSF or BB3	X	X	√	√
ac9+ or acs	X	X	√	√
a_p,a_{phy},a_{nap}	√	√	√	√
a_y	√	√	X	√
Pigments	√	√	√	√
SPM,PIM,POM	√	√	X	√
POC	X	X	√	X
Coulter Counter	X	X	√	√
FCM	X	X	√	X
Microscopy	X	X	X	√

As a conclusion from this chapter, several instruments were available to measure backscattering at the initial stages of this PhD work. From them, the backscattering slope (or better, the exponent of the power law that fits the backscattering spectrum) has been calculated. However, the adequacy of such power law to describe spectral variations in backscattering has not been studied. This uncertainty is added to the fact that the study of spectral variations falls outside the scope of the hypothesis being tested. These two factors cause that, although the spectral variations (in terms of

spectral slopes) will be shown throughout the thesis, the study of this property will be given secondary importance within the text and should be borne in mind when drawing conclusions from these slopes.

Chapter Four

Uncertainty of in-situ measurements of spectral backscattering

CHAPTER FOUR: UNCERTAINTY OF IN-SITU MEASUREMENTS OF SPECTRAL BACKSCATTERING

Synopsys

In this chapter, b_{bp} and γ measured by two different instruments (HOBILabs Hydroscat backscatter meter and Wetlabs BB3) are compared. Significant differences were found between instruments only for γ, which in this study is a parameter of secondary interest due to uncertainties in its calculation (see Chapter Three). Results presented in this Chapter are purely an illustrative exercise of the sensitivity to calibration and correction (σ correction) of the measurements collected with the Hydroscat backscatter meter (hereafter Hydroscat). The difficulties associated with the use of Hydroscat are highlighted in the conclusions of this Chapter.

4.1. Comparison of b_{bp} from Hydroscat-6 and BB3 instruments

The sensitivity of b_{bp} and γ_{BS} from HOBILabs Hydroscat-6 to the sigma correction parameters is important in the context of this thesis because this instrument was available for the ECOMAR cruise together with a Wetlabs BB-3 (see Chapter 3). However, during that cruise there were no concurrent valid measurements of absorption and scattering to produce an accurate sigma correction. Therefore the default parameters were used. The comparison between the two instruments at a similar wavelength was very close (Figure 4.1.a), with a slight underestimation by the Hydroscat-6 (on the linear scale, the regression was $b_{bp}(532)_{HS6}= 0.87\ b_{bp}(550)_{BB3}+ 0.0003$, $r^2=0.76$, N=1333). However, the spectral slopes did not show a significant correlation (Figure 4.1.b).

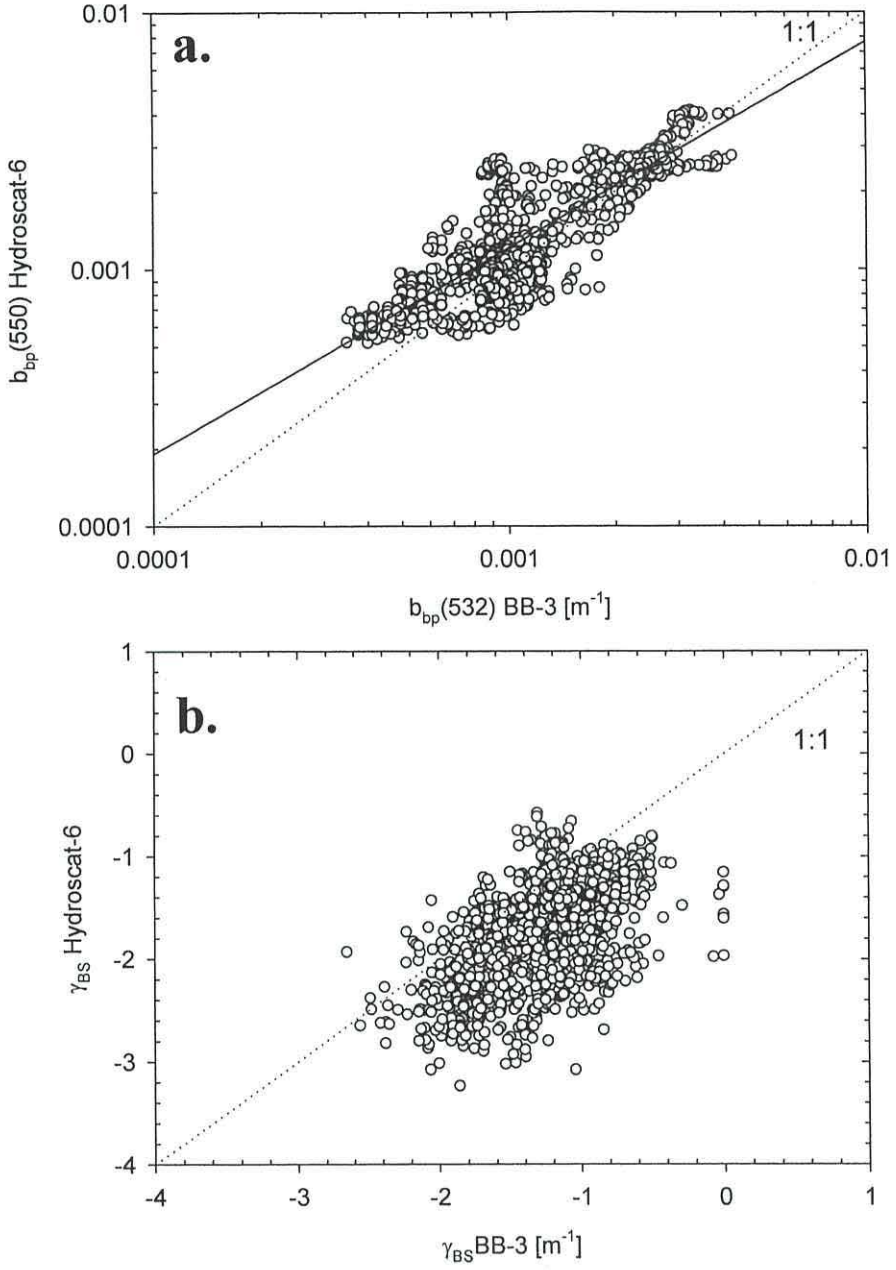

Figure 4.1 Comparison between HOBILabs Hydroscat-6 (HS6) and Wetlabs BB3 measurements of: a) b_{bp} .Note that the backscattering for the two instruments is given at two different wavelengths. Solid line is the power law fit to the data : $b_{bp}(532)_{HS6}= 0.31 \times b_{bp}(550)_{BB3}^{0.8}$, $r^2=0.76$, N=1333. b) γ_{BS}

4.2. Sensitivity analysis and parameters range

The sensitivity analysis presented here aims to quantify the effects of the optical calibration and of the in-situ attenuation on γ. In the first instance (hereafter Test A), two hypothetical spectra $b_{bp}^{u}(\lambda)$ were used as input to Equations 2.a and 9 in Chapter 3 and sequentially changed the parameters in Equations 8 and 9 in Chapter 3 according to the range in the literature and observed in-situ values. In Test B, $b_b^{u}(\lambda)$ in-situ from the same instrument at several stations was used as an input to the Equations 2a and 9 from Chapter 3, and the parameters measured at those stations were substituted in Equations 8 and 9 from Chapter 3.

For Test A, two hypothetical spectra were used as input values of $b_{bp}^{u}(\lambda)$ with wavelengths corresponding to some of the instruments (HS6-2001 and HS6-2002) from the inter-comparison: 442, 488, 550, 620 and 671 nm. These synthetic spectra of $b_{bp}^{u}(\lambda)$ had corresponding slope values of γ_u=0.1 and γ_u=2.0 and high and low absolute values respectively, which are typical of Case 2 and Case 1 scenarios. The γ_u were derived from theoretical studies (Morel and Maritorena, 2001) and Hydroscat measurements (Maffione and Dana, 1997b; Vaillancourt *et al.*, 2004). Then, $b_{bw}(\lambda)$ was added to $b_{bp}^{u}(\lambda)$ before applying the $\sigma[K_{bb}(\lambda)]$. A reference slope (γ_{ref}) for each scenario was obtained using the input spectra combined with the default parameters in Equations 8 and 9 from Chapter 3.

Once the input spectra were defined for Test A, $k_{exp}(\lambda)$ was varied in Equation 2.b (Chapter 3) according to the values in Figure 4.2.a, that shows how this constant varies among instruments and for the same instrument over time. To illustrate the sensitivity of the same instrument to different calibrations the values of $k_{exp}(\lambda)$ of HS6-2002 were changed from the calibration in 2002 to the 2005 calibration. Also were changed the parameters of Equations 8 and 9 (of Chapter 3) according to the measured values given in Table 3.4, from stations sampled in the North Sea and the Western English Channel in 2002 and 2003 (Figure 3.12 for the positions of the stations used). The range of in-situ values of $a(\lambda)$ and $a^*(\lambda)$ are shown in Figure 4.1.b and c and were collected using the methods described in Chapter 3. For the scattering term values in Equation 9 (Chapter 3), there were no concurrent $b(\lambda)$ available,

therefore the range in b_b was derived from the literature (Boss *et al.*, 2004; Ulloa *et al.*, 1994). The resulting γ from this sensitivity analysis was compared to the γ_{ref}.

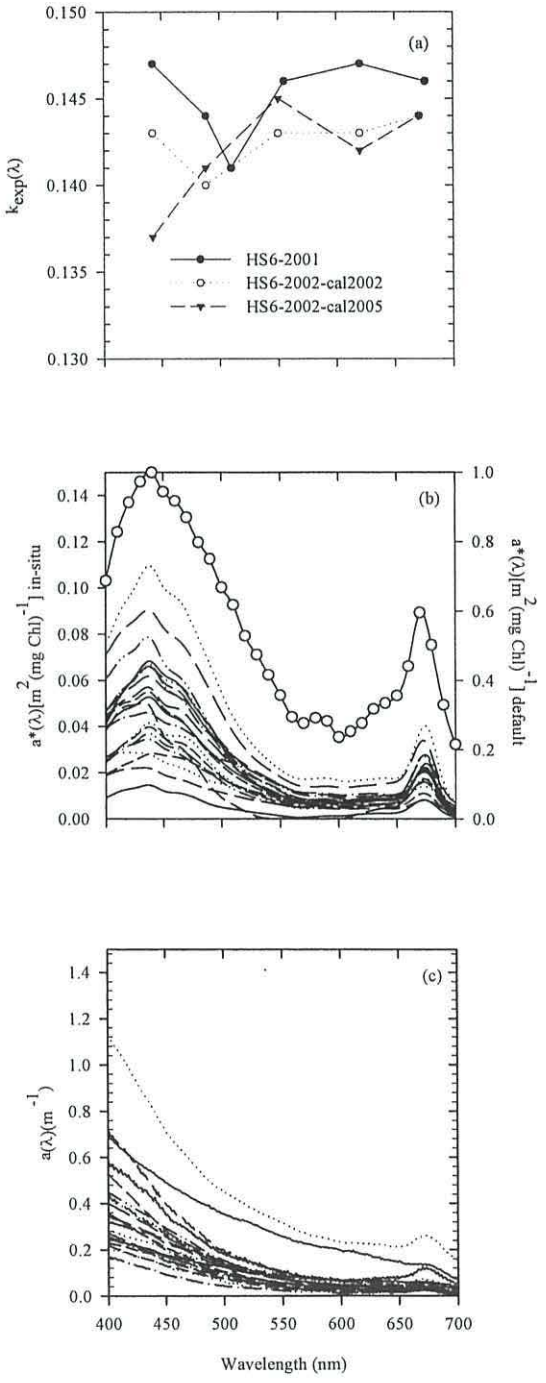

Figure 4.2 Range in default and measured spectral parameters used for the sensitivity analysis: a) $k_{exp}(\lambda)$, b) $a^*(\lambda)$, where the line with empty circles are the default values provided in Hydroscat and c) $a(\lambda)$.

Test B not only compared the effect of a simultaneous change in the parameters of the σ correction to the sequential change of the parameters (Test A), but it also included the effect of the natural variability of γ. The 20 $b_b^u(\lambda)$ in-situ profiles from one instrument (HS6-2002) were processed using two sets of parameters: the default parameters (Table 3.4) and the co-incident in-situ values of $a(\lambda)$ (Figure 4.2). At each position, γ was calculated for each set of parameters, producing γ_u, γ_{ref} and γ using in-situ $a(\lambda)$, as defined above. No scattering terms ($b(\lambda)$ or $\tilde{b}_b$) were concurrently measured, so the default values of these parameters were used.

4.3. Results of Hydroscat-6 intercomparison

The spectrally averaged $b_{bpu}(\lambda)$ of all instruments for tank 1 was 0.019±0.002 m^{-1} (mean ± standard deviation), but was higher for tank 2, 0.037±0.002 m^{-1}. While there was a difference between the tanks, there was an agreement between the instruments and no significant difference was recorded in the residuals of $b_{bpu}(\lambda)$ of each instrument in tank 1 ($p=0.68$) or in tank 2 ($p=0.94$) (Figure 4.2).

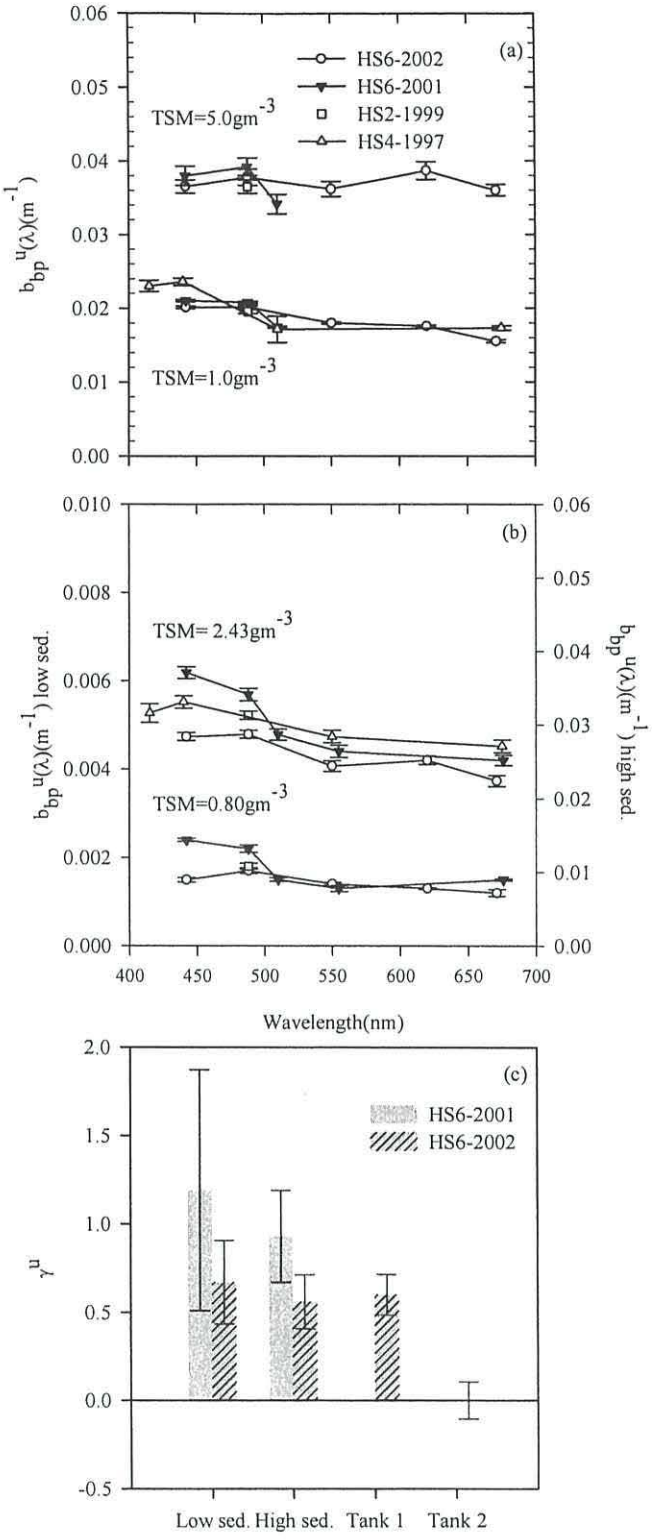

Figure 4.3 b_{bp}^{u} (λ) from instruments inter-comparison a) tank experiments b) field comparison. Symbols are averages over depth or time for each plot, error bars are S.D. c) γ of b_{bp}^{u} (λ), error bars are S.E. derived in the calculation of γ according to Equation 5 in Chapter 3.

However, there were significant differences between the residuals of $b_{bp}^{u}(\lambda)$ of each instrument at the Low Sediment station (p=0.004), but there were no differences at the High Sediment station (p=0.07) (Figure 4.2). For the Low Sediment station, HS4-1997 caused the differences observed. When this spectrum was removed from the analysis, V was reduced to 1.61% and the differences between the residuals of $b_{bp}^{u}(\lambda)$ were eliminated (p=0.28). The spectral average of $b_{bp}^{u}(\lambda)$ for the Low Sediment station was 0.0016±0.0004 m^{-1}, while for the High Sediment station was higher 0.029±0.004 m^{-1}. In order to have an independent estimate of the values expected at these two stations, the particle backscattering was calculated from a model for Case 1 waters (Morel and Maritorena, 2001). Chl-a values at the Low Sediment station were measured using HPLC: 1.91mg m^{-3} and at the High Sediment station as 2.46 mg m^{-3}. The backscattering for this model is spectrally constant and gives 0.0029 and 0.0033 m^{-1} for the Low Sediment and the High Sediment stations, respectively. The model gives the same order of magnitude as the measurements of $b_{bp}^{u}(\lambda)$ at the Low Sediment station but it underestimated $b_{bp}^{u}(\lambda)$ by a factor of 10 at the High Sediment station.

The percentage difference calculated from comparing the residuals of $b_{bp}^{u}(\lambda)$ for each instrument with the mean of the residuals in each situation (i.e. tank 1, tank 2, Low Sediment and High Sediment stations, Chapter 3) is summarized in Table 4.1. The precision (range of those differences) was higher for the tanks than at the stations of the inter-comparison.

Table 4.1: Percentage difference of the residuals from the mean for the instrument inter-comparison

Instrument	Difference (%)			
	Tank 1 (n=9)	Tank 2 (n=13)	Low Sediment (n=11)	High Sediment (n=15)
HS4-1997	-0.21			1.63
HS2-1999	-2.95	-1.83	0.96	1.97
HS6-2001	1.78	1.59	4.59	3.19
HS6-2002	-0.31	-0.59	-4.78	-4.89
Range	4.74	3.42	9.37	8.09

The γ^u was selected for only the two instruments with the most similar spectral configuration: HS6-2001 and HS6-2002. Generally, γ^u decreased with increasing suspended matter concentration (Figure 4.1). HS6-2001 had a greater variation in γ^u than HS6-2002 for the in-situ stations of the inter-comparison. For HS6-2001, γ^u varied from 1.19 to 0.93 and for HS6-2002 it ranged from 0.67 to 0.56, which followed the same decreasing trend with increasing SPM as the data from the in-situ stations.

4.4. Results of sensitivity analysis

The results of Test A in terms of γ^u, γ_{ref} and γ for each parameter and scenario are summarized in Table 4.2. The slopes increase slightly due to the σ correction in both scenarios and for all the parameters tested. The increase from γ^u to γ_{ref} was from 2.0 to 2.064 and from 0.1 to 0.134 for the Case 1 and Case 2 scenarios respectively.

Table 4.2: Values of γ and mean absolute variation † resulting from the sensitivity analysis (Test A)

	Case 1 scenario			Case 2 scenario		
	Min	Max	Mean absolute variation	Min	Max	Mean absolute variation
$k_{exp}(\lambda)$	2.061	2.064	0.001	0.121	0.121	0.013
Chl-a	2.145	2.071	0.044	0.195	0.140	0.033
$a^*(\lambda)$	2.060	2.059	0.004	0.132	0.131	0.003
$a_{det}(\lambda)$	2.118	2.062	0.028	0.184	0.133	0.025
γ_{det}	2.063	2.064	0.000	0.134	0.135	0.000
γ_y	2.064	2.064	0.000	0.134	0.134	0.000
$a(\lambda)$	2.316	2.120	0.154	0.330	0.179	0.120
$\tilde{b}_b$	2.024	2.175	0.075	0.115	0.184	0.035

† The mean of the absolute variation is defined as $\left| [(\gamma_{min} - \gamma_{ref}) + (\gamma_{max} - \gamma_{ref})]/2 \right|$

The magnitude of this result is more easily understood with an example: with a hypothetical $b_{bp}(550)=0.00496$ m^{-1}, one could use $\gamma^u = 2.0$ to extrapolate $b_{bp}(\lambda)$ spectrally to $b_{bp}(442)$ with a value of 0.00768 m^{-1}. However, if $\gamma_{ref} = 2.064$ was used instead, $b_{bp}(442)$ would equal 0.00779 m^{-1}. In this example, the percentage difference in $b_{bp}(442)$ would increase by 1.4% by using the γ_{ref}. Following the same reasoning but for $b_{bp}(550)=0.0495$ m^{-1} with $\gamma^u=0.1$ and $\gamma_{ref}=0.134$, $b_{bp}(442)$ would be 0.0506 and 0.0510 m^{-1} respectively, and would produce increase of 0.8% in the estimate of $b_{bp}(442)$. According to these results, there is a very small influence of $\sigma[Kbb(\lambda)]$ on γ_{ref} compared to γ^u. Consequently, the impact on point λ values is almost negligible and of similar magnitude in the two hypothetic situations (<2%).

After assessing the differences between γ^u and γ_{ref}, the effects of each parameter on the σ correction were analyzed. Surface plots of $b_{bp}(\lambda)$ are presented (Figure 4.4) for the Case 1 scenario ($\gamma^u=2.0$), for a parameter range derived from the literature (Kirk, 1994). The range derived from observations (Table 3.4) occurs at the lower limit of Figure 4.2. γ obtained from the maximum and the minimum of each parameter are summarized in Table 4.2. The factors that affected γ most were $a(\lambda)$, $\tilde{b}_b$, Chl-a and $a_{det}(400)$ in decreasing order of importance in both scenarios. The averaged absolute difference between γ_{ref} and γ from $a(\lambda)$, was 0.154 and 0.120 for Case 1 and Case 2 respectively. The same values calculated for the $k_{exp}(\lambda)$ produced 0.001 and 0.013 respectively. This suggested that the uncertainty due to the optical calibration was smaller than that due to $a(\lambda)$. These changes were also greater than those produced by the parameters in the absorption model Equation 8 (from Chapter 3), whose average variation was between 0.0 and 0.075 (Table 4.2). This suggests that the default model may not be describing correctly the absorption effects, for the range of our measured parameters. In addition, the effect of changing $a(\lambda)$ in Equation 3 (Chapter 3), was greater than the differences between γ_{ref} and γ^u: 0.154 and 0.120 for γ from $a(\lambda)$ versus γ_{ref}, compared to 0.064 and 0.034 for γ_{ref} versus γ^u in the Case 1 and Case 2 scenarios respectively.

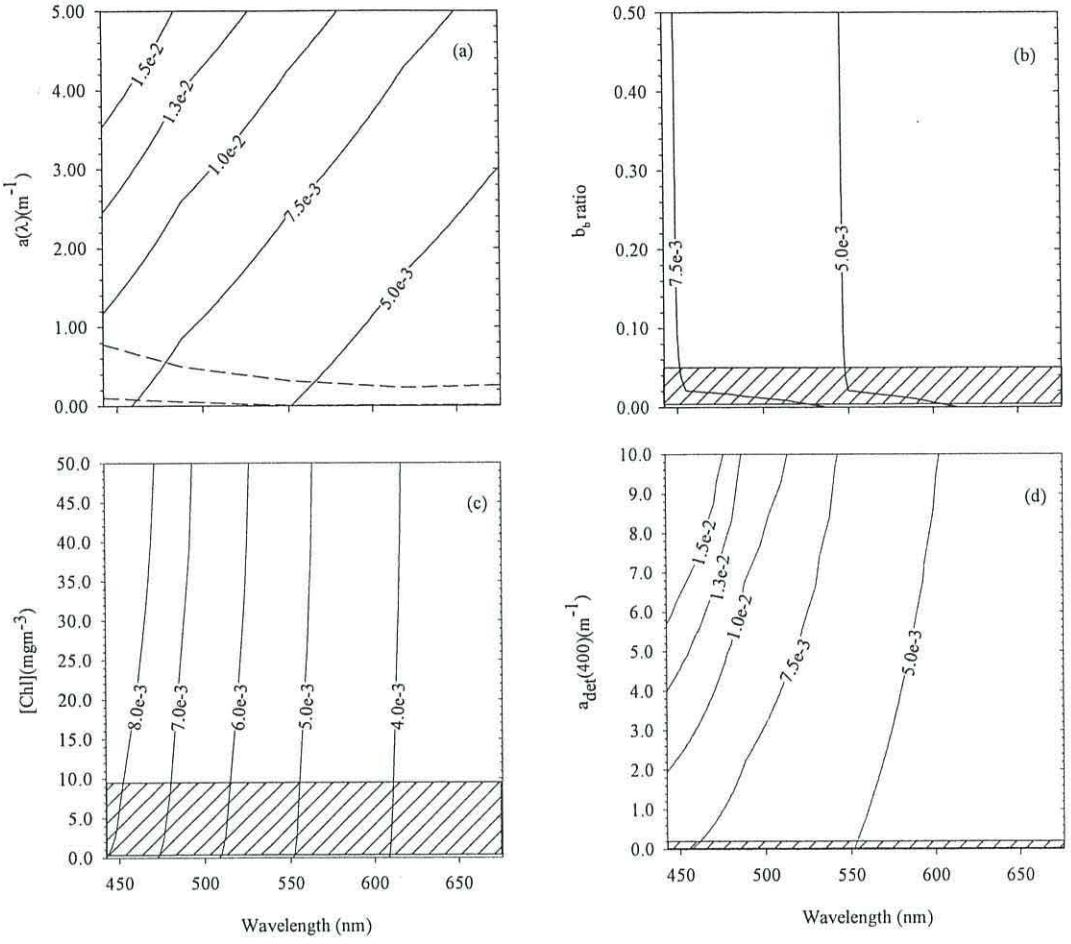

Figure 4.4 $b_{bp}(\lambda)$ results from the sensitivity analysis (Test A) at hypothetical Case 1 scenario for a range of values of: a) $a(\lambda)$, b) $\tilde{b}_b$, c) Chl-a ([Chl] label in the y axis) and d) $a_{det}(400)$. Superimposed to each sub-figure, the dotted lines in a) and the shadowed area in b), c) and d) define the range from the measured data (Table 3.5).

To estimate the influence of these variations in γ on point values of $b_{bp}(\lambda)$, the same example as above for a change in $a(\lambda)$ in Equation 7 (Chapter 3) can be used. The minimum $a(\lambda)$ from Figure 4.2.c, produces a γ=2.32. Using $b_{bp}(550)$=0.00496 m^{-1} and γ=2.32, one obtains $b_{bp}(442)$=0.00823 m^{-1}. This value, compared to the reference $b_{bp}(442)$=0.00779 m^{-1}, obtained with γ_{ref}=2.06, means an increase by 5.7% of the

estimated $b_{bp}(442)$. The same calculations for the Case 2 scenario, produced a similar increase (5.2%) in the estimate of $b_{bp}(442)$ with respect to the reference.

In Test B, the average γ^u, γ_{ref} and γ using in-situ surface $a(\lambda)$ between 2 and 5 m at each station was related to Chl-a (Figure 4.5). The tendency of γ to decrease with increasing Chl-a was not altered by the use of the σ correction with default or in-situ values. The trend in the data follows a similar one to the values predicted by the model for Case 1 waters by Morel and Maritorena (2001), although their estimates of γ are lower.

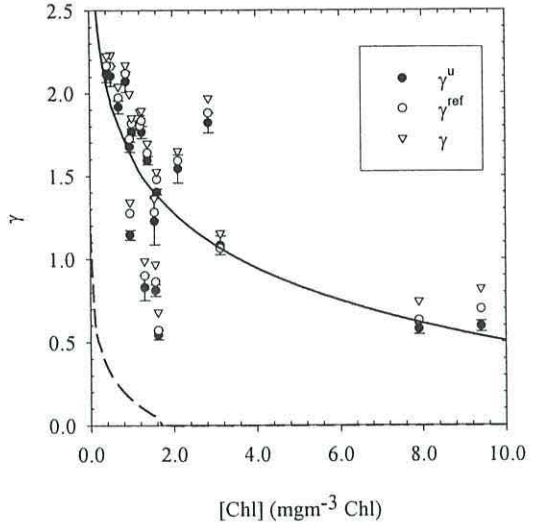

Figure 4.5 Spectral slopes for Test B: $-\gamma^u$, $-\gamma_{ref}$ and $-\gamma$ from using $a(\lambda)$ as a function of Chl-a ([Chl] in the x axis of the figure). Error bars on γ^u are standard deviation. Solid line are the predicted values of a non linear regression : $\gamma^u=1.61-0.48\log_{10}$(Chl-a), $r^2= 0.94$,n=20). Dotted line is the γ produced using Morel and Maritorena (2001) for comparison.

The mean γ^u over depth and stations was 1.284±0.160 (mean ± standard deviation), while for γ_{ref} gave 1.351±0.160 and for γ processed with $a(\lambda)$ gave 1.444±0.170. The calculated mean and standard deviation of the differences between γ^u and γ_{ref}, and between γ_{ref} and γ at each depth and for each station. Then the global mean of the differences for all the stations (N=20) and the mean of the standard deviations were calculated. The first comparison (γ^u with γ_{ref}) gave a mean difference and standard deviation of 0.039±0.028 and produced an increase in $b_{bp}(442)$ of 1.5%. The second

comparison (γ_{ref} with γ) gave a mean difference of 0.060±0.035 and gave an increase in $b_{bp}(442)$ of 2.1%.

4.5. Discussion and conclusions: effects of the sigma correction on backscattering measurements from Hydroscat-6

From observations of backscattering in controlled laboratory conditions, Vaillancourt *et al.* (2004) found that the variability of the spectral slope of the mean backscattering efficiency factor varied between 0.0046 and 2.32, which is within the range of our measurements. With respect to the uncertainties due to different absolute calibration parameters, on measuring in-situ γ, it has been shown (Maffione and Dana, 1997b) that the standard errors of γ are sensitive to changes from turbid to clear waters, increasing from turbid (0.01 to 0.14) to very clear waters (0.15 to 0.2). In the present comparison, it was also found that the standard error for γ increased in all situations from turbid to clear waters for two instruments (Figure 4.3.c). The comparison between the two Hydroscats (HS6-2001 and HS6-2002), produced two fold differences in γ. One explanation for these differences may be that these two instruments had different absolute calibration parameters (Figure 4.2). For these two instruments, the percentage differences derived from Figure 4.3 for the co-incident wavelengths (442 and 488 nm) were 18 and 58% respectively, which could account for most of the difference in γ. Given the few data analyzed, further research should analyze further the influence of the absolute calibration on the measurements of γ using Hydroscat.

In the sensitivity study, other possible sources of artificial changes in γ were addressed: the optical calibration parameter, $k_{exp}(\lambda)$, and the σ correction. By using a sensitivity analysis with a wide range of parameters (i.e. changing $k_{exp}(\lambda)$, $a^*(\lambda)$, Chl-a, γ_d, γ_y, $a_{det}(400)$ and $\tilde{b}_b$ and $a(\lambda)$ sequentially) from different calibration values, literature values and realistic values from measurement in coastal waters. The assumption in these results was that the spectral variation of $b(\lambda)$ was not significant compared to $a(\lambda)$. The maximum differences produced by the σ correction were found when $a(\lambda)$ was used in Equation 7 (Chapter 3). The effects of changing $k_{exp}(\lambda)$ compared to $a(\lambda)$ were insignificant for the range of values available. However, there were two limitations in this study, first was the assumption that there was not spectral

variation in χ_p. Some theoretical studies have addressed the spectral variation of the $b_b(\lambda)$,(Bricaud and Morel, 1986) but their work did not consider the spectral variations of the VSF to derive $b_b(\lambda)$. The second limitation of this study was that variations of $b(\lambda)$ were not considered in the sensitivity analysis. This was constrained by the lack of co-incident $b(\lambda)$ measurements. From a model of $b(\lambda)$ based on observations in Case 1 and Case 2 waters, (Gould *et al.*, 1999) the slope of $b(\lambda)$ can vary between -0.0044 in turbid waters and -0.00018 in clear waters. Spectral variations of $b(\lambda)$ would increase the difference between γ_{ref} and the corrected γ and would make the measurement truly independent, as $b_{bp}{}^{u}(\lambda)$ is used in the σ correction as an estimator of $b(\lambda)$ in Equation 9 (Chapter 3). In the last part of the sensitivity analysis, in-situ backscattering was processed with the default parameters and with coincident $a(\lambda)$ at a number of stations in European coastal waters. It was observed that using the σ correction with in-situ $a(\lambda)$ does not significantly affect the measured γ compared to the natural variation of γ.

The original description of σ correction (Maffione and Dana, 1997a, 1997b), follows an exponential law as it is derived from the ratio between the empirical weighting function of filtered sea water $W(z;c_w(\lambda))$ and the empirical weighting function of the sampled volume $W(z;c(\lambda))$, which is $\exp(-c(\lambda)r)$, where r is the sum of the distance between the lamp and the target volume and back to the sensor and $c(\lambda)$ the attenuation due to particles and water. Their empirical measurements (Maffione and Dana, 1997a) relating σ to $c(\lambda)$ showed that there was a 10% change in σ when $c(\lambda)$ varied from 0.02 to 1 m^{-1}. Variations in $c(\lambda)$ had only a small effect on σ for small values of $c(\lambda)$. However, for higher values of $c(\lambda)$, between 5 and 6 m^{-1}, a 10% change in σ was obtained, which is higher than the change in σ produced by lower $c(\lambda)$ values. HOBILabs Inc. modelled this dependency on $c(\lambda)$ as a function of the absorption and scattering coefficients (HOBILabs, 20004). The effect of the attenuation was considered to be merely to decrease the signal of the measured $b_b(\lambda)$. However, another effect of the attenuation on the Hydroscat measurements is the influence on the scattering angle measured (θ). Maffione and Dana (1997a) showed that the effect of changing $c(\lambda)$ from 0.02 m^{-1} to 0.5 m^{-1} had a very small effect on θ, and caused a change from 141° to 134°, higher values of $c(\lambda)$, however, were not considered in their study. Based on the Maffione and Dana (1997a) data, if one assumes a linear decrease in θ with increasing $c(\lambda)$, for $c(\lambda)=2$ m^{-1}, θ becomes ~112°. $K_{bb}(\lambda)$ (the $c(\lambda)$ for Hydroscat viewing geometry) can be derived at 442 nm using

Equations 7 and 9 (Chapter 3) and the maximum attenuation values in this study. The parameters used for this calculation were $a(442)=0.671\ m^{-1}$, $b_{bp}^{u}(\lambda)=0.0510$ and $\tilde{b}_b=0.015$. The resulting $K_{bb}(\lambda)$ was $2.031\ m^{-1}$ which was higher than the range of the attenuation considered by Maffione and Dana (1997a). It could therefore be necessary to take into account $c(\lambda)$ for the correction of θ in turbid waters, in addition to the current reduction of the signal. An explicit way of accounting for the effect of the change of angle of measurement due to $c(\lambda)$ should be formulated to retrieve the $b_{bp}(\lambda)$ based on a comparison of the Hydroscat measurements with angular measurements of VSF.

From the results from this exercise, the parameters of the model used in the correction of the backscattered signal are shown to have little influence on the spectral slope of the resulting $b_{bp}(\lambda)$. Accounting for the absorption using the default method and parameters had little effect on the final value of the spectral slope of $b_{bp}(\lambda)$, which is more sensitive to the parameters of the absolute calibration of the instrument. This study has not taken into account the role of scattering on the correction (typical of SPM dominated coastal waters).

It has been shown (in the Methods, Chapter 3) that the correction of Hydroscat-6 data depends heavily on the co-incident measurements of absorption and scattering, which in turn are difficult to obtain with high accuracy. Additionally, it has been shown in Chapter 4 that there is a sensitivity of backscattering from Hydroscat to the absolute calibration and that for some of the data collected there is uncertainty on where the variability comes from instrument artifacts. Therefore, as a conclusion from this chapter, all of the data available from Hydroscat-6 were not used in the remaining of this thesis and and only Wetlabs BB3 (and VSF3) will be used hereafter.

Chapter Five

Backscattering related to chlorophyll and particulate organic carbon in the open ocean

CHAPTER FIVE: BACKSCATTERING RELATED TO CHLOROPHYLL AND PARTICULATE ORGANIC CARBON IN THE OPEN OCEAN

Synopsys

In this chapter, simultaneous measurements of Chl-a, POC and particle backscatter coefficient (b_{bp}) are presented for the sub-polar front region of the North Atlantic collected during summer 2007. In this sampling region, the Mid-Atlantic Ridge (central Atlantic), the empirical relationships between b_{bp} and bulk biogeochemical indicators of phytoplankton stocks will be tested. The relationships between b_{bp} and chlorophyll-a concentration (Chl-a) and particulate organic matter concentration (POC) are compared to global relationships from the literature. The relationships with Chl-a are consistent with current knowledge, but diverge for POC. Results are discussed in terms of the particulate matter composition using as an indicator the POC:Chl-a ratio. The results presented in this chapter highlight the need for a new approach to gain better insight into the causes of variation of backscattering which are then presented in Chapter 6.

5.1 North Atlantic Sub-Polar Front environment

5.1.1. Hydrography

The Charlie Gibbs Fracture Zone (CGFZ), located over the Mid-Atlantic Ridge (Chapter 3), had a high surface temperature gradient (Figure 5.1.a) during the ECOMAR cruise (Figure 5.1.b). Southern casts of the CTD detected warmer (~15.5°C) and more saline (~35.6 psu) waters. Across the CGFZ subpolar front, average surface temperature dropped to ~13.4°C and salinity to 35.0, with cold waters at shallow depths (7°C at 40 m). North station average surface temperature to the West of the ridge was 10.5°C, slightly lower than to the East of the ridge (11.2°C), and salinity was slightly higher to the West than to the East (34.9 as compared to 34.8). These differences, however, were not statistically significant and therefore casts to the East and West of the ridge at the North of the subpolar front will be treated hereafter as one, the North station. Mean mixed layer depth at the South (N of casts =5) was 43.1 ± 7.3 m (mean± standard deviation). Across the front, at the TOPEX transect, the mixed layer became shallower (22.7± 9.5 m, N of casts =8). At the North the mixed layer deepened (40.6 ± 8.3 m, N of casts = 9).

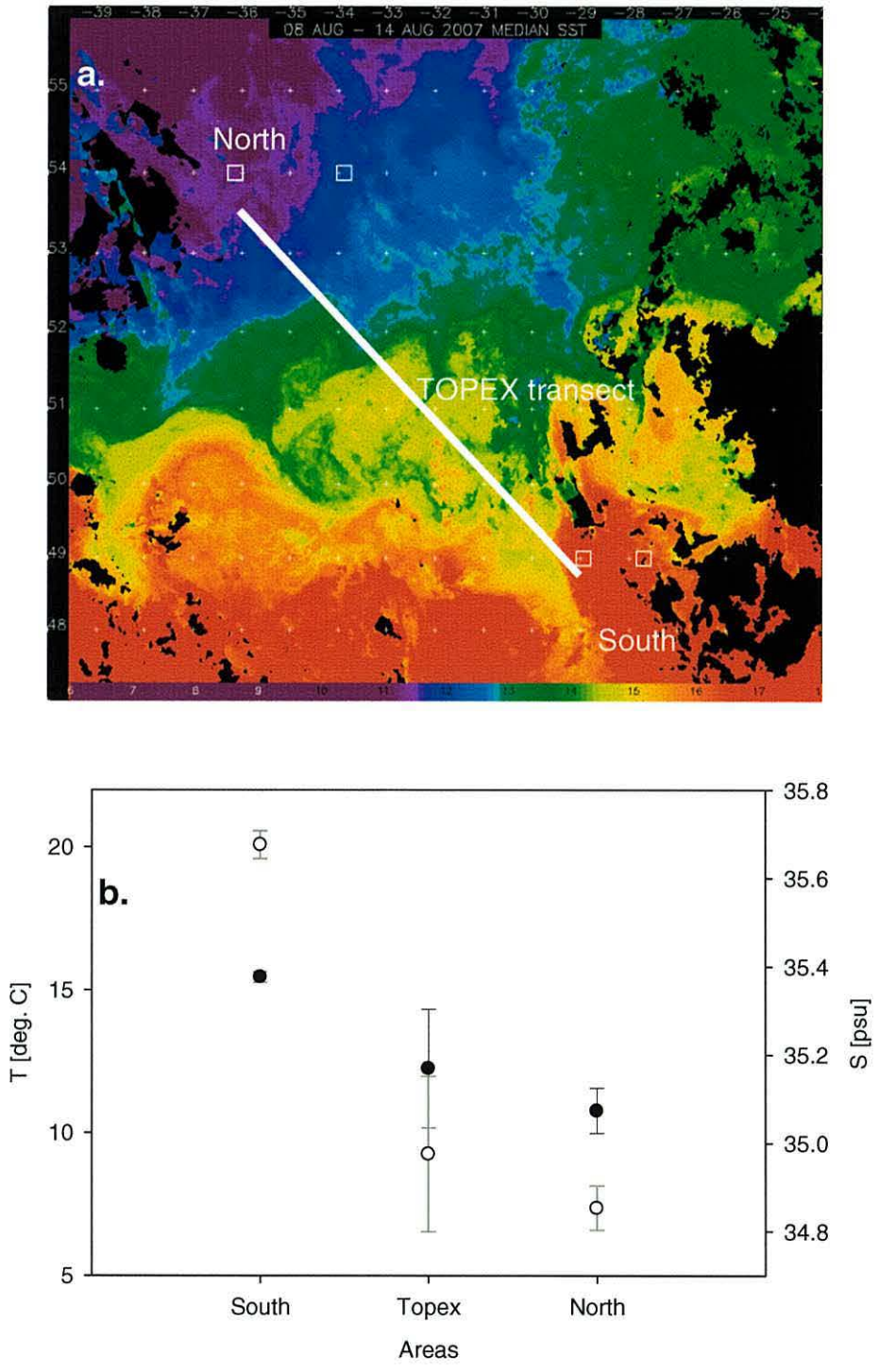

Figure 5.1 Physical environment at the CGFZ of the Mid-Atlantic ridge. a) Composite image of sea surface temperature from the AVHRR during the ECOMAR cruise. Scale goes from 6 °C (purple) to 18 °C (red). The squares mark the position of the stations at both sides of the ridge. b) In-situ near surface (0-40m) average temperature (filled circles) and salinity (empty circles). Error bars are standard deviations for the replicates at the three sites and from the water column between 0 and 40m.

5.1.2. Chl-a and POC

For most of the cruise, near surface Chl-a was less than 1 mgm^{-3}, suggesting mesotrophic conditions. The South had Chl-a values less than 0.5 mgm^{-3} throughout the water column (Figure 5.2.a), with a slight maximum at 50m. At the north edge of the TOPEX transect (Figure 5.3), Chl-a resided at 20 m and above the pycnocline and the Chl-a concentration increased to 1.3 mgm^{-3}. Chl-a at the North station (Figure 5.2.b) was on average less than 0.6 mgm^{-3} near the surface (less than 30 m). Overall, the South had the lowest Chl-a concentration and the TOPEX transect, the highest ($p<0.0001$, $F=14.3$, $N=79$).

Particulate organic carbon (POC) for the whole domain, from 0 to 40m, was on average 200.9 $mgCm^{-3}$ (std. deviation, 142.8 $mgCm^{-3}$, N=51). There were no significant differences between the North and South areas (with average POC 147.4 and 127.4 $mgCm^{-3}$), the TOPEX transect had significantly higher POC (average±std.dev, 334.2±187.9 $mgCm^{-3}$) ($p<0.0001$, $F=15.3$, $N=85$).

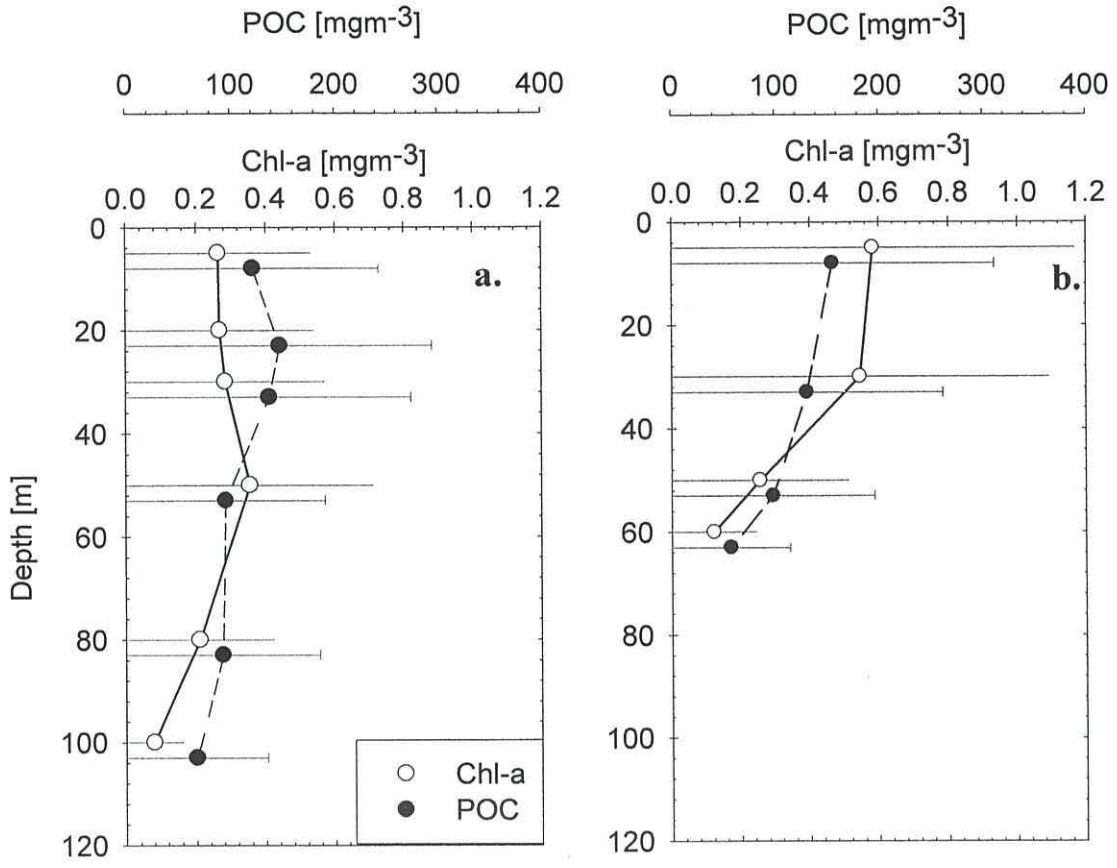

Figure 5.2 Mean profile and standard deviation (error bars) of Chl-a and POC for: a) South area. b) North area. Chl-a and POC samples are coincident, but POC is plotted with a slight vertical offset, for clarity

The South and North areas (Figure 5.2) have similar vertical POC distributions, with higher values in the surface layer than below 40m. For the TOPEX transect (Figure 5.3), POC was related to the position of the pycnocline and to the latitude change, being greater at depths less than 40 m in the southern part of the TOPEX transect compared to the northern part.

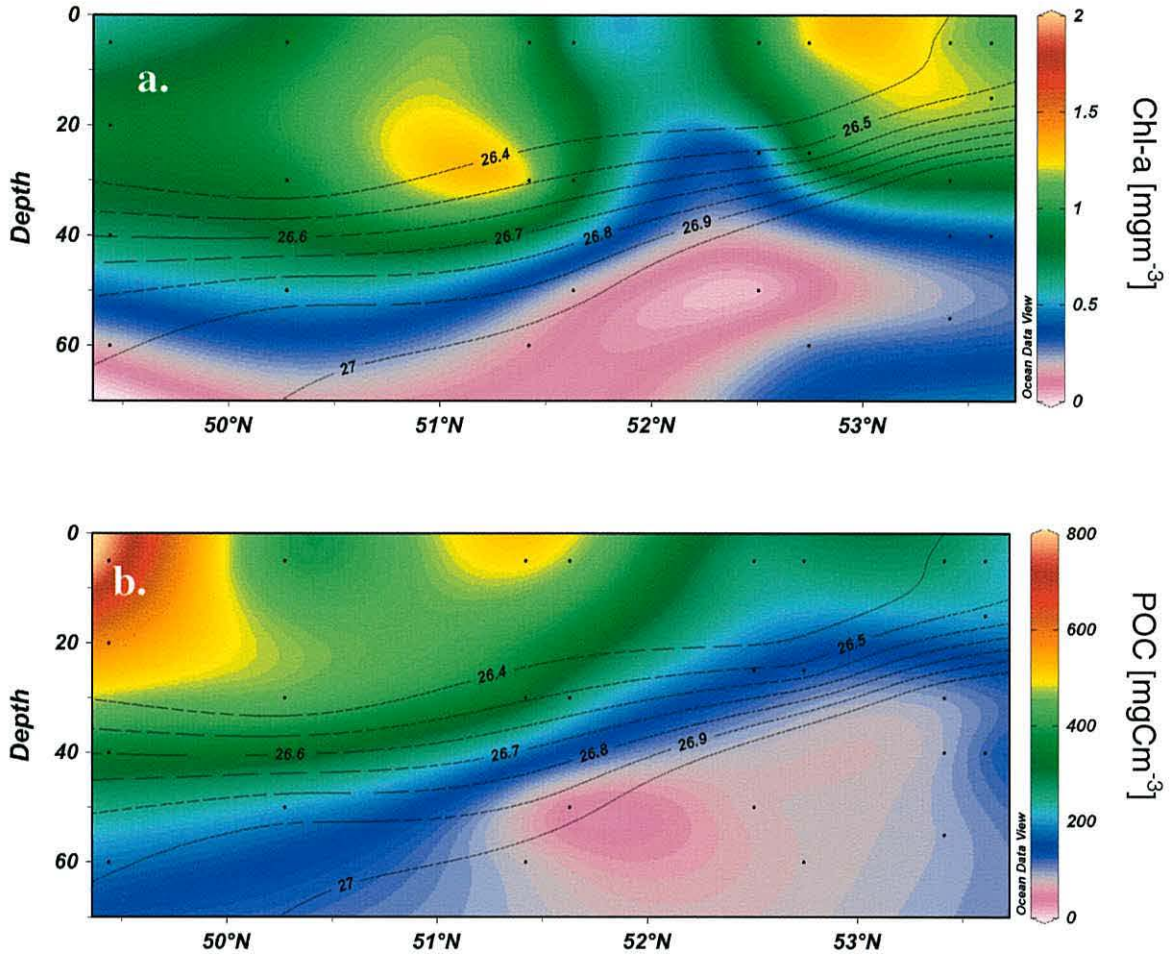

Figure 5.3 a) TOPEX section of Chl-a (mgm^{-3}). b) TOPEX section of POC ($mgCm^{-3}$). Contours are density anomalies.

For all data, the average POC:Chl-a ratio was 400±274 mgC $(mgChl\text{-}a)^{-1}$ (N=48), and values in the North were significantly lower than those in the South (260 and 561 respectively), and the higher dispersion along the TOPEX transect overlapped both areas (Figure 5.4). It is worth noting that the global relationship obtained by Sathyendranath *et al.* (2009) between POC and Chl-a from HPLC, is close to the relationship found in this study. Also, it is interesting that the relationship between phytoplankton carbon and Chl-a estimated by Sathyendranath *et al.* (2009) falls systematically below all the points from ECOMAR.

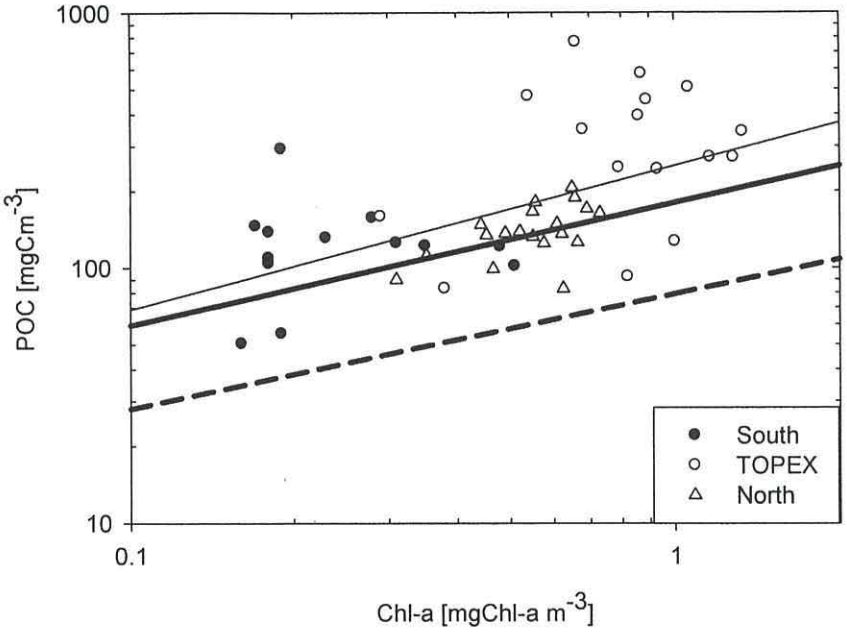

Figure 5.4 POC as a function of Chl-a for the three ECOMAR regions (see legend for region). Thin solid line corresponds to the power law fit to all the data: $POC=251\times Chl\text{-}a^{0.56}$, $R^2=0.29$, N=48. Thick solid line corresponds to the global power law fit in Sathyendranath *et al.* (2009): $POC=180\times Chl\text{-}a^{0.48}$. Thick dashed line corresponds to the expected phytoplankton carbon to Chl-a relationship from a quartile fit in Sathyendranath *et al.* (2009).

5.2 Horizontal and vertical distributions of particle backscattering and its spectral shape

For all data (0-120 m), $b_{bp}(532)$ was significantly lower in the South compared to the TOPEX transect and Northern stations ($p<0.0001$, F=15.5, N=54). There was no significant difference between the TOPEX and Northern stations (Figure 5.5). At the surface (0 to 40 m), b_{bp} (532) also increased towards the North, with an average increase of 62% from South to North at 532 nm (Table 5.1). The coefficient of variation (i.e.CV=SD/mean x 100) of $b_{bp}(532)$ was greatest for stations along the TOPEX transect across the sub-polar front (28.5%) and smallest for the Southern area (11%).

Table 5.1: Particle backscattering and backscattering slope (γ_{BS}) mean values for the surface mixed layer (0-40 m) for the different areas of this study. These aggregate means are obtained pooling together all available casts at each area and for all data available between 0 and 40 m (N~40).

Area		$b_{bp}(462)$ [m-1]	$b_{bp}(532)$ [m-1]	$b_{bp}(650)$ [m-1]	γ_{BS}
North	Mean	0.0032	0.0027	0.0022	-1.07
	CV(%)	14	15	17	14.4
Topex	Mean	0.0026	0.0023	0.0020	-0.79
	CV(%)	29	29	28	-21.1
South	Mean	0.0012	0.0010	0.0008	-1.36
	CV(%)	13	11	10	14.8

The backscattering spectral slope (γ_{BS}), for the whole dataset (0-120m), was significantly lower (higher in absolute value, steeper) in the South than in the TOPEX and North locations (p=0.001, F=8.76, N=54). Near the surface (0-40 m) it varied between -1.36, in the South and -0.79 in the TOPEX transect. Therefore, the spectra was flatter in the TOPEX transect than elsewhere. The variability of γ_{BS} was also greater in the TOPEX transect.

Vertically, the Southern area has higher and constant backscatter signal above the mixed layer. Backscatter then decreases with increasing depth. γ_{BS} is constant below the mixed layer down to 60 m and then it becomes steeper and noisier with depth. This shape of vertical variation is similar in the North and TOPEX transect, although the variations are larger in above the pycnocline. This pattern is what would be expected (e.g. Twardowski *et al.*(2007)): backscattering magnitude is related to particle load (which is higher near to the surface); when particle concentration reduces, the spectral shape becomes steeper (i.e. more negative) and more similar to that of the pure water.

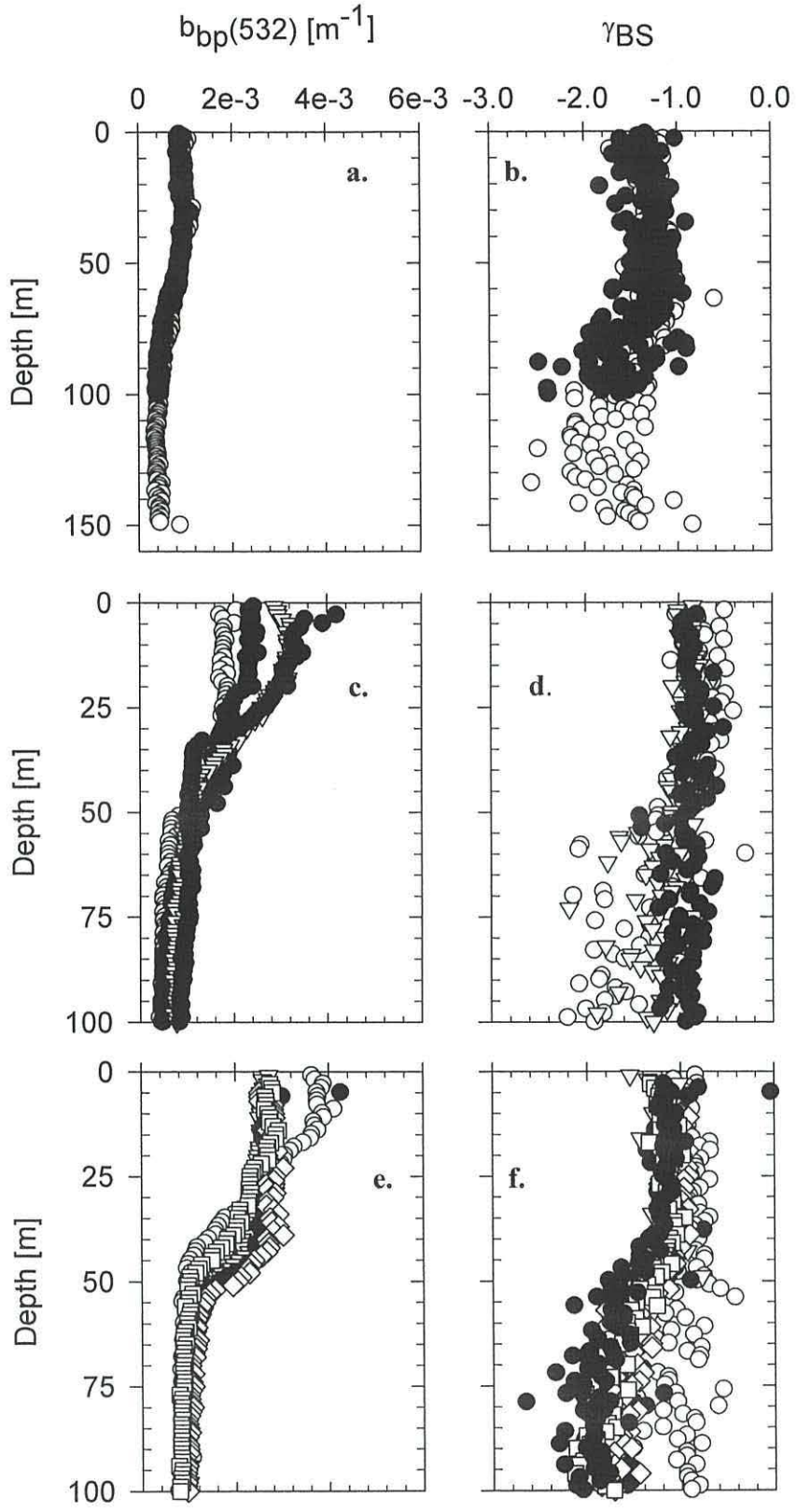

Figure 5.5 a),c),e)$b_{bp}(532)$ for the South, TOPEX and North areas respectively. b),d),f) γ_{BS} for the South, TOPEX and North areas respectively. Different symbols correspond to different casts at each area.

Backscattering along the TOPEX transect increased towards the north in the surface layer, while below the pycnocline it remained constant. Despite the variability in backscattering at the surface, the backscattering slope was quite constant, becoming steeper and noisier below the pycnocline.

5.3 Relationship between b_{bp} and γ_{BS} with Chl-a

$b_{bp}(532)$ as a function of Chl-a for the ECOMAR cruise is shown in Figure 5.6, for all coincident data (N=50). There is an increase of $b_{bp}(532)$ with Chl-a (and also of b_{bp} at 462 and 650 nm, not shown). The R^2 is quite high (R^2=0.62 in log space, Table 5.2) despite the narrow range of the data available when fitting a power law of the type:

$$b_{bp}(\lambda) = \alpha \times \text{Chl-a}^{\beta} \qquad \textbf{Eq.1}$$

where α and β are the coefficients of the fit corresponding to published empirical models (Huot *et al.*, 2008).

Table 5.2: Regression results of the fits for the particulate backscattering (number of observations, N=50) as a function of Chl-a. The equation fitted is $b_{bp}(\lambda) = \alpha \times \text{Chl-a}^{\beta}$

λ [nm]	α (Std. Err)	β (Std. Err)	R^2	RMSE,[m^{-1}]* (MAPE, [%])**
462	0.003 (0.030)	0.45 (0.05)	0.57	0.15 (4.8)
532	0.003 (0.030)	0.51 (0.05)	0.63	0.15 (4.5)
650	0.002 (0.031)	0.55 (0.05)	0.62	0.16 (4.7)

*Root Mean Square Error, RMSE = $\sqrt{\sum_i \left(y_{pred,i} - y_{meas,i}\right)^2 / N}$, on the decimal log transformed data, where y_{pred} and y_{meas} are the predicted and measured values respectively of the i-th sample. N is the number of samples

** Mean absolute percent error, MAPE = $100/N \times \sum_i \left|\left(y_{pred,i} - y_{meas,i}\right)/ y_{meas,i}\right|$

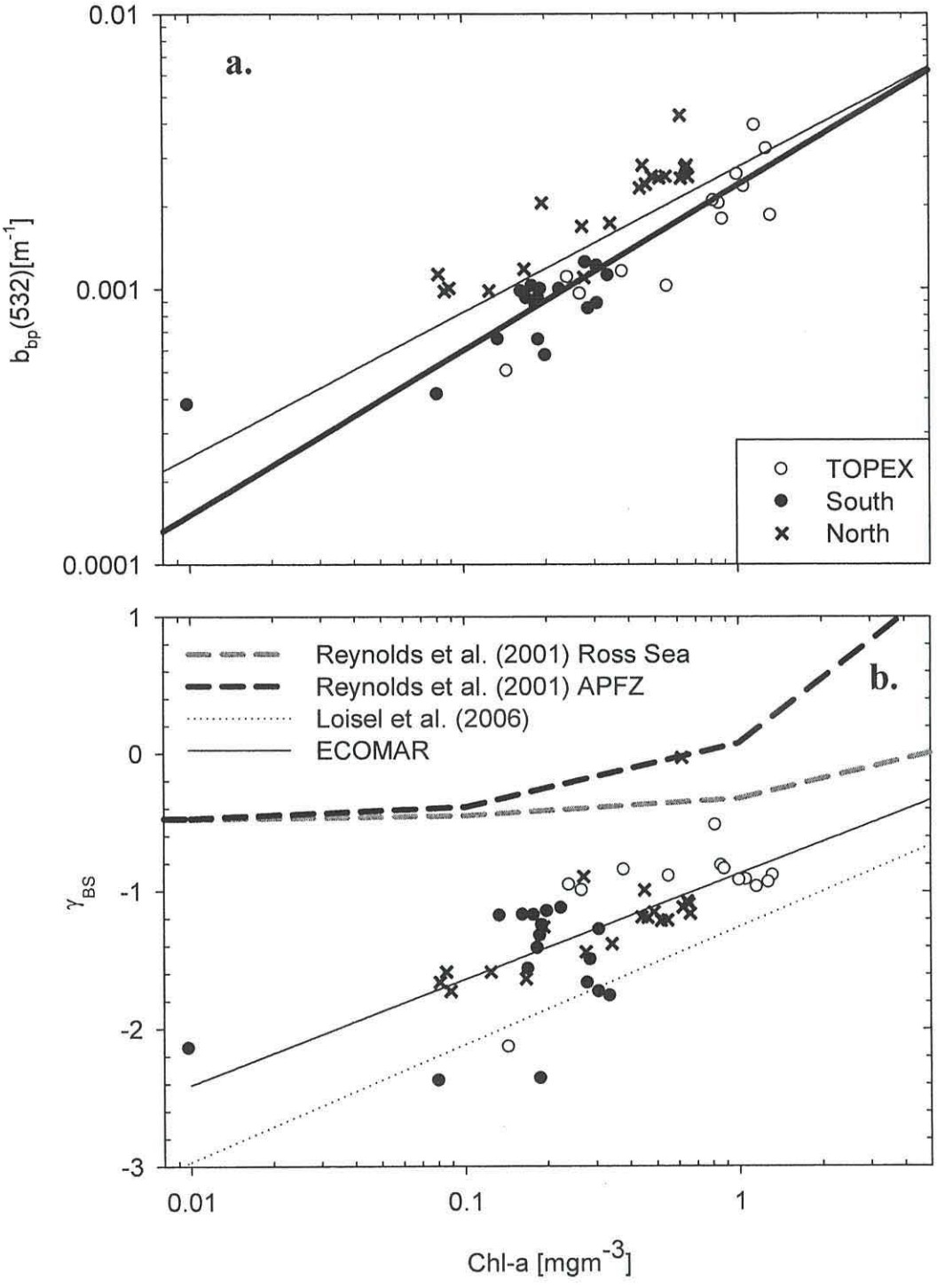

Figure 5.6 a) Variation in $b_{bp}(532)$ as a function of Chl-a. Thin line is the power law fit on the data from the ECOMAR cruise in Table 5.2. Thick line is the regression computed using the model by Huot *et al.* (2008). b) γ_{BS} variation with Chl-a. ECOMAR regression: γ_{BS}= -0.77 x $\log_{10}$(Chl-a)+0.87 (r^2=0.46, for the log transformed Chl-a, N=50). APFZ stands for Antartic Polar Front Zone

The backscattering spectral slope (γ_{BS}), becomes less negative with increasing Chl-a (Figure 5.6.b). In other words, the spectra become flatter with increasing Chl-a. The regression fit to the log-transformed Chl-a data gives a root mean squared error (RMSE) of 0.31 m^{-1} and a mean absolute percent error of 82 % with no significant differences among areas. Data are comparable to other in-situ studies in the Antarctic Ocean (Reynolds *et al.*, 2001) and satellite algorithms (Loisel *et al.*, 2006).

5.4 Relationship between b_{bp} and γ_{BS} with POC

The relationships between POC and $b_{bp}(532)$ and the backscattering spectral slope (γ_{BS}) are shown in Figure 5.7. Only a small fraction of the variance of $b_{bp}(532)$ is explained by a linear regression applied to all the POC data.

If the five points with POC greater than 290 mgm^{-3} are not considered in the regression, the variance on $b_{bp}(532)$ explained by the linear model is 43% (line fitted in Figure 5.7.a). Of these five points four are located in casts in the TOPEX transect, and coincide with the highest values of Chl-a. By area, the samples at the South station are concentrated around the lower values of POC, while North and TOPEX samples make up for most of the variability encountered.

Concerning the relationship between POC and γ_{BS}, there is not a clear pattern (Figure 5.7.b). The set values with high POC discarded above, present a constant γ_{BS}. There are no values in the literature to verify these findings concerning the variation of the spectral slope with POC.

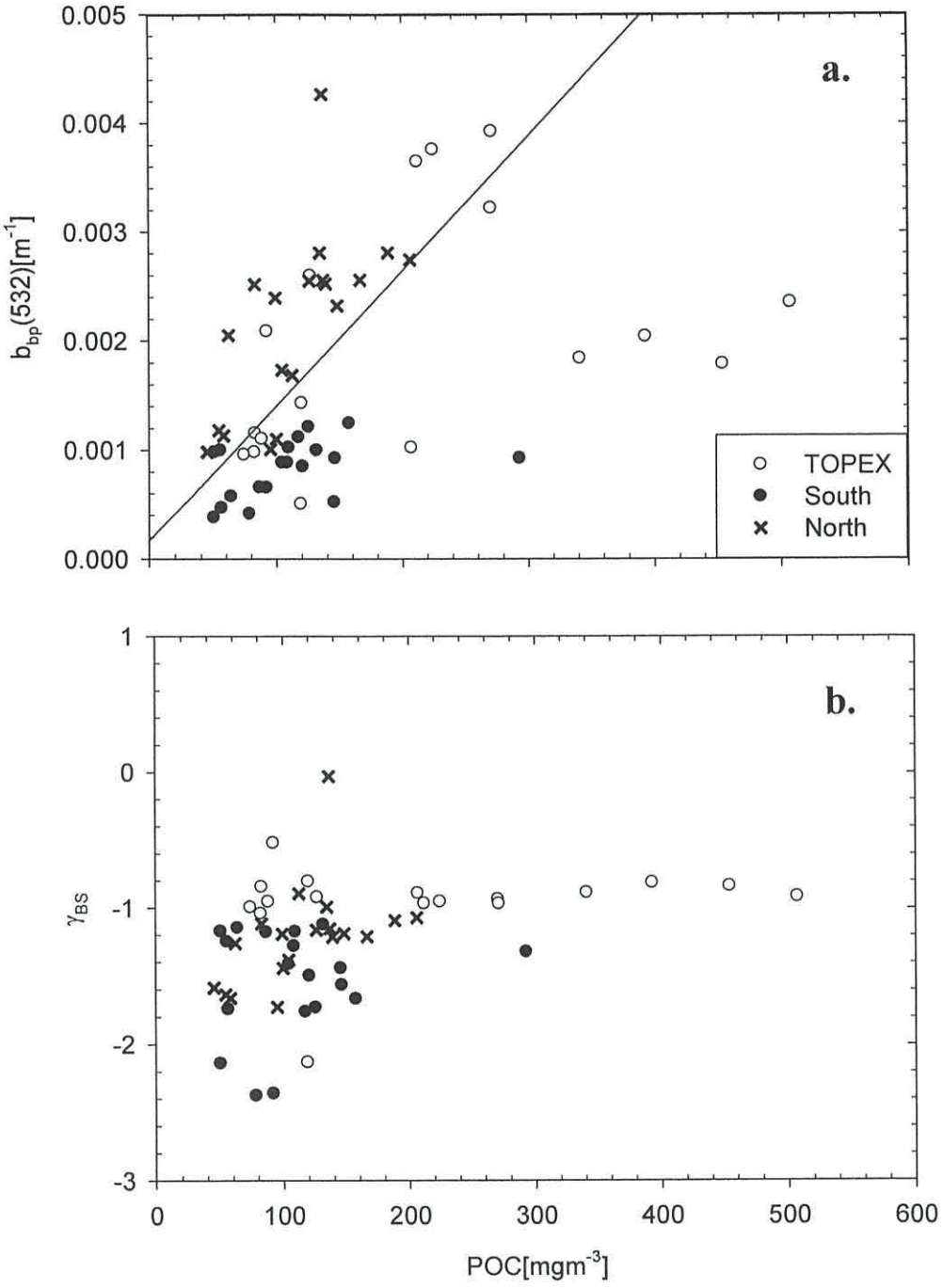

Figure 5.7 a) $b_{bp}(532)$ variation with POC. Thin line is the regression on the data from the ECOMAR cruise: $b_{bp}(532)= 1.2x10^{-5}x$ POC+0.0002 (r^2=0.43, N=50). b) γ_{BS} variation with POC.

Specific backscattering with respect to Chl-a ($b^*_{bp,Chl\text{-}a}(532)$) and with POC ($b^*_{bp,POC}(532)$) are commonly reported in the literature. The mean $b^*_{bp,Chl\text{-}a}(532)$ at the surface layer, between 0 and 40 m was 0.004±0.001 [m^2 $(mgChl\text{-}a)^{-1}$] (N=29), and $b^*_{bp,POC}(532)$ was 1.4 x 10^{-5}±0.8 x 10^{-5} [m^2 $(mgC)^{-1}$] (N=29).

By area, $b^*_{bp,Chl\text{-}a}(532)$ between 0 and 40 m at South and North is similar (~0.005 m^2 $(mgChl\text{-}a)^{-1}$), while at the the TOPEX transect it is halved in average (~0.002 m^2 $(mgChl\text{-}a)^{-1}$), and this reduction is statistically significant ($p<0.0001$, $F=38.0$, $N=27$). The mean of $b^*_{bp,POC}$ (532) for all data is smaller than for the surface layer only, however, this difference is not statistically significant. The $b^*_{bp,POC}$ (532) does not follow the same distribution as $b^*_{bp,Chl\text{-}a}(532)$. Lower values are encountered in the South and TOPEX stations (~1.0 x 10^{-5} m^2 $(mgC)^{-1}$) whereas values twice as high are encountered in the North (~1.9 x 10^{-5} m^2 $(mgC)^{-1}$). These differences are statistically significant ($p<0.01$, $F=7.31$, $N=30$).

5.5 Discussion and conclusions

During the ECOMAR cruise, there was a doubling in the particle backscattering coefficient from the South to the North of the sub-polar front. These variations were explained better by the variations of Chl-a than by the variations in POC.

The backscattering values observed in ECOMAR are low, but the minimum recorded is about four times higher than the values measured in clearer waters in the Pacific (Twardowski *et al.*, 2007). Backscattering slope tends to -4 with depth , which is the expected value for the backscattering slope of pure seawater according to Morel (1974).

Considering the relationship between backscatter and Chl-a, the regression line from ECOMAR is comparable to the model of Huot *et al.* (2008) (Figure 5.6.a). The coefficients of both regressions are comparable: at 532 nm, α is 0.0025 while for Huot *et al.*(2008) it is 0.0024 and β is 0.5, while for Huot *et al.* (2008) it is 0.6. The model by Huot *et al.* (2008) was developed using a wider range of Chl-a than those of the current work, however, there is an agreement between their relation and the data from ECOMAR. For measurements in the north polar Atlantic (Stramska *et al.*, 2003), collected with different instrumentation, the agreement is also notable: α was 0.0019 and β was 0.5.

Concerning the γ_{BS}, the overall value for ECOMAR (-1.07) is slightly less negative than the value obtained by Huot *et al.* (2008) (-1.14). It is an interesting result that a proportion of the variations in γ_{BS} was explained by variations in Chl-a (R^2=0.46, $p<0.0001$). One of the few studies that assessed the variation in γ_{BS} in oceanic waters also predicts a reduction of γ_{BS} with the increase of Chl-a, with a slope of 0.86 (Loisel *et al.*, 2006), which is similar to the one obtained in this work (0.77, see Figure 5.6.b). In a laboratory study (Vaillancourt *et al.*, 2004) γ_{BS} of 29 phytoplankton species ranged from -0.0046 to -2.32, but no relationship was found with any descriptor of phytoplankton concentration. This overall agreement between the most current empirical models and the models derived for ECOMAR, indicates that the measurements performed are in line with current knowledge.

The relationship between POC and particle backscattering for ECOMAR was comparable with other oceanic studies (Stramski *et al.*, 2008). However, these authors obtained better relationships in comparable conditions (R^2=0.77, when removing upwelling areas from the regression and using Buiteveld values for b_{bw}). No significant trend was found between POC and γ_{BS} and it is worth noting the lack of published relationships in the literature.

Mass-specific backscattering coefficients with respect to Chl-a and POC were obtained from simultaneous in-situ water samples, unlike some published studies which derive the biogeochemical variables from optical measurements (e.g. Sullivan *et al.* (2005)). Mass-specific backscattering with respect to Chl-a falls within the expected range (Reynolds *et al.*, 2001). Mass-specific backscattering with respect to POC for the ECOMAR cruise is 38 % lower than that of the BIOSOPE (central Pacific Ocean) but more similar to values recorded in the East Atlantic ocean (16% lower) (Stramski *et al.* 2009). One interpretation could be that there are different assembleges of particles in different regions, however, more data on the nature of particles would be required. (Chapter 6).

This variability of the mass-specific backscattering coefficients can be discussed in terms of the variations in the POC:Chl-a ratio due to variations in the non-phytoplankton carbon or variations in the phytoplankton carbon. The variations in the non-phytoplankton carbon are the result of the ecosystem functioning as a whole, while

the variations in the phytoplankton carbon are a result of phytoplankton diversity and/or the adaptation to the environment (light and nutrients).

If all changes in POC:Chl-a ratio could be attributed to phytoplankton diversity, in the South, the high Chl-a specific backscattering, coincides with the lowest POC:Chl-a. According to the assumptions above, this means that smaller phytoplankton dominated. Also, in the North, Chl-a specific backscattering is similar to the South (high), but here, the POC:Chl-a ratio is similar or slightly higher, implying that there is a dominance of slightly larger phytoplankton there. Finally, in the TOPEX transect, where the Chl-a specific backscattering is significantly lower, the POC:Chl-a ratio is highest, indicating the largest cells of the domain. This explanation would agree with the widely accepted theory that sustains the backscattering is related to the smallest cells (e.g Stramski *et al.* (2001)). However, the POC could also be due to the biogenic detritus. Hence the necessity to expand this study to include some indication of the size of the living cells as well as the detrital fraction.

A number of conclusions can be drawn from this study: firstly, in the particular region of study of the Mid-Atlantic Ridge and for the summer period, it has been found that a large part of the backscattering measured is well correlated to Chl-a, but not so well to POC. Secondly, there is also a relationship between the spectral shape of the backscattering coefficient and the Chl-a (but not POC). Finally, although significant changes have been found in the mass-specific backscattering coefficients with respect to Chl-a and POC, there is a need for additional information about the phytoplankton groups present and the amount of non-phytoplankton carbon in the water. Therefore, further analysis of the backscattering data will be done in the next Chapter, using information on the abundances of plankton organisms and the detrital fraction.

Chapter Six

Backscattering related to phytoplankton using flow cytometry in the open ocean

CHAPTER SIX: BACKSCATTERING RELATED TO PHYTOPLANKTON USING FLOW CYTOMETRY IN THE OPEN OCEAN

Synopsys

In Chapter Five, a high percentage of the variation in particle backscattering coefficient (b_{bp}) during the ECOMAR cruise was explained by phytoplankton chlorophyll-a (Chl-a) (r^2=63%) using a power law, which was consistent with previous studies. Particulate organic carbon concentration (POC) was also related to b_{bp}, but a lower percentage of the variance could be explained compared to Chl-a. In this chapter results are presented which demonstrate that in the ECOMAR region in the summer of 2007 a high fraction of the variability in backscatter is due to variations in phytoplankton abundance in the size range between 2 and 20μm (R^2=0.67, N=46). This evidence is presented in two ways: firstly by the statistical relationships between the in-situ measured data and secondly via sensitivity analysis based both on literature and in-situ data. The results are discussed in relation to potential sources of error and current literature.

6.1 Pico and nano plankton contributions to particle backscattering: formulation of the "reductionist approach" for the ECOMAR cruise

The main hypothesis of this thesis is that the phytoplankton component is an important contributor to b_{bp} in oceanic waters. The phytoplankton, according to size can be classified into pico (diameter, d<2 μm), nano (2>d>20 μm) and micro (d>20 μm) phytoplankton. All of these groups contribute to the Chl-a concentration in the water column. The results presented in Chapter Five, showing that the variability in b_{bp} was significantly explained by Chl-a, suggest that the dominant signal in b_{bp} is phytoplankton. Which part of the phytoplankton community contribute most to this signal or whether the signal is due to other components such as bacteria and non-living particles which also co-vary with Chl-a, is yet to be resolved.

One way to separate Chl-a bearing organisms into size groups and to distinguish them from bacteria is by means of counting cell abundances using flow cytometry. The analytical method of flow cytometer (see Chapter Three) has been adapted in PML (Tarran *et al.*, 2006; Tarran *et al.*, 2001; Zubkov *et al.*, 2000) to use side scattering, forward scattering and three different fluorescence channels to distinguish between bacteria, *Synecococcus spp.*, *Prochlorococcus spp*, picophytoeukaryotes (hereafter picoeukaryotes), nanophytoeukaryotes (hereafter nanoeukaryotes), cryptophytes (a type of nanoeukaryotes) and coccolithophorids. Only microphytoplankton abundance is missing when this method is used. Then, the separate components can be related to the backscattering signal, similarly to what has been done for attenuation and scattering (Chung *et al.*, 1998; Claustre *et al.*, 1999; Durand and Olson, 1996; Green *et al.*, 2003; Grob *et al.*, 2007; Montes-Hugo *et al.*, 2009; Oubelkheir *et al.*, 2005).

During summer 2007, a cruise took place at the Mid-Atlantic Ridge - MAR (between 48 and 54°N), providing the opportunity to sample the abundance of these organisms in a region away from the influence of the continental shelf (i.e. far from sources of minerals or coastal organic detritus). Absorption by phytoplankton and non-algal particles (a_{phy} and a_{NAP}, respectively) are presented to quantify (indirectly) the amount of detritus present in the water column. This specific oceanic region has not been previously sampled for bio-optical parameters, hence, the added importance of these measurements. Some studies have sampled water masses south of the MAR (north of

the Sargasso Sea), where it has been reported that non-photosynthetic bacteria represent the same amount of carbon as the sum of prochlorophytes, non-photosynthetic bacteria and photosynthetic eukaryotes (Li, 2002; Li *et al.*, 1992; Li and Harrison, 2001).

Therefore, the main assumptions of the study are that: the main contributors to b_{bp} are those detected by flow cytometry and that minerals, non-living organic detritus and bubbles are not significant contributors to b_{bp} above the Mid-Atlantic Ridge, Equation 1 in Chapter One, becomes:

$$b_{bp} = \sum_{i=1}^{n} b_{bppla,i} =$$
$$= \sum_{i=1}^{7} C_{ppla,i}\sigma_{bbp,pla,i} = \quad \textbf{Eq.1}$$
$$= C_{pBACT}\sigma_{bbpBACT} + C_{pPROC}\sigma_{bbpPROC} + C_{pSYN}\sigma_{bbpSYN}$$
$$+ C_{pPICO}\sigma_{bbpPICO} + C_{pNANO}\sigma_{bbpNANO} + C_{pCRYP}\sigma_{bbpCRYP} + C_{pCOCCO}\sigma_{bbpCOCCO}$$

where $C_{ppla,i}$ is the number concentration (in m^{-3}) for each type of plankton particle (*ppla,i*), detected by flow cytometry : bacteria - *BACT*, *Prochlorococcus spp.* – *PROC*, *Synecococcus spp.* – *SYN*, picoeukaryotes – *PICO*, nanoeukaryotes – *NANO* and coccolithophorids – *COCCO*. σ_{bbp} is the backscattering cross-section (in m^2) of a single particle of the *i*th component and is the result of the product of the geometric cross-section of the particle (S_i) by the efficiency factor (Q_{bbpi}, dimensionless) for backscattering of the particle. The efficiency factor is the ratio of radiant power backscattered by the particle to radiant power intercepted by S_i (Bricaud and Morel, 1986):

$$b_{bpi}=C_{pplai}\times[S_i \times Q_{bbpi}] \quad \textbf{Eq.2}$$

The first part of this chapter presents the spatial (vertical and horizontal) distributions of the different types of organisms detected by flow cytometry and the particulate absorption components, as an indirect measure of non-algal particles. This dataset is then explored statistically by means of linear regressions between the abundances of the different groups of organisms and b_{bp} to obtain σ_{bbp}. Finally, measured b_{bp} is compared to a re-constructed value based on the in-situ counts (C_i) and S_i and Q_{bbpi} obtained from the literature.

6.2 Results

6.2.1. Flow cytometry characterisation of bacterial, pico and nano phytoplankton standing stocks at the Mid-Atlantic Ridge

Figures 6.1, 6.2 and 6.3 illustrate the vertical variability of the different groups of plankton sampled. For this study, the profiles have been grouped into three areas: South (Figure 6.1), TOPEX (Figure 6.2) and North (Figure 6.3). The intra-area variability will not be addressed here (i.e. separation of each area further into East and West). In each area, the average profiles are presented alongside the profile for each station to illustrate the intra-area variability. The profiles show that the vertical distribution of bacteria (high nucleic acid + low nucleic acid) is similar throughout the region. *Prochlorococcus spp.* appeared only in the South and *Synecococcus spp.* was also more abundant in the South and decreased towards the North. Picoeukaryote abundance was similar throughout the region, with larger variability towards the North. The abundance of larger cells (nanoeukaryotes and cryptophytes) increased towards the North, but was also more disperse.

For the whole dataset (all the stations and depths), the abundance of pico and nanoplankton correlated with Chl-a. Only *Synecococcus spp.* was not correlated with the Chl-a. A large part of the variations in Chl-a (r^2 = 0.5, N=56, F=66, P<0.001) are explained by the larger phytoplankton groups (nanoplankton and cryptophytes). The remaining variability in Chl-a with respect to the cell abundances can be explained by photo-physiological changes in the Chl-a content of cells (like photo-acclimation, e.g. Geider *et al.* (1997)) and by presence of larger phytoplankton not identified by flow cytometry.

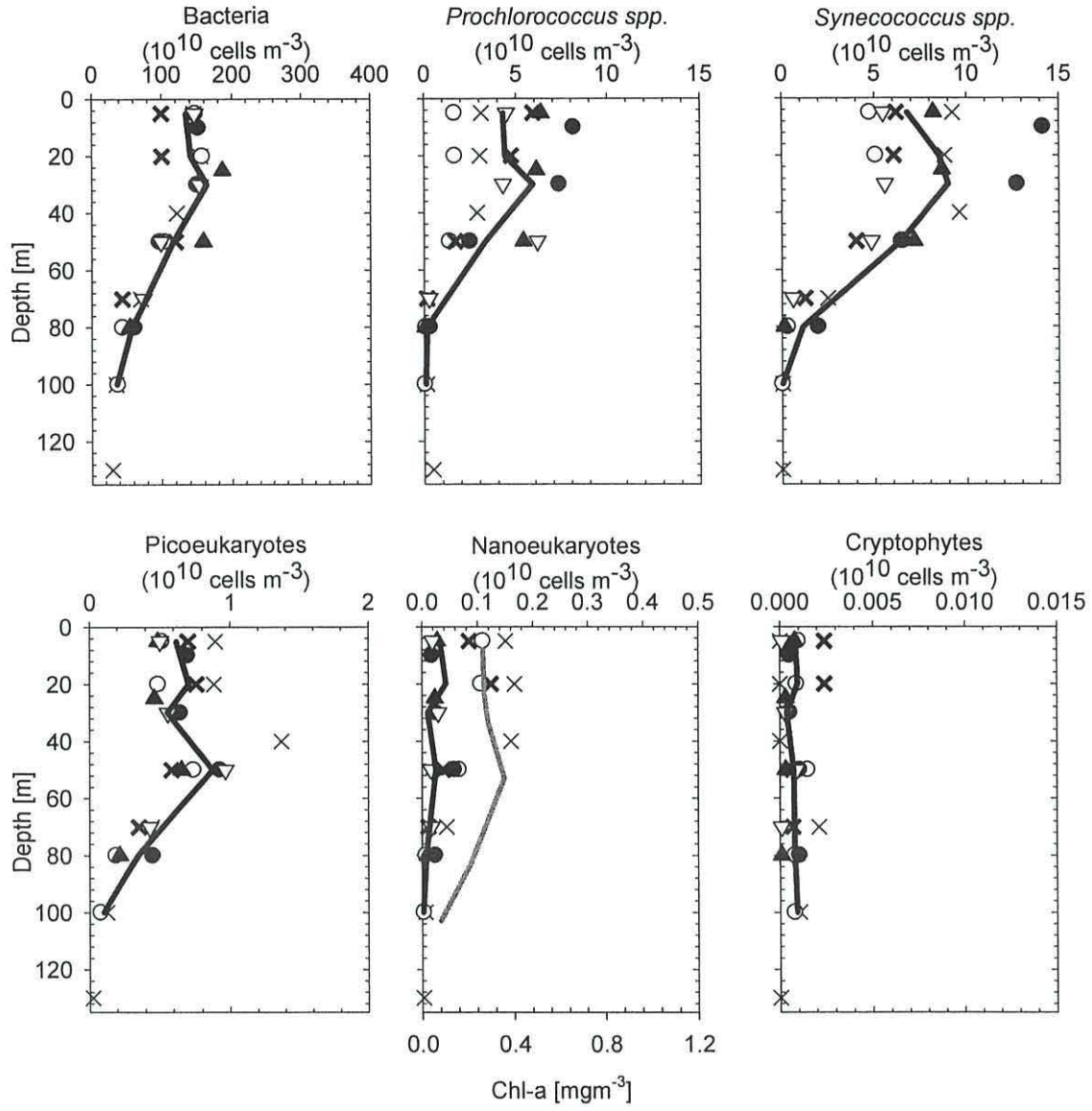

Figure 6.1 Depth profiles of bacteria, *Prochlorococcus spp.*, *Synecococcus spp.*, picoeukaryote, nanoeukaryote and cryptophyte abundances at the Southern station. Different symbols correspond to different casts at a given station. The average is indicated by a solid black line. The average Chl-a at the same depths is indicated by a solid grey line.

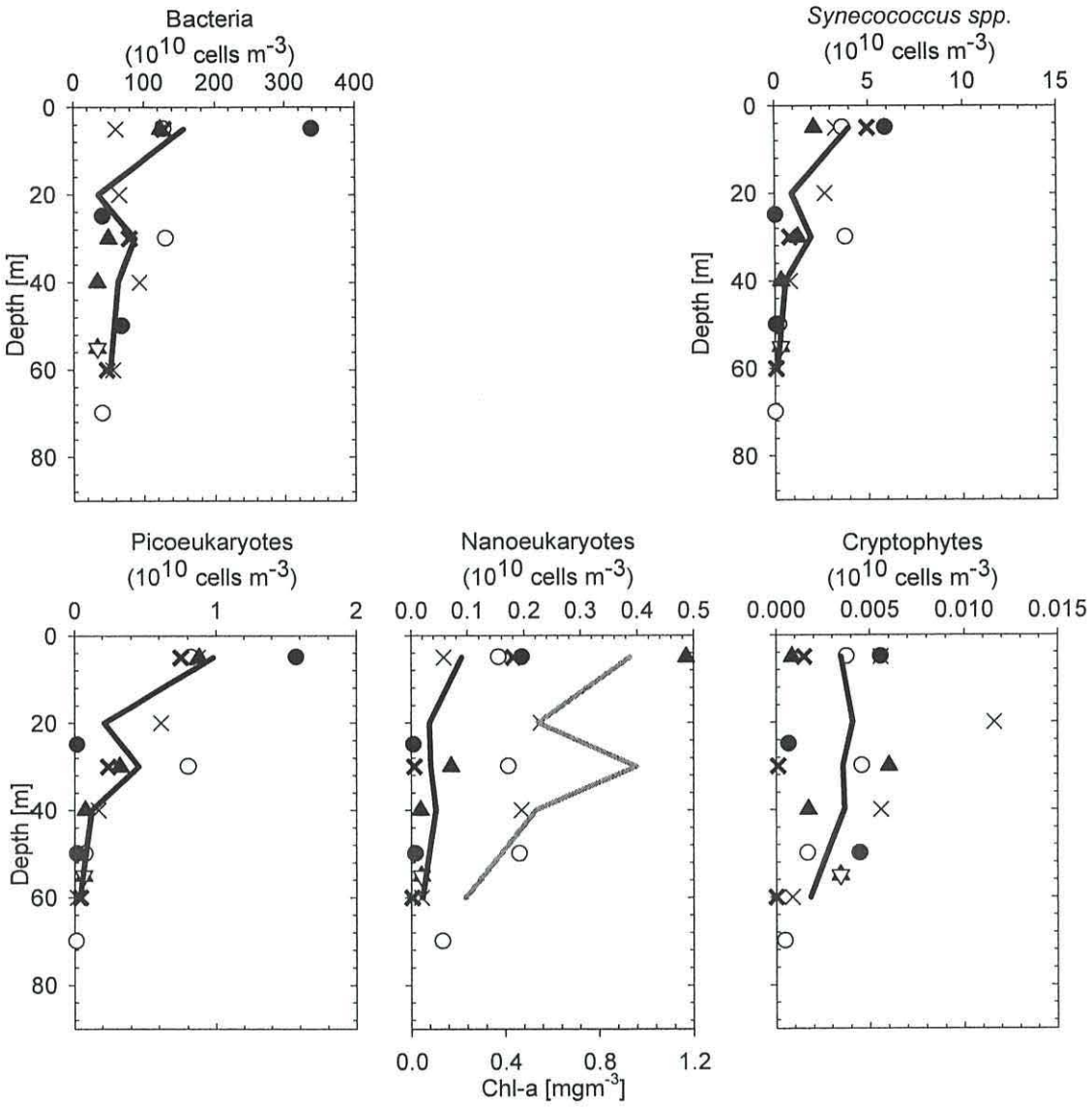

Figure 6.2 Same as Figure 6.1, except for all locations at TOPEX.

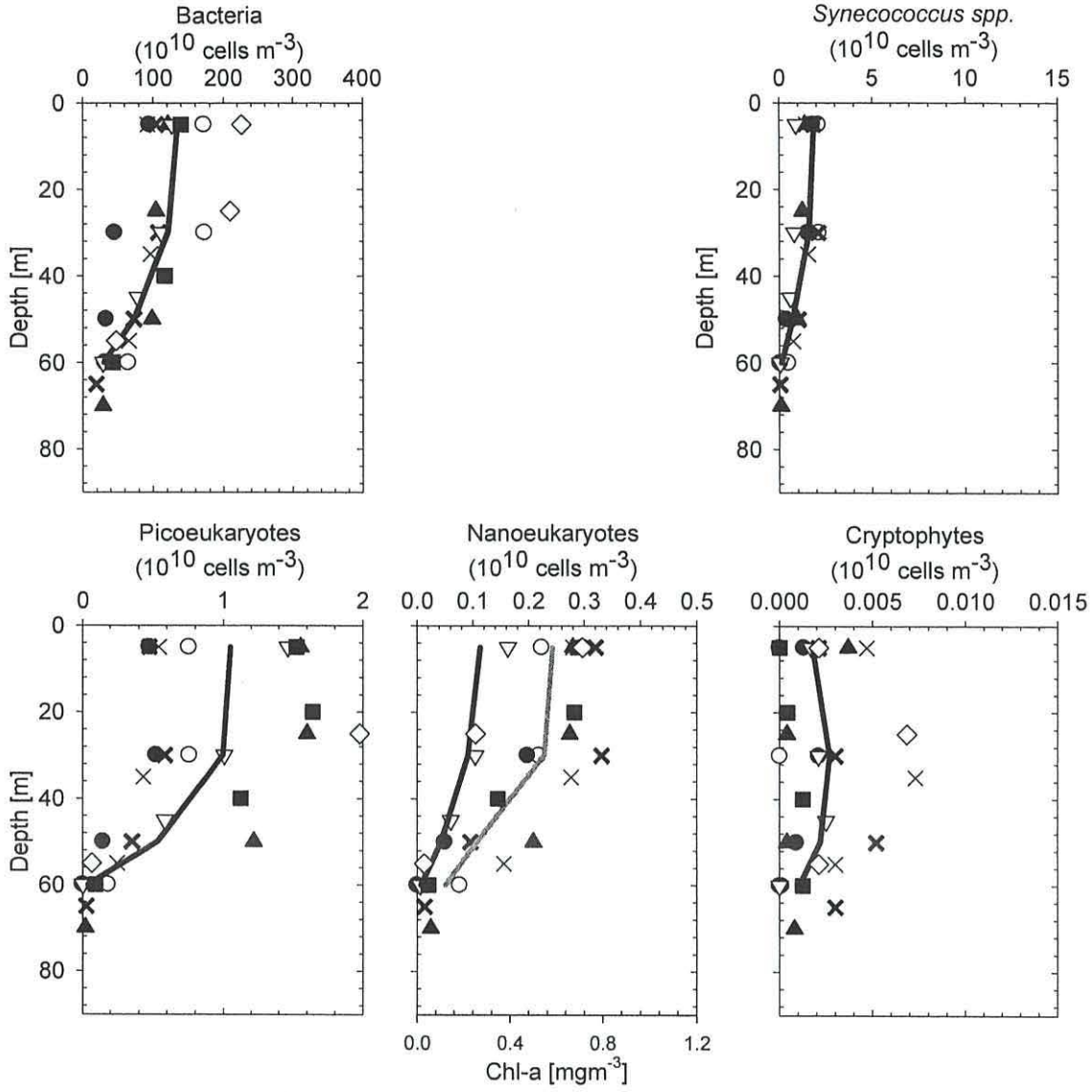

Figure 6.3 Same as Figure 6.1, except for all locations at North.

The contribution to total abundance of photosynthetic organisms by number (fractional numerical abundance) by the photosynthetic pico and nanoplankton was different at the Southern stations compared with the TOPEX and Northern stations (Figure 6.4). On average (between 0 and 40 m), *Synecococcus spp.* were the most abundant organisms at all sites. In the South area they represented 60 % of the photosynthetic plankton, whereas at the TOPEX and North, they represented 75 and 58 % respectively. *Prochlorochoccus spp.* was present only at the South (35 %) and absent at the TOPEX and North stations. Picoeukaryotes increased from 5 % in the South to 19 % and 33 % in the TOPEX and North, respectively. Nanoeukaryotes proportion also increased: from 1 % in the South to 6 % in the TOPEX and 8 % in the North. Cryptophyte abundances

were undetectable in the South and very low numbers (less than 0.2 %) in the TOPEX and North stations.

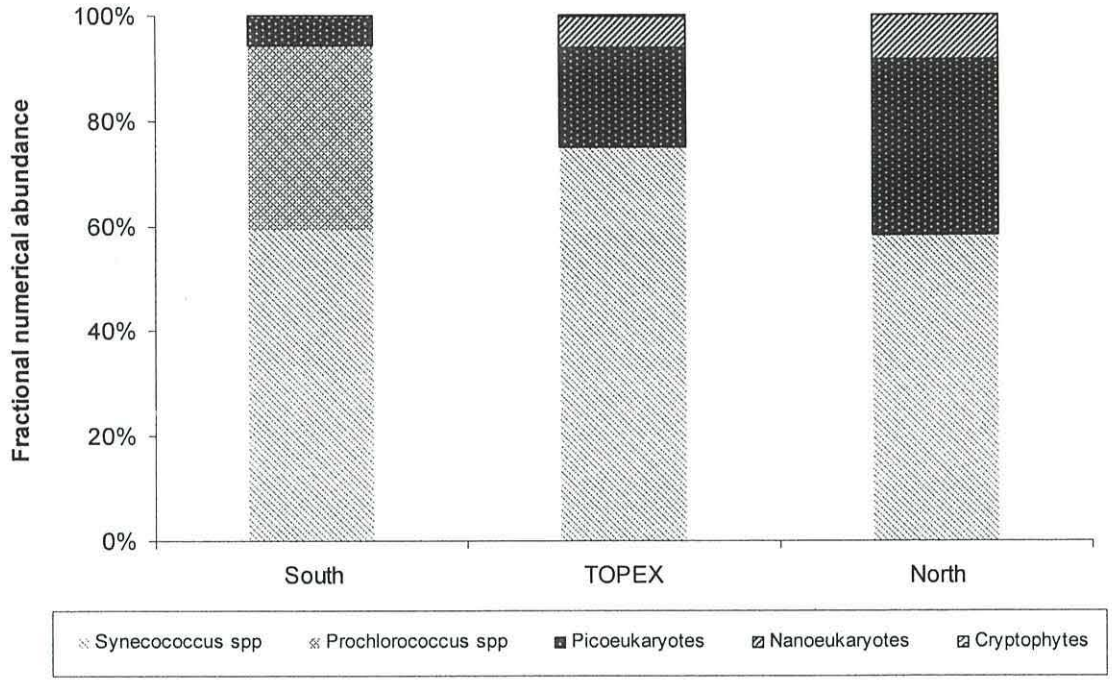

Figure 6.4 Contribution per area to the fractional numerical abundance of the photosynthetic organisms.

In summary, for the whole dataset, the Southern sites had a significantly different phytoplankton community structure than the rest of areas: *Prochlorococcus spp.* was present, *Synecococcus spp.* abundance was significantly higher (ANOVA with N=76, F=20.1, P<0.001). Larger phytoplankton was significantly lower there: cryptophyte (ANOVA with N=76, F=9.1, P=0.000) and nanoeukaryotes (ANOVA with N=76, F=10.0, P=0.000). Bacteria and picoeukaryotes were not significantly different between study areas.

6.2.2. Pigment characterisation of larger (diatoms and dinoflagellates) phytoplankton standing stocks

Pigment distribution information (see Chapter 5) was used to confirm and complement flow cytometry counts by indicating the presence of larger phytoplankton. Firstly, the presence of prochlorophytes at the South was confirmed by the presence of divynl-chl-a (not shown). Secondly, fucoxanthin, an indicator of diatoms, and peridinin, of dinoflagellates, were both found in the study region and correlated significantly with Chl-a (Figure 6.5). The fucoxanthin maximum matched the position of the deep chlorophyll maximum (0.27 mg m^{-3} at 30 m at 51°N), indicating diatom presence where no other pico or nanophytoplankton group was detected by flow cytometry. The other fucoxanthin maximum (marker for diatoms) was also deep (0.25 mg m^{-3} at 40 m at 49°N), where nanoeukaryotes and cryptophytes were detected, but not picoplankton. Peridinin (marker for dinoflagellates) was generally low and only found in concentrations greater than 0.03 mg m^{-3} in some profiles of the TOPEX transect, but generally did not match the Chl-a maxima. Therefore, it is possible that diatoms and dinoflagellates play a role in the particulate pool, explaining the remaining variability of Chl-a.

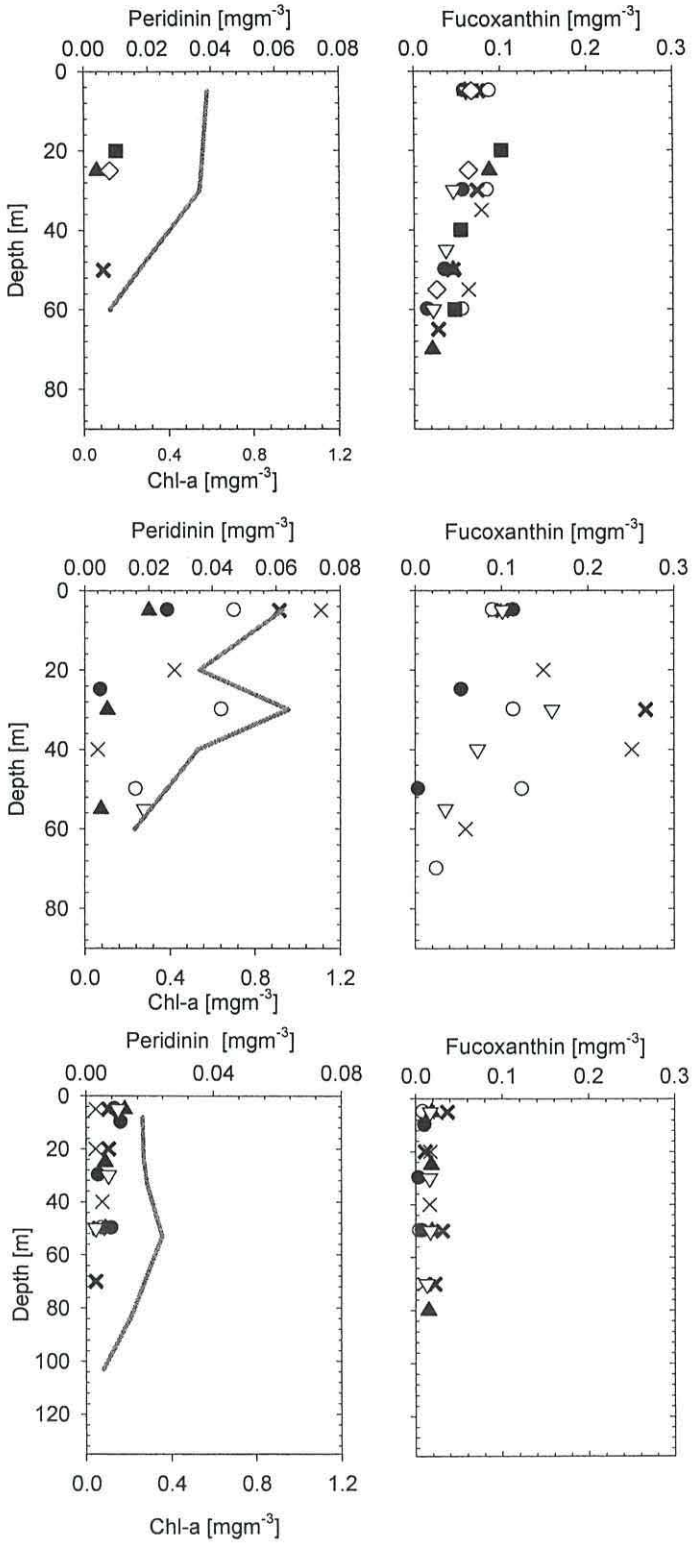

Figure 6.5 Depth profiles of a),c),e) Peridinin at the North, TOPEX and South stations respectively. Solid line is the Chl-a average profile. b),d),f) Fucoxanthin at the North, TOPEX and South respectively. Absence of points in the figure (especially 6.5.a.) is due to data below limit of detection.

Fucoxanthin concentration (from diatoms) was different in all three areas and increased from South (lowest) to TOPEX to decrease from TOPEX to North areas (ANOVA with N=78, F=30.3, P=0.000). Peridinin concentration (from dinoflagellates) was highest in the TOPEX transect (ANOVA with N=38, F=8.7, P=0.001) and similarly low in the other two areas. The combined pattern emerging from flow cytometry and pigments analysis indicates three different particle assemblages in the study region: the South, stable, with the lowest Chl-a and smaller organisms, the TOPEX, across the front, with higher Chl-a and the largest cells and the North with intermediate size organisms.

6.2.3. Fractionation of the particulate absorption as an indirect quantification of the non-algal component

A brief description of the total particulate absorption (a_p) distribution and the proportions between photosynthetic (a_{phy}) and detritus (or absorption by non-algal particles, a_{NAP}) fractions is provided. The importance of a_{NAP} in this study is that it provides an indicator of the amount of organic detritus and mineral particles present, as it was used by Stramski *et al.* (2001), given that although organic detritus, minerals have also a significant absorption signal (Stramski *et al.*, 2007). This provides an indicator of the amount of non-pigmented matter that can be backscattered in the water column. The particulate absorption at 440 nm for depths less than 40 m was significantly lower in the South (mean±std.dev., 0.018±0.003 m^{-1}, N=13) than in the TOPEX (0.060±0.031 m^{-1}, N=16) or North stations (0.052±0.021 m^{-1}, N=22). The average contribution of a_{phy} to a_p at 440 nm increasing slightly towards the North. For the South, TOPEX and North, it was 86, 91 and 93% respectively. Importantly for the backscattering, this implies a small and constant (no significant difference between regions, Fisher test, P=0.213) proportion of non-algal particles (Figure 6.6).

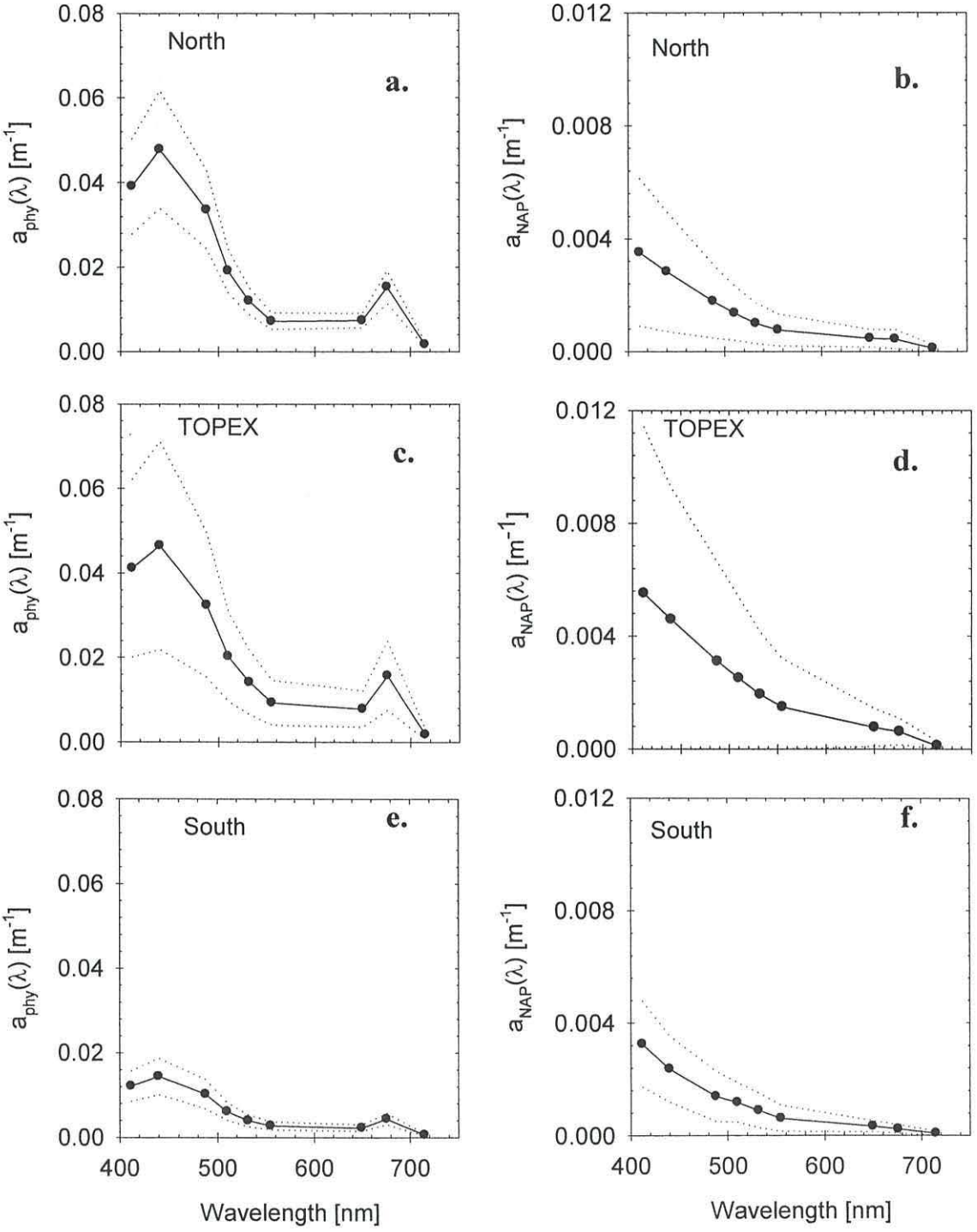

Figure 6.6 a),c),e)Phytoplankton absorption coefficient at the North, TOPEX and South stations respectively. b),d),f) Non-algal particulate absorption (a_{NAP}) at the North, TOPEX and South stations respectively. Selected wavelengths are shown (filled circles). Solid lines with filled circles are means between 0 and 40m and dotted lines are ± standard deviation.

To validate the phytoplankton absorption measurements with published values, Figure 6.7.a is presented, showing a_{phy} (440) as a function of Chl-a concentration and its comparison with the model by Bricaud *et al.*(2004). It is important to verify the absorption measurements because they are a key supporting evidence that demonstrates the lack of particles not related to phytoplankton (i.e. minerals). The non-algal fraction of the particulate (a_{NAP}:a_p ratio) shows that it is related to Chl-a (Figure 6.7.b) in a similar fashion to a previously published work (Bricaud and Stramski, 1990). Therefore a_{NAP} not only represents a small proportion of the particulate absorption, but also its contribution to the total particulate absorption pool is significantly correlated to Chl-a and its variations partially explained by those of Chl-a.

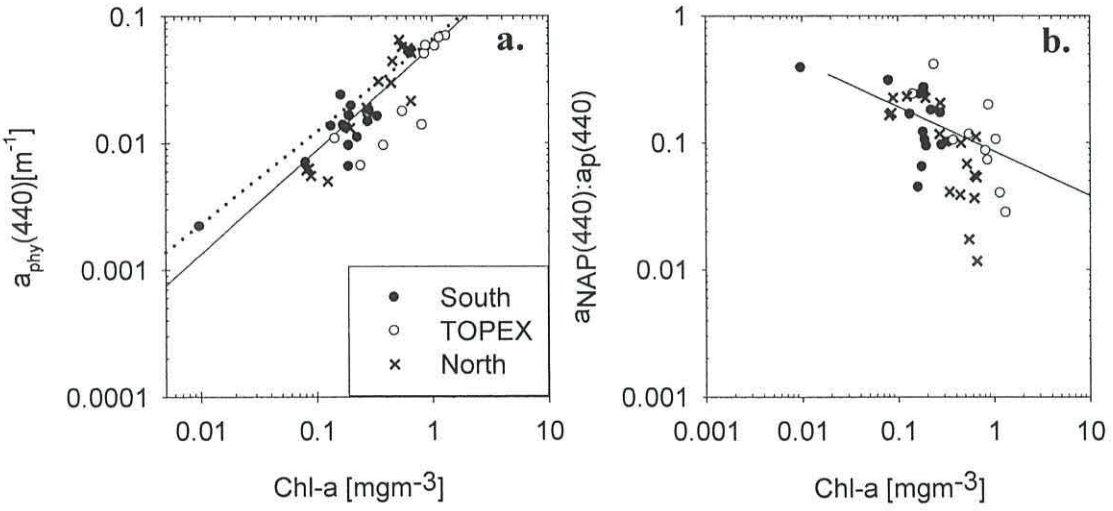

Figure 6.7 a) Phytoplankton absorption as a function of Chl-a. Solid line is the power fit to the data: $a_{phy}(440)= 0.06xChl\text{-}a^{0.8}$, $r^2=0.7$, N=42. Dotted line is the model presented in Bricaud *et al.* (2004). b) Non-algal fraction of the particulate absorption as a function of Chl-a. Solid line is the power fit to the data: $a_{NAP}(440):a_{phy}(440)= 0.09xChl\text{-}a^{-0.4}$, $r^2=0.4$, N=42.

6.2.4. Relationship between b_{bp} and the abundance of pico and nano phytoplankton

Pico and nano plankton components (including bacteria) are compared one by one with $b_{bp}(532)$ for each area of the Charlie Gibbs Fracture Zone. The data ensemble consisted of 46 coincident points (including all depths). Stepwise multiple linear regression was firstly used to assess if different components of the phytoplankton assemblage explained a significant portion of the variation in $b_{bp}(532)$. The results revealed that nanoeukaryote and cryptophyte abundances alone describe highest variation in $b_{bp}(532)$ with an r^2=0.70. These two variables were independent among them (Pearson correlation analysis, P>0.05). For this reason, the slopes of the regression can be considered a direct estimate of backscattering cross-section (σ_{bbp}) for those components (Table 6.1). Figure 6.8 shows the relationships between the abundance of nanoeukaryotes and cryptophytes (the two groups that combined using multiple linear regression) explained most of the variability in $b_{bp}(532)$. The relationship between $b_{bp}(532)$ and nanoplankton abundance was significant:

$$b_{bp}(532) = 0.0008 + 6.48\times10^{-13} C_{pNEUK}\ ,\ R^2=0.67,\ N=46,\ F=90.99,\ P<0.0001 \qquad \textbf{Eq.3}$$

Whereas that for cryptophytes alone was not significantly correlated with backscattering (P=0.02).

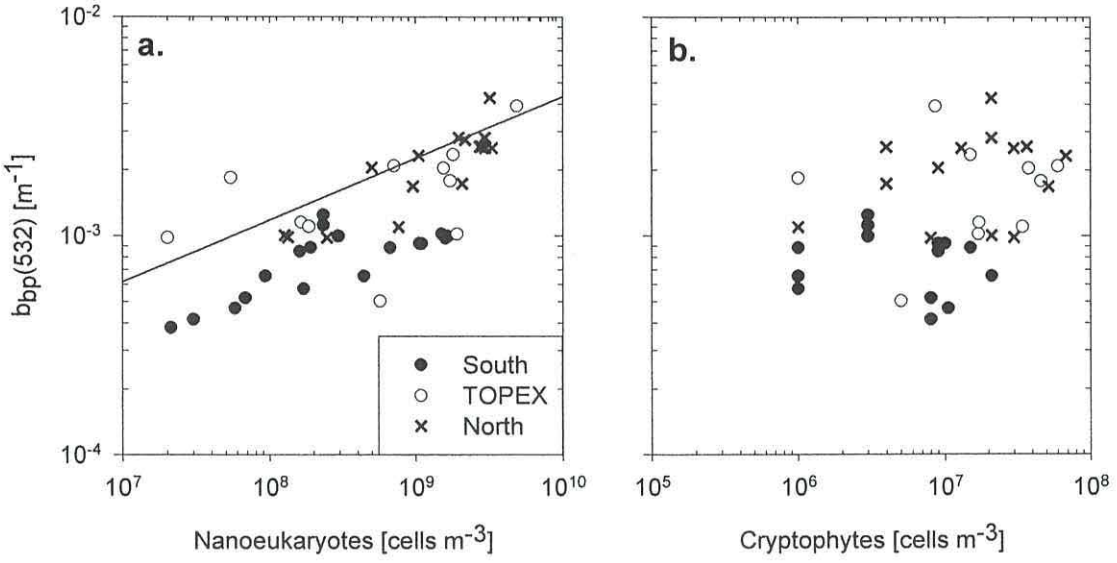

Figure 6.8 $b_{bp}(532)$ for each area at the CGFZ of the Mid-Atlantic ridge, as a function of: a) nanoeukaryote abundance. Solid line is the power law fit to all data for visualisation purposes b) cryptophyte abundance.

Differences in the relationships between groups for the areas are evidenced in Figure 6.9. To explain the causes of variability of $b_{bp}(532)$, correlations and regressions with phytoplankton and bacteria abundances (in cells m^{-3}) were done for the three separate domains of this study: South, TOPEX and North.

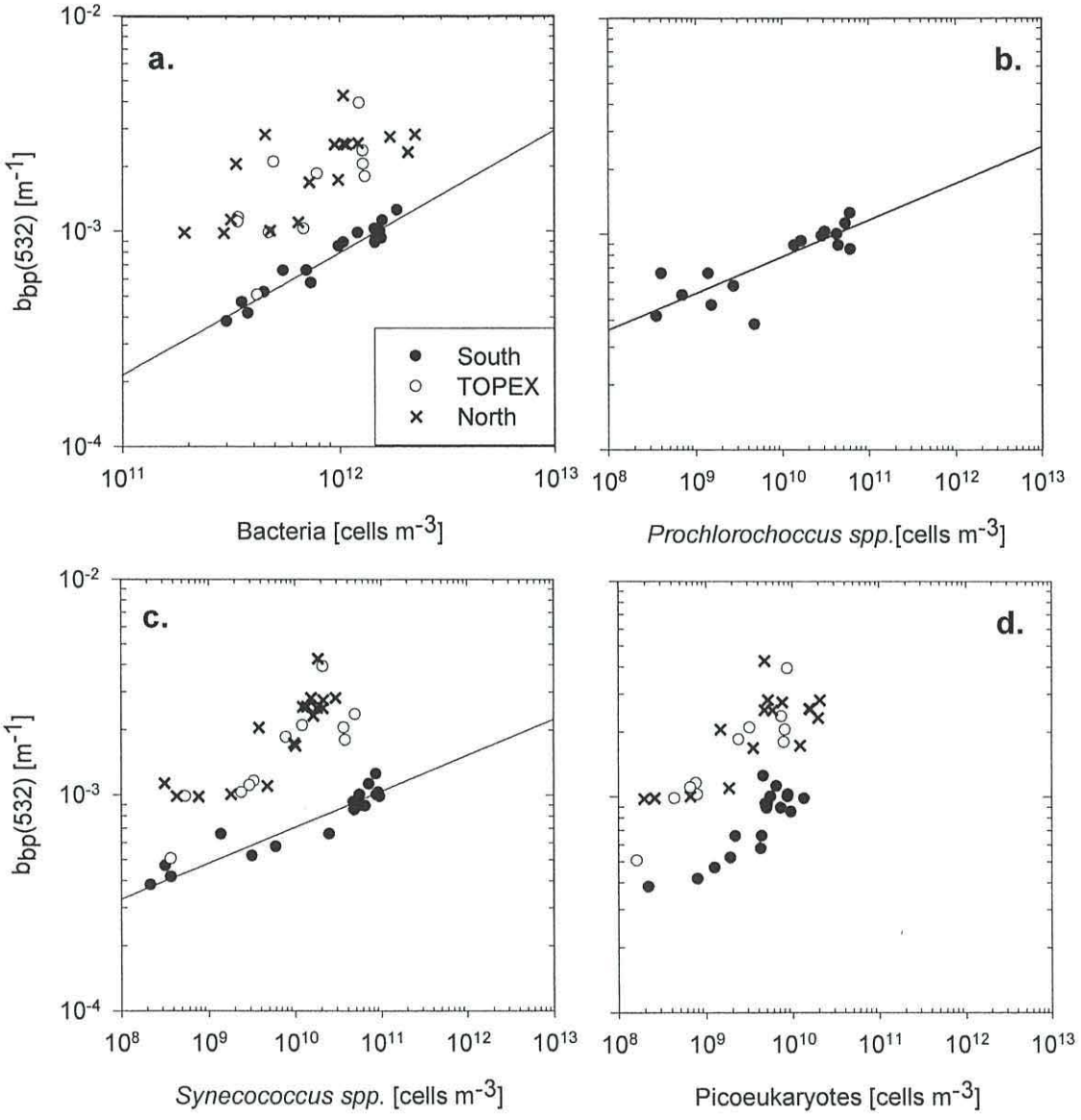

Figure 6.9 $b_{bp}(532)$ for each area at the CGFZ of the Mid-Atlantic ridge, as a function of: a) bacteria abundance. b) *Prochlorochoccus spp.* abundance. c) *Synecococcus spp.* abundance. d) Picoeukaryote abundance. Solid line in each plot is the power law fit to South data only for visualisation purposes. The corresponding linear fit model is shown in Table 6.1

A summary of the regression results by area is given in Table 6.1. In the South (N=18), the total bacteria (the sum of high and low nucleic acid bacterial counts), *Synecococcus spp.*, *Prochlorococcus spp.*, picoeukaryotes and nanoeukaryotes were significantly ($p<0.01$) and positively correlated (correlation coefficient, R, greater than 0.5) to $b_{bp}(532)$. Using a stepwise multiple linear regression, bacteria abundance, on its own, was able to explain the variability in $b_{bp}(532)$ in the South. Including picoeukaryotes in the stepwise regression increased the variance explained to 93%. Adding the *Prochloroccocus spp.* and nanoeukaryotes compartments did not increase the variance explained. Since the plankton groups were highly correlated with each other, the multiple linear regression with $b_{bp}(532)$ cannot be used to provide estimates of backscattering cross-section. Separate linear regressions with each group of organisms are reported as a way to quantify the variance explained by each phytoplankton component (Table 6.1). The estimates of backscattering cross section (σ_{bbpi}) produced in this way must be treated with caution, as they may be overestimating the role of each individual phytoplankton component being used to explain the variability of the backscattering coefficient separately. It is reassuring, however, that the backscattering cross section derived in this way increases with increasing nominal size of the organisms (i.e. from bacteria to nanoplankton) and that the order of magnitude ($\sim 10^{-12}$ to 10^{-15}) for each component is in agreement with current literature (Stramski *et al.*, 2001).

Concerning the unexplained variance, the residuals of the fit of cryptophytes and nanoeukaryotes for the whole dataset were significantly correlated with fucoxanthin concentrations, which explained 10% of the variability of the residuals through a linear fit ($P<0.05$, $F=6.14$, $N=45$, figure not shown). This indicates that diatoms may contribute to the backscattering signal at this region, but are not being accounted for using flow cytometry. Also, the alloxanthin, indicator of cryptophytes, was significantly correlated to the residuals, indicating that the cryptophytes counts may be underestimating the amount of cryptophytes, which may be larger than what was measured by flow cytometry.

Table 6.1: Linear regression estimates of the backscattering cross-section 532nm (mean±SE) for the plankton components (see text). The coefficient units are m^{-2} $part.^{-1}$ and have to be multiplied by a 10^{-15} factor. The regression statistics are summarized by the coefficients of determination (R^2) and the F-ratio (NS-not significant, P>0.05; *, 0.001<P<0.05;,P<0.001). CONST is the intercept. An example of how the table should be read is: $b_{bp}(532)=0.30x10^{-15}+0.47x10^{-15}C_{pBACT}$, $R^2=0.91$, N=18.**

Area		Coefficient ± SE ($\times 10^{-15}$)	R^2	F	N
All data	CONST	0.64± 0.12 **	70.2	53.97**	46
	NANOEUKARYOTES	621 ± 65 **			
	CRYPTOPHYTES	11143 ± 4475*			
South	CONST TOTAL BACT	0.30 ± 0.04** 0.47± 0.04**	91.2	177.95**	18
	CONST SYNECHOCCOCUS	0.51 ± 0.04** 6.64 ± 0.71**	83.5	87.18**	18
	CONST PROCHLOROCOCCUS	0.59 ± 0.05** 9.32 ± 1.73**	62.4	29.25**	18
	CONST PICOEUKARYOTES	0.54 ± 0.08** 50.27 ± 13.30*	43.9	14.29*	18
	CONST NANOEUKARYOTES	0.68 ± 0.07** 226.23 ± 93.69*	22.1	5.83*	18
TOPEX	CONST TOTAL BACT	0.48 ± 0.48 NS 1.56 ± 0.54*	42.3	8.33*	11
	CONST PICOEUKARYOTES	0.9 ± 0.26* 207.49 ± 50.70*	61.2	16.75*	11
	CONST NANOEUKARYOTES	1.06± 0.24* 526.9 ±130.6*	60.4	16.27*	11
North	CONST TOTAL BACT	1.36 ± 0.35** 0.8 ± 0.3*	25.5	6.47*	17
	CONST SYNECHOCOCCUS	1.13 ± 0.23** 83.65 ± 15.95**	62.4	27.52**	17
	CONST NANOEUKARYOTES	1.10 ± 0.21** 607.7± 105.0**	67.0	33.49**	17

In the TOPEX area, across the sub-polar front, *Prochlorochoccus spp.* were absent (N=11). Backscattering was significantly correlated with total bacteria (P = 0.018), and picoeukaryotes and nanoeukaryotes (P=0.003). Pico and nanoeukaryotes explained the highest variance in particle backscattering (r^2=0.6), whereas bacteria explained only 40% of the variability. Backscattering cross-sections were lower for bacteria and higher for picoeukaryotes and nanoeukaryotes, following the same pattern as in the South.

In the North, b_{bp} was correlated with bacteria, *Synechococcus spp.* and nanoeukaryotes abundances (N=17). *Synechococcus spp.* and nanoeukaryotes abundances explained 62 and 67% of the variance while total bacteria explained only 25% of the variance and again, the backscattering cross-section increased from smaller to larger particles.

Across areas, b_{bp} variability is explained differently by different plankton types. In the South, picoplankton dominated, *Synecococcus spp.*, *Prochlorococcus spp.* and total bacteria explained most of the variance. Whereas in the TOPEX and North nanoeukaryote abundance explained the highest percentage variance in $b_{bp}(532)$ followed by *Synecococcus spp.*.

The main result here is that the larger phytoplankton detectable by flow cytometry, nanoeukaryotes, are mainly responsible for the variation in b_{bp} in this dataset. However, locally, this relationship breaks down, and other phytoplankton components are more important explaining the variability of the b_{bp}. For instance, the South is an environment where smaller plankton dominates the pico and nano particle pool (bacteria, *Prochlorochoccus spp.* and *Synecococcus spp.*) and in the absence of larger nanoeukaryotes, smaller plankton dominates the variations of b_{bp}.

Using $a_{NAP}(412)$ as an indicator of detrital material, the relationship with backscatter was explored. No significant relationships between $a_{NAP}(412)$ and $b_{bp}(532)$ either for the whole of the dataset or for the separate areas.

6.2.5. Budget of the contributions of pico and nanoplankton to backscattering

The parameters used to derive the contribution of organisms to $b_{bp}(532)$ are size and backscattering efficiency factors for each particle type (Q_{bbpi}). These values are combined according to Equations 1 and 2 to obtain $b_{bp}(532)$. Size and Q_{bbpi} from the literature are summarized in Tables 6.2, 6.3 and 6.4. The values in italics in Tables 6.2 and 6.3 have been used for the reference calculation of σ_{bbpi} (Table 6.4). Multiplying σ_{bbpi} with the measured abundance of each type of particle (from flow cytometry) and adding all the contributions as in Equation 1, one obtains the reference $b_{bp}(532)$.

The size and Q_{bbpi} chosen for the reference calculation come mostly from experimental values obtained by Vaillancourt *et al.* (2004). This work has been chosen as it provides evidence that the greatest efficiency is due to phytoplankton (which is the hypothesis to be tested). All parameters come from that study, except those concerning *Synecococcus spp.*, as the representative species used by Vaillancourt *et al.* (2004), *Synecococcus elongatus*, is a freshwater species, and *Prochlorococcus spp.*, which was not measured in the Vaillancourt *et al.* (2004) study. No microscopy was available during the cruise, therefore representative species have been chosen as typical of the province under study (G. Tarran pers. comm.). Further, in the construction of the reference calculation, larger species (microplankton, d>20μm) and organogenic detritus have not been used, as no direct quantification of those was available for this cruise.

Table 6.2: Mean cell diameters (± standard deviations or ranges, in µm) from literature used in the computation of S_i to obtain σ_{bbp}. Values in italics have been used for the reference calculation. Additional values illustrate the range of observations or laboratory cultures (Lab. culture).

Group	Diameter	Reference and area of sampling
Total bacteria	*0.50*	Vaillancourt et al. (2004): Lab. culture
	0.46±0.14	Zubkov *et al.* (2000): Subtropical Atlantic
	0.50	Grob *et al.* (2007): Pacific
	0.56	Chung *et al.* (1996): Pacific
	0.50 to 0.65	Ulloa *et al.* (1992): Western North Atlantic
	0.15 to 0.73	Gundersen *et al.* (2002): Bermuda Atlantic
	0.34 to 0.75	Montes-Hugo *et al.* (2009): Various locations
	0.45 to 0.46	Green *et al.*(2003): Coastal Atlantic
	0.55	Stramski *et al.* (2001): Lab. Culture
Prochlorococcus spp.	*0.71*	Morel *et al.* (1993): SARG strain, Lab. culture
	0.59	Morel *et al.* (1993): MED strain, Lab. culture
	0.54	Heywood *et al.* (2006): Atlantic
	0.68±0.08	Grob *et al.* (2007): Pacific
	0.63±0.20	Zubkov *et al.* (2000): Subtropical Atlantic
	0.74	Chung *et al.* (1996): Pacific
	0.70	Claustre *et al.* (1999): Pacific
Synecococcus spp.	*1.05*	Ahn *et al.* (1992) : ROS strain. Lab culture
	2.50	Vaillancourt *et al.* (2004): Lab. culture
	0.93	Heywood *et al.* (2006): Atlantic
	0.86±0.10	Grob *et al.* (2007): Pacific open ocean
	1.16±0.02	Grob *et al.* (2007): Pacific coastal station
	0.95±0.31	Zubkov *et al.* (2000): Atlantic
	0.90	Chung *et al.* (1996): Pacific
	1.20	Claustre *et al.* (1999): Pacific
	1.09 to 1.38	Green *et al.*(2003): Coastal Atlantic
	0.92 to 1.43	Morel *et al.* (1993): Lab. culture
Picoeukaryotes	*1.40*	Vaillancourt *et al.* (2004): *Micromonas pulsilla*, Lab. culture
	1.90	Vaillancourt et al. (2004): *Pelagomonas calceolata*, Lab. culture
	1.56	Tarran et al. (2006): Atlantic
	1.37 to 1.99	Grob *et al.* (2007): Pacific
	2.35	Zubkov *et al.* (2000): Atlantic
	1.26	Chung *et al.* (1996): Pacific
	2.28	Claustre *et al.* (1999): Pacific
Nanoeukaryotes	*6*	Vaillancourt et al. (2004): *Chrysocromulina polylepis,* Lab. culture
	2.0 to 18.0	Vaillancourt *et al.* (2004): Lab. culture
	2.60	Tarran *et al.* (2006): Atlantic oligotrophic
	6.60	Tarran *et al.* (2006): Atlantic temperate
	2.05 to 2.31	Green *et al.*(2003): Coastal Atlantic
	3.97 to 7.73	Stramski *et al.* (2001): Small nanoplankton, Lab. culture
	11.77	Ahn *et al* (1993): *Hymenomonas elongata*, Lab. culture
Cryptophytes	*5.4*	Vaillancourt et al. (2004): *Guillardia theta*
	17.1	Tarran *et al.* (2006): Atlantic
	5.57	Ahn *et al.* (1993) : *Chroomonas fragarioides,* Lab. culture
	3.0 to 7.0	Vaillancourt *et al.* (2004): Lab. culture

Table 6.3: Backscattering efficiency factors (Q_{bbpi}, dimensionless) from the literature used in the computation of σ_{bbpi}. Values in italics have been used for the reference calculation. Additional values illustrate the range of observations or laboratory cultures (culture).

Group	Q_{bbpi}	Reference for Q_{bbp}, Species, Wavelength of Q_{bbp}
Total bacteria	*0.0039*	Vaillancourt *et al.* (2004): Undefined species, culture, 510 nm
	0.005 to 0.0090	Morel and Ahn (1990): Strain from Villefranche-sur-Mer coast, culture, 530 nm
	0.0023 to 0.0026	Green *et al.*(2003): Coastal Atlantic, 488 nm
Prochlorococcus spp.	*0.0008*	Morel *et al.* (1993): SARG strain, culture, 500 nm
	0.0011	Morel *et al.* (1993): MED strain, culture, 500 nm
Synecococcus spp.	*0.0007*	Ahn *et al.*(1992): ROS strain, culture, 550 nm
	0.0024	Vaillancourt *et al.* (2004): *Synecococcus elongatus*, culture, 510 nm
	0.0006	Morel *et al.* (1993): MAX01-Low light, culture, 500 nm
	0.0004	Morel *et al.* (1993): ROS and MAX at cultured different light intensities, culture, 500 nm
	0.0013 to 0.0022	Green *et al.*(2003): Coastal Atlantic, 488 nm
Picoeukaryotes	*0.0065*	Vaillancourt et al. (2004): *Micromonas pulsilla*, culture, 510 nm
	0.0030	Vaillancourt et al. (2004): *Pelagomonas calceolata*, culture, 510 nm
Nanoeukaryotes	*0.019*	Vaillancourt et al. (2004): *Chrysocromulina polylepis,* culture, 510 nm
	0.0018 to 0.0643	Vaillancourt et al. (2004): culture, 510 nm
	0.0015	Ahn *et al* (1993): *Hymenomonas elongata*, culture, 550 nm
	0.0013 to 0.0019	Ahn *et al* (1993): Other nanoplankton, culture, 550 nm
	0.0013 to 0.0020	Green *et al.*(2003): Coastal Atlantic, 488 nm
Cryptophytes	*0.0029*	Vaillancourt et al. (2004): *Guillardia theta* , culture, 510 nm
	0.0095 to 0.0258	Vaillancourt *et al.* (2004): culture , 510 nm
	0.0015	Ahn *et al.* (1993) : *Chroomonas fragarioides,* culture, 550 nm

The reference calculation of σ_{bbpi} computed from the literature are comparable with those derived from the linear fit to in-situ data (Table 6.4). For instance, the nanoeukaryote σ_{bbp} calculated from the whole dataset was 6.2×10^{-13} m^2 $cells^{-1}$ while the value from the reference calculation was 5.7×10^{-13} m^2 $cells^{-1}$. Bacteria and *Prochlorococcus spp.* σ_{bbp} calculated was also close to the in-situ. *Synecococcus spp.* and picoeukaryotes default calculated values are lower than in-situ.

The overall agreement between reference (calculated) σ_{bbpi} and measured σ_{bbpi} confirms that the efficiency factors and sizes used are representative of the observations at the ECOMAR region. This provides confidence on the use of those parameters to proceed with the calculation of b_{bp}.

Table 6.4: Backscattering cross-section (σ_{bbpi}) computed from the geometrical cross-section (calculated from the diameter in Table 6.2) and Q_{bbpi} (in Table 6.3). Values in italics have been used for the reference calculation. Additional values illustrate the range of observations (slopes of regressions extracted from Table 6.1).

Group	σ_{bbpi} from reference calculation (m^2 $cells^{-1}$) $\times10^{-15}$	σ_{bbpi} from regressions of in situ data (m^2 $cells^{-1}$) $\times10^{-15}$		
		South	TOPEX	North
Total bacteria	0.77	0.47	1.56	0.80
Prochlorococcus spp.	0.61	9.3	-	-
Synecococcus spp.	0.32	6.6	NS	83
Picoeukaryotes	10	50	207	NS
Nanoeukaryotes	570	226	527	607
Cryptophytes	66	NS	NS	NS

To calculate a reference $b_{bp}(532)$ from the contributions of each organism type, σ_{bbpi} (as calculated above) and C_i (i.e. the particle abundance of each type) measured were used. Reference σ_{bbpi} combined with C_i from flow cytometry samples coincident with b_{bp} in-situ data form the dataset for this analysis (N=26, depth ≤40 m). The final contribution of each organism to total b_{bp} (i.e. $b_{bpi}/b_{bp}x100$) is a product of cell size, efficiency factors and cell abundances. These contributions (in %) are averaged for the ensemble of data and by region. The most important contributors to the reference $b_{bp}(532)$ for all data are bacteria (52 %) and nanoeukaryotes (47 %), followed by picoeukaryotes (4 %). *Synechococcus spp.* and cryptophytes contribute both with less than 1%. These contributions were variable by area due to variations in cell abundances: bacteria contribution to b_{bp} decreases from 66 % in the South (N=8), to 54 % in TOPEX (N=7) and to a minimum of 38 % in the North (N=11). The contribution of nanoeukaryotes to b_{bp} increases from 27 % in the South, to 42 % in TOPEX, up to 64 % in the North. Therefore, the final contributions to b_{bp} are controlled by cell size and efficiency factors,

but assuming constancy of these, cell abundances modulate their change, causing changes in the dominance of the b_{bp}.

Reference b_{bp} were compared with in-situ measurements in Figure 6.10. The comparison falls around the one to one line. A number of factors could be invoked to modify the results: for instance, if data from southern stations were not considered, the variance explained would be similar but the slope of the regression would be closer to one (i.e. 0.9, instead of 0.7). Other factors that could significantly affect the fit are the choice of the cell size and the backscattering efficiency factors (Q_{bbpi}). Therefore a sensitivity analysis was performed to assess the impact of these parameters on σ_{bbpi} and b_{bp}.

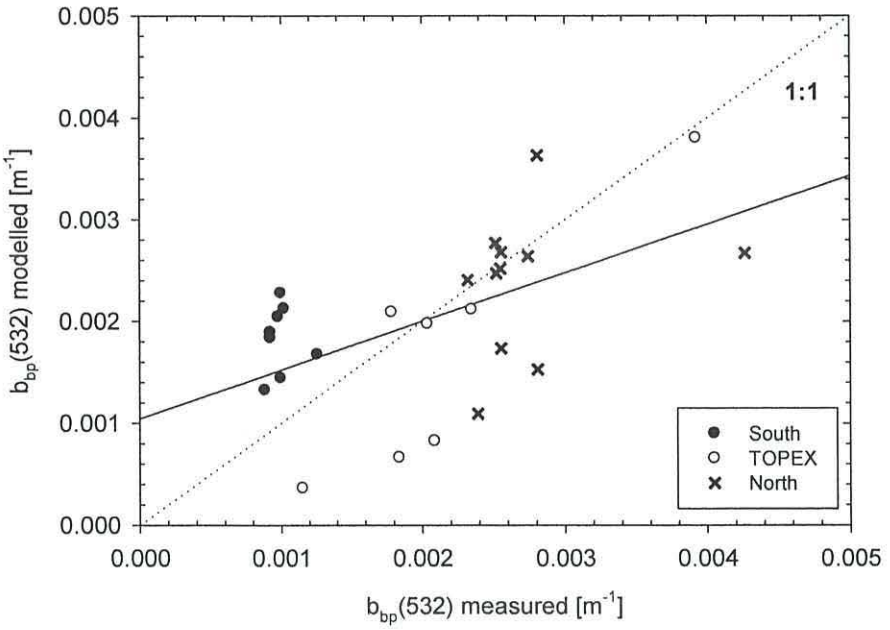

Figure 6.10 Measured versus modelled particulate backscattering at 532 nm for each region at the Mid-Atlantic Ridge. Solid line represents the linear regression fit to the data, with the equation: $b_{bp}(532)_{modelled} = 0.0010+0.48 \times b_{bp}(532)_{measured}$, $r^2= 0.27$, N=26. Dotted line is the 1-to-1 line.

In the sensitivity analysis, Q_{bbpi} and diameter were changed to the maximum and minimum reported in Tables 6.2 and 6.3 for each organism type. The impact of those changes are measured on terms of % of change in the slope and r^2 of the fit between $b_{bp}(532)$ modelled and measured, and referred to the reference calculation (i.e. slope = 0.48 and r^2=0.3) (Figure 6.11). The effects of changes on Q_{bbpi} and diameter on b_{bp} are

magnified by the particle abundance of each type. Therefore the greatest effects on the fit are on changes to the parameters of bacteria and nanoplankton. Only reducing the bacteria Q_{bbpi} or diameter there is an improvement of the fit: increase of r^2 (Figures 6.11.b and d) and a small increase of the slope (Figures 6.11.a and c). Importantly, increasing the efficiency of bacteria, does not improve the fit between observed and calculated b_{bp}. Another observation is that reducing the diameter or efficiency of the nanoeukaryotes, worsens the fit. Increasing their efficiency improves the amount of variance explained but produces a slope near to 1.5. This result points towards a potential greater role of nanoeukaryotes than bacteria in controlling the backscattering signal.

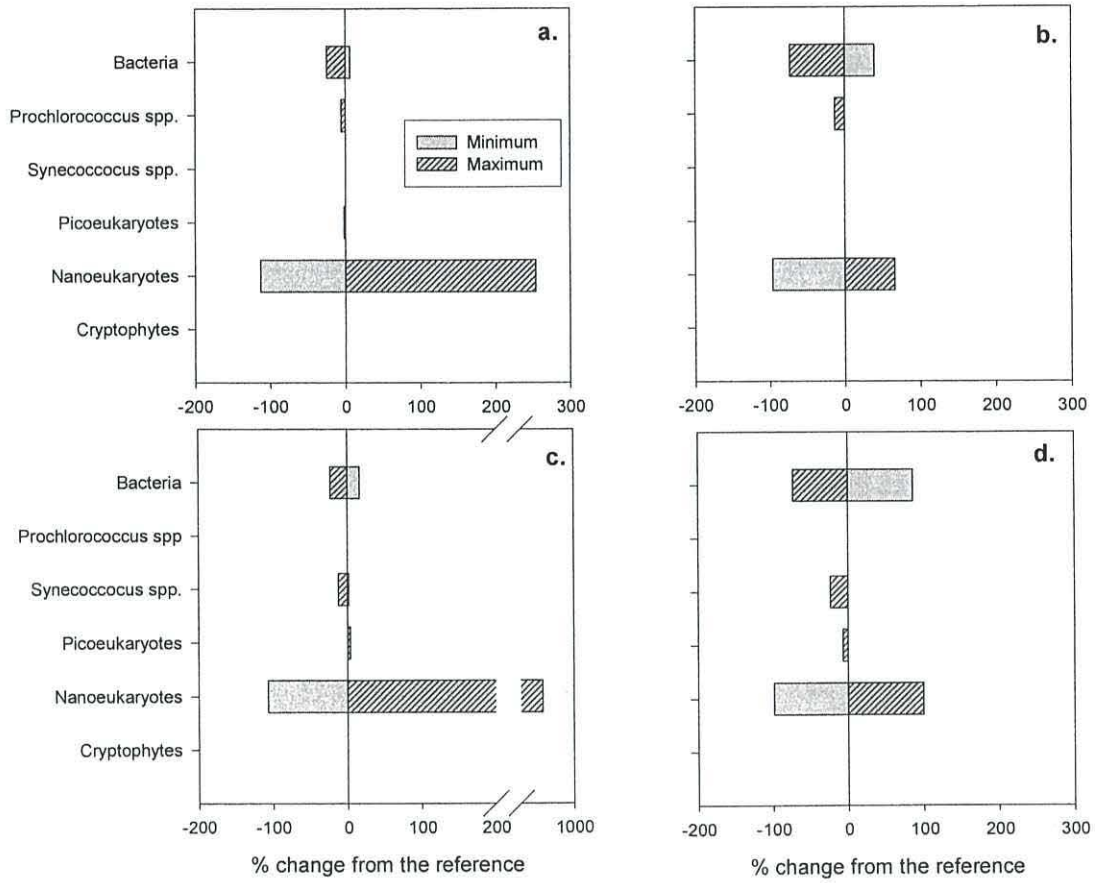

Figure 6.11 Sensitivity of the fit between b_{bp} measured and b_{bp} calculated (reference). With respect to changes of Q_{bbpi} in terms of % change in a) slope of the fit and b) r^2 of the fit. With respect to changes in diameter in terms of % change in c) slope of the fit and d) r^2 of the fit.

In particular, if for nanoeukaryotes, two different diameters were used, a smaller (2.6μm) in the South; the larger (6.6 μm) in the TOPEX and North data (Tarran *et al.*, 2006) the slope of the fit would become 0.82 and the r^2=0.6. Similarly, if one changed the size of bacteria to 0.2 μm in the South, leaving 0.5 μm in the TOPEX and North, the slope would become 0.9 and the r^2=0.6.This highlights the importance of measurements of typical sizes.

However, for a given cell size, it is interesting to test the effect of backscattering efficiency factors to verify the results by Stramski *et al.* (2001), that affirm that the greatest living contributors to backscattering are bacteria in oceanic conditions. For instance, if Q_{bbp} for bacteria increased from 0.0039 to 0.008 and Q_{bbp} for nanoeukaryotes decreased by a factor of four, from 0.019 to 0.0013, in these calculations, the overall contribution of bacteria would rise to 92%, coinciding with published results. However, the measured and simulated backscatter would lose any relationship (i.e. r^2 <1% and slope <0). Therefore, using a higher efficiency factor for bacteria and a lower one for nanoeukaryotes increases the contribution of bacteria but does not explain the observations in this dataset, suggesting a larger than expected contribution of nanoeukaryotes to particulate backscatter for this dataset.

6.3 Discussion and conclusions

During the ECOMAR cruise, there was a doubling in the particle backscattering coefficient from the South to the North of the sub-polar front. The increase in backscattering was related to an increase in nanoeukaryotes and, to a lesser extent, cryptophytes abundance, which together explained a large fraction of the variance in particle backscatter. In addition, the particulate detritus absorption at 440 nm was low and decreased towards the North.

These findings can be compared with theoretical predictions that support the role of bacteria as the main living backscatterers (Stramski *et al.*, 2001). The Stramski *et al.*, (2001) theoretical study (based on pre-existent measurements) predicts that the major cause of backscattering is minerals, which contribute 80-85 % of the signal, followed by biogenic detritus (~9%) and bubbles (3.6-7%). In their reference simulation, all the planktonic microorganisms contribute to a small fraction of backscatter (1.8-3.6%), of

which the most important are bacteria. The reference modelling scenario proposed by Stramski *et al.*, (2001) is in oligotrophic state (Chl-a of 0.18mgm^{-3}) and the detritus absorption ($a_{NAP}(440)$, including mineral and biogenic absorption) is ~29% of the particulate absorption. This scenario produced a $b_{bp}(532)$~0.0019m^{-1}. In a scenario with bloom conditions (i.e. Chl-a equal to 0.72 mgm^{-3}; a_{NAP} (440) proportion remained constant), Stramski *et al.* (2001) predict an increase of 3% or less in backscattering due to the increase of different types of phytoplankton. In the South, with a Chl-a of 0.26 mgm^{-3} and a_{NAP} (440) proportion of 14%, the measured $b_{bp}(532)$ was 0.001m^{-1}. This area had 44% more Chl-a and half a_{NAP} (440) proportion than the reference simulation from Stramski *et al.* (2001), and yet, the $b_{bp}(532)$ measured was half the predicted value in their reference simulation. In the TOPEX and North, however, the a_{NAP} (440) proportion of the particulate absorption decreased (to 8.5 and 6.4% respectively), but the $b_{bp}(532)$ did not (0.0027m^{-1} and 0.0026m^{-1}, respectively). Furthermore, a small (but significant) fraction of the variance of the residual (from the multiple linear regression between backscattering and nanoeukaryotes and cryptophytes) was explained by the variation in a pigment marker of diatoms.

Particulate backscattering, derived using parameters from laboratory experiments (Morel *et al.*, 1993; Vaillancourt *et al.*, 2004) and in-situ estimates of pico and nanoplankton size (Heywood *et al.*, 2006; Tarran *et al.*, 2006; Zubkov *et al.*, 2000) were then used in the present work in an approach similar to the one used to fractionate the optical attenuation coefficient into different phytoplankton components (Chung et al., 1998; Claustre et al., 1999; Durand and Olson, 1996). For a realistic range of assumed sizes and measured particles concentrations, the combination of Q_{bbpi} that better explained the observations were those that gave a higher importance to larger phytoplankton. However, it is worth noting that these calculations are very sensitive to the typical size used, especially for the bacteria and nanoeukaryotes. It is therefore crucial in future work to have accurate estimates of the representative sizes for each compartment.

Another potential source of error is the uncertainty in the dominant phytoplankton species, to attribute Q_{bbpi}. No visual identification of species was available for this cruise, the representative species for a particular phytoplankton is assumed to be the typical one for the corresponding province (G. Tarran, pers. comm.), for which Q_{bbi}

value is available from the literature. It is also important to highlight the caveat that the calculations have by not considering the larger phytoplankton (at least diatoms) and detritus in the simulation. Secondly, given the small change in spectral backscattering, the mismatch between the measured wavelength used (532 nm) and the wavelengths used for the calculations (Table 6.3).

The two separate comparisons above provide indirect evidence that the nanophytoplankton could be more important than expected from bio-optical modelling, as being suggested by recent field studies (Dall'Olmo *et al.*, 2009). It could be that homogeneus contents increase the backscattering efficiency (Aden and Kerker, 1951; Bernard et al., 2009; Meyer, 1979). If the limitations of the models are their simplifications, the main limitations of field studies such as the present one are: its confinement in time and space, the limited amount of co-incident backscatter and flow cytometry data, the lack of direct measurements of mineral concentrations, unavailability of wind data at the moment of this study to calculate the bubble concentrations and the lack of direct measurements of cell diameters. Therefore, similar studies to this one in different oceanographic conditions with large variations in dominant phytoplankton sizes, that include the above measurements, are desirable to verify the findings presented.

To definitively test the role of nanoeukaryotes as important backscatterers, in-situ populations need to be identified and the appropriate species specific Q_{bbi} need to be attributed. Concerning size measurements, it is now normal practise to do size fractionation tests to measure pico and nanoplankton sizes so that uncertainty in parameters can be reduced, and better backscattering estimates can be produced (Grob *et al.* 2007).

As a conclusion, in the particular region of study of the Mid-Atlantic Ridge in the summer period, it has been found that a large part of the backscattering measured is well correlated with Chl-a and explained mainly by variations in nanoplankton cell abundance. This could be representative of larger areas of the ocean, where there are no terrigenous sources.

Chapter Seven

Seasonal changes in the Western English Channel and their effect on particulate backscattering and scattering

CHAPTER SEVEN: SEASONAL CHANGES IN THE WESTERN ENGLISH CHANNEL AND THEIR EFFECT ON PARTICULATE BACKSCATTERING AND SCATTERING

Synopsis

In the two previous chapters (Chapters 5 and 6) results have shown that in an open ocean location, in the summer of 2007 (away from coastal areas), it is possible to relate the backscattering coefficient variations to the amount of chlorophyll-a (Chapter 5). According to the results from Chapter 6, a proportion (60%) of the variability in backscattering can be explained by the variations in abundance of nanoplankton (between 2 and 20 μm). This result challenges current knowledge about backscattering. To verify the extent of the validity of the relationship between backscattering and phytoplankton, when other sources can be present (i.e. minerals or organic detritus not locally produced), the 'reductionist approach' is applied to a Western English Channel dataset. Results in this chapter show that suspended mineral particles explain part of the variability of the b_{bp} (R^2=58%, N=16, P<0.001) whilst none of the organisms (greater than 2 μm) considered in this study were related significantly to the variations in backscattering. This is discussed in terms of the composition of the suspended matter. Additionally to the study on the relationship between particulate matter and backscattering, the variations of the backscattering spectral slope are presented but less emphasis should be placed on these results due to the caveats mentioned in Chapter Three.

A part of this chapter has been submitted, with contributing data from other authors, to Journal of Plankton Research (title: *Particulate scattering and backscattering related to water constituents and seasonal changes in the western English Channel*) and is currently (December 2009) under revision (in press).

7.1 "Reductionist approach" equations at L4

Following on the rationale from the previous chapter, the particle backscattering (b_{bp}) is considered to be the result of a sum of influences due to different types of suspended matter. To recapitulate, the measurements at L4 (list presented in full detail in Chapter 3) were taken near the surface on a weekly basis for a period of ten years. Apart from b_{bp}, particulate scattering (b_p) was also available and will also be studied in this Chapter. Concerning the matter composition, several indicators of the organic and inorganic matter amount were available: suspended particulate matter (SPM), the organic and inorganic fractions of the SPM (i.e. POM and PIM) and the phytoplankton carbon (phytoplankoton-C) from microscopy abundances separated in the following groups: diatoms, dinoflagellates, phyto-flagellates (between 2 and 10μm), *Phaeocystis* spp., coccolithophorids and heterotrophic Dinophyceae. Phytoplankton-C, is hereafter referred to the sum of the carbon contributions from each of the phytoplankton groups above (i.e. **diatoms, dinoflagellates, phyto-flagellates, *Phaeocystis spp.* and coccolithophorids**) plus the **heterotrophic Dinophyceae**, because of the presence of photosynthetic pigments (Roger Harris pers. comm.). Percentages of each phytoplankton component are referred to the total phytoplankton-C as defined here. It is worth stressing that no picoplankton or bacteria counts were included in this phytoplankton-C estimate. It is also important that all the study hereafter will be done in mass concentrations as opposed to number concentration (in Chapter 5). The reason for using mass rather than number concentration is to keep phytoplankton abundance comparable with the SPM (in mass).

Therefore, the main assumptions of the study that follows are: that the main contributors to b_{bp} are those organisms detected by optical counting, SPM (fractionated into minerals and organic matter). Bacteria, picoplankton (less than 2 μm) are not considered separately and bubbles are assumed not to be significant contributors to b_{bp} at L4. With these assumptions, Equation 1 in Chapter One, becomes:

$$
\begin{aligned}
b_{bp} &= b_{bpSPM} = b_{bpPOM} + b_{bpPIM} = b_{bpliving} + b_{bpnonliving} + b_{bpPIM} = \\
&= \sum_{i=1}^{n} b_{bppla,i} + b_{bpnonliving} + b_{bpPIM} = \\
&= \sum_{i=1}^{n} C_{ppla,i}\sigma_{bbp,pla,i} + C_{nonliving}\sigma_{bbp,nonliving} + C_{PIM}\sigma_{bbp,PIM} = \\
&= C_{pFLAGEL}\sigma_{bbpFLAGEL} + C_{pCOCCO}\sigma_{bbpCOCCO} + C_{pPHAEO}\sigma_{bbpPHAEO} + \\
&\quad C_{pDIAT}\sigma_{bbpDIAT} + C_{pDINO}\sigma_{bbpDINO} + C_{pHETDINO}\sigma_{bbpHETDINO}
\end{aligned}
\qquad \textbf{Eq.1}
$$

where $C_{ppla,i}$ is the mass concentration (in $mgCm^{-3}$) for each type of plankton particle (*ppla,i*), detected by optical microscopy : phyto-flagellates - *FLAGEL*, coccolithophorids – *COCCO*, *Phaeocystis spp.* – *PHAEO*, diatoms – *DIAT*, dinoflagellates – *DINO* and heterotrophic Dinophyceae – *HETDINO*. σ_{bbp} is the backscattering cross-section (in m^2mgC^{-1}) of a single particle of the *i*th component and is the result of the product of the geometric cross-section of the particle (S_i) by the efficiency factor (Q_{bbi}, dimensionless) for backscattering of the particle. The efficiency factor is the ratio of radiant power backscattered by the particle to radiant power intercepted by S_i (Bricaud and Morel, 1986):

$$b_{bpi}=C_{pplai} \times [S_i \times Q_{bbi}] \quad \textbf{Eq.2}$$

Equation 1 also includes the role of minerals (PIM) and non-living organic matter. The latter is quantified by the particulate organic fraction of SPM (POM). Conceptually there is an overlapping on the definition of this variable using POM, as it includes the contributions of living photosynthetic organisms as well as bacteria and organogenic detritus. These equations are also used for b_p.

The first part of this chapter presents the seasonal variations of the variables under study. Seasonal averages and standard deviations were calculated by separating the dataset by solstices and equinoxes to define seasons and pooling the data together from different years. By doing this, it is assumed that no inter-annual trends can be detected with the current dataset, due to the length of the data record and frequency of observations (Section 7.2).

Then the dataset is explored statistically by means of linear regressions between the abundances of the different groups of organisms and suspended matter composition and b_{bp} to obtain σ_{bbp} (as well as b_p). Finally, global relationships among the descriptors of the composition of suspended matter are presented to interpret the seasonal variability of σ_{bbp} and σ_{bp} .

7.2 The overall picture at L4: particle composition and scattering properties

A dataset from samples collected in different ways and for different time periods has been assembled at L4. The diversity of sampling methods (Chapter 3) is reflected in the amount of data available for each variable (Table 7.1). For a time series of 10 years sampled every week there should be a grand total of 520 samples. However, due to logistics and weather, the number of effective sampling opportunities per year at L4 is on average 40. Samples that were collected from the ship's non-toxic water supply (i.e. pigments and SPM) are the most abundant (N equal to 405 and 307), given that the pigments time series started earlier than the SPM. Discrete samples for phytoplankton-C (N=364) were not as abundant, however, as they are sampled from a Niskin bottle on a CTD rosette which is not deployed during adverse sea conditions at the station. Finally, the least frequently collected data were from the optics rig, which is lighter than the CTD, and has a narrow weather window making its deployment even more reliant on the sea conditions. Intermittent instrument failures and post-processing quality checks further reduced the availability of the optics data.

Mixed layer depth (obtained from CTD data) at L4 followed the typical temperate region pattern (Figure 7.1.a.), ranging from a peak of 35 m during autumn-winter (i.e. mixing most of the water column) to a minimum of ~5m during summer. Interestingly, the full water column is never completely mixed, reducing the possibility of presence of locally re-suspended matter near the surface. Also the euphotic layer depth (depth at which the surface PAR irradiance is reduced to 1%) is always deeper than the mixed layer depth (data not shown, global mean±std. dev. 32.5±7.2 m). The water column at L4 is significantly more stratified during the summer and spring months (mean±std. dev. 15.2±6.6 m) compared to the autumn and winter period (26.1±8.2m).

Table 7.1: Descriptive statistics at L4, including number of samples for each variable (N), average and standard deviation (SD), range (minimum and maximum) and the period of sampling or the actual years sampled.

Variable	N	Average	SD	Minimum	Maximum	Years
SPM (gm^{-3})	309	1.00	0.88	0.17	9.94	2001 - 2008
PIM (gm^{-3})	293	0.71	0.80	0.02	8.45	2001 - 2008
POM (gm^{-3})	290	0.31	0.22	0.01	1.48	2001 - 2008
POM/SPM (%)	287	35.5	21.1	1.7	97.6	2001 - 2008
Chl-a (mgm^{-3})	405	1.38	1.09	0.09	12.23	1999 - 2008
Phytoplankton-C ($mgC\ m^{-3}$)	366	41.7	49.1	2.8	378.8	1999 - 2008
Phytoplankton-C:Chl-a	296	36.05	43.05	2.07	408.14	1999 - 2008
Phyto-Flagellates ($mgC\ m^{-3}$)	366	13.7	17.1	0.6	212.2	1999 - 2008
Coccolithophorid ($mgC\ m^{-3}$)	366	0.8	2.2	0.0	30.0	1999 - 2008
Phaeocystis spp. ($mgC\ m^{-3}$)	366	1.9	11.2	0.0	135.0	1999 - 2008
Heterotroph-Dinophyceae ($mgCm^{-3}$)	366	5.6	14.1	0.0	170.3	1999 - 2008
Diatoms ($mgCm^{-3}$)	366	10.8	20.5	0.1	173.8	1999 - 2008
Dinoflagellates ($mgC\ m^{-3}$)	366	8.9	29.0	0.0	312.1	1999 - 2008
Particle size distribution slope, *j*	80	2.42	0.67	1.35	4.84	2005,2007,2008
b_p (532) (m^{-1})	99	0.555	0.272	0.125	1.760	2003 - 2008
γ_S	99	0.3	0.7	-0.6	4.1	2003 - 2008
b_{bp}(532) (m^{-1})	23	0.003	0.002	0.000	0.008	2003 - 2008
γ_{BS}	23	-0.2	1.7	-5.0	4.1	2003 - 2008
b_{bp}: b_p (532)	16	0.004	0.002	0.001	0.009	2003 - 2008
γ_{BSR}	16	-0.6	1.0	-2.3	1.2	2003-2008

The suspended particulate matter (SPM) global mean value was low for a coastal site ($1.00\pm0.88 gm^{-3}$, Table 7.1), although large peaks (Figure 7.1.b., maximum of 9.94 gm^{-3}) appeared mainly during winter. This seasonal variation appears to be related to the variations of the inorganic suspended matter, PIM (Figure 7.1.c). The overall split of the SPM is 70% PIM to 30% POM. The present study adds a temporal dimension: Table 7.2 shows that SPM almost halves from winter to summer and the POM:SPM ratio, indicative of the fraction of combined living and non-living organic material in the suspended matter, more than doubles from 20 % in the winter to about 50% in the spring and summer.

Table 7.2: Seasonal separation (means and standard deviations, SD) of the SPM and POM:SPM

	SPM (g m-3)		POM:SPM (%)	
Season	N	Mean±SD	N	Mean±SD
Winter	65	1.51±1.49	65	19.5±7.0
Spring	86	0.80±0.40	85	48.2±20.9
Summer	92	0.81±0.66	83	51.9±16.4
Autumn	64	1.03±0.57	54	32.8±12.7
All data	309	1.00±0.88	287	35.5±21.1

The phytoplankton amount and diversity was monitored in terms of Chl-a and phytoplankton-C (Table 7.3). Chl-a was generally lower than 2 mg Chl-a m^{-3}, but highly variable (Figure 7.1.d and Table 7.1). The main phytoplankton Chl-a bloom at L4 typically occurred in spring (late April to early May) and a secondary bloom typically appeared late in the summer (September). In between these two maxima there was usually a period of low Chl-a concentration, except for some events (e.g. a peak of 7 mg Chl-a m^{-3} occurred on the 14th July 2008). Seasonally, the Chl-a was significantly higher in the summer and spring compared to winter and autumn.

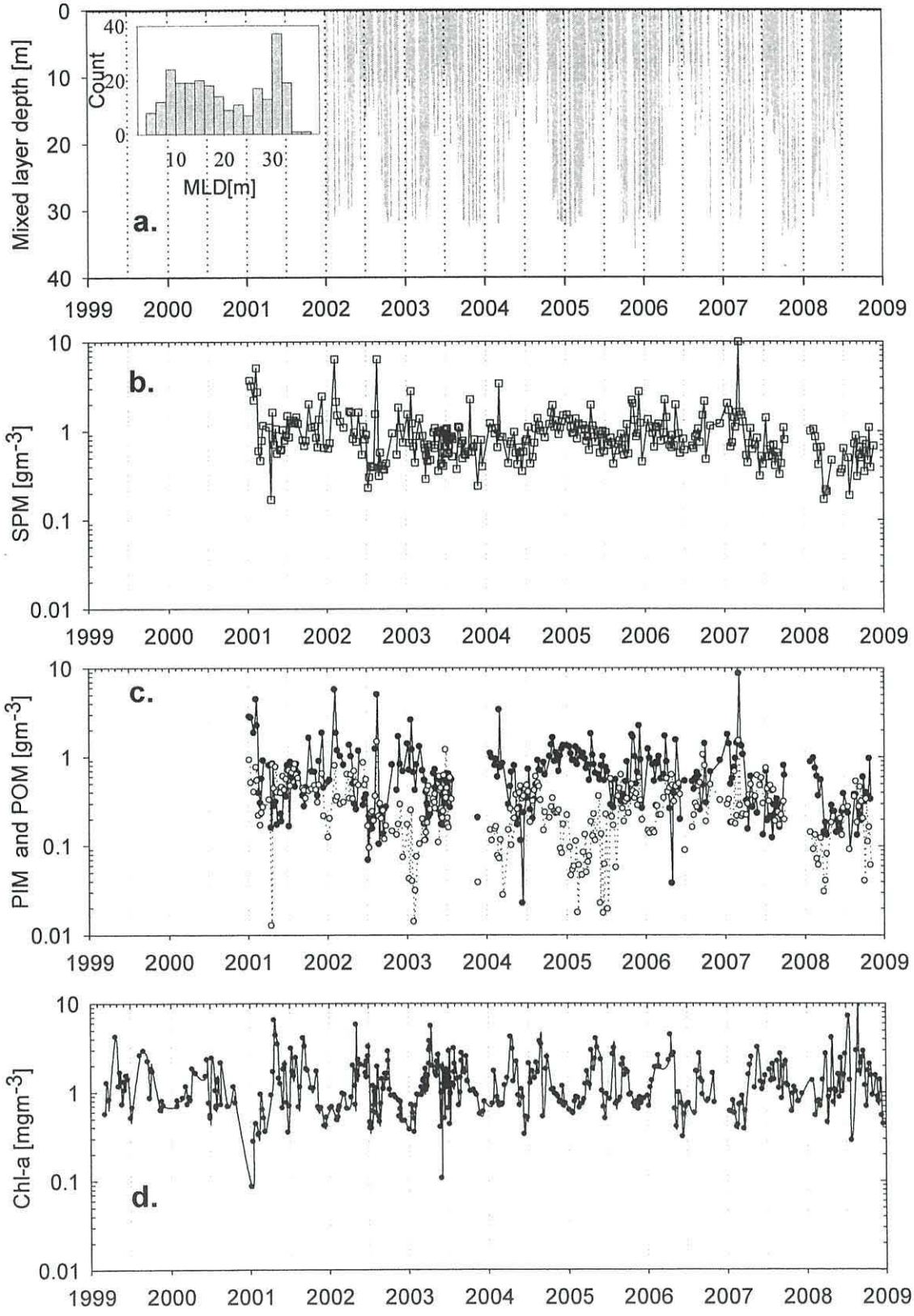

Figure 7.1 Weekly time series at L4 between January 1999 and January 2009 : a) mixed layer depth (insert is histogram of frequency),b) SPM, c) PIM, solid line and filled dots; POM, dotted line and empty dots, d) Chl-a.

The phytoplankton-C presented a large overall standard deviation (41.6±49.12 mg C m^{-3}) indicating large seasonal variability. Similarly to Chl-a, there was lower phytoplankton-C in winter and autumn and higher in summer and spring, with summer significantly higher than spring. In order to explain these variations, the temporal evolution of the contributions to the phytoplankton-C pool has to be invoked. The small phyto-flagellates were present and very abundant throughout the year (Figure 7.2). The large phytoplankton-C components (diatoms, dinoflagellates and heterotrophic Dinophyceae) present a succession typical of temperate regions: spring bloom dominated by diatoms and late summer bloom dominated by dinoflagellates and heterotrophic Dinophyceae (Figure 7.2). This can explain the mismatch between the maximum in Chl-a (spring) and the maximum in phytoplankton-C (summer): dinoflagellates and heterotrophic Dinophyceae have a larger C:Chl-a ratio than diatoms. *Phaeocystis* spp. appeared sporadically in blooms only in spring while coccolithophorid blooms occurred in spring, summer or autumn.

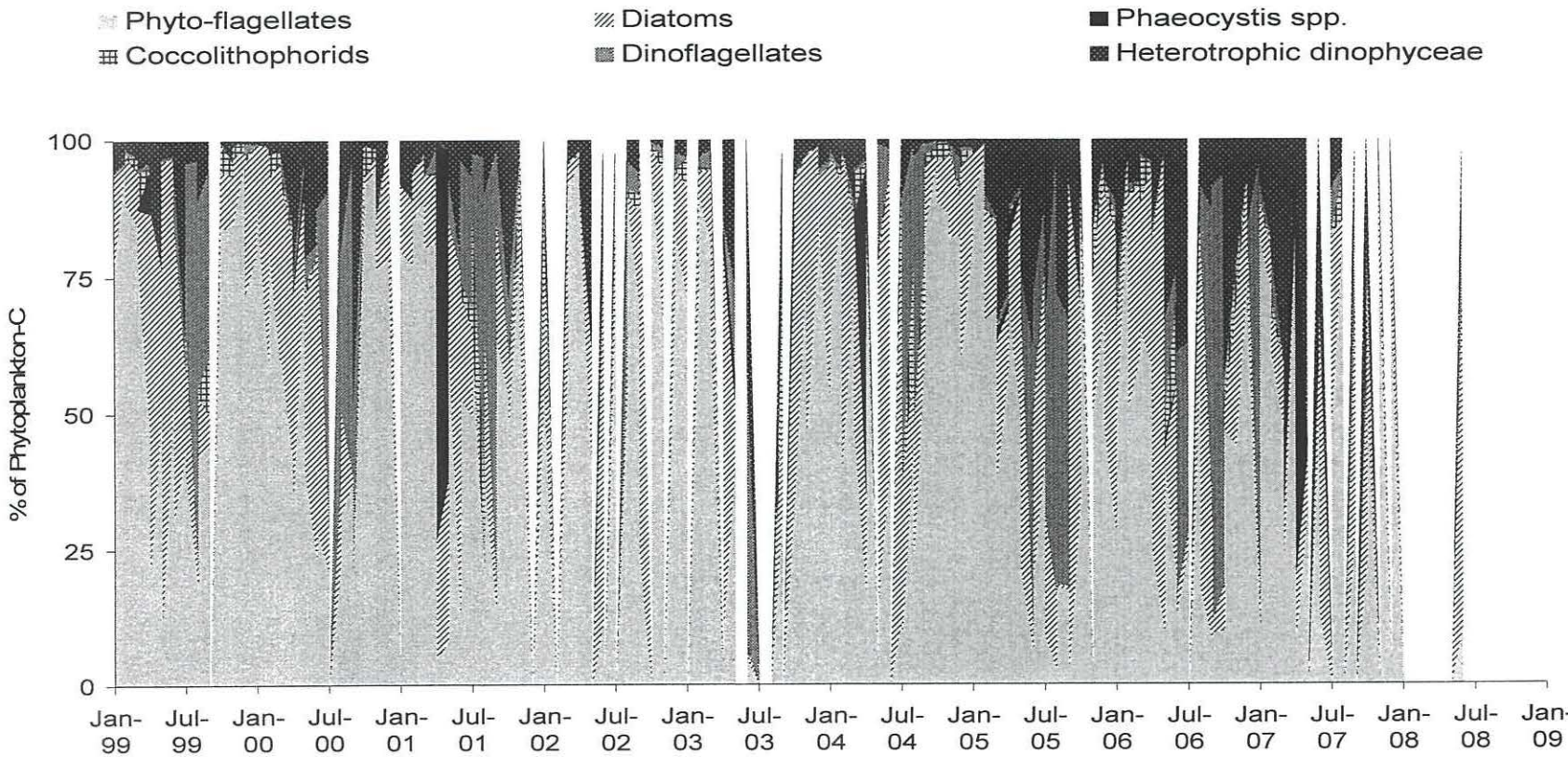

Figure 7.2 Relative abundance (in percentage) to the total phytoplankton-C by the different phytoplankton groups considered (diatoms, dinoflagellates, flagellates, *Phaeocystis* spp., coccolithophorids and heterotrophic Dinophyceae) between January 1999 and January 2009 at L4. White spaces are missing data.

The particle size distribution was measured intermittently during the study (Table 7.1). The Junge exponent derived from it, j, was generally low (2.4±0.7), indicating the dominance of larger particles in the size range considered (2 – 60 μm). Seasonally, the Junge exponent was significantly higher in winter than spring and summer, while autumn values were intermediate (Figure 7.3 and Table 7.2).

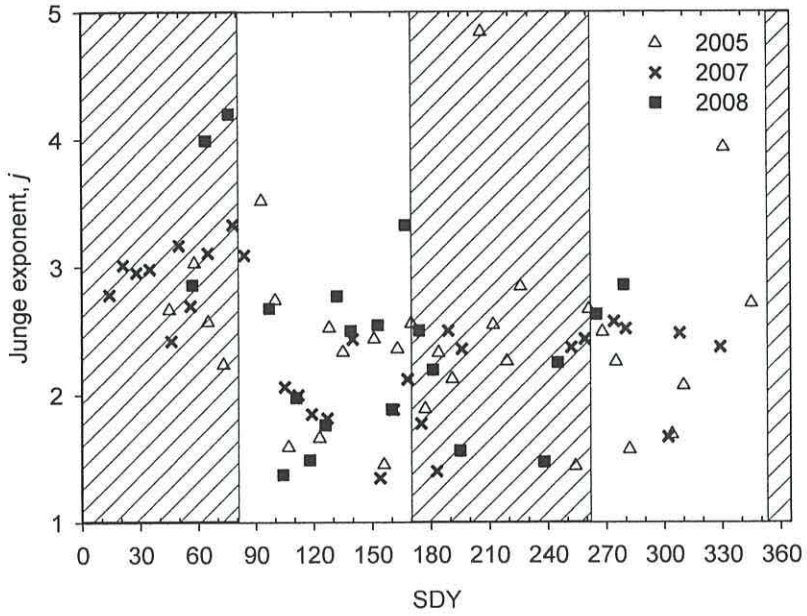

Figure 7.3 Particle size distribution slope or Junge exponent, j for three years. Data are superimposed relative to the standard day of the year (SDY) for the three years.

For particulate scattering (b_p), the 532 nm channel was used because this matches the equivalent band in b_{bp}. There was a significant seasonal signal in b_p at all wavelengths: lower mean values were found in spring and winter compared to summer and autumn (Figure 7.4.a and Table 7.3).

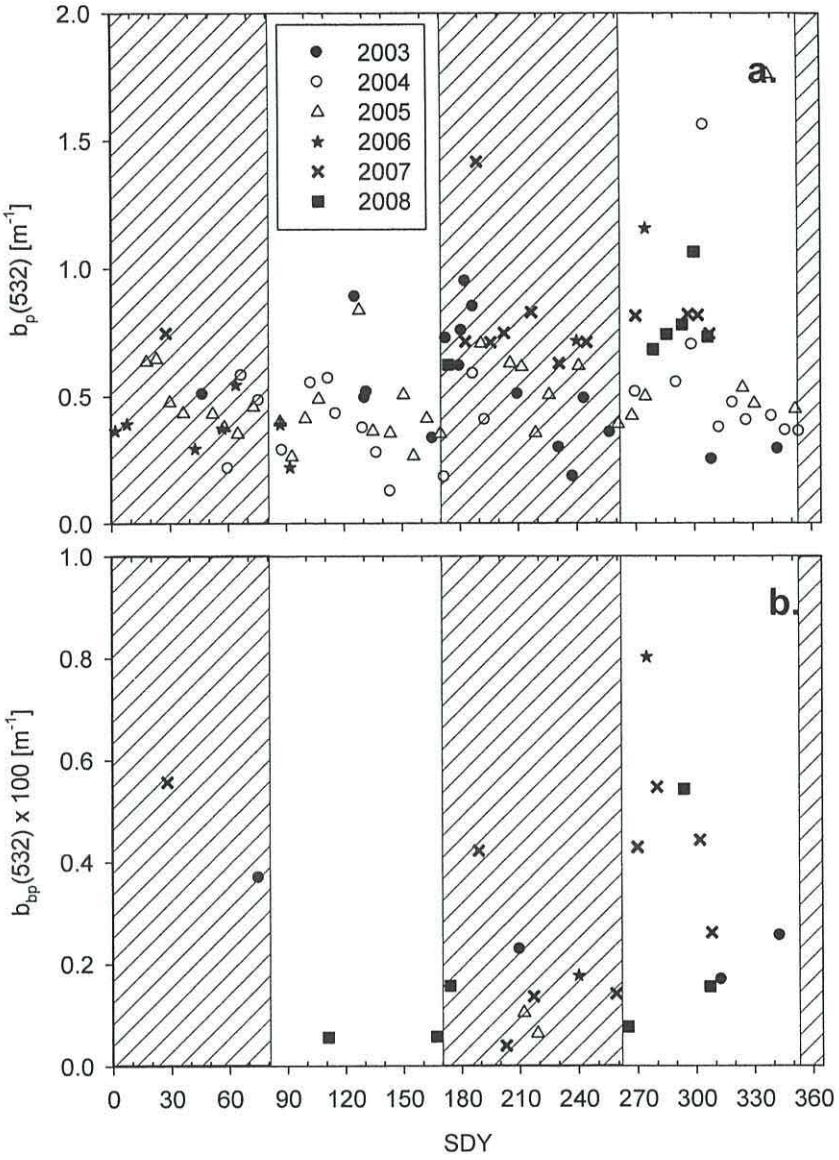

Figure 7.4 Time series of at L4 for 6 years:a) $b_p(532)$; b) $b_{bp}(532)$. Data are superimposed relative to the standard day of the year (SDY) for the six years.

The particulate backscattering coefficient at 532nm, $b_{bp}(532)$, had a global average and standard deviation of 0.0027±0.0020 m^{-1}. $b_{bp}(532)$ was statistically significantly lower during spring and summer compared with autumn and winter (Figure 7.4.b. and Table 7.4).

Table 7.3: Seasonal separation (means and standard deviations, SD) of the Chl-a, phytoplankton-C, phytoplankton-C:Chl-a ratio and Junge parameter, *j*.

	Chl-a ($mg\ m^{-3}$)		Phytoplankton-C ($mg\ m^{-3}$)		Phytoplankton-C: Chl-a ($mgC\ mg\ Chl\text{-}a^{-1}$)		Particle size distribution slope, *j*	
Season	N	Mean±SD	N	Mean±SD	N	Mean±SD	N	Mean±SD
Winter	83	0.81±0.41	79	12.2±11.1	61	17.87±17.4	17	3.0±0.5
Spring	117	1.71±1.17	105	51.9±45.1	84	39.18±34.59	29	2.2±0.6
Summer	116	1.67±1.39	99	70.3±61.4	83	56.48±57.38	20	2.3±0.7
Autumn	89	1.09±0.53	83	22.6±34.8	68	23.53±37.24	14	2.4±0.6
All data	405	1.38±1.09	366	41.7±49.1	296	36.05±43.05	80	2.4±0.7

Table 7.4: Seasonal separation of the particulate scattering, backscattering and backscattering ratio coefficients at 532 nm (means and standard deviations, SD) together with their respective spectral slopes. NA means not available.

	$b_p(532)$ (m^{-1})		γ_S	$b_{bp}(532)$ $\times 10^{-3}$ (m^{-1})		γ_{BS}	$b_{bp}(532)$: $b_p(532)$ $\times 10^{-3}$		γ_{BSR}
Season	N	Mean±SD	Mean±SD	N	Mean±SD	Mean±SD	N	Mean±SD	Mean±SD
Winter	18	0.46±0.13	0.0±0.3	2	5.00±1.41	-0.3±1.3	1	7.5±NA	-1.5±NA
Spring	25	0.41±0.18	0.8±1.0	2	0.57±0.01	0.5±2.1	0	NA	NA
Summer	28	0.63±0.24	0.3±0.4	9	1.63±1.10	-0.4±1.1	8	2.3±1.2	-0.6±1.2
Autumn	28	0.67±0.36	0.1±0.7	10	3.68±2.20	-0.1±0.9	7	5.6±2.3	-0.5±0.8
All data	99	0.56±0.27	0.3±0.7	23	2.72±2.10	-0.2±1.7	16	4.0±2.5	-0.6±1.0

The $b_p(532)$ and $b_{bp}(532)$ were correlated when all coincident data were considered (Figure 7.5, N=16), but presented a large dispersion (R^2=25%). The overall mean backscattering ratio $\tilde{b}_{bp}(532)$ is 0.0040±0.0025. Seasonally, sampling was un-balanced, with one observation in winter, none in spring, 8 in summer and 7 in autumn. Values recorded in winter and autumn (0.0058±0.0022, N=8) were significantly higher than in summer (0.0023±0.0012, N=8).

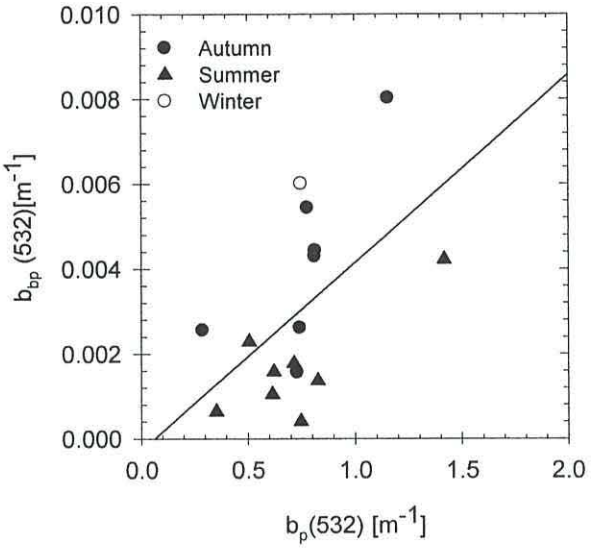

Figure 7.5 Scatter plot of $b_p(532)$ and $b_{bp}(532)$ for the whole dataset, with different symbols for each season. The solid black line is the corresponding linear regression to the whole dataset: $b_{bp}(532)=0.0042\times b_p(532)-0.00028$, $R^2=0.25$, N=16. The constant is not significant (p>0.05).

The mean spectra of b_p and of b_{bp} are presented for the different seasons (Figure 7.6 and 7.7). It can be observed for scattering that overall spectral features appear in all seasons with different intensity and for the backscattering that the spectra are not flat. The spectral shapes suggest a large influence of the absorption (Doxaran *et al.*, 2009). Seasonally (Table 7.4), the spectra were compared with modelled spectra produced using Chl-a as input (Huot *et al.*, 2008).

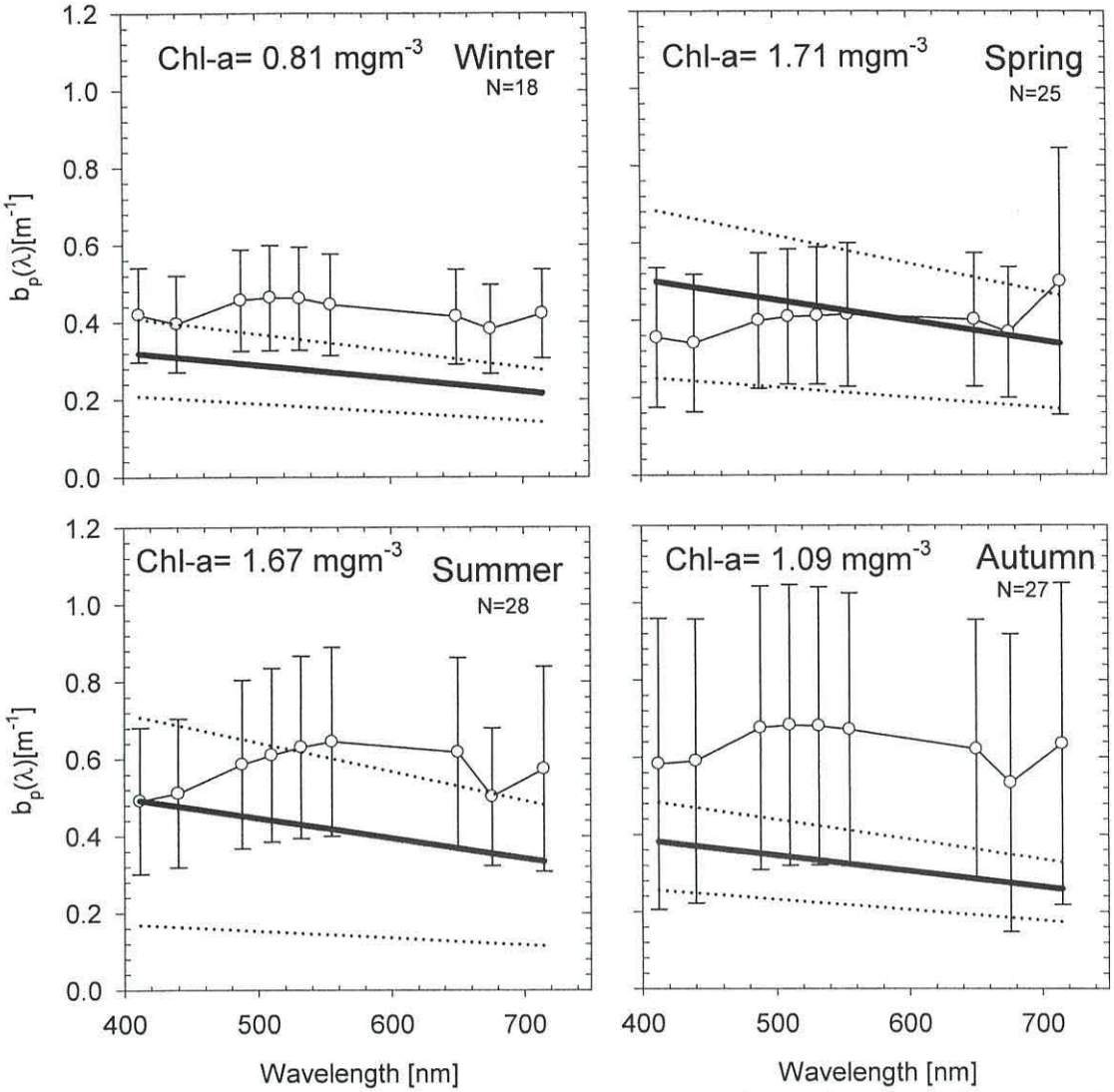

Figure 7.6 Average (solid line) and standard deviation (error bars) of the seasonal $b_p(\lambda)$ at L4. The statistics are computed from N spectra obtained for each season, irrespectively of the year of collection. $b_p(\lambda)$ computed using the Huot *et al.* (2008) model: thick solid line corresponds to the seasonal mean of Chl-a (in plots) and dotted lines to the mean±SD (Table 7.3).

For $b_p(\lambda)$ there is some agreement between modelled and measured values, especially in the spring, although Huot *et al.* (2008) do not reproduce the 'dips' around 440 and 676 nm (Figure 7.6). In all the other seasons, the model average line falls typically below the observed seasonal mean. However, given the dispersion of the in-situ data (especially in winter), it is not possible to quantify these differences statistically. Rather, it could be speculated that there could be particles (other than Chl-a) present in winter and autumn that produces a larger than expected signal.

The comparison of the Huot *et al.* (2008) model with $b_{bp}(\lambda)$ highlights the lower than expected observations of $b_{bp}(532)$, which could be due to a small instrumental problem

(but consistent over time). Seasonally, the observed $b_{bp}(\lambda)$ agrees with the modelled values only in summer. In winter, the model significantly underestimates, but observations are too limited to draw statistically robust conclusions. It has been shown that the highest PIM occurs during winter, and this could be a cause of mismatch. In spring, the model overestimates the observations, while autumn is similar to winter, although with a larger dispersion of the observations. However, in order to quantify and explain the seasonal variations of the whole spectra, the spectral slopes are needed.

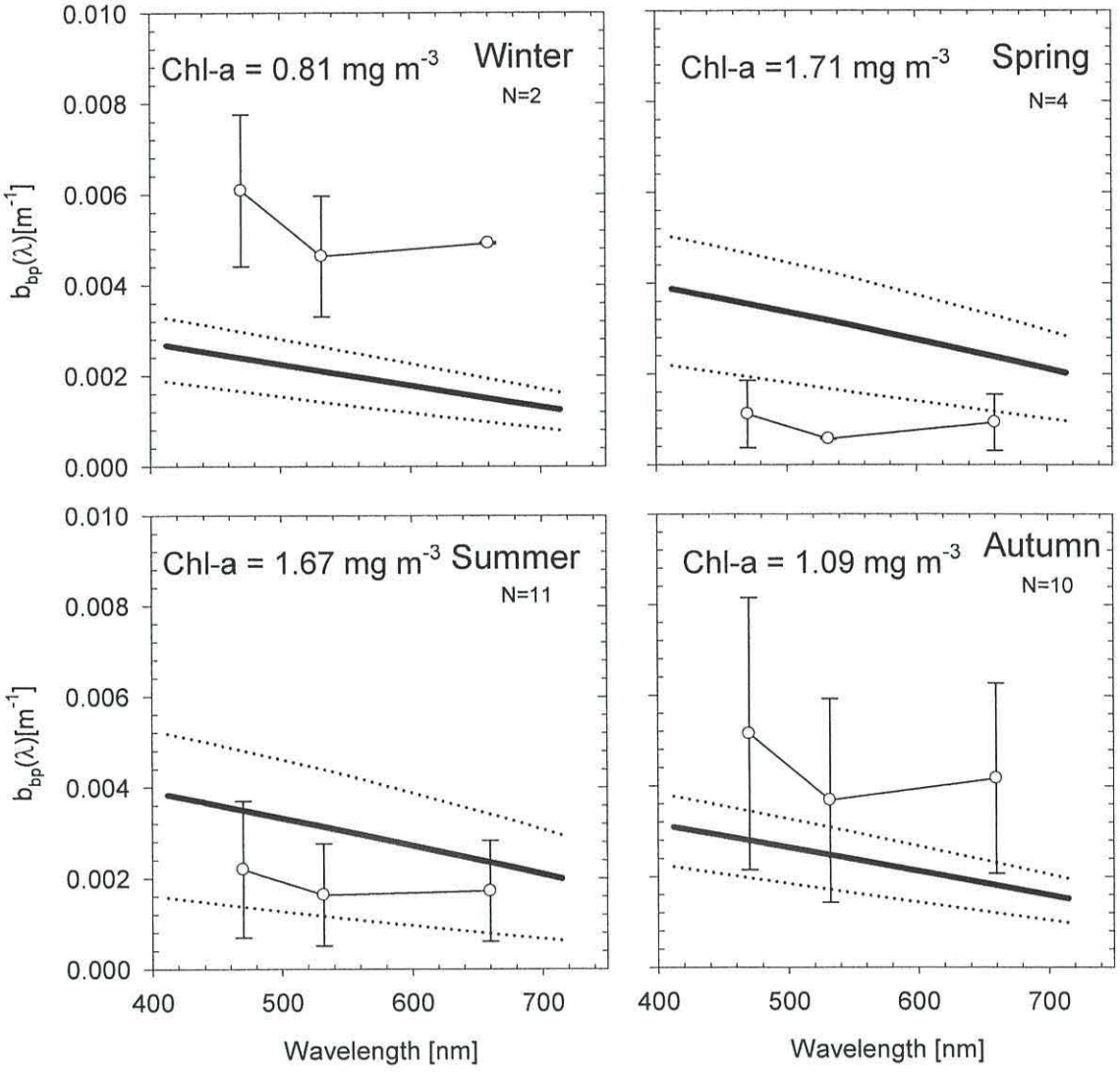

Figure 7.7 Average (solid line) and standard deviation (error bars) of the seasonal $b_{bp}(\lambda)$ at L4. The statistics are computed from N spectra obtained for each season, irrespectively of the year of collection. $b_{bp}(\lambda)$ computed using the Huot *et al.* (2008) model: thick solid line corresponds to the seasonal mean of Chl-a (in plots) and dotted lines to the mean±SD (Table 7.3).

For all years under study and all seasons, the spectral slopes of scattering in the visible (γ_S) and in the near-infrared channels (γ_{S3}) were correlated (see Chapter 3). However, γ_{S3} was not correlated with any visible channel and γ_S was only correlated with $b_p(440)$, therefore only γ_S will be related to $b_p(440)$ in the following. The γ_S are mostly positive or near to zero (Figure 7.8.a.), with a global mean and standard deviation of 0.33±0.74.

There is a seasonal trend on the data: spring and summer present the greater spectral variability especially where $b_p(440)<0.5m^{-1}$. The autumn-winter group of data present less variability in the spectral slope. In fact, the spectral slope in spring is significantly different to the rest of seasons (Table 7.4).

There was a negative and significant correlation between the backscattering slope (γ_{BS}) and $b_{bp}(532)$ in the whole dataset (Figure 7.8.b). The overall mean γ_{BS} and standard deviation is -0.14±1.10, which represents spectra flatter than those measured around the U.S. coast (Snyder *et al.*, 2008) and in the northern Adriatic Sea (Berthon *et al.*, 2007). The large variability is linked to the seasonality in our dataset: when data are split in seasons, significant relationships emerge (Figure 7.8.b). The gradient of γ_{BS} against $b_{bp}(532)$ in the spring-summer is more than twice that in the autumn-winter.

The backscattering ratio slope (γ_{BSR}) global average was -0.6±1.0 (N=16), which is what would be expected of a low $\tilde{b}_{bp}(532)$ and fits with larger published datasets (Snyder *et al.*, 2008). Given the small amount of data per season it is not possible to identify significant relationships between $\tilde{b}_{bp}(532)$ and γ_{BSR} (Fig. 7.8.c).

The overall picture of the particle composition at L4 is the result of two superimposed seasonal cycles: the inorganic matter (the minimum proportion of PIM is 50% of the total SPM) and the living phytoplankton (with seasonal variation of phytoplankton species), with an overall domination of large particles throughout the year. This interplay of variable composition and size produces significant seasonal changes in scattering but not in its slope. However, seasonal changes in backscattering and its associated spectral slope are significant.

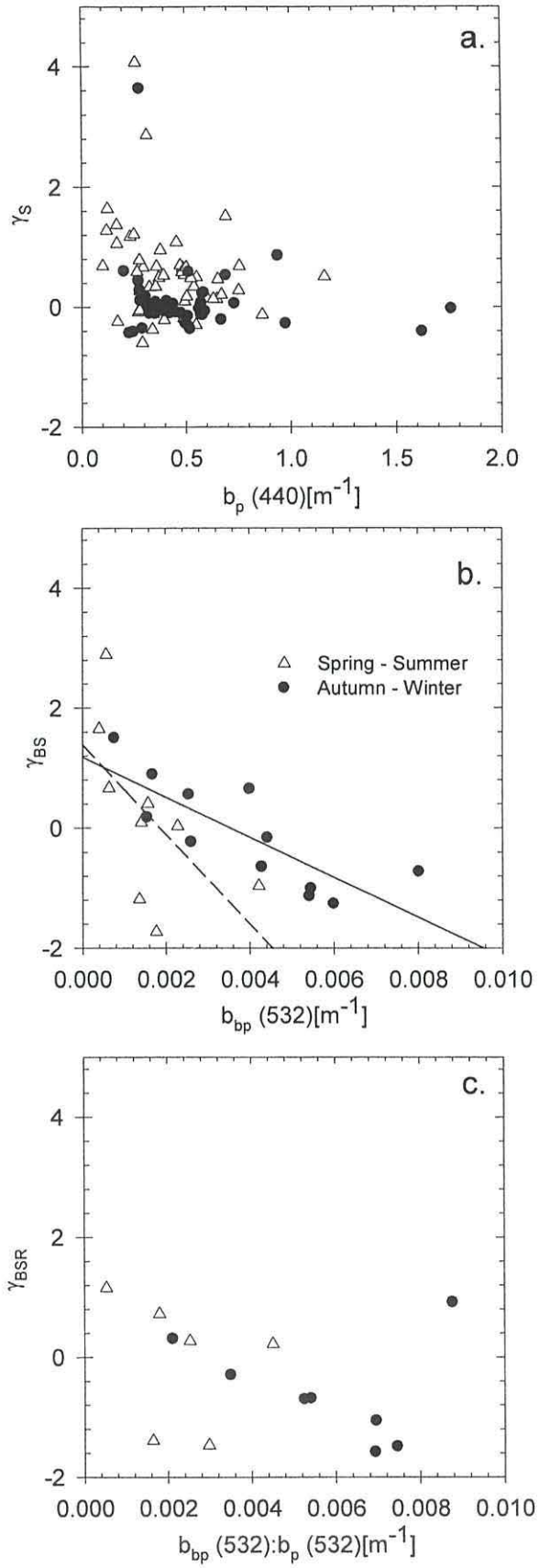

Figure 7.8 Scatter plots of : a) $b_p(440)$ and γ_S, b) $b_{bp}(532)$ and γ_{BS}, the solid line is the linear fit to the autumn-winter subset : $\gamma_{BS} = -333 \times b_p(532) + 1.18$, $R^2 = 0.61$, N=12; the dash line is the linear fit to the spring-summer subset: $\gamma_{BS} = -746 \times b_p(532) + 1.39$, $R^2 = 0.27$, N=9. c) $b_{bp}(532)$: $b_p(532)$ and γ_{BSR}, with different symbols for each season.

7.3 Seasonal changes in mass-specific coefficients and causes of spectral variability

The source of variation of the scattering properties was investigated using linear regressions with the suspended particulate matter composition, phytoplankton-C groups and particle size distribution, both globally and seasonally. The coefficients derived from these regressions are the mass-specific particulate scattering coefficients ($b_p^*(\lambda)$ in m^2g^{-1}).

In the relationship between $b_p(532)$ and the suspended matter (i.e. SPM, PIM or POM) significant correlations were found only with POM, which explained 17% of the variability of the dataset as a whole (Table 7.5). Grouping the data according to the mixed layer depth (i.e. autumn-winter and spring-summer) improved the % variance explained (Figure 7.9.a.). POM for the period autumn-winter, explained 33% of the variance in $b_p(532)$, but less (16%) for the spring-summer period.

Table 7.5: Linear regression coefficients (constant and slope) and their standard error (SE) between the $b_p(532)$ and $b_{bp}(532)$ and the components of the suspended matter for the whole L4 dataset (see text). The regression statistics are summarized by the coefficients of determination (R^2) and the F-ratio (NS-not significant, P>0.05; *, 0.001<P<0.05;,P<0.001). N is the number of data available for each regression. An example of how the table should be read is: $b_p(532)=0.42+0.63xPOM$, $R^2=0.17$, N=83.**

Variable	Components	Coefficient	SE	R^2	F	N
$b_p(532)$	Constant	0.42	0.05(**)	16.9	17.6(**)	83
	POM	0.63	0.15(**)			
$b_p(532)$	Constant	0.45	0.05(**)	4.9	5.8(*)	94
	Chl-a	0.08	0.03(*)			
$b_p(532)$	Constant	0.48	0.03(**)	8.6	8.8(*)	83
	Diatoms-C	0.003	0.001(*)			
$b_{bp}(532)$	Constant	7.71E-05	0.0007(NS)	48.2	17.72(**)	19
	SPM	0.0034	0.0008(**)			
$b_{bp}(532)$	Constant	0.0002	0.0007(NS)	57.8	21.51(**)	16
	PIM	0.0055	0.0012(**)			

When looking at the stability of the $b_p^*(532)-POM$ value, for the whole dataset, was 0.63 m^2g^{-1} POM with a standard error (SE) of 0.15, close to the lowest value of Snyder et al. (2008). For the autumn-winter data, $b_p^*(532)$-POM was significantly higher (1.2 m^2g^{-1}) than for the spring-summer (0.48 m^2g^{-1}), when the relationship was worse

(Fig.7.9.a). The fact that the particulate scattering only related to the POM is significant in so far as it challenges an explanation where the variability of b_p is related to changes in refractive index due to minerals (Babin *et al.*, 2003). The seasonality of the organic matter implies changes either in the size distribution of the organic particles or in their composition. Because no significant relationships were found between the size distribution slope and b_p, the effects of changes in the composition of POM were investigated.

The phytoplankton abundance measured as: Chl-a, total phytoplankton-C and individual phytoplankton-C for the groups considered, was related to $b_p(532)$ for the dataset as a whole and seasonally split as above. For the whole dataset, Chl-a and diatom-C were correlated significantly to $b_p(532)$, but only explained a small fraction of the variability in $b_p(532)$, i.e. less than 10% (Table 7.5). Seasonally (Figure 7.9.b and c), in the spring-summer period, the same factors as for the global dataset are related to $b_p(532)$, and the amount of the variance explained increased up to 31% for the diatom-C. In the autumn-winter period, the relationships found for the whole data set do not hold. The $b_p^*(532)$-diatom-C from the total dataset (coefficient±SE, 0.003±0.001 m^2mg^{-1} diatom-C) was similar to the one obtained in the spring-summer period.

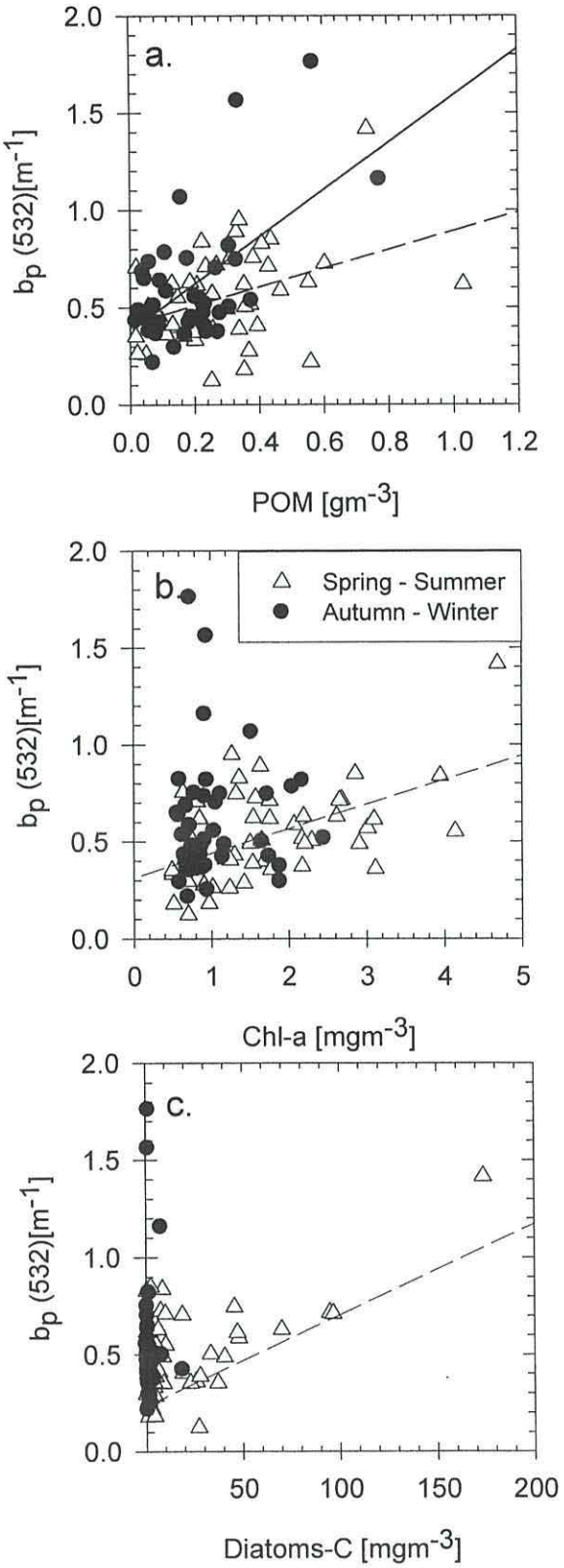

Figure 7.9 Scatter plots of : a) $b_p(532)$ and POM, the solid line is the linear fit to the autumn-winter subset : $b_p(532)=1.2\times POM+0.38$, $R^2=0.32$, N=38; the dash line is the linear fit to the spring-summer subset: $b_p(532)=0.48\times POM+ 0.41$, $R^2=0.14$, N=45; b) $b_p(532)$and Chl-a; the dash line is the linear fit to the spring-summer subset: $b_p(532)=0.13\times Chl\text{-}a+0.31$, $R^2=0.26$, N=49;. c) $b_p(532)$ and diatoms-C; the dash line is the linear fit to the spring-summer subset: $b_p(532)=0.004\times$diatoms-C+0.41 , $R^2=0.34$, N=45; with different symbols for each season.

Only SPM and PIM presented a positive and significant correlation with $b_{bp}(532)$ when the whole dataset was considered. The variation of SPM explained significantly ($P<0.001$, $N=19$) up to 48% of the variation in $b_{bp}(532)$, while PIM explained up to 58% (Table 7.5). In order to test the validity of these relationships in the different seasons, the dataset was split as above (Figure 7.10.a and b). When there was higher $b_{bp}(532)$, i.e. winter and autumn group, the relationships remained similar as for the whole dataset, with SPM explaining 37% and PIM explaining 49% of the variability in $b_{bp}(532)$. For the summer-spring group, PIM was still correlated to backscattering, but it was SPM which explained more of the variation in $b_{bp}(532)$: 36% and 60% explained by PIM and SPM respectively.

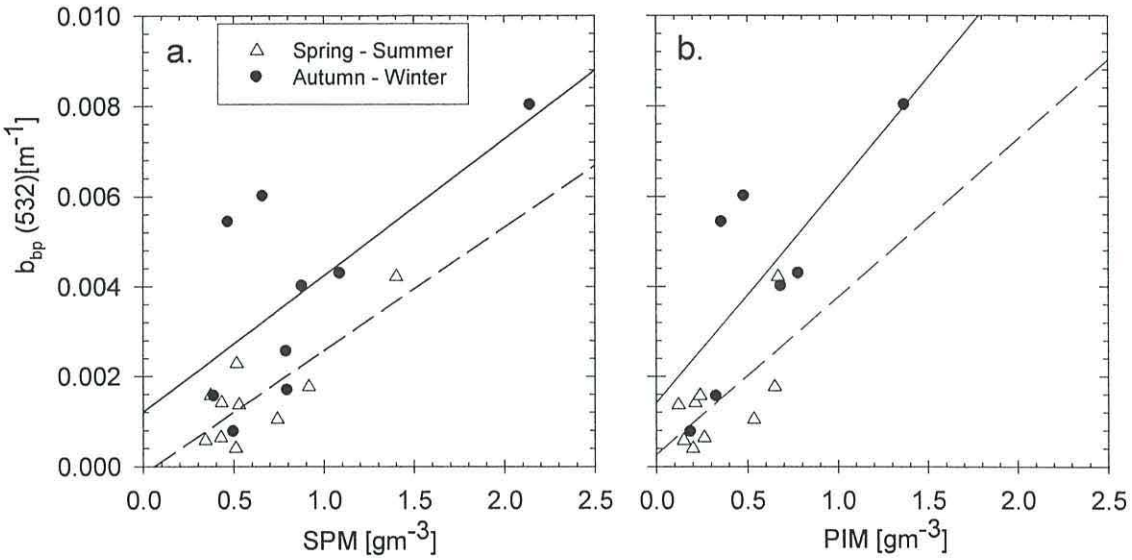

Figure 7.10 Scatter plots of : a) $b_{bp}(532)$ and SPM; the solid line is the linear fit to the autumn-winter subset : $b_{bp}(532)=0.003\times SPM+0.001$, $R^2=0.37$, N=9; the dash line is the linear fit to the spring-summer subset: b_{bp} (532)=0.003×SPM-0.0002, $R^2=0.60$, N=10; b) $b_{bp}(532)$ and PIM; the solid line is the linear fit to the autumn-winter subset : b_{bp} (532)=0.0048×PIM+0.0014 , $R^2=0.49$, N=7, the dash line is the linear fit to the spring-summer subset: b_{bp} (532)=0.0035×PIM+0.0003 , $R^2=0.36$, N=9; with different symbols for each season.

The mass-specific backscattering coefficient derived from the regressions on the whole dataset, $b^*_{bp}(532)$ with respect to SPM was 0.0034±0.0008 m^2g^{-1} SPM, while $b^*_{bp}(532)$ was higher with respect to PIM (0.0055±0.0010 m^2g^{-1} PIM). For the winter-autumn period, both coefficients were reduced by 15%. For the spring-summer period, $b^*_{bp}(532)$ with respect to SPM was similar to the mean value for the whole data set and PIM specific particulate scattering was smaller than in autumn-winter (0.0048±0.0010 m^2g^{-1}

PIM). However, given the small amount of data available, it is difficult to draw conclusions about the seasonality of these coefficients.

Overall, the small spectral variation in the scattering, described by the spectral slope (γ_S) correlated significantly only to Chl-a, with small variance explained (less than 10%) and a positive slope (Figure 7.11.a.), pointing to the effect of Chl-a related absorption on the spectral shape of the particulate scattering. However, seasonally, no significant correlations appeared between γ_{BS} and different components of the particulate matter composition or the size distribution slope. The backscattering ratio spectral slope (γ_{BSR}) was found to be globally related to Chl-a explaining up to 20% of the variance. This relationship is driven seasonally, by the correlation with Chl-a in the spring-summer (R^2=30%) as there is no significant relationship with the Chl-a in the autumn-winter. In terms of the seasonality of this relationship, the coefficient for the regression between Chl-a and γ_{BSR} was -0.51±0.22 ($p<0.05$), while for the spring-summer period is -0.67±0.30, although not significant statistically ($p=0.06$).

When γ_S and γ_{BS} are plotted against the Junge exponent, *j* (Figure 7.11.c and d), results are broadly consistent with the expected theoretical relationship $\gamma = 3 - j$ (Morel, 1973) but with large dispersion.

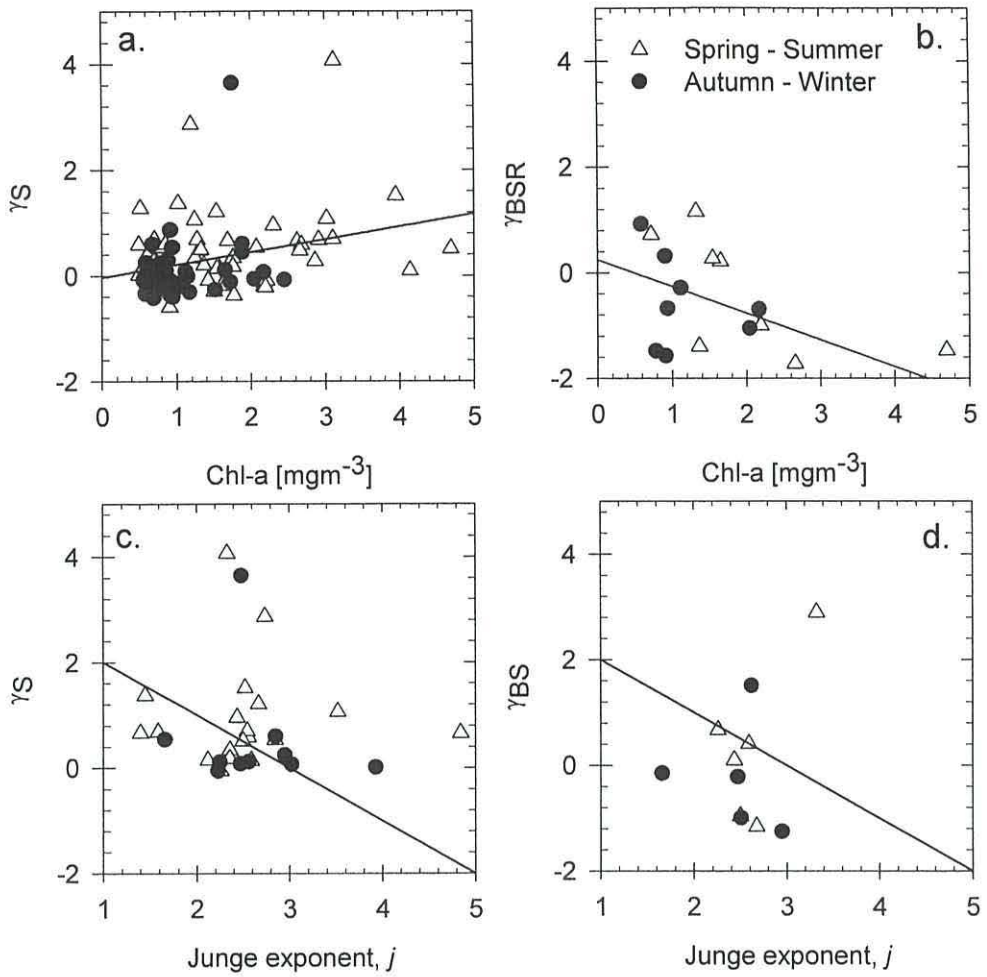

Figure 7.11 Scatter plots of: a) γ_S and Chl-a, the solid line is the linear fit to whole dataset : γ_S =0.24×Chl-a-0.03, R^2=0.07, N=94; b) γ_{BSR} and Chl-a, the solid line is the linear fit to whole dataset : γ_{BSR} =-0.51×Chl-a+0.25 , R^2=0.20, N=17; c) γ_S and the Junge parameter, *j*, d) γ_{BS} and *j*, with different symbols for each season. The solid line in c) and d) is the expected modelled relationship (Morel, 1973) between γ_S and *j* : γ_S=3-*j*

7.4 Particle matter composition changes at L4: non-living and living contributions

According to the results above, the particulate scattering coefficient is related to POM. The relationship is better for the autumn-winter period than for the spring-summer. It is necessary now to attempt to characterise the composition of the POM. It is expected that POM has living and non-living components and therefore it would be interesting to test which component explains the greatest variance in POM. To do so, the living component is characterised through phytoplankton-C and Chl-a, neglecting non-photosynthetic organisms (e.g. bacteria). Phytoplankton-C also neglects organisms less than 2μm.

For the whole data set, phytoplankton-C correlated with POM ($p<0.01$, Figure 7.12.a.) and all the phytoplankton-C groups were significantly correlated with POM, except the small phyto-flagellates, which do not have a strong annual variation (Figure 7.2). Overall the phytoplankton-C:POM ratio (0.24±0.48 gC g^{-1}) presents a large dispersion (Figure 7.12.a.), which also appear for the lower values in winter-autumn (0.13±0.23 gC g^{-1}) and the higher values in spring-summer (0.31±0.60 gC g^{-1}). This means that there is a larger proportion of living organic matter forming the POM pool during the spring and summer, although given the large dispersion of this indicator, no significant differences can be implied.

The linear relationship between the phytoplankton-C and POM for the whole dataset, although statistically significant, provides a very small explanation of the variance in POM (5%). Using forward stepwise regression between POM and the phytoplankton-C components (phyto-flagellates, coccolithophorids, *Phaeocystis spp.*, diatoms, dinoflagellates and heterotrophic-Dinophyceae) explains similarly low variance in POM. Only coccolithophorids, *Phaeocystis* spp. and heterotrophic Dinophyceae remained as variables in the multiple linear regression (6.2%, N=234). Seasonally, there is no relation between the phytoplankton-C and POM (Figure 7.12.a.).

Chl-a was also correlated to POM (Figure 7.12.b.), and globally the ratio POM:Chl-a presents a large dispersion (347±713 mg POM mg Chl-a^{-1}), with lower values in spring-summer (282±303 mg POM mg Chl-a^{-1}) and higher in autumn-winter (436±1037 mg POM mg Chl-a^{-1}). Unlike phytoplankton-C, these seasonal differences are statistically significant. It would appear from these results that Chl-a:POM could be a better indicator than phytoplankton-C:POM of the phytoplankton mass proportion in the suspended matter pool, because the Chl-a measurement includes the contribution by smaller phytoplankton not detected with the optical counting (less than 2μm in size).

The weak correlations with phytoplankton-C suggest that phytoplankton larger than 2 μm are not a strong source of POM variability, while the similarly weak correlations with Chl-a suggest the same for smaller phytoplankton. These results point to the dominance of POM by organic detritus and bacteria.

The total phytoplankton-C correlated significantly with Chl-a for the whole data set (Figure 7.12.c.), but only three phytoplankton groups correlated significantly with Chl-a

(N= 283): diatoms, *Phaeocystis* spp. and dinoflagellates. Seasonally, peaks observed in spring-summer were correlated with diatom-C and phaeocystis-C. Interestingly in autumn-winter, diatom-C and coccolithophorid-C correlated with Chl-a.

The backscattering coefficient variations were better related to the variations of PIM in autumn-winter and to POM in the spring-summer. The variability of the suspended mineral concentration, PIM, explained 95% of the SPM variability at L4 for the global data set (Figure 7.12.d.).

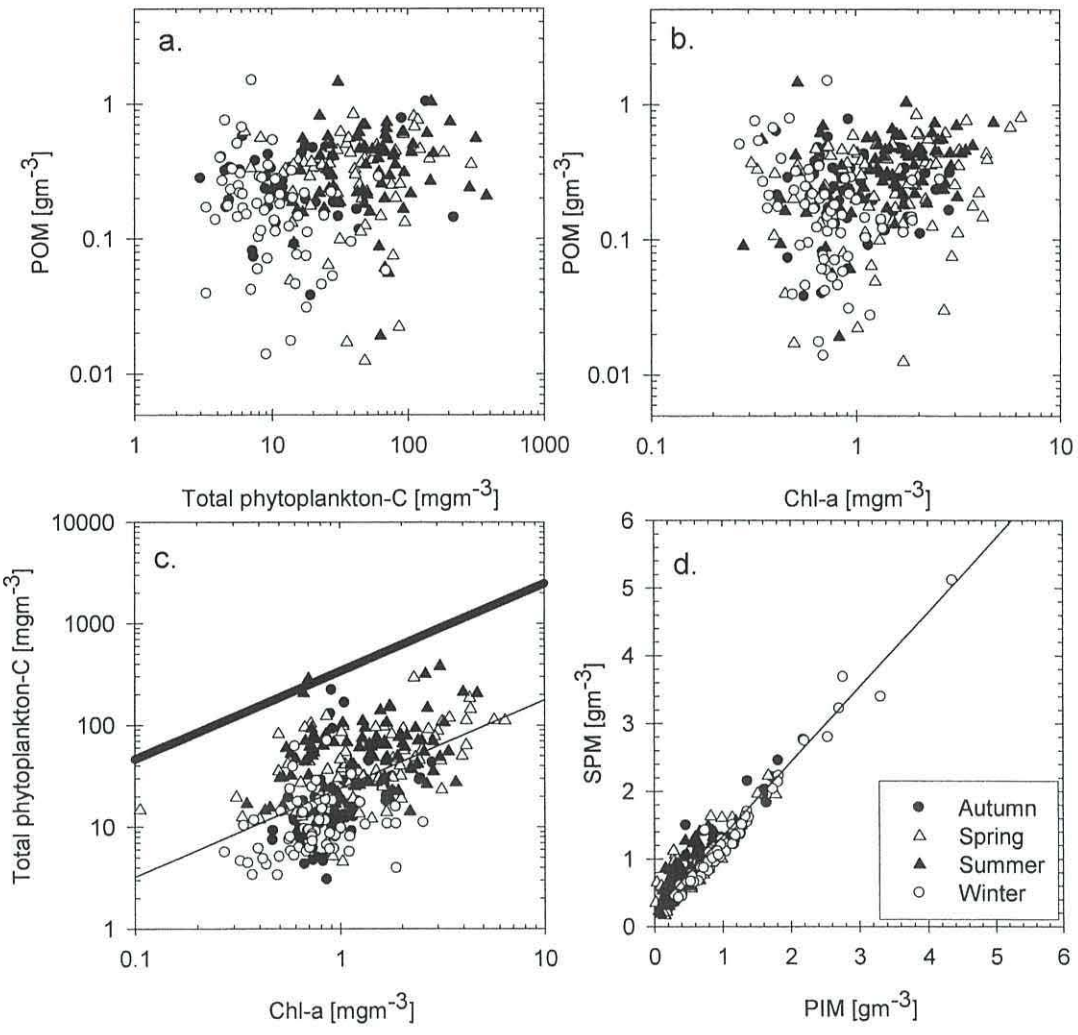

Figure 7.12 Scatter plots of : a) phytoplankton-C and POM; b) Chl-a and POM; c) Chl-a and phytoplankton-C, thick solid line is the statistical model at the lower quartile of Sathyendranath *et al.* (2008) : Particulate-C=79×Chl-a$^{0.65}$, thin solid line is the power-fit to the whole dataset: Phytoplankton-C = 24×Chl-a$^{0.87}$, R^2=0.27, N=295; d) PIM and SPM, thin solid line is the linear regression for the whole dataset: SPM= 0.23+1.10×PIM , R^2=0.95, N=288. Different symbols are used for data in each season (see legend).

During spring-summer, the POM:SPM ratio is 50% and halves in autumn-winter. Therefore, only about half of the particulate matter is organic in spring-summer and yet, it explains the greater part of the backscattering variability in that period. The above relationship (or lack of them) between phytoplankton-C and POM, may suggest that the organic detritus and bacteria are responsible for the backscattering when PIM is low.

7.5 Discussion and conclusions

In the discussion that follows, a comparison of the results from this Chapter with the relevant literature is done. For the suspended matter composition, a previous study in the area (Babin *et al.*, 2003) provided a snapshot of the suspended matter concentration (0.84 gm^{-3}) and composition (36% POM) at the beginning of September. In the corresponding season of this study (i.e. all summer data), our observations (Table 7.2), had a similar SPM load (0.81 gm^{-3}), but with a greater fraction of the organic matter in them (52%).

Concerning the particulate scattering, overall, $b_p(532)$ was 0.56±0.27 m^{-1}, low for a coastal site compared to observations in clear coastal waters of Monterrey Bay (Snyder *et al.*, 2008) or the Adriatic Sea (Berthon *et al.*, 2007) and slightly lower than values at the eastern part of the English Channel (Loisel *et al.*, 2007). Particulate backscattering is at the lower end of values reported for coastal waters (Berthon *et al.*, 2007; Snyder *et al.*, 2008).

The overall backscattering ratio, $\tilde{b}_{bp}(532)$, is 0.0040±0.0025, that is, 0.4% of the scattered light is in the backward direction. This low value is considered typical of marine particles with dominance of large particles and low refractive index (Ulloa *et al.*, 1994) and is in the lower limit of observations (Whitmire *et al.*, 2007). Its seasonal variations (higher values in winter-autumn and lower in summer) was consistent with observations made in the eastern English Channel (Loisel *et al.*, 2007), although the actual $\tilde{b}_{bp}(532)$ at L4 was lower. The model of Twardowski *et al.*, 2001 that uses $\tilde{b}_{bp}$ and size distribution slope to derive the bulk refractive index is not applicable to this dataset because the particle size distribution slope is below the range of applicability of the model.

In the literature the mass-specific particle scattering value is provided as the ratio of $b_p(\lambda)$ to SPM (Babin *et al.*, 2003; Doxaran *et al.*, 2009) as well as the coefficients of the regressions to $b_p(\lambda)$ (Snyder *et al.*, 2008). The average of the ratio $b_p(555)$:SPM is provided only for comparison with previous studies in the area (Babin *et al.*, 2003; Doxaran *et al.*, 2009). Globally (N=90), $b_p(555)$:SPM at L4 is higher than those studies (mean±std.dev, 0.7±0.4 m^2g^{-1} SPM) but variable between a winter mean of 0.5 and a summer mean of 0.9, validating the model proposed by Babin *et al.* (2003), in the sense that the SPM shifts from mineral dominated in the winter (~0.5 m^2g^{-1}) to phytoplankton dominated in the summer (1m^2g^{-1}). The comparison between seasonal means of the scattering coefficient with a published model (Huot *et al.*, 2008) resulted generally in an underestimation by the model, for all seasons, except during spring, where predictions were close to the seasonal mean. For backscattering, observations are larger or similar to predictions of the model, except during spring. It has been shown that there is a higher amount of minerals during winter and autumn and these are well correlated with backscattering, hence the underestimation of the model in comparison with the data. The model of Huot *et al.* (2008) was based on observations in the open ocean or in an upwelling region. It is likely that the particle ensemble (living and non-living) during the spring bloom at L4, and dominating the backscattering, has got different sizes or efficiency factors compared to the open ocean as discussed in Chapter Five. However, more likely, the paucity of backscattering data in spring could be producing a distortion in the seasonal value. Therefore more sampling effort is required to verify this result, eventually including an intensive targeted sampling during the spring bloom.

The phytoplankton-C:Chl-a ratio changes with photoadaptation and nutrient limitation, but also it is phytoplankton group specific (Geider *et al.*, 1997; MacIntyre *et al.*, 2002): larger phytoplankton tend to have higher phytoplankton-C:Chl-a ratio than smaller phytoplankton groups. At L4 the overall ratio was 36.05±43.05 mgC mgChl-a^{-1}, and the power-law relationships (Figure 7.12.c) are lower than similar estimates from in-situ data (Sathyendranath *et al.*, 2009). This difference can be attributed to methodological differences between the two estimates: while the estimate of phytoplankton-C comes from counts of living cells between 2 and 60μm, the particulate-C from Sathyendranath et al. (2009) comes from elemental analysis on filters which retains all suspended matter (living and non-living) greater than 0.47μm nominal pore size (S. Sathyendranath, pers. comm.). The phytoplankton-C:Chl-a ratio varies seasonally as expected (Table 7.3), being lower in autumn-winter, when phyto-flagellates dominated than in spring-

summer, when larger phytoplankton (diatoms and dinoflagellates) dominated. Overall, the particle population was dominated by large particles, as the particle size distribution slope was low (Jonasz and Fournier, 2007).

A number of conclusions can be drawn from the results presented. Firstly, the b_p is low and related to POM overall and seasonally at the surface of L4, with significantly different mass-specific coefficients in the spring-summer to the autumn-winter. These variations are related to variations in the composition of the POM pool, which has been shown to contain a greater amount of larger living phytoplankton-C in the spring-summer than in autumn-winter. Secondly, the b_{bp} is also low, but it is related to PIM, although no firm conclusions can be drawn about the seasonality of the mass-specific parameter. Significantly, no relationship between b_{bp} has been found with Chl-a or any of the phytoplankton groups considered, although γ_{BS} was significantly related to Chl-a.

Chapter Eight

Discussion, conclusions and recommendations for future work

CHAPTER EIGHT: DISCUSSION, CONCLUSIONS AND RECOMMENDATIONS FOR FUTURE WORK

8.1 Discussion

The question addressed by this thesis has been whether **the contribution of phytoplankton to particulate backscattering is significant**. To respond to this question, backscattering and particles properties (including phytoplankton diversity) were sampled **in-situ** in oceanic and coastal waters. Backscattering measurements have been related to particle properties using conventional bulk properties relationships as well as using a new proposed **'reductionist approach'**. Spectral variability and instrumental effects have also been explored.

In oceanic waters (Chapter 5), it has been shown that chlorophyll-a concentrations (Chl-a) are well correlated to backscattering. This finding corroborates previous studies in different oceanic regions and wider ranges of chlorophyll (e.g. Huot *et al.* (2008)). This result is a good indicator that the measurements collected in the ECOMAR area can be treated as a case study to further test the sources of the particle backscattering. Additionally, significant differences among Chl-a-specific particle backscattering for the areas in the Mid-Atlantic region were found: the North and South were higher than along the TOPEX transect.

The relationship between POC and particle backscattering for ECOMAR was comparable to other oceanic studies (Stramski *et al.*, 2008). Although these authors obtained better relationships in comparable conditions (R^2=0.77, when removing upwelling areas from the regression and using Buiteveld values for b_{bw}) the slope of their regression (1.87×10^{-5}) is of the same order of magnitude as the relationship found in this study. No significant trend was found between POC and γ_{BS} and it is worth noting the lack of published relationships in the literature.

The relationship between POC and Chl-a is close to recently published global estimates (Sathyendranath *et al.*, 2009). The relationship between backscattering, Chl-a and POC is important in the context of new algorithms for estimating primary production

(Behrenfeld *et al.*, 2005). These algorithms use the relationship between b_{bp} and Chl-a to use b_{bp} as a proxy for phytoplankton-C (C for Carbon) as the currency for phytoplankton biomass instead of using Chl-a directly as has been done in precedent models (e.g. Morel (1991)). An example of the results at ECOMAR with respect to estimations of phytoplankton-C based on b_{bp} can be illustrated using Figure 8.1. In this example the phytoplankton-C to b_{bp} from Behrenfeld *et al.* (2005) is compared to phytoplankton-C computed in two ways from the relationships obtained in Chapter 6:

1. Using the total POC to $b_{bp}(532)$ relationship, equation in Figure 5.9. The relationship of total POC to b_{bp} from Stramski *et al.*(2008) is also shown for comparison. (ECOMAR 1)
2. Substituting the Chl-a to $b_{bp}(532)$ relationship (from Figure 5.8.a and Table 5.2) into the relationship of POC to Chl-a for phytoplankton from Sathyendranath *et al.* (2009), results in the following equation: Phytoplankton-C=79xChl-a$^{0.65}$ (ECOMAR 2)

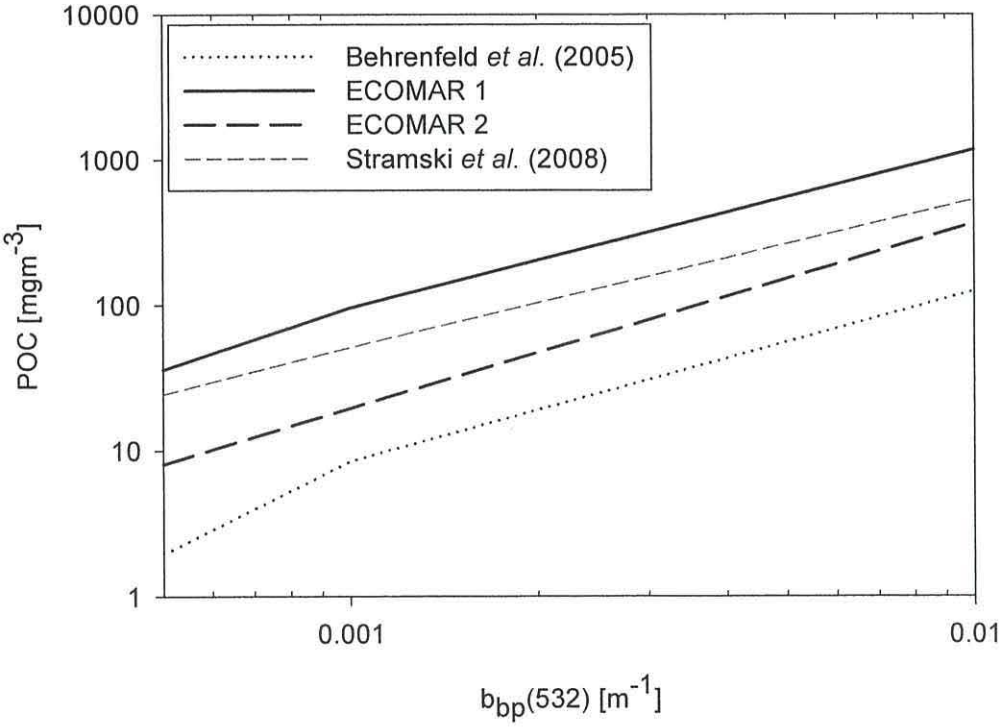

Figure 8.1 $b_{bp}(532)$ as an indicator of POC and phytoplankton-C for models from the literature compared to models derived from this study (see text).

Figure 8.1 highlights two main points. First is that the relationships found at ECOMAR between b_{bp} and POC (ECOMAR 1) and between b_{bp} and phytoplankton-C derived from the Chl-a relation to b_{bp} (ECOMAR 2) are consistent with the bio-optical relationships used for global primary production calculations (Behrenfeld *et al.*, 2005). Second is that the phytoplankton-C estimates from the Chl-a to b_{bp} relationship (ECOMAR 2) are closer to the estimates of phytoplankton-C from Behrenfeld *et al* (2005) than the relationship between the total particulate organic pool (POC) and b_{bp} (ECOMAR 1). This result suggests that the use of b_{bp} as an estimator of phytoplankton-C could be justified. However this is still a matter of discussion in the literature (e.g. Huot *et al.* 2008) and an active area of research.

The connection between b_{bp} and the phytoplankton-C needed to be demonstrated. This was attempted in Chapter 6, where additional information on the phytoplankton, bacteria and detrital matter was presented. The major result was that, considering the ensemble of data, the abundance of phytoplankton (in particular nanoeukaryotes and cryptophyta, between 2 and 20 μm) explained most of the variability (70%, $P<0.0001$) of the particle backscattering observed. This result points towards the importance of phytoplankton as a contributor to particle backscattering. Regional variations of this relation highlighted the importance of the differences in particle assemblages. For instance, in the South, where nanoeukaryotes and cryptophytes were less abundant, backscattering variations were produced by bacteria and *Synecococcus spp.*. A further significant result was that the role of detrital matter on backscattering was small, because the detrital matter contribution (quantified indirectly through its absorption) to the total particulate was constant throughout the domain and unrelated to the changes of b_{bp}. Further, the proportion of detritus to total particulate absorption was related to Chl-a similarly to the study by Bricaud and Stramski (1990), meaning that it is unlikely that the mineral contribution (non correlated to Chl-a) be of some optical importance in the ECOMAR area.

The backscattering is the result of the product of backscattering cross section and the amount of particles of each type. Therefore, it is important to stress the point that the backscattering cross section for nanoeukaryotes derived from the measurements in-situ resulted from changes in composition of the pico and nano plankton communities across the areas of ECOMAR. This implies that abundance of particles in each area played a

role on the final backscattering measurement (i.e. at a similar backscattering cross section value, the signal would be dominated by the type of organisms in greater number concentration). In the South it has been shown that nanoeukaryote and cryptophyte abundances were low, whereas smaller cells (bacteria, *Synecococcus spp.* and *Prochlorococcous spp.*) were more abundant. In this ecosystem, because of their larger numbers, the smaller cells dominate the variability of the backscattering and hence are well correlated to it in this area. However, shifts in the community towards domination of larger cells, in the TOPEX transect and the North, produced changes in the backscattering measured. Furthermore, even larger cells (diatoms, indicated by fucoxanthin), not quantified directly in this study could be able to explain part of the variation of the remaining unexplained backscattering variations. Simultaneous quantification of abundance of larger cells is therefore required.

To complement the linear regressions from the in-situ data, in Chapter 6 a sensitivity analysis was used which combined literature values of cell diameter and backscattering efficiency factors. The reference calculation was done using a set of backscattering efficiency factors that gave more importance to phytoplankton. According to this reference computation, the majority of the particle backscattering signal comes from the bacteria, due to their large numbers. However, in terms of backscattering efficiency, only a combination of parameters that gave greater importance to nanoeukaryotes were capable of improving the fit between observed and modelled backscatter. The main limitations to the computations presented in this study are caused by the indirect nature of the measurements through the use of flow cytometry.

The direct (from measurements) and indirect (from calculations) evidence presented in Chapter 6, leads to the conclusion that for the open ocean water, at least on the Mid-Atlantic Ridge, during the period of study, the major contributors to particle backscattering (i.e. those with the highest backscattering efficiency factors) were nanophytoplankton. Also, the need for phytoplankton cell identification data (using microscopy) was highlighted.

In order to extend the validity of this result, and to test whether the use of microscopy data (instead of flow cytometry) and therefore the consideration of larger cells could yield a better understanding of the variability of backscattering, a similar study to that in

the open ocean was carried out in coastal waters (Chapter 7). In this case, a station near to the coast (L4) was monitored weekly for almost 10 years, and the variations in optical properties and particle composition were due to seasonal changes rather than spatial differences. At L4, the surface bulk properties of particles (Chl-a, suspended particulate matter-SPM, particulate inorganic matter-PIM and particulate organic matter-POM) were complemented with information about the diversity of the phytoplankton groups. This chapter has been accepted as a paper in a peer reviewed journal.

The main result from Chapter 7 concerning the particle backscattering was the lack of relationship with phytoplankton carbon or to Chl-a content. The majority of the variation of backscattering was related to PIM and SPM. The enhancement that PIM produces on b_{bp} resulted in a deviation from models that use Chl-a to predict backscattering (e.g. Figure 7.7). The measured seasonal means of b_{bp} were compared with predictions from a model based solely on Chl-a (Huot *et al.*, 2008), and the enhancement of b_{bp} occurs in winter and autumn, coinciding with the higher seasonal proportion of PIM in the suspended matter. In spring and summer, when the concentration of suspended minerals was lower, the predicted values were higher than the measurements. The dominance of large particles during the spring and summer could be the cause of this disagreement. Larger particles were shown by the phytoplankton counts (dominance of diatoms and dinoflagellates) and by measurements of particle size distribution (particle size distribution slope was lowest in spring, i.e. greater proportion of larger particles).

The comparison between the two study sites (coastal and oceanic) in terms of backscattering magnitude and mass-specific coefficients deserves some attention. At L4 $b_{bp}(532)$ reached 0.008 m^{-1}, whereas at the Mid-Atlantic Ridge it reached 0.003 m^{-1}. Overall the organic load (POM at L4 ~300 mgm^{-3} and POC at the Mid-Atlantic Ridge ~200 mgm^{-3}) and Chl-a (Chl-a at L4 ~1.4 mgm^{-3} and at Mid-Atlantic Ridge ~0.8 mgm^{-3}) were higher at L4 than at the Mid-Atlantic Ridge. Additionally, minerals were measured in L4 and were considered to be negligible in the Mid-Atlantic Ridge. So overall, a larger amount of particulate matter at L4 produced a larger b_{bp} signal.

There are three methodological differences between the study at L4 and in the Mid-Atlantic Ridge area that need to be highlighted as potential sources of differences between the sites. Firstly, the data on the phytoplankton groups at L4, came from optical microscopy whereas the study at the Mid-Atlantic Ridge was done using flow cytometry. Microscopy includes cells between 2 and 200 μm particles, but not picoeukaryotes, *Prochlorococcus spp.*, *Synecoccocus spp.* or bacteria. Secondly, phytoplankton at L4 is expressed in terms of carbon content, whereas at the Mid-Atlantic Ridge it has been expressed as cell numbers. This approach was preferred because the measurements of SPM and its related components are also in mass units. Thirdly, the backscattering has been measured using different instruments. At L4 a Wetlabs VSF-3 and at the Mid-Atlantic Ridge a Wetlabs BB3. During this study it has not been possible to simultaneously measure the backscattering with the two instruments. However, there are a number of publications that have compared the different instruments in the market for measuring backscattering and the global consensus now is that the discrepancies between different instruments are not greater than 5% (Berthon *et al.*, 2007; Boss *et al.*, 2004; Sullivan *et al.*, 2005; Twardowski *et al.*, 2007).

The fact that no correlations were found between b_{bp} and phytoplankton-C at L4 may be due to the methodological differences highlighted and the interference with the SPM load. This highlights an area that requires further effort: the inclusion of flow cytometry measurements in the routine monitoring or any optics work attempting to relate the backscattering to the particle composition.

The main conclusion from this PhD is that in the open ocean location (over the North Atlantic mid oceanic ridge) in the summer of 2007, taking into account different size fractions, phytoplankton helped in understanding the causes of variation in backscattering. However, in a time series study over 10 years of observations at a fixed station in the Western English Channel (station L4), backscattering variations were better explained by the presence of mineral particles.

The application of these results to other areas of the ocean is desirable to test the generality of the conclusions, but the two sites (Mid-Atlantic Ridge and L4 station) have been chosen to provide a test bed for the 'reductionist approach', and it is hoped

that similar studies will be carried out in the future, as the interpretation of remote sensing imagery is limited by the consideration of bulk components (like chlorophyll-a or total suspended matter).

8.2 Conclusions

The **main conclusion** of this thesis is that, *in absence of minerals, the phytoplankton between 2 and 20μm have the highest backscattering efficiency (Q_{bb}) over the Mid-Atlantic Ridge (in the North Atlantic) during the summer of 2007. However, bacteria make up the largest contribution to particulate backscattering (52% of b_{bp}) through their large abundance. Minerals, when present, are more efficient backscatterers than any other particle.* There are spatial and temporal variations of these efficiencies but they could not be elucidated from this study and more data are required.

A number of specific conclusions can be drawn from the results that have been presented in this thesis, concerning the specific objectives set up initially:

- Spatial and temporal variations of backscattering have been measured using different instruments. Higher b_{bp} has been found in coastal waters at slightly higher Chl-a and organic matter concentrations
- Relationships of b_{bp} with bulk descriptors of the suspended matter have been found to agree with previous published results in oceanic waters, however a deviation from previous knowledge is significant in the coastal waters studied
- Using the 'reductionist approach', b_{bp} has been found to correlate significantly with phytoplankton in oceanic waters. This result, if found consistent in other oceanic areas, may have a significant impact in the way of interpreting ocean colour remote sensing and on primary production algorithms.
- In a coastal station, the 'reductionist approach' has not yielded similar results. Methodological differences and the role of minerals have been invoked to explain this. At this station, mineral load has been found to be the major cause of variation of backscattering.

8.3 Recommendations for future work

- It is crucial to test the result concerning the importance of phytoplankton on backscattering in other oceanic areas to verify its validity. Preliminary tests with the AMT dataset are underway.

- The reductionist approach used has been shown to be a powerful tool that may allow for better interpretation of the role of the different types of pico and nanoplankton in the remote sensing images. This approach should be used systematically as a complement to bulk particle properties.

- The reductionist approach should be extended to larger sizes of phytoplankton (using microscopy or other methods) to verify whether diatoms play an important role on backscattering.

- The lack of backscattering data in the coastal zone limits the study of the bio-optical relationships with the particulate matter composition. Autonomous continuous measurements should be conducted to improve the possibility of matching in-situ backscattering measurements with discrete water sampling.

- This study has uncovered a relationship through an statistical study of the empirical data. This is only the first step, as a mechanistic description (via a physical model) should be used to explain the physical causes of the enhanced backscattering by nanoeukaryotes. As such models may exist (e.g. multiple layered spheres), then the efforts should be directed towards the measurement of the parameters required for the models (e.g. thickness of layers) and the construction of suitable validation datasets.

Appendix I

List of symbols

LIST OF SYMBOLS

Symbol	Definition	Units
Chl-a	Chlorophyll-a concentration	mgm^{-3}
POC	Particulate organic carbon concentration	mgm^{-3}
SPM	Suspended particulate matter concentration	gm^{-3}
PIM	Particulate inorganic matter concentration	gm^{-3}
POM	Particulate organic matter concentration	gm^{-3}
a	Total absorption coefficient	m^{-1}
a_w	Pure seawater absorption coefficient	m^{-1}
a_y	Dissolved absorption coeffiecient, or yellow substance or CDOM, coloured dissolved organic matter	m^{-1}
a_p	Particle absorption coefficient	m^{-1}
a_{phy}	In vivo phytoplankton absorption coefficient	m^{-1}
a_{NAP}	Non-algal or detrital particle absorption coefficient	m^{-1}
b	Total scattering coefficient	m^{-1}
b_w	Pure seawater scattering coefficient	m^{-1}
b_p	Particle scattering coefficient	m^{-1}
b_b	Total backscattering coefficient	m^{-1}
b_{bw}	Pure seawater backscattering coefficient	m^{-1}
b_{bp}	Particle backscattering coefficient	m^{-1}
$\tilde{b}_b$	Particle backscattering ratio	No units
γ_y	Spectral slope of a_y	No units
γ_S	Spectral slope of b_p	No units
γ_{BS}	Spectral slope of b_{bp}	No units
γ_{BSR}	Spectral slope of $\tilde{b}_b$	No units
j	Junge exponent of a particle size distribution	No units
σ_{bbpi}	Backscattering cross section of a particle of type i in terms of -mass concentration -number concentration	 m^2mgC^{-1} m^2
S_i	Geometric cross section of the particle type i	m^2
Q_{bbpi}	Particulate backscattering efficiency factor of the particle type i	No units
$\beta(\theta,\lambda)$	Volume scattering function	$(m^{-1}sr^{-1})$
$\beta_w(\theta,\lambda)$	Volume scattering function of pure sea-water	$(m^{-1}sr^{-1})$
$\beta_p(\theta,\lambda)$	Volume scattering function of particles	$(m^{-1}sr^{-1})$
χ_p	Factor that multiplies $\beta_p(\theta,\lambda)$ at one angle to provide an approximation for the integrated value	No units

Appendix II

List of references cited

LIST OF REFERENCES CITED

Aas, E. 1996. Refractive index of phytoplankton derived from its metabolite composition. *Journal of Plankton Research,* Vol. 18, pp. 2223-2249.

Ackleson, S. G., R. W. Spinrad, C. M. Yentsch, J. Brown and W. Korjeffbellows. 1988. Phytoplankton Optical-Properties - Flow Cytometric Examinations of Dilution-Induced Effects. *Applied Optics,* Vol. 27, pp. 1262-1269.

Aden, A. L. and M. Kerker. 1951. Scattering of electromagnetic waves from two concentric spheres. *Journal of Applied Physics,* Vol. 22, pp. 1242-1246.

Ahn, Y. H., A. Bricaud and A. Morel. 1992. Light Backscattering Efficiency and Related Properties of Some Phytoplankters. *Deep-Sea Research Part a-Oceanographic Research Papers,* Vol. 39, pp. 1835-1855.

Babin, M., A. Morel, V. Fournier-Sicre, F. Fell and D. Stramski. 2003. Light scattering properties of marine particles in coastal and open ocean waters as related to the particle mass concentration. *Limnology and Oceanography,* Vol. 48, pp. 843-859.

Babin, M., D. Stramski, G. M. Ferrari, H. Claustre, A. Bricaud, G. Obolensky and N. Hoepffner. 2003. Variations in the light absorption coefficients of phytoplankton, nonalgal particles, and dissolved organic matter in coastal waters around Europe. *Journal of Geophysical Research-Oceans,* Vol. 108(C7), doi:10.1029/2001JC000882.

Bader, H. 1970. The hyperbolic distribution of particle sizes. *Journal of Geophysical Research,* Vol. 75, pp. 2822-2830.

Balch, W. M., D. T. Drapeau, J. J. Fritz, B. C. Bowler and J. Nolan. 2001. Optical backscattering in the Arabian Sea - continuous underway measurements of particulate inorganic and organic carbon. *Deep-Sea Research Part I-Oceanographic Research Papers,* Vol. 48, pp. 2423-2452.

Balch, W. M., J. M. Vaughn, J. F. Novotny, D. T. Drapeau, J. I. Goes, E. Booth, J. M. Lapierre, C. L. Vining and A. Ashe. 2002. Fundamental changes in light scattering associated with infection of marine bacteria by bacteriophage. *Limnology and Oceanography,* Vol. 47, pp. 1554-1561.

Balch, W. M., J. Vaughn, J. Navotny, D. T. Drapeau, R. Vaillancourt, J. Lapierre and A. Ashe. 2000. Light scattering by viral suspensions. *Limnology and Oceanography,* Vol. 45, pp. 492-498.

Balch, W. M., K. A. Kilpatrick, P. Holligan, D. S. Harbour and E. Fernandez. 1996. The 1991 coccolithophore bloom in the central North Atlantic .2. Relating optics to coccolith concentration. *Limnology and Oceanography,* Vol. 41, pp. 1684-1696.

Barlow, R., D. G. Cummings and S. W. Gibb. 1997. Improved resolution of mono- and Divinyl chlorophylls a and b and Zeaxanthin and Lutein in phytoplankton extracts using reverse phase C-8 HPLC. *Marine Ecology Progress Series,* Vol. 171, pp. 303-307.

Behrenfeld, M. J. and P. G. Falkowski. 1997. A consumer's guide to phytoplankton primary productivity models. *Limnology and Oceanography,* Vol. 42, pp. 1479-1491.

Behrenfeld, M. J., E. Boss, D. A. Siegel and D. M. Shea. 2005. Carbon-based ocean productivity and phytoplankton physiology from space. *Global Biogeochemical Cycles,* Vol. 19, GB1006, doi:10.1029/2004GB002299

Behrenfeld, M. J., R. T. O'Malley, D. A. Siegel, C. R. McClain, J. L. Sarmiento, G. C. Feldman, A. J. Milligan, P. G. Falkowski, R. M. Letelier and E. S. Boss. 2006. Climate-driven trends in contemporary ocean productivity. *Nature,* Vol. 444, pp. 752-755.

Bernard, S., T. A. Probyn and A. Quirantes. 2009. Simulating the optical properties of phytoplankton cells using a two-layered spherical geometry. *Biogeosciences Discussions,* Vol. 6, pp. 1497-1563.

Berthon, J. F., E. Shybanov, M. E. G. Lee and G. Zibordi. 2007. Measurements and modeling of the volume scattering function in the coastal northern Adriatic Sea. *Applied Optics,* Vol. 46, pp. 5189-5203.

Bogucki, D. J., J. A. Domaradzki, D. Stramski and J. R. Zaneveld. 1998. Comparison of near-forward light scattering on oceanic turbulence and particles. *Applied Optics,* Vol. 37, pp. 4669-4677.

Bohren, C. F. and D. R. Huffman. 1983. *Absorption and scattering of light by small particles.* Wiley, New York, 530 pp.

Boss, E. and W. S. Pegau. 2001. Relationship of light scattering at an angle in the backward direction to the backscattering coefficient. *Applied Optics,* Vol. 40, pp. 5503-5507.

Boss, E. S., R. Collier, G. Larson, K. Fennel and W. S. Pegau. 2007. Measurements of spectral optical properties and their relation to biogeochemical variables and processes in Crater Lake, Crater Lake National Park, OR. *Hydrobiologia,* Vol. 574, pp. 149-159.

Boss, E., M. S. Twardowski and S. Herring. 2001b. Shape of the particulate beam attenuation spectrum and its inversion to obtain the shape of the particulate size distribution. *Applied Optics,* Vol. 40, pp. 4885-4893.

Boss, E., W. S. Pegau, M. Lee, M. Twardowski, E. Shybanov, G. Korotaev and F. Baratange. 2004. Particulate backscattering ratio at LEO 15 and its use to study particle composition and distribution. *Journal of Geophysical Research-Oceans,* Vol. 109, doi:10.1029/2002JC001514.

Boss, E., W. S. Pegau, W. D. Gardner, J. R. V. Zaneveld, A. H. Barnard, M. S. Twardowski, G. C. Chang and T. D. Dickey. 2001a. Spectral particulate attenuation and particle size distribution in the bottom boundary layer of a continental shelf. *Journal of Geophysical Research-Oceans,* Vol. 106, pp. 9509-9516.

Bowers, D. G. and C. E. Binding. 2006. The optical properties of mineral suspended particles: a review and synthesis. *Estuarine Coastal and Shelf Science,* Vol. 67, pp. 219-230.

Bricaud, A. and A. Morel. 1986. Light Attenuation and Scattering by Phytoplanktonic Cells - a Theoretical Modeling. *Applied Optics,* Vol. 25, pp. 571-580.

Bricaud, A. and D. Stramski. 1990. Spectral Absorption-Coefficients of Living Phytoplankton and Nonalgal Biogenous Matter - a Comparison between the Peru Upwelling Area and the Sargasso Sea. *Limnology and Oceanography,* Vol. 35, pp. 562-582.

Bricaud, A., A. L. Bedhomme and A. Morel. 1988. Optical-Properties of Diverse Phytoplanktonic Species - Experimental Results and Theoretical Interpretation. *Journal of Plankton Research,* Vol. 10, pp. 851-873.

Bricaud, A., A. Morel and L. Prieur. 1983. Optical-Efficiency Factors of Some Phytoplankters. *Limnology and Oceanography,* Vol. 28, pp. 816-832.

Bricaud, A., H. Claustre, J. Ras and K. Oubelkheir. 2004. Natural variability of phytoplanktonic absorption in oceanic waters: Influence of the size structure of algal populations. *Journal of Geophysical Research-Oceans,* Vol. 109, C11010, doi: 10.1029/2004JC002419

Buiteveld, H., J. H. M. Hakvoort and M. Donze. 1994. The Optical Properties of Pure Water. *Ocean Optics Xii,* Vol. 2258, pp. 174-183.

Chami, M., E. B. Shybanov, T. Y. Churilova, G. A. Khomenko, M. E. G. Lee, O. V. Martynov, G. A. Berseneva and G. K. Korotaev. 2005. Optical properties of the particles in the Crimea coastal waters (Black Sea). *Journal of Geophysical Research-Oceans,* Vol. 110, C11020, doi:10.1029/2005JC003008

Chami, M., E. Marken, J. J. Stamnes, G. Khomenko and G. Korotaev. 2006. Variability of the relationship between the particulate backscattering coefficient and the volume scattering function measured at fixed angles. *Journal of Geophysical Research-Oceans,* Vol. 111, C05013, doi: 10.1029/2005JC003230

Chung, S. P., W. D. Gardner, M. J. Richardson, I. D. Walsh and M. R. Landry. 1996. Beam attenuation and microorganisms: spatial and temporal variations in small particles along 140W during the 1992 JGOFS EqPac transects. *Deep-Sea Research Part Ii-Topical Studies in Oceanography,* Vol. 43, pp. 1205-1226.

Chung, S. P., W. D. Gardner, M. R. Landry, M. J. Richardson and I. D. Walsh. 1998. Beam attenuation by microorganisms and detrital particles in the equatorial Pacific. *Journal of Geophysical Research-Oceans,* Vol. 103, pp. 12669-12681.

Ciotti, A. M., J. J. Cullen and M. R. Lewis. 1999. A semi-analytical model of the influence of phytoplankton community structure on the relationship between light attenuation and ocean color. *Journal of Geophysical Research-Oceans,* Vol. 104, pp. 1559-1578.

Claustre, H., A. Morel, M. Babin, C. Cailliau, D. Marie, J. C. Marty, D. Tailliez and D. Vaulot. 1999. Variability in particle attenuation and chlorophyll fluorescence in the tropical Pacific: Scales, patterns, and biogeochemical implications. *Journal of Geophysical Research-Oceans,* Vol. 104, pp. 3401-3422.

Claustre, H., F. Fell, K. Oubelkheir, L. Prieur, A. Sciandra, B. Gentili and M. Babin. 2000. Continuous monitoring of surface optical properties across a geostrophic front: Biogeochemical inferences. *Limnology and Oceanography,* Vol. 45, pp. 309-321.

Dall'Olmo, G. and A. A. Gitelson. 2006. Effect of bio-optical parameter variability and uncertainties in reflectance measurements on the remote estimation of chlorophyll-a concentration in turbid productive waters: modelling results. *Applied Optics,* Vol. 45, pp. 3577-3592.

Dall'Olmo, G., T. Westberry, M. J. Behrenfeld, E. Boss and W. H. Slade. 2009. Significant contribution of large particles to optical backscattering in the open ocean. *Biogeosciences,* Vol. 6, pp. 947 - 967.

Doxaran, D., K. Ruddick, D. McKee, B. Gentili, D. Tailliez, M. Chami and M. Babin. 2009. Spectral variations of light scattering by marine particles in coastal waters, from visible to near infrared. *Limnology and Oceanography,* Vol. 54, pp. 1257-1271.

Dunne, J. P., J. L. Sarmiento and A. Gnanadesikan. 2007. A synthesis of global particle export from the surface ocean and cycling through the ocean interior and on the seafloor. *Global Biogeochemical Cycles,* Vol. 21, GB4006, doi: 10.1029/2006GB002556

Durand, M. D. and R. J. Olson. 1996. Contributions of phytoplankton light scattering and cell concentration changes to diel variations in beam attenuation in the equatorial Pacific from flow cytometric measurements of pico-, ultra- and nanoplankton. *Deep-Sea Research Part Ii-Topical Studies in Oceanography,* Vol. 43, pp. 891-906.

Eisma, D. 1993. *Suspended matter in the aquatic environment.* Springer-Verlag, Berlin. 315 pp

Eppley, R. W., E. Stewart, M. R. Abbott and U. Heyman. 1985. Estimating ocean primary production from satellite chlorophyll: introduction to regional differences and

statistics for the southern California Bight. *Journal of Plankton Research,* Vol. 7, pp. 57-70.

Gardner, W. D., A. V. Mishonov and M. J. Richardson. 2006. Global POC concentrations from in-situ and satellite data. *Deep-Sea Research Part Ii-Topical Studies in Oceanography,* Vol. 53, pp. 718-740.

Garver, S. A. and D. A. Siegel. 1997. Inherent optical property inversion of ocean color spectra and its biogeochemical interpretation .1. Time series from the Sargasso Sea. *Journal of Geophysical Research-Oceans,* Vol. 102, pp. 18607-18625.

Geider, R. J., H. N. MacIntyre and T. M. Kana. 1997. Dynamic model of phytoplankton growth and acclimation: responses of the balanced growth rate and the chlorophyll-a:carbon ratio to light, nutrient-limitation and temperature. *Marine Ecology-Progress Series,* Vol. 148, pp. 187-200.

Geider, R. J., H. N. MacIntyre and T. M. Kana. 1997. Dynamic model of phytoplankton growth and acclimation: responses of the balanced growth rate and the chlorophyll-a:carbon ratio to light, nutrient-limitation and temperature. *Marine Ecology-Progress Series,* Vol. 148, pp. 187-200.

Geider, R. J., H. N. MacIntyre and T. M. Kana. 1997. Dynamic model of phytoplankton growth and acclimation: responses of the balanced growth rate and the chlorophyll-a:carbon ratio to light, nutrient-limitation and temperature. *Marine Ecology-Progress Series,* Vol. 148, pp. 187-200.

Gordon, H. R. and A. Morel. 1983. *Remote assessment of ocean color for interpretation of satellite visible imagery: A review.* Lecture notes on Coastal and Estuarine studies. Springer-Verlag, Berlin.114 pp

Gordon, H. R. and T. Du. 2001. Light scattering by nonspherical particles: Application to coccoliths detached from Emiliania huxleyi. *Limnology and Oceanography,* Vol. 46, pp. 1438-1454.

Gordon, H. R., O. B. Brown, R. H. Evans, J. W. Brown, R. C. Smith, K. S. Baker and D. K. Clark. 1988. A semianalytic radiance model of ocean color. *Journal of Geophysical Research-Oceans,* Vol. 93, pp. 10909-10924.

Gould, R. W., R. A. Arnone and P. M. Martinolich. 1999. Spectral dependence of the scattering coefficient in case 1 and case 2 waters. *Applied Optics,* Vol. 38, pp. 2377-2383.

Green, R. E. and H. M. Sosik. 2004. Analysis of apparent optical properties and ocean color models using measurements of seawater constituents in New England continental shelf surface waters. *Journal of Geophysical Research-Oceans,* Vol. 109, C03026, doi: 10.1029/2003JC001977

Green, R. E., H. M. Sosik and R. J. Olson. 2003a. Contributions of phytoplankton and other particles to inherent optical properties in New England continental shelf waters. *Limnology and Oceanography,* Vol. 48, pp. 2377-2391.

Green, R. E., H. M. Sosik, R. J. Olson and M. D. DuRand. 2003b. Flow cytometric determination of size and complex refractive index for marine particles: comparison with independent and bulk estimates. *Applied Optics,* Vol. 42, pp. 526-541.

Grob, C., O. Ulloa, H. Claustre, Y. Huot, G. Alarcon and D. Marie. 2007. Contribution of picoplankton to the total particulate organic carbon concentration in the eastern South Pacific. *Biogeosciences,* Vol. 4, pp. 837-852.

Groom, S. B., V. Martinez-Vicente, J. Fishwick, G. H. Tilstone, G. F. Moore, T. J. Smyth and D. S. Harbour. 2009. The western English Channel observatory: Optical characteristics of station L4. *Journal of Marine Systems,* Vol. 15, pp. 20-50.

Gundersen, K., M. Heldal, S. Norland, D. A. Purdie and A. H. Knap. 2002. Elemental C, N, and P cell content of individual bacteria collected at the Bermuda

Atlantic Time-series Study (BATS) site. *Limnology and Oceanography,* Vol. 47, pp. 1525-1530.

Heywood, J. L., M. V. Zubkov, G. A. Tarran, B. M. Fuchs and P. M. Holligan. 2006. Prokaryoplankton standing stocks in oligotrophic gyre and equatorial provinces of the Atlantic Ocean: Evaluation of inter-annual variability. *Deep-Sea Research Part Ii-Topical Studies in Oceanography,* Vol. 53, pp. 1530-1547.

Hilton, J., J. P. Lishman, S. Mackness and S. I. Heaney. 1986. An automated method for the analysis of particulate organic carbon and nitrogen in natural waters. *Hydrobiologica,* Vol. 141, pp. 269-271.

Holligan, P., M. Viollier, D. S. Harbour, P. Camus and M. Champagne-Pilippe. 1983. Satellite and ship studies of coccolithophore production along a continental shelf edge. *Nature,* Vol. 304, pp. 339-342.

Huot, Y., A. Morel, M. S. Twardowski, D. Stramski and R. A. Reynolds. 2008. Particle optical backscattering along chlorophyll gradient in the upper layer of the eastern South Pacific Ocean. *Biogeosciences,* Vol. 5, pp. 495-507.

Jonasz, M. and G. Fournier. 2007. *Light scattering by particles in water: Theoretical and experimental foundations.* Academic Press - Elsevier. 704 pp

Kirk, J. T. O. 1994. *Light and Photosynthesis in Aquatic Ecosystems.* Cambridge University Press. 525 pp

Kitchen, J. C. and J. R. Zaneveld. 1992. A three-layered sphere model of the optical properties of phytoplankton. *Limnology and Oceanography,* Vol. 37, pp. 1680-1690.

Koike, I., H. Shigemitsu, T. Kazuki and K. Kazuhiro. 1990. Role of sub-micrometre particles in the ocean. *Nature,* Vol. 345, pp. 242-244.

Kostadinov, T. S., D. A. Siegel, S. Maritorena and N. Guillocheau. 2007. Ocean color observations and modeling for an optically complex site: Santa Barbara Channel, California, USA. *Journal of Geophysical Research-Oceans,* Vol. 112, C07011, doi: 10.1029/2006JC003526

Kudela, R. M., N. Garfield and K. W. Bruland. 2006. Bio-optical signatures and biogeochemistry from intense upwelling and relaxation in coastal California. *Deep-Sea Research Part Ii-Topical Studies in Oceanography,* Vol. 53, pp. 2999-3022.

Lee, M. E. and M. R. Lewis. 2003. A new method for the measurement of the optical volume scattering function in the upper ocean. *J. Atmos. Oceanic Technol.,* Vol. 20, pp. 563– 571.

Lee, Z. P., K. L. Carder and R. A. Arnone. 2002. Deriving inherent optical properties from water color: a multiband quasi-analytical algorithm for optically deep waters. *Applied Optics,* Vol. 41, pp. 5755-5772.

Li, W. K. W. 1995. Composition of ultraphytoplankton n the central North Atlantic. *Marine Ecology Progress Series,* Vol. 122, pp. 1-8.

Li, W. K. W. 2002. Macroecological patterns of phytoplankton in the northwestern North Atlantic Ocean. *Nature,* Vol. 419, pp. 154-157.

Li, W. K. W. and W. G. Harrison. 2001. Chlorophyll, bacteria and picophytoplankton ecological provinces of the North Atlantic. *Deep-Sea Research Part Ii-Topical Studies in Oceanography,* Vol. 48, pp. 2271-2293.

Li, W. K. W., P. M. Dickie, B. D. Irwin and A. M. Wood. 1992. Biomass of bacteria, cyanobacteria, prochlorophytes and photosynthetic eukariotes in the Sargasso Sea. *Deep-Sea Research Part I,* Vol. 39, pp. 501-519.

Llewellyn, C. A., J. Fishwick and J. C. Blackford. 2005. Phytoplankton community assemblage in the English Channel: a comparison using chlorophyll a derived from HPLC-CHEMTAX adn carbon derived from microscopy cell counts. *Journal of Plankton Research,* Vol. 27, pp. 103-119.

Loisel, H. and A. Morel. 1998. Light scattering and chlorophyll concentration in case 1 waters: A reexamination. *Limnology and Oceanography,* Vol. 43, pp. 847-858.

Loisel, H. and D. Stramski. 2000. Estimation of the inherent optical properties of natural waters from the irradiance attenuation coefficient and reflectance in the presence of Raman scattering. *Applied Optics,* Vol. 39, pp. 3001-3011.

Loisel, H., E. Bosc, D. Stramski, K. Oubelkheir and P. Y. Deschamps. 2001. Seasonal variability of the backscattering coefficient in the Mediterranean Sea based on Satellite SeaWiFS imagery. *Geophysical Research Letters,* Vol. 28, pp. 4203-4206.

Loisel, H., J. M. Nicolas, P. Y. Deschamps and R. Frouin. 2002. Seasonal and inter-annual variability of particulate organic matter in the global ocean. *Geophysical Research Letters,* Vol. 29, doi:000181230500007.

Loisel, H., J.-M. Nicolas, A. Sciandra, D. Stramski and A. Poteau. 2006. Spectral dependency of optical backscattering by marine particles from satellite remote sensing of the global ocean. *Journal of Geophysical Research,* Vol. 111, C09024, doi: 10.1029/2005JC003367

Loisel, H., X. Meriaux, J. F. Berthon and A. Poteau. 2007. Investigation of the optical backscattering to scattering ratio of marine particles in relation to their biogeochemical composition in the eastern English Channel and southern North Sea. *Limnology and Oceanography,* Vol. 52, pp. 739-752.

MacIntyre, H. N., T. M. Kana, T. Anning and R. J. Geider. 2002. Photoacclimation of photosynthesis irradiance response curves and photosynthetic pigments in microalgae and cyanobacteria. *Journal of Phycology,* Vol. 38, pp. 17-38.

Maffione, R. A. and D. R. Dana. 1997a. Instruments and methods for measuring the backward-scattering coefficient of ocean waters. *Applied Optics,* Vol. 36, pp. 6057 - 6067.

Maffione, R. A. and D. R. Dana. 1997b. Recent measurements of the spectral backward-scattering coefficient in coastal waters. *Ocean Optics XIII.*

Markwardt, C. B. 2008. Non-linear squares fitting in IDL with MPFIT. *Astronomical data analysis software and systems XVIII.*Vol. 411, Quebec, Canada.

McManus, M. A., A. L. Alldredge, A. H. Barnard, E. Boss, J. F. Case, T. J. Cowles, P. L. Donaghay, L. B. Eisner, D. J. Gifford, C. F. Greenlaw, C. M. Herren, D. V. Holliday, D. Johnson, S. MacIntyre, D. M. McGehee, T. R. Osborn, M. J. Perry, R. E. Pieper, J. E. B. Rines, D. C. Smith, J. M. Sullivan, M. K. Talbot, M. S. Twardowski, A. Weidemann and J. R. Zaneveld. 2003. Characteristics, distribution and persistence of thin layers over a 48 hour period. *Marine Ecology-Progress Series,* Vol. 261, pp. 1-19.

Menden-Deuer, S. and E. J. Lessard. 2000. Carbon to volume relationships for dinoflagellates, diatoms, and other protist plankton. *Limnology and Oceanography,* Vol. 45, pp. 569-579.

Meyer, R. A. 1979. Light scattering from biological cells: dependence of backscatter radiation on membrane thickness and refractive index. *Applied Optics,* Vol. 18, pp. 585-588.

Meyer, R. A. 1979. Light scattering from biological cells: dependence of backscatter radiation on membrane thickness and refractive index. *Applied Optics,* Vol. 18, pp. 585-588.

Mishchenko, M. I., J. W. Hoveneier and L. D. Travis. 2000. *Light scattering by nonspherical particles.* Academic Press. New York. 147 pp

Mobley, C. D. 1994. *Light and water; radiative transfer in natural waters.* Academic Press, Inc. 592 pp

Montagnes, D. J., J. A. Berges, P. J. Harrison and F. J. R. Taylor. 1994. Estimation of carbon, nitrogen, protein and chlorophyll a from volume in marine phytoplankton. *Limnology and Oceanography,* Vol. 39, pp. 1044-1060.

Montes-Hugo, M. A., H. Ducklow and O. M. Schofield. 2009. Contribution by different marine bacterial communities to particulate beam attenuation. *Marine Ecology-Progress Series,* Vol. 379, pp. 13-22.

Moore, C. M., M. S. Twardowski and J. R. V. Zaneveld. 2000. The ECO-VSF: a multiangle scattering sensor for determination of the volume scattering function in the backward direction. *Ocean Optics XV.* October 16-20, Monaco

Morel, A. 1987. Chlorophyll-Specific Scattering Coefficient of Phytoplankton - a Simplified Theoretical Approach. *Deep-Sea Research Part a-Oceanographic Research Papers,* Vol. 34, pp. 1093-1105.

Morel, A. 1988. Optical Modeling of the Upper Ocean in Relation to Its Biogenous Matter Content (Case-I Waters). *Journal of Geophysical Research-Oceans,* Vol. 93, pp. 10749-10768.

Morel, A. 1991. Light and Marine Photosynthesis - a Spectral Model with Geochemical and Climatological Implications. *Progress in Oceanography,* Vol. 26, pp. 263-306.

Morel, A. and A. Bricaud. 1981. Theoretical Results Concerning Light-Absorption in a Discrete Medium, and Application to Specific Absorption of Phytoplankton. *Deep-Sea Research Part a-Oceanographic Research Papers,* Vol. 28, pp. 1375-1393.

Morel, A. and B. Gentili. 1991. Diffuse Reflectance of Oceanic Waters - Its Dependence on Sun Angle as Influenced by the Molecular-Scattering Contribution. *Applied Optics,* Vol. 30, pp. 4427-4438.

Morel, A. and S. Maritorena. 2001. Bio-optical properties of oceanic waters: A reappraisal. *Journal of Geophysical Research-Oceans,* Vol. 106, pp. 7163-7180.

Morel, A. and Y. H. Ahn. 1990. Optical-Efficiency Factors of Free-Living Marine-Bacteria - Influence of Bacterioplankton Upon the Optical-Properties and Particulate Organic-Carbon in Oceanic Waters. *Journal of Marine Research,* Vol. 48, pp. 145-175.

Morel, A. and Y. H. Ahn. 1991. Optics of Heterotrophic Nanoflagellates and Ciliates - a Tentative Assessment of Their Scattering Role in Oceanic Waters Compared to Those of Bacterial and Algal Cells. *Journal of Marine Research,* Vol. 49, pp. 177-202.

Morel, A., Y. H. Ahn, F. Partensky, D. Vaulot and H. Claustre. 1993. Prochlorococcus and Synechococcus - a Comparative-Study of Their Optical-Properties in Relation to Their Size and Pigmentation. *Journal of Marine Research,* Vol. 51, pp. 617-649.

Oishi, T. 1990. Significant relationship between the backward scattering coefficient of sea water and the scatterance at 120. *Applied Optics,* Vol. 29, pp. 4658-4665.

O'Reilly, J. E., S. Maritorena, B. G. Mitchell, D. A. Siegel, K. L. Carder, S. A. Garver, M. Kahru and C. McClain. 1998. Ocean color chlorophyll algorithms for SeaWiFS. *Journal of Geophysical Research-Oceans,* Vol. 103, pp. 24937-24953.

Oubelkheir, K., H. Claustre, A. Sciandra and M. Babin. 2005. Bio-optical and biogeochemical properties of different trophic regimes in oceanic waters. *Limnology and Oceanography,* Vol. 50, pp. 1795-1809.

Pegau, W. S. and J. R. Zaneveld. 1993. Temperature dependent absorption of water in the red and near infrared portions of the spectrum. *Limnology and Oceanography,* Vol. 38, pp. 188-192.

Preisendorfer, R. W. 1961. Application of radiative transfer theory to light measurements in the sea. *Int. Geophys. Geod. Monogr.,* Vol. 10, pp. 11-29.

Prieur, L. and S. Sathyendranath. 1981. An Optical Classification of Coastal and Oceanic Waters Based on the Specific Spectral Absorption Curves of Phytoplankton Pigments, Dissolved Organic Matter, and Other Particulate Materials. *Limnology and Oceanography,* Vol. 26, pp. 671-689.

Quirantes, A. and S. Bernard. 2004. Light scattering by marine algae: two-layer spherical and nonspherical models. *Journal of Quantitative Spectroscopy & Radiative Transfer,* Vol. 89, pp. 311-321.

Reynolds, R. A., D. Stramski and B. G. Mitchell. 2001. A chlorophyll-dependent semianalytical reflectance model derived from field measurements of absorption and backscattering coefficients within the Southern Ocean. *Journal of Geophysical Research-Oceans,* Vol. 106, pp. 7125-7138.

Sathyendranath, S., L. Prieur and A. Morel. 1989. A 3-Component Model of Ocean Color and Its Application to Remote-Sensing of Phytoplankton Pigments in Coastal Waters. *International Journal of Remote Sensing,* Vol. 10, pp. 1373-1394.

Sathyendranath, S., V. Stuart, A. Nair, K. Oka, T. Nakane, H. A. Bouman, M.-H. Forget, H. Maass and T. Platt. 2009. Carbon-to-chlorophyll ratio and growth rate of phytoplankton in the sea. *Marine Ecology-Progress Series,* Vol. 383, pp. 73-84.

Shifrin, K. 1988. *Physical optics of ocean water.* American Institute of Physics. 285 pp

Shutler, J. D., T. J. Smyth, P. E. Land and S. B. Groom. 2005. A near-real time automatic MODIS data processing system. *International Journal of Remote Sensing,* Vol. 26, pp. 1049-1055.

Smith, R. C. and K. S. Baker. 1981. Optical properties of the clearest natural waters (200-800 nm) *Applied Optics,* Vol. 20, pp. 177-184.

Smyth, T. J., G. F. Moore, S. B. Groom, P. E. Land and T. Tyrrell. 2002. Optical modeling and measurements of a coccolithophore bloom. *Applied Optics,* Vol. 41, pp. 7679-7688.

Smyth, T. J., G. F. Moore, T. Hirata and J. Aiken. 2006. Semianalytical model for the derivation of ocean color inherent optical properties: description, implementation, and performance assessment. *Applied Optics,* Vol. 45, pp. 8116-8131.

Snyder, W. A., R. A. Arnone, C. O. Davis, W. Goode, R. W. Gould, S. Ladner, G. Lamela, W. J. Rhea, R. Stavn, M. Sydor and A. Weidemann. 2008. Optical scattering and backscattering by organic and inorganic particulates in U.S. coastal waters. *Applied Optics,* Vol. 47, pp. 666-677.

Southward, A. J., O. Langmead, N. J. Hardman-Mountford, J. Aiken, G. T. Boalch, P. R. Dando, M. J. Genner, I. Joint, M. A. Kendall, N. C. Halliday, R. P. Harris, R. Leaper, N. Mieszkowska, R. D. Pingree, A. J. Richardson, D. W. Sims, T. Smith, A. W. Walne and S. J. Hawkins. 2005. Long-term oceanographic and ecological research in the western English Channel. *Advances in Marine Biology,* Vol. 47, pp. 1-105.

Stramska, M. and D. Stramski. 2005. Variability of particulate organic carbon concentration in the north polar Atlantic based on color observations with Sea-viewing Wide Field-of-View Sensor (SeaWiFS). *J. Geophys. Res,* Vol. 111, pp.

Stramska, M., D. Stramski, R. Hapter, S. Kaczmarek and J. Ston. 2003. Bio-optical relationships and ocean color algorithms for the north polar region of the Atlantic. *Journal of Geophysical Research-Oceans,* Vol. 108, pp.

Stramska, M., D. Stramski, S. Kaczmarek, D. B. Allison and J. Schwarz. 2006. Seasonal and regional differentiation of bio-optical properties within the north polar Atlantic. *Journal of Geophysical Research-Oceans,* Vol. 111, pp.

Stramski, D. 1999. Refractive index of planktonic cells as a measure of cellular carbon and chlorophyll a content. *Deep-Sea Research Part I-Oceanographic Research Papers,* Vol. 46, pp. 335-351.

Stramski, D. and A. Morel. 1990. Optical-Properties of Photosynthetic Picoplankton in Different Physiological States as Affected by Growth Irradiance. *Deep-Sea Research Part a-Oceanographic Research Papers,* Vol. 37, pp. 245-266.

Stramski, D. and D. A. Kiefer. 1991. Light-Scattering by Microorganisms in the Open Ocean. *Progress in Oceanography,* Vol. 28, pp. 343-383.

Stramski, D. and S. B. Wozniak. 2005. On the role of colloidal particles in light scattering in the ocean. *Limnology and Oceanography,* Vol. 50, pp. 1581-1591.

Stramski, D., A. Bricaud and A. Morel. 2001. Modeling the inherent optical properties of the ocean based on the detailed composition of the planktonic community. *Applied Optics,* Vol. 40, pp. 2929-2945.

Stramski, D., E. Boss, D. Bogucki and K. J. Voss. 2004. The role of seawater constituents in light backscattering in the ocean. *Progress in Oceanography,* Vol. 61, pp. 27-56.

Stramski, D., M. Babin and S. B. Wozniak. 2007. Variations in the optical properties of terrigenous mineral-rich particulate matter suspended in seawater. *Limnology and Oceanography,* Vol. 52, pp. 2418 - 2433.

Stramski, D., R. A. Reynolds, M. Babin, S. Kaczmarek, M. R. Lewis, R. Rottgers, A. Sciandra, M. Stramska, M. S. Twardowski, B. A. Franz and H. Claustre. 2008. Relationships between the surface concentration of particulate organic carbon and optical properties in the eastern South Pacific and eastern Atlantic Oceans. *Biogeosciences,* Vol. 5, pp. 171-201.

Stramski, D., R. A. Reynolds, M. Kahru and B. G. Mitchell. 1999. Estimation of particulate organic carbon in the ocean from satellite remote sensing. *Science,* Vol. 285, pp. 239-242.

Sullivan, J. M. and M. S. Twardowski. 2009. Angular shape of the oceanic particle volume scattering function. *Applied Optics,* Vol. 48, pp. 6811-6819.

Sullivan, J. M., M. S. Twardowski, P. L. Donaghay and S. A. Freeman. 2005. Use of optical scattering to discriminate particle types in coastal waters. *Applied Optics,* Vol. 44, pp. 1667-1680.

Tarran, G. A., J. L. Heywood and M. V. Zubkov. 2006. Latitudinal changes in the standing stocks of nano- and picoeukariotic phytoplankton in the Atlantic Ocean. *Deep Sea Research II,* Vol. 53, pp. 1516 - 1529.

Tarran, G. A., M. V. Zubkov, M. A. Sleigh, P. H. Burkill and M. Yallop. 2001. Microbial comunity structure and standing stocks in the NE Atlantic in June and July of 1996. *Deep Sea Research II,* Vol. 48, pp. 2001.

Tassan, S. and G. M. Ferrari. 1995. An alternative approach to absorption measurements of aquatic particles retained on filters. *Limnology and Oceanography,* Vol. 40, pp. 1358-1368.

Twardowski, M. S., E. Boss, J. B. Macdonald, W. S. Pegau, A. H. Barnard and J. R. V. Zaneveld. 2001. A model for estimating bulk refractive index from the optical backscattering ratio and the implications for understanding particle composition in case I and case II waters. *Journal of Geophysical Research-Oceans,* Vol. 106, pp. 14129-14142.

Twardowski, M. S., H. Claustre, S. A. Freeman, M. Stramski and Y. Huot. 2007. Optical backscattering properties of the "clearest" natural waters. *Biogeosciences,* Vol. 4, pp. 1041-1058.

Tzortziou, M., A. Subramaniam, J. R. Herman, C. L. Gallegos, P. J. Neale and L. W. Harding. 2007. Remote sensing reflectance and inherent optical properties in the mid Chesapeake Bay. *Estuarine Coastal and Shelf Science,* Vol. 72, pp. 16-32.

Ulloa, O., S. Sathyendranath and T. Platt. 1994. Effect of the Particle-Size Distribution on the Backscattering Ratio in Seawater. *Applied Optics,* Vol. 33, pp. 7070-7077.

Ulloa, O., S. Sathyendranath, T. Platt and R. A. Quinones. 1992. Light-Scattering by Marine Heterotrophic Bacteria. *Journal of Geophysical Research-Oceans,* Vol. 97, pp. 9619-9629.

Vaillancourt, R. D., C. W. Brown, R. R. L. Guillard and W. M. Balch. 2004. Light backscattering properties of marine phytoplankton: relationships to cell size, chemical composition and taxonomy. *Journal of Plankton Research,* Vol. 26, pp. 191-212.

van de Hulst, H. C. 1957. *Light scattering by small particles.* Wiley. 470 pp

Verardo, D. J., P. N. Froelich and A. McIntyre. 1990. Determination of organic carbon and nitrogen in marine sediments using the Carlo Erba - 1500 analyzer. *Deep Sea Research I,* Vol. 37, pp. 157 - 165.

Vold, R. D. and M. J. Vold. 1983. *Colloid and interface chemistry.* Addison-Wesley. Reading,269 pp

Volten, H., J. F. de Haan, J. W. Hoveneier, R. Schreurs, V. Vassen, A. G. Dekker, H. J. Hoogenboom, F. Charlton and R. Wouts. 1998. Laboratory measurements of angular distributions of light scattered by phytoplankton and silt. *Limnology and Oceanography,* Vol. 43, pp. 1180-1197.

Wells, M. L. and E. D. Goldberg. 1991. Occurrence of small colloids in sea water. *Nature,* Vol. 353, pp. 342-344.

Wells, M. L. and E. D. Goldberg. 1992. Marine submicron particles. *Marine Chemistry,* Vol. 40, pp. 5-18.

Whitmire, A. L., E. Boss, T. J. Cowles and W. S. Pegau. 2007. Spectral variability of the particulate backscattering ratio. *Optics Express,* Vol. 15, pp. 7019-7031.

Wozniak, S. B. and D. Stramski. 2004. Modeling the optical properties of mineral particles suspended in seawater and their influence on ocean reflectance and chlorophyll estimation from remote sensing algorithms. *Applied Optics,* Vol. 43, pp. 3489-3503.

Zaneveld, J. R. and J. Pak. 1973. Method for the determination of the index of refraction of particles suspended in the ocean. *Journal of the Optical Society of America,* Vol. 63, pp. 321-324

Zaneveld, J. R. V. and J. C. Kitchen. 1995. The Variation in the Inherent Optical-Properties of Phytoplankton near an Absorption Peak as Determined by Various Models of Cell Structure. *Journal of Geophysical Research-Oceans,* Vol. 100, pp. 13309-13320.

Zhang, X. D., M. Lewis and B. Johnson. 1998. Influence of bubbles on scattering of light in the ocean. *Applied Optics,* Vol. 37, pp. 6525-6536.

Zhang, X. D., M. Lewis, M. Lee, B. Johnson and G. Korotaev. 2002. The volume scattering function of natural bubble populations. *Limnology and Oceanography,* Vol. 47, pp. 1273-1282.

Zubkov, M. V., M. A. Sleigh, P. H. Burkill and R. J. G. Leakey. 2000. Picoplankton community structure on the Atlantic Meridional Transect: a comparison between seasons. *Progress in Oceanography,* Vol. 45, pp. 369-386.